Study on the Performance Enhancement of the Adsorption Heat Pump applied Natural Meso-porous Material

天然メソポーラス材料を用いた吸着式ヒートポンプの

性能向上に関する研究

He Fang

2022.8

Supervisor

Katsunori Nagano

Environmental system engineering

Division of human environmental system

Graduate school of Engineering

Hokkaido University

Acknowledgment

Author would like to express my gratitude to all those who helped me during the writing of this thesis.

First of all, the deepest gratitude goes foremost to Prof. Katsunori Nagano, author's supervisor. All the guidance and help, greatly encourage author in overcoming the problems and advancing the reaches. Not only the study, Prof. Katsunori Nagano also always talk to author on the culture, history, popularity and so on, which provided author comfortable humanistic solicitude. This guidance and help support author on the academy reaches, and these talk cure author psychologically.

Author also wants to express my gratitude to Prof. Takao Katsura, who is gentle and encourage author in daily life. On the other hand, Prof. Takao Katsura always give author critical and valuable comments on the presentation, which remind author the problem of the current study and help author figure out the way to improve the studies.

Then the special gratitude is for Dr. Junya Togawa. Author has achieved a mountain of guidance on studies from Dr. Junya Togawa, which became the motivation of author for study as a researcher. The moral standard as a researcher for the author is influenced and established by Dr. Junya Togawa. The word from Dr. Junya Togawa, "Never cheat at the academy reaches", has been the tenet of author as a researcher.

The gratitude from author also to all the members of Nagano's laboratory. With your help and support, author's research can advance and finish. Especially, great gratitude to all the guys who belong to the same team to author. Thanks for the senior students, your kind sharing of ideas give author inspiration to overcome the problem of research. Thanks for the junior students, your trust make the author confident to progress the research.

Besides, author wants to express the gratitude to his bad guys, or called intimate friends, who are Chang Liu, Jingyi Zhong and Zhi You. Thanks for you guy's sneer or encouragement, bother or accompanying. You guy remind me that I am nothing, and also trust that I am everything.

Of course, the sincerest gratitude goes to author's family and parents. Without their support, all the growth and achievement of author will not exist. Thanks for the financial and spiritual support. On the other hand, author want to lament the death of Uncle Ping He, who is an energetic and sagacious elder. Author grew up under the caring from Uncle Ping He, they had lots of happy and funny memory. It is very regrettable that Uncle Ping He left author due to drowning on 2022.7.9, R.I.P.

Abstract

Global energy consumption has increased with technological advances, the air conditioner market is expected to burgeon. As a side effect of the use of traditional compress-type air conditioners, problems such as CO_2 emissions and ozone layer depletion need to be addressed. Adsorption heat chiller or adsorption heat pump (AHP) is a type of thermally driven heat pump that provides cooling capacity using low-grade heat sources from 60 - 80 °C, e.g., factory exhaust or hot water from a solar water heater. The utilization of water as adsorbate leads it to be environment friendly. Therefore, AHP is considered an attractive solution. However, some disadvantages such as the low Coefficient of cooling Performance (COP), exorbitant initial cost and huge entire size compared to other types of thermally driven heat pump such as Absorption Heat Pump, result in market barriers for AHPs.

A composite adsorbent of Wakkanai Siliceous Shale (WSS) impregnated with 20 wt. % of LiCl, which is a kind of salt inside porous matrix and has been developed by our laboratory in the prior studies to reduce the initial cost. This study focuses on the practical application of the composite adsorbent and the cooling performance enhancement of the AHP. The topics of each chapter are shown as following:

In Chapter 1, the study background is introduced. The global energy consumption and the domestic energy consumption are introduced, which indicate the energy consumption increasing for the space cooling. Then the performance and specification of several thermal driven heat pumps are compared.

In Chapter 2, a comprehensive review of the AHP is conducted. The working pair, the advanced cycle for performance enhancement and the prior study in our laboratory are shown. Based on this review, the position and objective of this study are determined.

In Chapter 3, the WSS composite adsorbent is applied in a labo-scale AHP as the practical application study. The acrylics who inner diameter of 450 mm is used as the container to observe inside the AHP. The adsorbent is filled into the aluminum corrugated micro channel heat exchanger (HEX, W400 × H300 × D12) to manufacture the adsorbent-filled HEX (ad-HEX). Foundation performance experiments were conducted, and the COP of 0.45 and Specific Cooling Power (SCP) of 0.41 kW/kg are obtained under the following experimental conditions: regeneration at 80 ℃, condensation, and sorption at 30 ℃, chilled water of 15 ℃, and cycle time of 14 min. Further, Heat Recovery (HR) is introduced and experimentally studied to reduce the regeneration heat amount, and the heat balance for this AHP was evaluated. It is confirmed that two types of heat recoveries could improve the COP for this AHP up to 0.54 when the outlet temperature of both adsorbers is 55 °C. The COP could be further improved to 0.57, based on the calculation for the heat balance. This AHP has advantages of high SCP as compared with AHPs in other formal studies.

In Chapter 4, author focuses on the improvement of the ad-HEX. A filling method known as the dip-coating method is introduced to improve the heat transfer and packing density of the ad-HEX. However, the dip-coating method results in the leakage of the impregnated LiCl, which effects on the adsorption ability of the adsorbent. Hence the dip-coating method is adapted to accommodate the WSS composite adsorbent, and two types of adsorbent-filled HEX (ad-HEX), i.e., the dip-HEX and dip-filled-HEX, are compared with the conventional ad-HEX known as the filled-HEX. The dip-HEX comprises a few mass transfer channels and has a packing density similar to that of the filled-HEX. Meanwhile, the dip-filled-HEX exhibits a 30% higher packing density compared with the filled-HEX. A basic performance experiment is performed, and the results indicate that the dip-HEX outperforms the filled-HEX owing to its higher COP and SCP. The dip-filled-HEX exhibits a slightly lower SCP than the filled-HEX; however, it exhibits the highest COP among three types of ad-HEXs. Subsequently, mass recovery is applied to enhance the cooling performance. In a typical mass recovery period of 10 s, the COP and SCP of the dip-HEX increases to 0.46 and 0.74 W/g, respectively.

In Chapter 5, a three-dimensional model is formulated to predict and analyze the performance of an AHP with HR and Mass Recovery (MR). A new value factor index (VF) is proposed to determine the parameters for optimal

system performance. It was confirmed that this model is suitable for performance prediction. COP can be improved from 0.503 to 0.604 at a cycle period of 14 min, which is consistent with the results of our previous study. An optimal HR period of 24 min is determined based on VF. Subsequently, MR was introduced. In cases where the MR of 1 s is utilized, SCP is increased from 0.389 kW/kg to 0.393 kW/kg, while the COP is increased to 0.607 with the HR. In addition, the COP decreased with an increase in the mass recovery period. It was found that the accumulated recoverable sensible heat is shared by the HR and MR. The HR reduces the accumulated regeneration heat. The MR not only reduced the regeneration heat but also enhanced the sorption process.

In Chapter 6, the conclusions for each chapter are summarized. The Passive Heat Recovery, which is one type of the heat recovery, is proved to improve COP from 0.45 up to 0.51. The adapted Dip-coating method also effective to enhance both COP and SCP. Based on the simulation result, both COP and SCP can be enhanced with the Mass Recovery. However, the performance improvement is negligible and the fulfilling is difficult. As the prospective topic, the case study using the simulation model built in Chapter 5 is needed. The specification design of the AHP can be evaluated according to the performance prediction results, which fit the climatic conditions of different area. In order to overcome the disadvantage that the unavailable cooling output below 0 ℃, the methanol is applied in some AHP as the adsorbate instead of the water. Moreover, it is possible to produce pure water by the adapted AHP system, which called water harvesting. With these study and development, AHP and other adsorption-based system are expected to be attractive.

Contents

List of Figures

List of Tables

Chapter 1

Introduction

1.1. Energy Consumption

1.1.1. Energy Consumption of the World

Energy is a critical point for modern society. Huge amount of energy consumption is needed to support our society. The global energy consumption versus the year is shown in **Fig. 1.1**. The total energy consumption in 2019 is around 14000 million of TOE (ton of oil equivalent), grown up to 375 % compared with that in 1965 year, it is 48 % increased from 2000 year. The Asian where we lived in shows the obvious rising of the energy consumption from 2000 year due the economic grow of the developing countries. The Middle East area also shows the rapid increase of the energy consumption (224 % than that in 2000 year) though its ratio is small. On the other hand, the energy consumption of the developed countries such as OECD increased very slowly. The lower economic and population grow rates, change of industry structure and energy-saving may be the reasons.

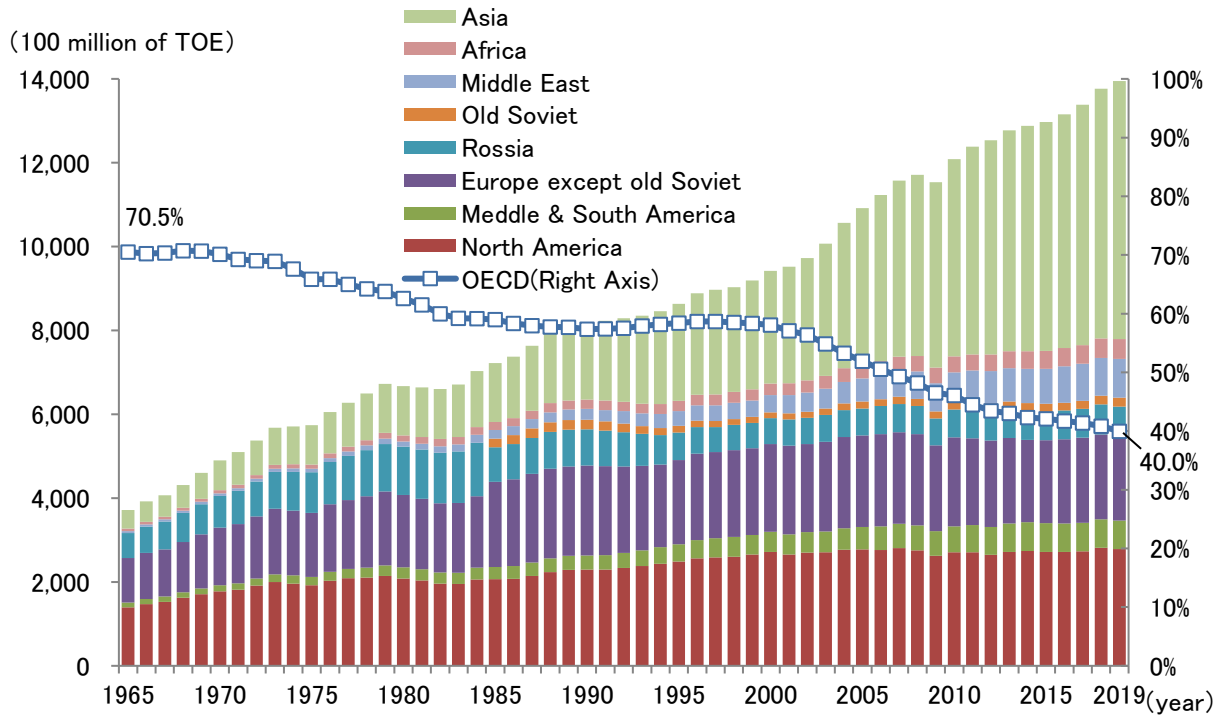

Fig.1.1 Global energy consumption.

The global energy consumption based on different primary energy (PE) source is shown in **Fig. 1.2**. The petroleum has been the major PE for more than 50 years, its share in all is 33.1 %. Not only applied to generate electricity, the petroleum is sold to the world also the transportable fuels. As the second PE, the consumption of coal increased average 2 % per year. Especially after 2000 year, with the quick economic growth of the

developing countries, such as China, the coal consumption increases quickly in Asia area as the electric generate fuel. However, the coal consumption increasing became mildly in 2015 year due to the coal requirement of China and U.S.A decrease. On the other hand, the Liquid Natural Gas (LNG) consumption have been kept increase as the electric generate fuel and domestic resident application (average 3.4% per year), especially in developed countries which is very positive to responds the global warming. The nuclear energy consumption increases fast until 2000, then became mildly. It was decreased 6.8% in 2012 due to the Fukushima Daiichi Nuclear Disaster and keep slightly increase of 1-2% per year after that year. In addition, other renewable source such as wind-power and solar power consumption grown rapidly in average 34.1 % per year from 2010 to 2019 due to the energy-saving and reduction of CO_2 emission. Its share rises rapidly up to 5% in 2019 from 1.4% in 2010.

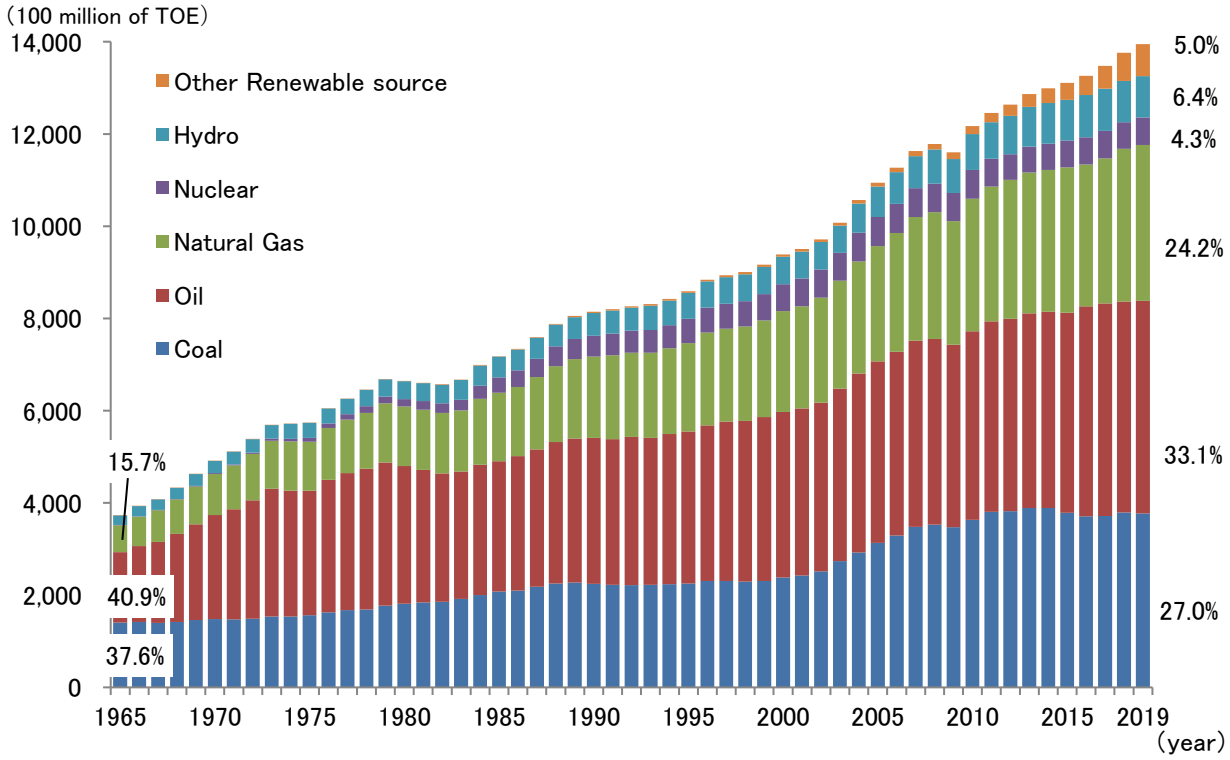

Fig.1.2 Global energy consumption different from the source.

Fig. 1.3 shows the global final energy consumption different from the department. The global final energy consumption in 2018 increased 2.3 times than 1971. The increase of the industry, the traffic and the resident in 2018 are 2, 2 and 3.2 times than those in 1971. The final energy consumption of the industry increases due to the widespread of the automation. The motorization needs large amounts of fuels, it contributes to the global final energy consumption increasing of the traffic. Especially, with the population growth and economic development in developing countries such as China and India, final energy consumption of the industry and the traffic are supposed to be enhanced further in the future.

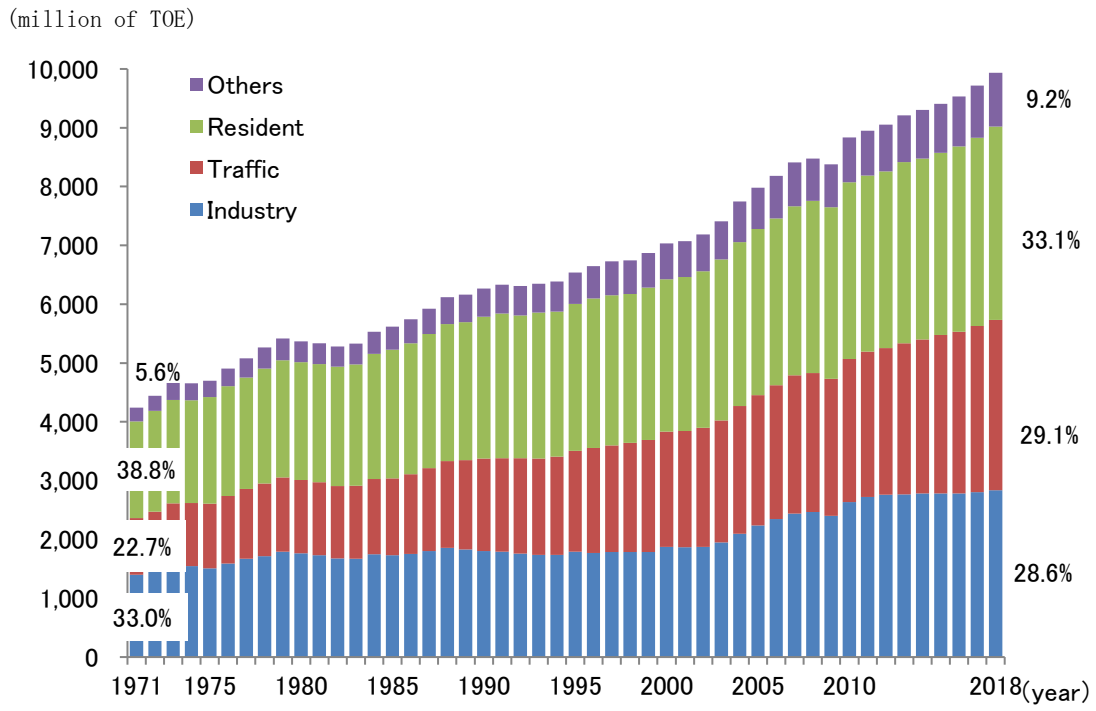

Fig.1.3 Global final energy consumption different from the department.

1.1.2. Electricity Consumption of the World

The global electricity consumption by year are shown in **Fig.1.4**, it have kept increasing except for 2009. The electricity consumption in Asia area started rapid rising from 2000. It rises up to 10.2 trillion kWh in 2018, which is 3.1 times than that of 3.25 trillion kWh in 2000. The electricity consumption in Middle East area is increased to 1 trillion kWh in 2018 from 0.38 trillion kWh in 2000, which is 1/10 compared with the Asia area. In additions, the electricity consumption of Oceania, Europe and North America in 2018 increased 1.2, 1.1 and 1.1 times than those in 2000. The rapid increase of the electric consumption in Asia area is because of the fast economic growth of China result in huge electric requirement, which is increased up to 6.01 trillion kWh in 2018 from 1.04 trillion kWh in 2000. India also shows great increase of electricity consumption from 0.37 trillion kWh in 2000 to 1.2 trillion kWh in 2018. Vietnam shows 8.4 times higher electricity consumption of 2018 than that of 2000, however, the absolute electricity consumption in 2018 is only 0.19 trillion kWh. Compared with the electricity consumption in 2000, those of the developing countries in Middle East area shows 2.63 times growth, meanwhile those of Africa area shows 1.87 times of growth due to the development support from China. The electricity consumption of both Middle East and Africa areas is around 7.5%, which is not large at present but can be proposed to be enhanced with the developing in the future. On the other hand, the electricity consumption of Japan is slightly increased to 0.95 from 0.89 due to the policy implement of energy-saving.

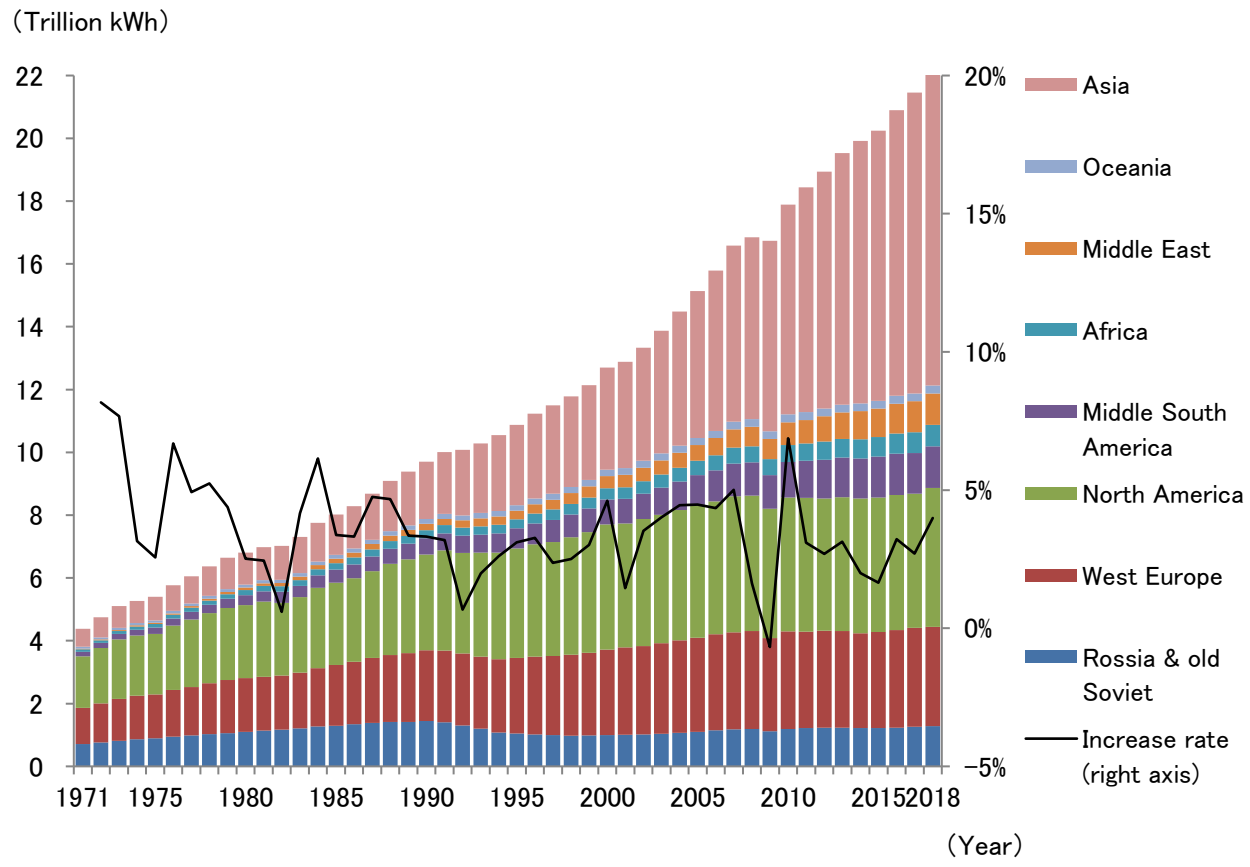

Fig.1.4 Electricity consumption of the world.

1.1.3. Electricity Supply of the World

The power generation amounts in different source are shown in **Fig. 1.5**, it has kept increasing from 1971 and up to 26.6 thousand trillion in 2018. The thermal power generation is the obviously main power generation way, which is about 64.1 % in all.

The power generation by the coal have been increased except for 2009 and 2015. It shows a stable share of about 39 % from 1971 to 2018. The power generation by the oil kept increased and started decreasing from 1980s owing to the oil crisis, the share of oil in 2018 fell down to 2.6 % from that of 20 % in 1980. As the substitute for oil, the natural gas shown an increased share of power generation from 13 % in 1980 up to 23.2 % in 2018. The nuclear technology has been developed and applied to the power generation since 1954, and the amount of the power generation by the nuclear increased rapidly until 1990. Then the amount of the power generation by the nuclear increased very slight every year, and its share was 10.2 % in 2018. With introduction and spread of the renewable source energy, it shown the share of 9.8 % in 2018. It can be predicted that the share of the power generation by the nuclear will increase further in the future.

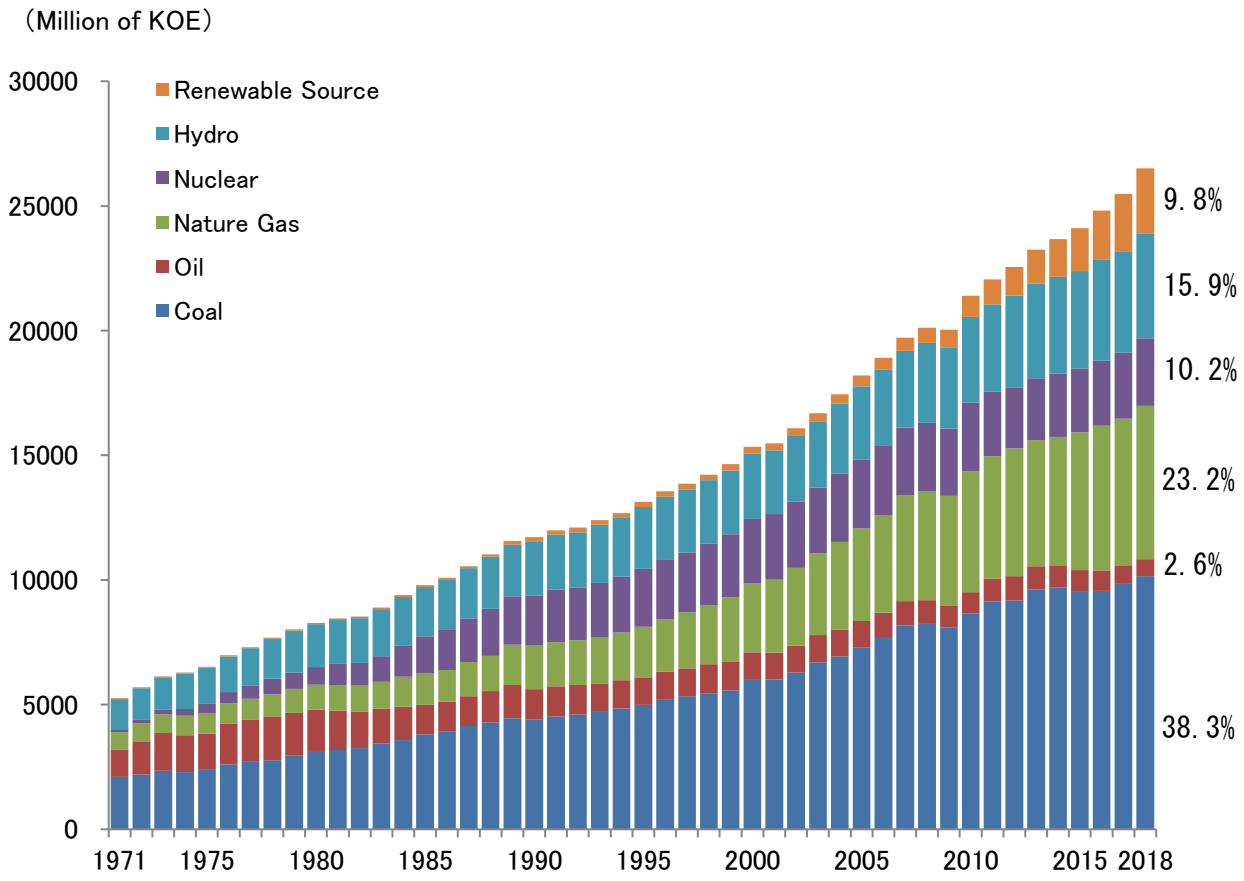

Fig.1.5 Power generation amount in different source.

The generation amount proportion of major countries different from energy source in 2018 is shown in **Fig.1.6**. With the production of shale gas in U.S.A, the proportion of generation amount by coal decreased and that of natural gas increased to 34.3 % in 2018. The coal was plentiful in U.K, it was used as the major fuel for power generation; however, with the development of natural gas mineral in north ocean, the proportion of generation amount by coal fell to 5.3 %. France shown an extreme high proportion of generation amount by the nuclear at 71.6 %, which is the highest proportion of the world. Germany shown the highest proportion of generation amount by the renewable source at 33.8 %; however, a relatively high proportion of generation amount by the coal at 37.5 % was still needed. The power generation in Italy mainly depended on the natural gas, hydro and renewable source. The power consumption of China increased rapid with the economic development, hence the large proportion of the coal at 66.8 % was used for power generation due to its cheap prices, meanwhile it causes the environmental problem. The proportion of generation amount by coal, natural gas and nuclear were 44.1 %, 26.5 % and 22.8 %, respectively.

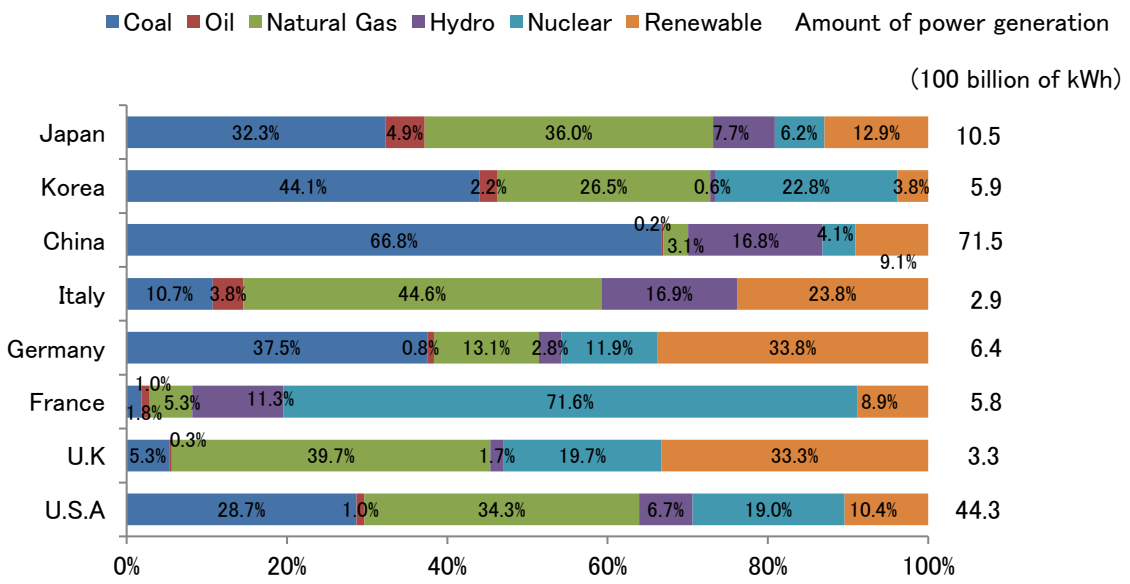

Fig.1.6 Proportion of generation amount different from energy source (Major Countries).

The generation amount proportion of some developing countries different from energy source in 2018 is shown in **Fig.1.7**. The total power generation of Africa was 830 billion of kWh, the proportion of generation amount by coal and natural gas, which were the main source of power generation, were 31.2 % and 40.1 %, respectively. 8 % of the generation amount was oil and 15.7 % of that was hydro. Moreover, the proportion of generation amount by nuclear and renewable source is extreme small in all. The Middle East have the richest oil field in the world, hence the oil and the natural gas applied in power generation were obviously more than other sources. The proportion of generation amount by oil and natural gas were 25.3 % and 73 %, respectively. In recent years, India has been rapidly developed in economy and shown a similar proportion of generation amount to China. The power generation was mainly by the coal in 73.5 % due to the cheap price; meanwhile, it can be predicted that the environmental problem will occur in the future. Viet Nam, Peru and Chile shown a small amount of power generation, meanwhile a relatively high proportion of generation amount by hydro at 34.9 %, 55.9 % and 28.4 % were obtained. The proportion of generation amount by coal in Peru was extremely low 0.2 %, meanwhile, the total power generation amount in Peru was only 50 billion of kWh. The power generation in Mexico was mainly by the natural gas at 60.3 %, proportion of power generation by other sources were from 4.1 % to 10.5 %. Brazil shown a very high proportion of power generation by hydro at 64.7 % owing to the applicant of its rich water source. The fossil fuel of coal, oil and natural gas were only 3.9 %, 2.1 % and 9.1%, respectively. The proportion of power generation by nuclear and renewable source were 2.6 % and 17.7 %, respectively.

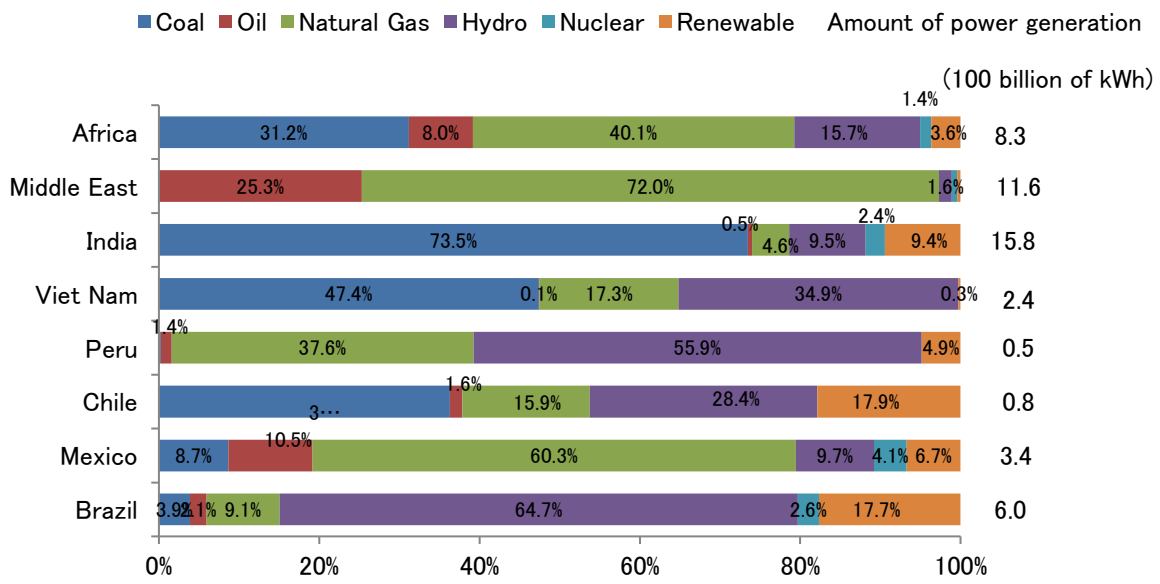

Fig.1.7 Proportion of generation amount different from energy source (Developing Countries).

The developed countries have a relatively large proportion of power generation by the nuclear and renewable. The proportion of power generation by the nuclear in France is astonishing 71.6 %, and the proportion of power generation by the renewable in Italy, Germany and U.K. are 23.8 %, 33.8 % and 33.3 %, respectively. On the other hand, some developing countries use the hydro to generate power mainly. The proportion of power generation by the hydro in Peru and Brazil are 55.9 % and 64.7 %, respectively. Owing the large production of oil, Middle East shown a very high proportion of power generation by the oil and natural gas at 25.3 % and 72 %, respectively. From all these data above, it is indicated that more than half of the power generation depends on the fossil fuel. The coal is the most general source for power generation, especially its cheap price result in its large proportion of power generation in developing countries. Moreover, it can be predicted that the power consumption in developing countries will increase with the economic development, which result in increase of coal requirement and environmental problem.

1.1.4. Energy Consumption of Japan

The energy consumption of business department based on purpose in Japan is shown in **Fig. 1.8**. As a developed country, its energy consumption can be used to predicted those of developing countries such as China, India and Viet Nam.

With the development of economy, the energy consumption of power/lighting increased owing to the office automation. Meanwhile, the energy consumption of space heating/cooling increased with the increasing comfort requirement. After 2000, the energy consumption of space heating decreased because of the coefficient

improvement of air conditioner, the development of thermal insulation materials and the policy spread of energy-saving. Moreover, the development of industry and cogeneration result in energy consumption of water heating decreasing mildly. On the other hand, the requirement of space cooling has been kept increasing. It can be predicted that the energy consumption in developing countries for space cooling and heating will increase with the economic development. China and India have a large and potential air conditioner market because of their great amount of population, which enhance the energy consumption. Meanwhile, Africa, North America and Middle East need large cooling amount with the spread of air conditioner in the future.

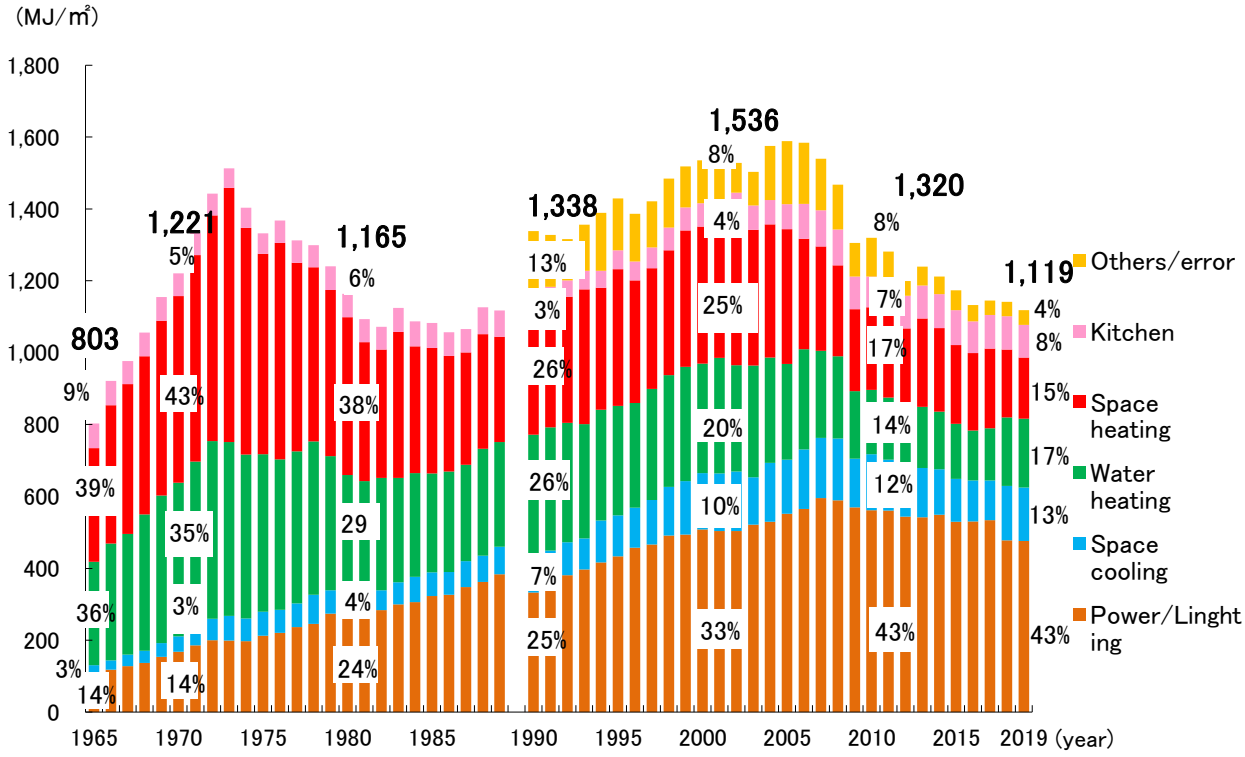

Fig.1.8 Energy consumption structure of business department base on purpose in Japan. [2]

1.1.5. Dependence Increase of Fossil Fuel

As mentioned above, the global energy consumption has kept increasing year by year. Especially, the comfort requirement in developing countries can be predicted to increase rapidly with the fast economic development, which results in the increase of energy consumption for space cooling/heating and water heating. The development of cogeneration contributes to reduce the energy for space heating and water heating. Meanwhile, the energy consumption for space cooling will increase owing to the spread of air conditioner.

In 2018, 64.1 % of all the power generation amount depends on the fossil fuel, as shown in **Fig. 1.5**. Though some countries applied large proportion of clear source, such as France used nuclear for 71.6 % and Brazil used hydro for 64.7 %, the fossil fuel and natural gas are the most general source for power generation in both

developing and developed countries. Moreover, the energy consumption of developing countries will increase with the development of economy and industry, the proportion of power generation by coal will increase. The dependence of power generation on fossil fuel can be predicted to increase further in the future.

However, the dependence increase of power generation on fossil fuel leads to environmental problem, which is the emission increase of CO_2. The emission of global warming gas include CO_2 is 1.343 billion ton in 2012, which is increased by 6.9 % than that in 2010. More than 30 % of all global warming gas emission owing to power generation.

With all mentioned above, the renewable energy has been studies as the alternative source of fossil fuel. This study focuses on the utilization of industry waste heat and solar heat, moreover, apply thoes heat to drive heat pump.

1.2. Thermal Driven Machine

1.2.1. Potential of Thermal Energy Application

After applied for work, energy is generally changed into heat and exhausted with exhaust gas under 200 ℃. The exhaust gas temperature proportion of different department is shown in **Fig.1.9**. It was found that the exhaust gas over 200 ℃ is about 20 %, half of all exhaust gas is less than 100 ℃. Because of the low energy density and high cost of recovery devices, almost all of those energy under 100 ℃ is exhausted as the exhaust gas. Not only the industry exhaust gas, but although the heat from vehicle and domestic cogeneration is exhausted directly without application.

Fig.1.9 Temperature distribution of exhaust.

On the other hand, more and more attention has been paid to the application of renewable energy in recent years, as shown in **Fig.1.10**. It can be predicted that the power generation amount by solar power will increase rapid in the future. Thus, the application technology of heat source under 100 ℃ in summer will be the key to the solar power development.

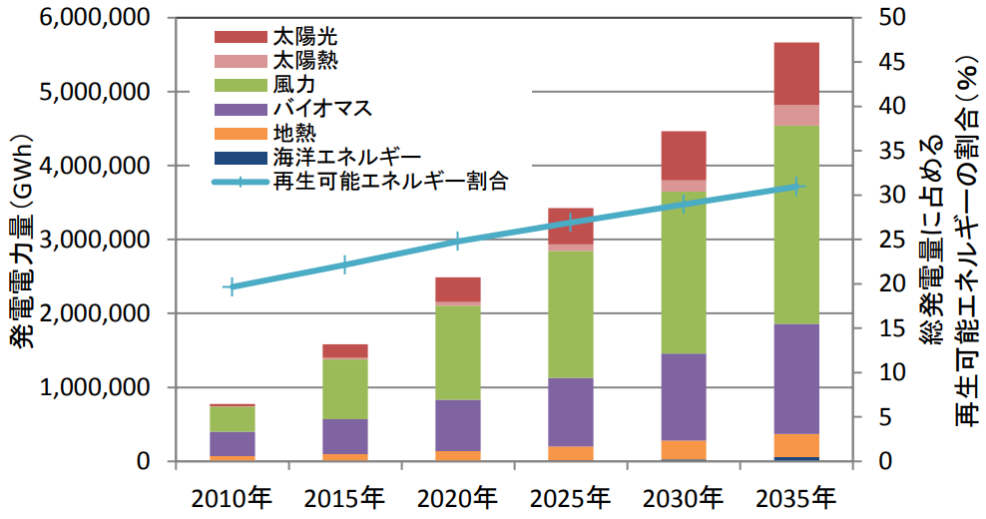

Fig.1.10 Prediction of generation by different source. [3]

As the alternative energy source of electricity, the exhausted heat under 100 ℃ is proposed to drive machine, especially air conditioners. With the utilization of heat source under 100 ℃, which is abundant in summer, the dependence on fossil fuel can be reduced. This section introduced the Adsorption Heat Pump (AHP), which is the major studied target. Moreover, another type of heat driven heat pump called Absorption Heat Pump is introduced to compared with AHP.

1.2.2. Absorption Heat Pump

Absorption Heat Pump is one of the heats driven heat pump. A kind of liquid that can strongly absorb the refrigerant vapor is applied as the absorbent, hence the evaporation of liquid refrigerant can be enhanced to provide the cooling power. Absorption heat pump was studied since 1930, and its commercial production has been sold in market from 1945.

Absorption heat pump is shown in **Fig.1.11**. The boiling point of water is 100 ℃ under atmosphere and

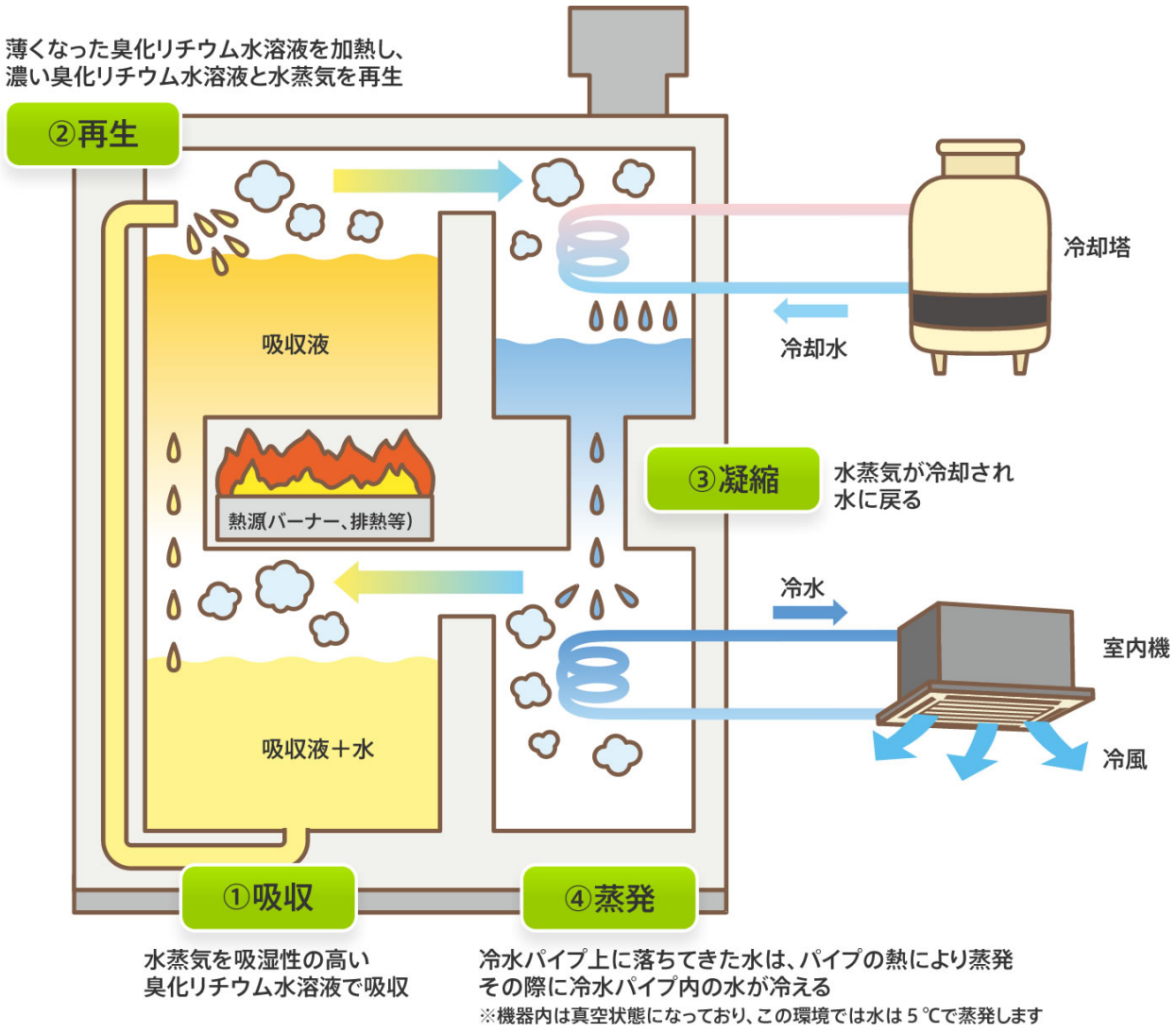

Fig.1.11 Conception of Absorption Heat Pump.

decreases down to 7 ℃ in vacuum, hence the absorption heat pump system inside is in vacuum to enhance the evaporation of refrigerant. The refrigerant is vaporized in evaporator (④), the circulation water in the heat exchanger (HEX) is cooled down to provide the cooling ability. The vaporized refrigerant move to absorber (①) and absorbed by the liquid absorbent. It leads to decrease of liquid absorbent concentration and absorption ability. Then the low-concentration liquid absorbent is sent to the regenerator (②) and heated to vaporize the refrigerant, thus the liquid absorbent can be concentrated and applied in absorber again. Meanwhile, the vaporized refrigerant move to the condenser (③) to be condensed, then return to evaporator to be reused again. Absorption heat pump usually applies water/LiBr as the absorbate(refrigerant)/absorbent working pair for space cooling. Ammonia/water is generally used as the absorbate(refrigerant)/absorbent working pair of absorption heat pump for chilling. Those absorption heat pump have been sold in market.

The circulation water for space cooling and the refrigerant evaporator exchanges their heat with the HEX in evaporator. The pressure of evaporator increases with the evaporation of refrigerant, meanwhile, the refrigerant vapor is absorbed by the absorbent in absorber, hence the pressure in evaporator can be kept at a relative low level to provide enough cooling ability. The absorption of refrigerant in absorber leads to temperature increase of liquid absorbent and absorption ability decrease, therefore the absorber is always cooled down by the cooling water from cooling tower. The low-concentration liquid absorbent is generated in generator by the heat source under 100 ℃, which comes from solar power or exhaust gas. The concentrated liquid absorbent return to absorber to be reuse. The vaporized refrigerant moves to the condenser to be condensed by the cooling water from cooling tower, then return to evaporator to be reused again.

The merits of absorption heat pump are shown as following:

1. Driven by the heat source under 100 ℃ from solar heater or industry exhaust gas, which is abundant and generally useless in summer.
2. Both Ozone Depletion Potential (ODP) and Global Warming Potential (GWP) are 0 because freon is not used.
3. Vibration and noise are little, and easy to maintain owing to heat driven.
4. Simple structure, output is easy to adjust by the flowrate change.
5. Coefficient of Performance (COP) for cooling is 1.0 ~ 1.5 and no electricity is needed except for circulation pump of heat source.

The demerits of absorption heat pump are shown as following:

1. Because of the corrosivity of LiBr, some hazardous material such as chromic acid is added to prevent corrosion.
2. The cooling ability under 0 ℃ is unavailable while water is applied as the refrigerant or circulation water.

3. Periodical maintenance and vacuuming are needed to keep the absorption heat pump inside at a high vacuum degree.
4. Bigger cooling tower is needed compared with the compress type air conditioner in same capacity.

Despite absorption heat pump have those demerits above, its commercial production have been sold in market and applied in lots of large building.

1.2.3. Adsorption Heat Pump

Adsorption Heat Pump (AHP) is another kind of heat driven heat pump. Mesoporous material such as silica-gel is able to sorb gas such as vapor, this phenomenon is applied in AHP to enhance the vaporization of refrigerant such as vapor hence the cooling ability can be obtained. **Fig.1.12** shows the schematic of silica-ge/water AHP. Water in evaporator is vaporized to provide cooling ability, then the vaporized vapor moves to and sorbed by the silica-gel. The silica-gel became saturated and the adsorption ability decrease with the progress of adsorption, hence the generation process is conducted. Hot water is circulated to heat the saturated silica-gel and the sorbed vapor is desorbed. Finally, the desorbed vapor is condensed in condenser and return to evaporator to be used again.

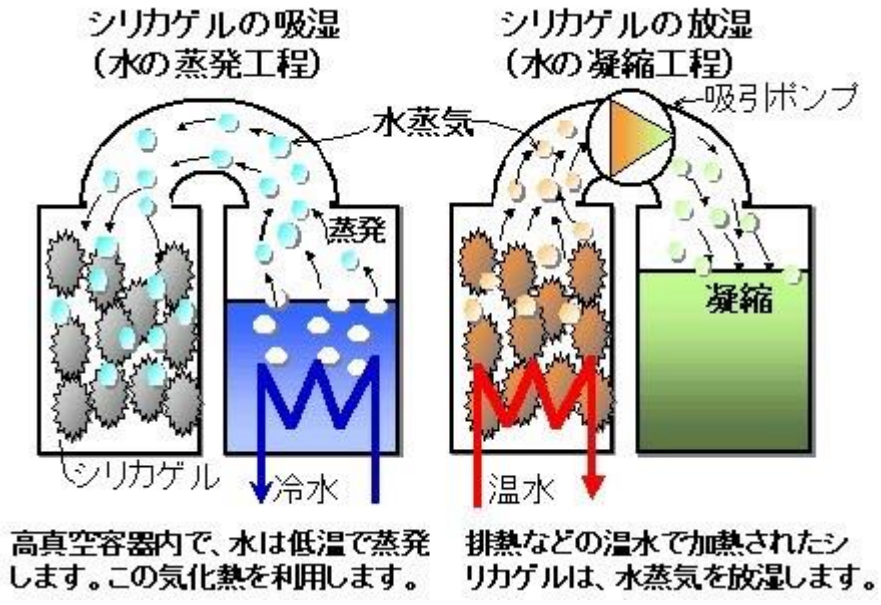

Fig.1.12 Conception of Adsorption Heat Pump. [4]

A general structure of AHP is shown in **Fig.1.13**. AHP consists an evaporator and a condenser, moreover, 2 adsorber are applied to provide cooling ability consecutively. The circulation water is flowed into the HEX in the evaporator and chilled with the vaporization of refrigerant water, thus the chilled water for space cooling at can be obtained at 7-15 ℃. The vaporized refrigerant water is sorbed by the adsorbent in the adsorber of right

side, hence the evaporator can be kept at a low pressure and the vaporization of refrigerant continue smoothly. Lots of heat is released with the water sorption, therefore cooling water at 30 ℃ from the cooling tower is flowed into adsorber to cool the adsorbent down. It called sorption process. On the other hand, the adsorber of left side is heated by the hot water at 60-80℃, which comes from the exhaust gas or solar heater. The sorbed water refrigerant is desorbed and move to condenser. The cooling water from cooling tower (or from the outlet of adsorber in sorption process) is circulated into the condenser, hence the vapor refrigerant can be condensed and return to the evaporator to be reused. This called regeneration process. The hot/cooling water supply of adsorber, valves action between each chamber are switched with the time past to switch the regeneration and sorption process.

The common sorbent/sorbate working pairs of AHP are as follows: Activated carbon/Alcohol, Activated carbon/Ammonia, natural Zeolites/Water, AQSOA-FAM/Water.

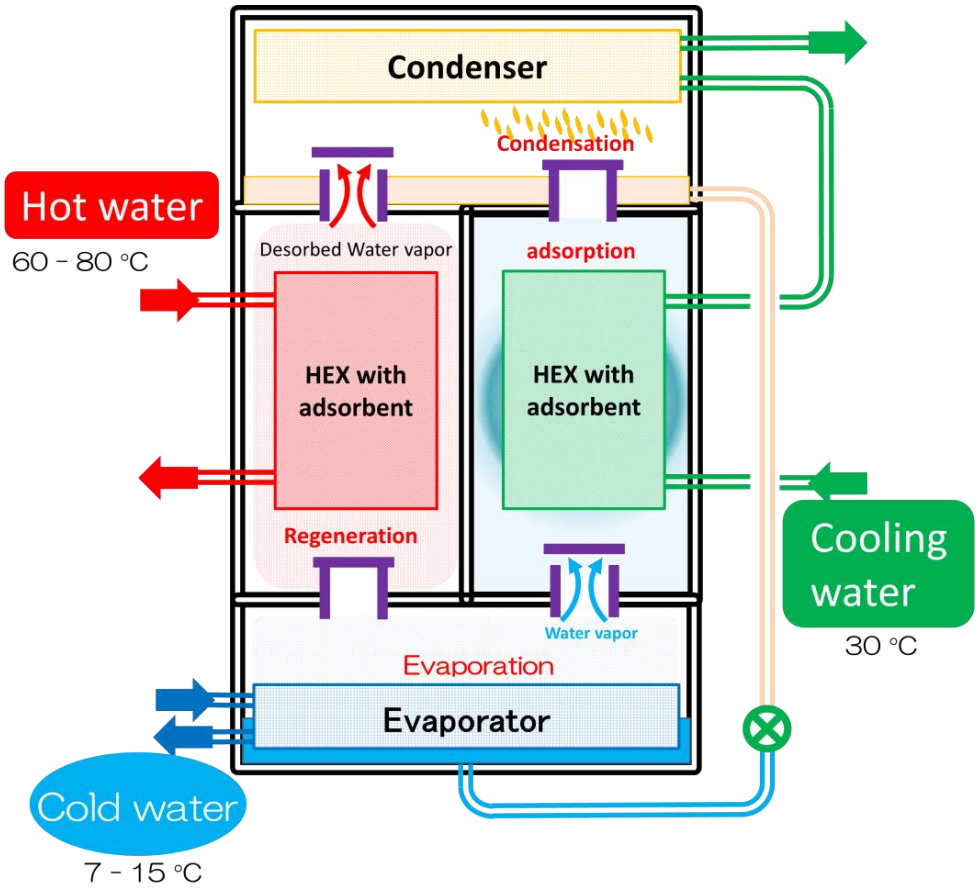

Fig.1.13 Principle and structure of normal Adsorption Heat Pump.

1.2.4. Practical Application of Adsorption Heat Pump

Some commercial AHP have been sold in market, as shown in **Fig.1.14**. **Fig.1.14 (a)** is a 10 kW-scale AHP made by Invensor Co. Ltd., AQSOA-Fam is applied as the adsorbent. Its dimension is 1100mm × 1370mm × 750mm and the weight of entire AHP is 445 kg. This AHP shows a high COP of 0.55, however, its price is more

than 300 million Japanese yen. An 80 kW-scale AHP made by Mayekawa MFG. Co., Ltd. is shown in **Fig.1.14(b)**, its dimension is 3900mm × 2100mm × 2350mm. However, other information such as prices and adsorbent are unavailable.

(a) Invensor Company. [5] **(b) Mayegawa Company. [6]**

Fig.1.14 Commercial AHP sold in the market.

1.2.5. Merits and Demerits of Adsorption Heat Pump

The merits of AHP are shown as following:

1. AHP can keep a relatively high performance than absorption heat pump
2. Compared with the performance of absorption heat pump, that of AHP decreases mildly with heat source temperature decrease. As **Fig.1.15** shows, the cooling performance of AHP decrease to 90 % while that of absorption heat pump drop to 48 % at 80 ℃.
3. No corrosive salts used; thus, the hazardous material is not necessary.
4. Little deterioration owing to low temperature and pressure inside the AHP.
5. Simple structure.
6. Only several minutes is needed to start (Absorption heat pump need more than 10 minutes).
7. The electricity consumption, noise and vibration are little owing to heat driven.

Not only all those merits mentioned above, AHP also have following demerits:

1. The relative low COP (0.5) compared with that of absorption heat pump (1.5), which is another type of heat driven heat pump.
2. Expensive initial coat. About 1/3 of this is for adsorbent.
3. The adsorbent is fixed in the adsorber, hence the mass transfer channel for adsorbate refrigerant vapor moving need to design. Moreover, the weight of adsorbent need increases to enhance the cooling power.
4. The small effective heat conductivity within adsorbent and the thermal resistant between the HEX and

adsorbent leads to bad heat conductivity inside. Larger heat transfer surface area is necessary, which result in large volume of AHP.

5. The micronization of adsorbent and the integration of adsorbent/HEX for the enhancement of heat transfer result in cost increase.
6. The cooling power output under 0 ℃ is unavailable while water is applied as the adsorbate refrigerant.

The spread of AHP is disturbed by all those demerits result, especially 1, 2 and 3. Hence the major barriers for AHP spread are performance improvement, initial cost reduction and compaction.

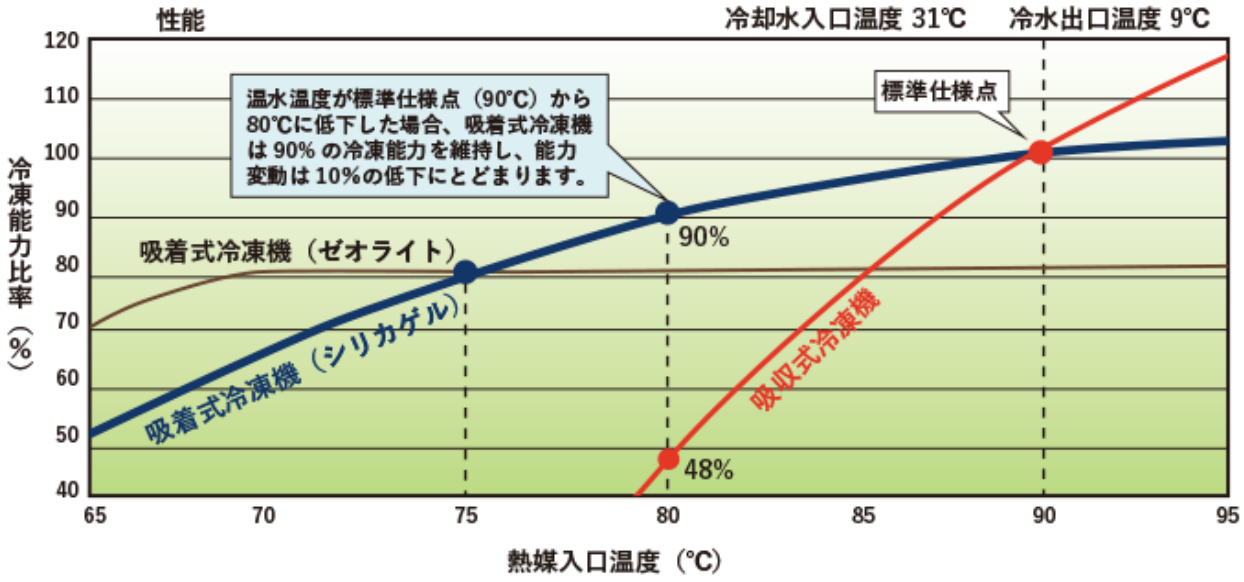

Fig.1.15 Performance comparing of Adsorption Heat Pump and Absorption Heat Pump of temperature.

1.3. Study Objective

As mentioned in the previous sections, the energy consumption has kept and is predicted to increase in the future. Lots of fossil fuel is applied in power generation especially in developing countries due to cheap price, which emits lots of CO_2 and causes environmental problem. On the other hand, the requirement of comfort increases with the economic development of developing countries, large amount of power generation is needed. The AHP, which is a kind of thermal driven heat pump, is one of the possible solutions to solve these two problems. The AHP is an environment-friendly space cooling machine driven by heat, which causes the AHP to be an alternative of air conditioner. However, huge volume of the device, expensive initial cost and relative low coefficient of performance result in market barriers of the AHP. Especially the expensive initial cost disturbs the spread of AHP introduction in developing countries, in which the air conditioner requirement will greatly increase in the future.

The purpose of this research is shown as following:

1) Building a laboratory-scale AHP prototype to practically using the mesoporous material developed by our prior studies. Experimentally evaluate the cooling performance of the AHP.
2) Introducing some advanced cycle and new filling method, comparing the different type of the heat exchangers to enhance the cooling performance of the AHP.
3) Building a three-dimensional model to predict the cooling performance of the AHP for numerically studies.

Reference

[1] Energy Consumption Report of 2019,

http://www.enecho.meti.go.jp/about/whitepaper/2020html/ , (2021-9-1)

[2] Energy Consumption Report on Department, Research Organization for Information Science and Technology,

http://www.rist.or.jp/atomica/data/dat_detail.php?Title_No=01-02-03-07 , (2021-9-1)

[3] Home Page of Japan Valve Manufacturer's Association,

https://j-valve.or.jp/environment/env-info/p160323.html , (2021-9-1)

[4] Home Page of Chubu Electric Power,

https://www.chuden.co.jp/corpo/publicity/press2002/0220_2_2.html , (2019-2-4)

[5] Home Page of AAAmachine Japan, Inc,

http://www.aaamachine.co.jp/ , (2021-9-1)

[6] Home Page of Mayekawa MFG. Co., Ltd,

http://www.mayekawa.co.jp/ja/news/2012/pdf/news20120418.pdf , (2021-9-1)

Chapter 2

Reviews on Adsorption Heat Pump

2.1. Working Pair of Adsorbent/Adsorbate

As the core of AHP, working pair of adsorbent/adsorbate determine the performance and properties of AHP mostly. AHP applied different working pair of adsorbent/adsorbate shows different working temperature, COP, cooling power output, temperature of chilled water. Common working pairs of adsorbent/adsorbate are shown as following.

2.1.1. Zeolite/Water

Swedish mineralogist Axel Fredrik Cronstedt observed that rapidly heating this material produced large amount of steam from water that had been adsorbed by the material in 1756, therefore he named this material “zeolite” from the Greek “zeo”, meaning “to boil” and “lithos”, meaning “stone”. Zeolite is a kind of microporous, aluminosilicate minerals. The combination of water and aluminosilicate is weak; hence water is easy to escape and be boiled when the zeolite is heated. The formation of zeolite can be indicated as Mn+x/nAlxSiyO2x+2yx-·zH2O.

Zeolite is general used to dehumidification and dehydration because of property of great hydrophilic. Meanwhile, zeolite possess micropores within 0.2～1.0 nm, thus it also used as molecular sieve. Moreover, zeolite can strongly adsorb some molecules then desorbed them when the zeolite is heated. This ability can be changes and adapted a lot with different parameters of zeolites, they are summarized as following:

(1) Structure of micropores

(2) Pore size which depends on ion exchange and chemical reaction

(3) Hydrophilia and hydrophobia depend on the proportion of Si/Al

(4) Molecule polarity of adsorbate/adsorbent

(5) Diameter of adsorbate molecule

(6) Distribution coefficient based on temperature

Zeolites have been investigated since the last century [1], [2]. Some alkalified zeolites are still stable even at 800°C, however, porous structure of most zeolites will be destroyed within 600-700°C [3]. Hence AHPs applied zeolite as adsorbent are mainly driven by heat source at 200-300°C. F. Meunier (1985) built a simulation of AHP applied zeolite 13X as the adsorbent, and result indicate COP of 0.425 [1]. Douss (1988) reported another study on AHP, in which Zeolite NaX was used as adsorbent. The simulation result shown a relative high COP of 0.73 and the experiment result of COP was 0.673 [2]. The regeneration temperature in studies of both F. Meunier and Douss were relatively high (F. Meunier : 350°C, Douss : 200°C), moreover, lots of water sorption/desorption

occurred at very low relative humidity range. These properties did not fit AHP, thus studies on zeolite-base AHP is few in recent years. On the other hand, zeolites are employed in steam generation system and lots of studies have been conducted [4], [5].

Zeolite is a kind of natural mineral. Lots of research have been conducted to artificially synthesize zeolites. It was indicated that the adsorption ability of artificially synthesized zeolites can be adjusted by changing the ratio of Si and Al, thus its efficient heat transfer and density can be adapted to AHP system. For example, Mitsubishi chemical Co.Ltd.. has developed a kind of artificially synthesized zeolite called AQSOA-FAM, and there was applied in some commercial production of AHP. However, the price of artificially synthesized zeolite is much more than that of natural zeolite, which result in a great barrier [6].

2.1.2. Silica-gel/Water

Silica-gel is a kind of adsorption material. It can be achieved by adding acid into sodium silicate, hydrolysis and drying. Silica-gel generally used as dessicant and accelerant owing to its porous structure and large surface area. Some silica-gel in which indicator of $CaCl_2$ is added to make the silica-gel shows blue color for low water adsorbed amount and light peachblow for high water adsorbed amount. These silica-gel that used as dessicant can be reused after regeneration.

Silica-gel can be classified to A and B type with the pore diameter and pore volume. The pore diameter and pore volume of A type silica-gel are 2.4 nm and 0.46 mL/g, respectively. Water vapor can be adsorbed by the A type silica-gel at a low relative humidity (**Fig. 2.1**) and desorbed with regeneration, hence it is general used as dessicant. B type silica-gel shows the pore diameter of 6 nm and the pore volume of 0.75 mL/g. The water vapor

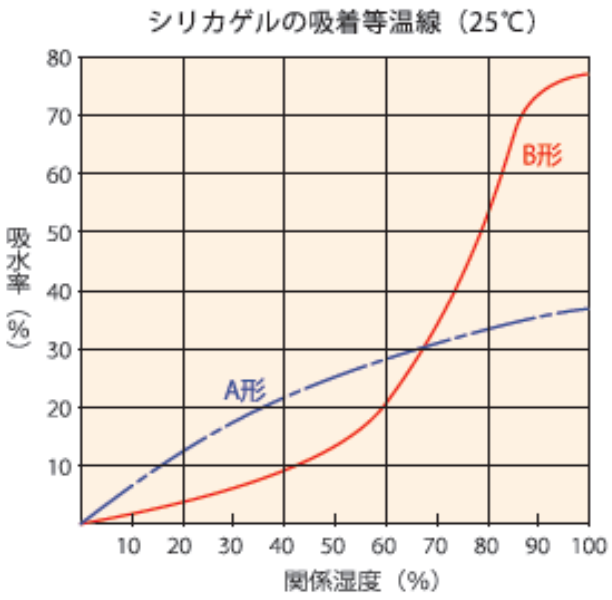

Fig. 2.1 Adsorption isothermal of A and B type silica-gel.

adsorption amount keeps mild at a low relative humidity and increases fast at a high relative humidity, therefore B type silica-gel can be employed to control the humidity. Silica-gel is not only used as dessicant, but although applied as food additive. A type silica-gel is general employed as adsorbent of AHP owing to its water sorption ability at a low relative humidity condition, which is necessary for AHP.

Pan (2015) and his team make a serial of study on silica-gel based AHP [7], [8], [9]. A COP of 0.35 and a SCP of 130 W/kg can be achieved by AHPs that employ silica gel at the following conditions: 80 °C regeneration, 30 °C condensation/sorption, 15 °C at the chiller inlet, and a cycle period of 600 s. In addition, performance of AHP applied solar heater as regeneration heat source at different temperature has been studied with simulation [10]. Silica-gel based AHP is also studied by Akahira (2004) and his team. With the mass recovery and two stage of cascade, this AHP shown COP of 0.51 and SCP of 130 W/kg at conditions of 80 °C regeneration and 7 °C evaporation [6], [11].

As a common working pair of adsorbent/adsorbate, silica-gel/water takes a good balance of driven temperature, price, cooling performance, environment friendly. That leads to lots of studied on silica-gel based AHP. It will be introduced later.

2.1.3. Activated Carbon/Alcohol · Propane · Ammonia

Activated carbon is a carbon porous material. It can be made from botanic material such as wood/bamboo/ cocoanut shell or coal/oil, even animal bone. In Okinawa of Japan, sugar cane leavings have been tried to be applied to product activated carbon. With the physical/chemical treatment, the adsorption ability of activated carbon can be enhanced and employed to selective separation/removing/refining. Because of the porous structure, activated carbon own ability of adsorbing other particles. Polar molecules such as water is difficult to be adsorbed by activated carbon for its nonpolar surface, however, organic granule such as alcohol can be selectively adsorbed. The activated carbon can be reused after regeneration, which is like another adsorbent. Moreover, activated carbon is more stable than other chemical adsorbent [12].

Alcohol, propane, and ammonia are generally employed as the adsorbate of activated carbon. Ammonia has advantages of large vaporization latent heat, harmless to ozone layer, low GWP and low boiling point of - 33 °C, it is usually applied in low temperature AHP system [12]. However, ammonia is poisonous and corrosive to copper, which result in few research in recent years. Alcohol such as methanol is harmless to ozone layer, low boiling point at - 114 °C, and it fits a lot of activated carbon but is as poisonous as ammonia. Propane is an environmentally friendly and low boiling point (- 42.1 °C) adsorbate. Its natural reserve is very abundant thus its price is very cheap [12].

H.J.Dakkama [12] and his teams studied on a high performance activated carbon call Maxsorb. The Maxsorb

was used as adsorbent, R143a and propane were applied as adsorbate in a two stages cascade system. COP of 0.04 was obtained at 70 °C regeneration and - 5 °C of chilled water. M. Kumita and his team fucus on density increasing of activated carbon. A simulation has been built and it was found that the sorption speed of methanol can be up to 0.811 kg/m^3・s by activated carbon whose density was increase up to 380 kg/m^3 [13]. The compactness of AHP can be expected with this technology.

The working pair of activated carbon/alcohol・propane・ammonia can produce cooling amount under 0°C owing to the low boiling point of adsorbate. However, poisonous and ignitable adsorbates need maintenance periodically, and lower latent heat than that of water is the demerit [3].

2.1.4. AQSOA-FAM/Water

AQSOA-FAM is a kind of artificially synthesized zeolite developed by Mitsubishi Chemical Co.Ltd.. **Fig.2.2** shows its isotherms of water. AQSOA-FAMs show different shape of isotherms to those of conventional adsorbents (Silica-gel, Y type zeolite and activated carbon). This kind of material can be regenerated at a lower temperature than conventional adsorbents, and its “S” shape curve of isotherm indicates that a large amount of water adsorption/desorption can occurred in a narrow relative humidity range.

AQSOA-FAM has a serial of Z01, Z02 and Z05. Their isotherms are similar to each other; however, their generation temperature and relative humidity range of sorption/desorption are different. AQSOA-FAM Z05 can be generated at a very low temperature of 50°C, and its water sorption/desorption amount change a lot at a high relative humidity range of 0.2-0.3. AQSOA-FAM Z02 shows the largest amount of water sorption/desorption at a very low relative humidity range of 0~0.1, but it needs a high temperature of 90°C to generate. AQSOA-FAM Z01 shown a sorption amount change around 0.1~0.2, it can be generated at 60 °C [14], [15], [16], [17]. On the other hand, Y type zeolite adsorbs a large amount of vapor at an extreme low relative humidity, which is very similar to AQSOA-FAM Z02. On the contrary, the generation temperature higher than 150 °C is needed, thus Y type zeolite is unfit to AHP system.

Because of all these properties mentioned above, AQSOA-FAM is a very valuable adsorbent material of AHP. A. Sapienza (2011) and his team made an AHP prototype employed AQSOA-FAM Z02 as adsorbent. COP of 0.6 and SCP of 395 W/kg are achieved under the following conditions: 90 °C generation, 15 °C evaporation. In addition, COP of 0.44 and SCP of 235 W/kg are obtained even the generation temperature is decreased down to 80 °C [17]. Some commercial products of AHP applied AQSOA-FAM were sold in market, as section 1.2.4 shown. However, the expensive price of AQSOA-FAM result in high initial cost of AHP, which disturb the spread [18].

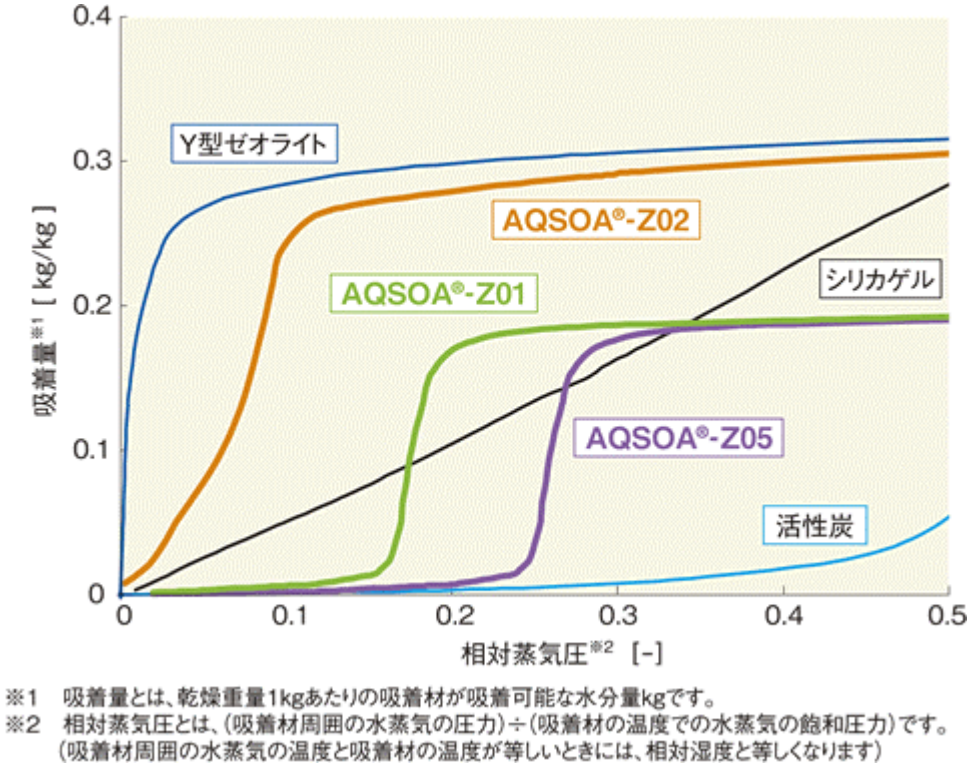

※1 吸着量とは、乾燥重量1kgあたりの吸着材が吸着可能な水分量kgです。
※2 相対蒸気圧とは、(吸着材周囲の水蒸気の圧力)÷(吸着材の温度での水蒸気の飽和圧力)です。
(吸着材周囲の水蒸気の温度と吸着材の温度が等しいときには、相対湿度と等しくなります)

Fig. 2.2 Comparing of adsorption isothermal between AQSOA and other materials.

2.1.5. Composite Adsorbent

Composite adsorbents generally consist of more than two types of adsorbents. Additives are impregnated into the matrix to produce composite adsorbents. Deliquesced salts are generally used as the additive of composite adsorbent. Those salts deliquesce with the progress of sorption and lump after drying, which causes worse mass transfer. The impregnation of deliquesced salts into porous material adsorbent as the additive is effective to solve this problem. In addition, the sorption amount can be enhanced with this impregnation. Porous materials such as activated carbon, activated carbon fiber, expandable graphite, silica-gel, vermiculite, and Wakkanai Siliceous Shale (WSS) that developed by our laboratory are generally applied as the matrix. Moreover, Multi-Wall Carbon Nano-Tubes (MWCNT) is also proposed in recent years [6], [19].

Different deliquesced salts are impregnated into silica-gel to achieve Selective Water Sorbent (SWS, SWS-1L($CaCl_2$), SWS-8L($Ca(NO_3)_2$), SWS-9L($LiNO_3$)). Those composite adsorbents are affected by cycle period obviously. In case of cycle period within 20-30 minuntes, SCP was 200 W/kg and COP was 0.13-0.3. While a longer cycle period of 2 hours was taken, SWS-1L shown a higher COP of 0.4-0.6 but lower SCP of 20-40 W/kg. In addition, our prior research shown that the impregnation of chloride more than 5 wt. % leads to expansion of pores. The impregnated salts can not be held by those expanded pore and the system performance decrease after long time running [19].

MWCNT possesses a large gravimetric pore volume of 3 cm^3/g. After impregnated with 44 wt.% LiCl, the sorption amount of water and methanol are 1 g/g and 1.65 g/g, respectively. The AHP applied MWCNT require long cycle period because of high specific heat of 1.7 kJ/g. Short cycle period results in uncomplete of sorption/desorption and reduces performance [19].

In our laboratory, a natural meso-porous material of WSS was used as the matrix, and LiCl is impregnated into the WSS to produce this WSS composite. WSS can be mined from quarry, which contribute to cheap price. With the impregnation of LiCl, water sorption of this composite adsorbent was improved and it can be employed as the a potential adsorbent. Our prior researches shown that the AHP applied this composite adsorbent shown COP of 0.16 and SCP of 86 W/kg. On the contrary, COP and SCP of the AHP applied this composite adsorbent require further improvement [19].

2.1.6. Metal Organic Frameworks

Metal Organic Frameworks (MOFs) is a serials of novel artificially synthesized material. It consists of metal ions or clusters coordinated to organic ligands to form one-, two-, or three-dimensional structures. Its large surface area which is much more lager than that of activated carbon/zeolite and its network structure leads to its application on gas adsorption and accelerant.

The commonly used MOFs subclasses are as following: MIL-100(Al), Al fumarate, ACU-10-H, MIL-101(Cr), HKUST-1. MIL-101(Cr) possesses extreme high specific surface area and specific pore volume of 4000 m^2/g and 2.02 cm^3/g, respectively [20]. It shown the water sorption amount of 1.01 g/g. When the regeneration temperature is set at 80 °C, the heat capacity of 283 kJ/kg can be obtained applied working pair of MIL-101(Cr)/ethanol, which is 2.2 time than that of activated carbon/ethanol, and heat capacity can be enhanced up to 371 kJ/kg with the increased regeneration temperature of 120 °C [19]. It is expected to be the alternative of activated carbon. however, it is extreme expensive owing to artificially synthesizing.

2.1.7. Comparison

Some representative studies of different working pairs are shown in **Table 2.1**. Studies of F. Meunier and Douss indicated that zeolite-based AHP shown COP of 0.67 at low vaporization temperature, however, regeneration over 200 °C is necessary. The requirement of high regeneration temperature is not fit the AHP that can be driven by low temperature heat source, thus the studies on zeolite-based AHP decreased in recent years. H.J.Dakkama reported an activated carbon/alcohol・propane working pair AHP system, at the conditions of 70 °C regeneration and -5 °C evaporation, COP of 0.04 can be obtained. Moreover, the latent heat of these working pair is lower than other water applied system, and more attention is needed owing to combustibility of

adsorbates. Pan's and Akahira's teams employed silica-gel as the adsorbent of AHP, COP of 0.5-0.65 and SCP of 130-150 W/kg were achieved. Silica-gel/water is a common working pair owing to its good balance of price, safety, and performance. The artificially synthesized zeolite of AQSOA-FAM was applied as adsorbent in the study of A.Sapienza. At the condition of 80 °C generation and 15 °C vaporization, COP and SCP were 0.44 and 235 W/kg, respectively. AQSOA-FAM-based AHP shown a great cooling performance, however, its spread is disturbed by the expensive cost. H.Z. Liu's study indicated the potential of WSS composite as the adsorbent. The cheap price of WSS composite benefit AHP at initial cost reduction. On the other hand, its cooling performance need enhancement.

Table 2.1 Outline of research on adsorption heat pump

Working pair (adsorbent/adsorbate)	Author	Year	$T_{reg}/T_{sor}/T_{evp}$	Half cycle time [s]	COP [-]	SCP [W/kg]	Simulation/ Experiment
Zeolite 13X / Water	F. Meunier [1]	1985	350/50/0	-	0.425	-	Simulation
Zeolite NaX / Water	Douss [2]	1988	200/60/-	5400	0.673	-	Experiment
Silica-gel / Water	Q.W.Pan [8]	2016	86/30/15	784	0.65	146.4	Experiment
Silica-gel / Water	A.Akahira [11]	2005	80/30/7	600	0.51	130	Experiment
FAM-02 / Water	A.Sapienza [17]	2011	80/30/15	210	0.44	235	Experiment
Maxsorb / R143a and Propane	H.J.Dakkama [12]	2017	70/30/-5	590	0.04	-	Simulation
LiCl(40 wt.%) + WSS / Water	Hongzhi Liu [19]	2018	80/30/12	600	0.16	86	Experiment

2.2. Advanced Cycle

2.2.1. Heat Recovery

The generation heat amount is not only for the desorption of adsorbate. The whole adsorber include HEX, adsorbent, remained circulation water also need regeneration heat amount to heated from sorption temperature, which disturbs cooling performance improvement. Heat recovery is a kind of advanced cycle that can reduce the regeneration heat amount, it was firstly proposed by F. Meunier in 1985 [1], and N. Douss in 1988 [2] conduct study of heat recovery. In recent year, Pan summarized and proposed some types of heat recovery again.

At the end of sorption/regeneration process, the high temperature side (HTS) adsorber 1 is almost fully generated and the low temperature side (LTS) adsorber 2 almost fully adsorbed, as **Fig. 2.3 (a)** shown. Then the sorption/regeneration switch, the cooling water is flowed into the HTS of Ads.1 to cool it down, and the remained hot water in Ads.1 is pushed out to the cooling tower. Meanwhile the hot water is flowed into the LTS of Ads.2 to heat it, and the remained cooling water return to the hot tank to be heated again, which results in regeneration heat mount increase, as **Fig. 2.3 (b)** shown. One type of the heat recovery that proposed by Pan is shown in **Fig.2.3 (c)** [2], the remained hot water in the HTS of Ads.1 is circulated to the LTS of Ads.2 to preheat it, hence the regeneration amount can be reduced.

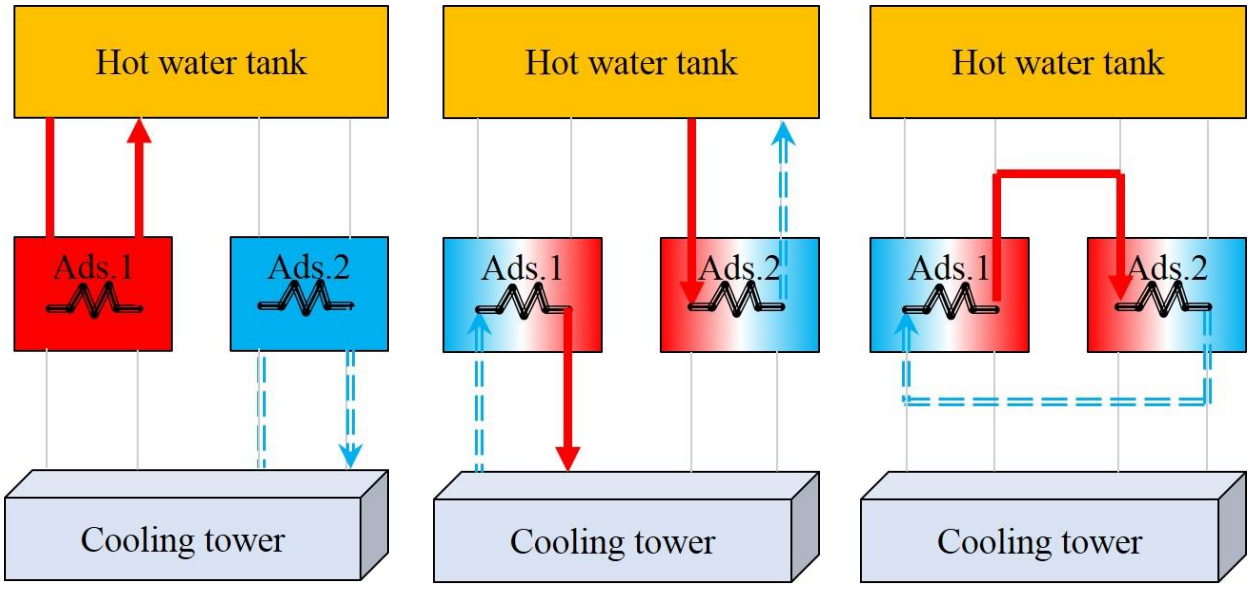

(a) Before state change **(b) Normal** **(c) Heat recovery**

Fig. 2.3 Different heat recovery types.

The recovered heat is generally the sensible heat of HEX, remained circulation water and adsorbent. Pan's simulation indicated that 14.6 %~15.7 % regeneration heat amount of an AHP system, in which applied the fin-tube HEX filled with the silica-gel, can be recovered. It was found that 90 % of the recovered heat amount was from the sensible heat of the remained water in the HTS Ads.1, only 9 % of the recovered heat amount was from

the tube, and less than 1 % of the recovered heat amount was from the adsorbent.

Though some extra valves, tubes and pumps may be necessary depends on the type of heat recovery, lots of studies were conducted on the heat recoveries because they are effective and easy to fulfill method to enhance COP [2], [8], [9], [10], [23]. Heat recovery method only reduce the regeneration heat amount; thus SCP is not affected. In addition, it is possible to combine heat recovery with other advanced cycle [8], [9], [10], [23].

2.2.2. Mass Recovery

A. Akahira and his team proposed an advance cycle called mass recovery to enhance the cooling performance of AHP [6]. The schematic of mass recovery in a representative AHP is shown in **Fig. 2.4**. At the end of sorption/regeneration process, the pressure of HTS is 4.2 kPa meanwhile that of LTS is 1.4 kPa, as shown in **Fig.2.4 (a)**. Then HTS and LTS are connected to each other, which indicate the start of mass recovery **(Fig. 2.4 (b))**. The pressure of both side adsorber become the same, hence the desorption of the HTS and the sorption of LTS can be enhanced. The HTS can be pre-cooling by the desorption and the LTS can be pre-heat by the sorption, which contribute to reduction of regeneration heat. In addition, because of the desorption during mass recovery, the HTS can be further dried, and it can adsorb more refrigerant adsorbate vapor in the next sorption process, the cooling performance can be improved.

The studies of A. Akahira indicate that COP of a silica-gel based AHP can be improved up to 0.5 from 0.4 with mass recovery [6]. Meanwhile SCP can be enhanced from 0.12 kW/kg to 0.13 kW/kg [11]. Though extra valves and large mass transfer channel between two adsorbers is necessary to fulfill mass recovery, mass recovery is a valuable advanced cycle which has been studied in lots of researches [8], [9], [10], [6], [11], [22].

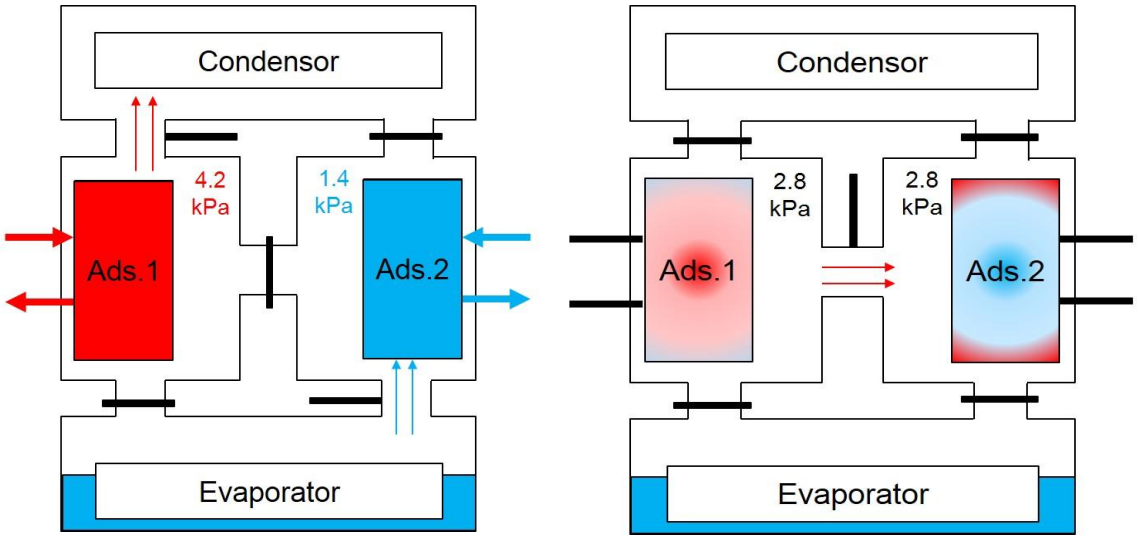

(a) Before state change **(b) Mass Recovery**

Fig. 2.4 Conception of Mass Recovery.

2.2.3. Cascade

In the low vaporization AHP system, more cooling heat amount is needed to cool down the water recovered from condenser owing to the large temperature difference between the evaporator and the condenser. It results in decrease of efficiency. Therefore several adsorption cycles are combined like in cascade, as shown in **Fig. 2.5**. Evaporator of the High Driving Temperature Adsorber (HDT) and condenser of the Low Driving Temperature Adsorber (LDT) are combined as the cascade HEX. Thus the temperature difference between condenser and cascade HEX of HDT, and that between cascade HEX and evaporator of LDT can be reduced, efficiency of the entire system can be improved. The cascade has been studied from 30 years ago, the theoretical simulation indicates that COP of AHP system can be enhanced up to 1.852 with cascading [1]. Moreover, because of the cascade AHP possess several cycles, it is possible to applied different working pairs that can adapted their working temperatures to enhance the cooling performance [11], [12]. On the other hand, extra chambers are required in cascade AHP system, which result in complex control. It causes the entire volume increase of these cascade AHP systems. Hence, the cascade AHP generally used in low temperature chilling chamber.

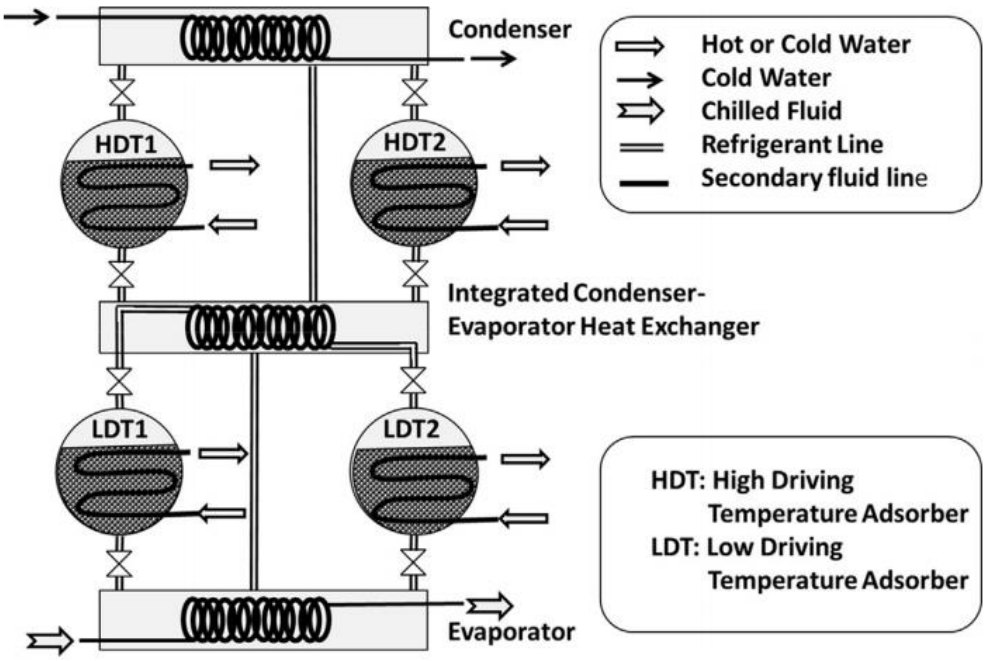

Fig. 2.5 Cascade adsorption heat pump.

2.2.4. Duration of Sorption/Regeneration Change

A representative complete cycle includes a sorption process and a regeneration process, the periods of them are generally the same. The speeds of sorption and regeneration are different owing to the different temperature of sorption and regeneration, thus the processes of sorption and desorption end at different time, the same period

result in uncomplete process of sorption or regeneration. Therefore, a method that changing the duration of sorption/regeneration to enhance the cooling performance of AHP was proposed.

Study of A.Sapienza [17] shown that the temperature different between the inlet and outlet of the HTS is smaller than that of the LTS, which indicated the regeneration process was finished earlier than sorption process. A.Sapienza developed a AHP, the cycle period was the fixed 7 minutes and the duration of sorption/regeneration was changed from 1 to 2.5, COP and SCP were enhance from 0.52 and 350 kW/kg to 0.6 and 400 kW/kg, respectively.

The method that the duration change of sorption/regeneration is easy to fulfill and effective to enhance the cooling performance. However, the different period of sorption and regeneration process require more than 2 of adsorber to provide stable cooling power output. It results in the entire volume increase, as the cascade AHP is.

2.3. Prior Studies in Our laboratory

2.3.1. Vapor Sorption Amount Enhancement of Natural Mesoporous [23]

To enhance the vapor sorption amount, $CaCl_2$, NaCl and LiCl were impregnated into a natural mesoporous material of WSS, and the composite material were investigated. The results shown that vapor sorption amount of WSS composite can be improved up to 7 times with the impregnation of chloride. Then the WSS composite impregnated with NaCl and LiCl was employed in a proto desiccant. In addition, silica-gel and zeolite were applied as adsorbent of the proto desiccant to compared with the WSS composite material. The experimental conditions are shown as following: RH 75 % at 30 °C for sorption process, RH 27 % at 40 °C for regeneration process. The results indicated that only the WSS composite desiccant can keep the indoor air at stable 18 g/kg_{DA}±1g (DA: Dry Air).

2.3.2. Development of Natural Mesoporous Material [24]

As mentioned in the previous section, the price of commercial AHP is up to 3 million Japanese Yen, 1/3 of the cost is for the adsorbent of AQSOA-FAM. The expensive initial cost leads to market barrier. Therefore, our laboratory proposed a natural mesoporous material called Wakkanai Siliceous Shale (WSS). Deliquescent chlorides were impregnated to develop the WSS composite material to enhance the sorption ability and reduce

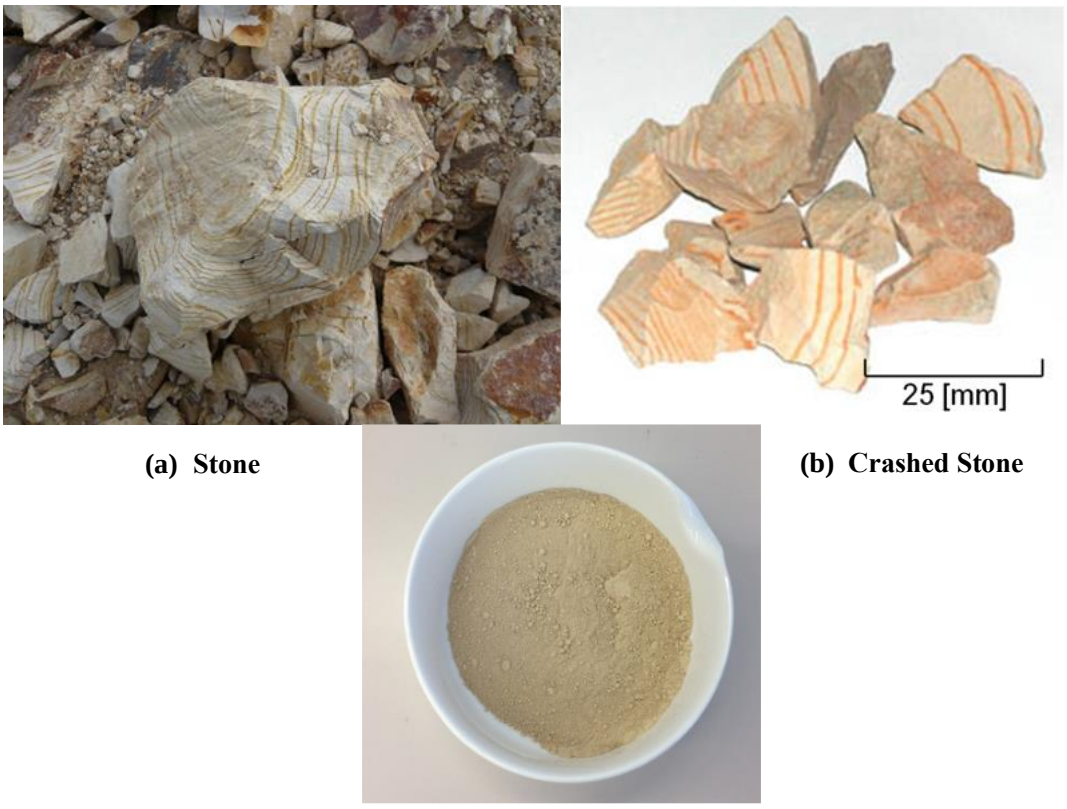

(a) Stone **(b) Crashed Stone**

(c) Powder

Fig. 2.6 Wakkanai Siliceous Shale.

the cost of adsorbent.

Fig. 2.6 shows the WSS from stone to power. The original WSS stone (**Fig. 2.6 (a)**) was mined from quarry, which contribute its cheap price. Then it was crashed into particle (**Fig. 2.6 (b)**) and powder (**Fig. 2.6 (c)**) to be applied as the host matrix of composite material. Impregnation of chloride did not cause pore size of WSS change, which is the advantage of WSS over the silica-gel as the host matrix. Some chloride such as $MgCl_2$, $CaCl_2$, LiBr and LiCl were impregnated to enhance the vapor sorption amount, the results indicated that the impregnated of LiCl improve sorption amount most. WSS with 40 wt. % shown the largest theoretical sorption amount of 0.92 g/g.

2.3.3. Manufacture of Small Scale AHP Prototype [18], [21]

As the first step of WSS composite application in AHP, a small scale AHP prototype was manufactured. The LiCl from 10 wt.% to 40 wt.% were impregnated into WSS to produce the WSS composites and their isotherms were measured. These WSS composites were filled into heat exchanger (HEX) and applied in the built experiment apparatus, as **Fig. 2.7** and **Fig. 2.8** shown. The WSS composite with 40 wt. % of LiCl shown the best COP of 0.3 and SCP of 60 W/kg at the following conditions: 90 °C-regeneration, 35°C-condensation [18]. Then the corrugated HEX was applied as the holder of adsorbent. The result indicated that SCP of this AHP was improved up to 86 W/kg while the cycle period was reduced from 120 min to 20 min though COP decreased to 0.16 [21].

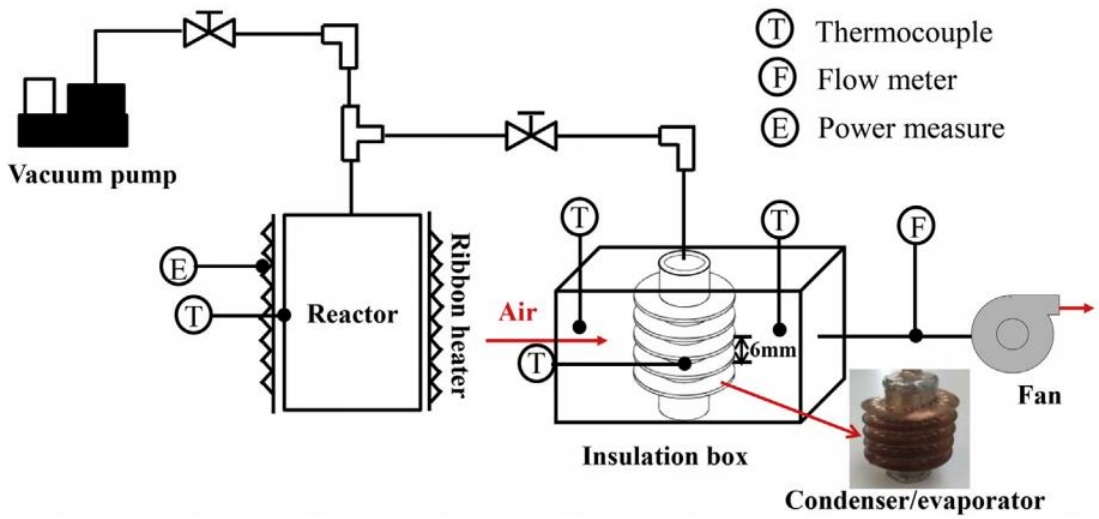

Fig. 2.7 Experiment schematic.

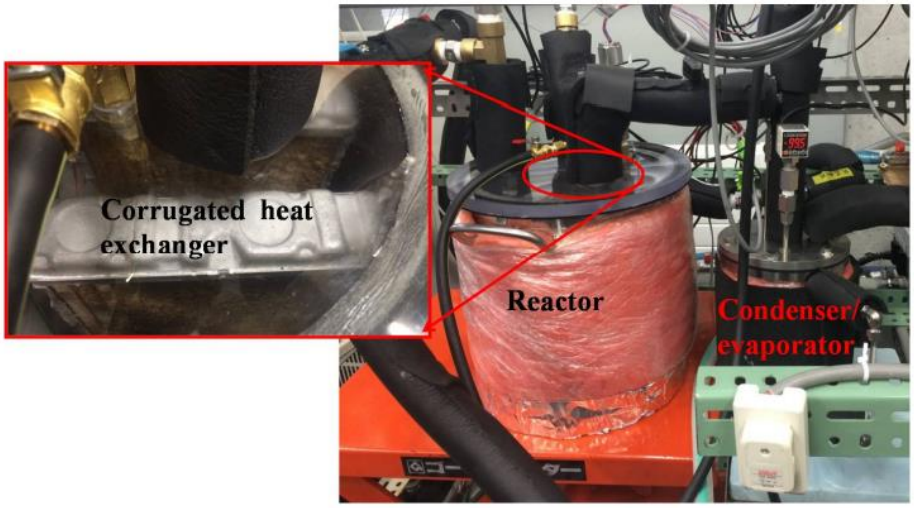

Fig. 2.8 Experiment apparatus.

2.3.4. Efficient Heat Conductivity Enhancement [25]

To enhance the efficient heat conductivity, some additive such as pure aluminum fiber, carbon fiber and graphite granule (**Fig. 2.9**) were mixed with the WSS composite. In addition, the total mass transfer coefficient depended on the aluminum fiber mixture was experimentally investigated.

The efficient heat conductivity of WSS composite was enhanced from 0.18 W/(m・K) up to 0.35 W/(m・K) with 40 wt. % of the pure aluminum fiber. The mixture with 50 wt. % of carbon fibers increased the efficient heat conductivity up to 0.4 W/(m・K). Moreover, mixture of graphite granule shown almost no enhancement on the efficient heat conductivity. The results indicated the positive effect of aluminum fiber and carbon fiber additive on the efficient heat conductivity enhancement. However, the high price of carbon fiber caused cost up of WSS composite. The pure aluminum fiber result in WSS composite decreasing and the risk of reaction with the adsorbate [25].

Fig. 2.9 Additives for enhancing heat transfer.

2.3.5. Cooling Performance Evaluation of Small Scale AHP based on Cycle Period [26]

A small scale AHP applied 20 wt. % LiCl-WSS as adsorbent was built to evaluate the cooling performance based on cycle period, the experimental schematic was shown in **Fig. 2.10**. The cycle period was changed from 8~16 minutes. The result indicated that the highest COP increased due to the progressing of sorption process and decreased while longer cycle period than 14 minutes was taken. On the other hand, SCP decreased with the cycle period increased. At the cycle period of 14 minutes, COP and SCP were 0.44 and 0.43 kW/kg, respectively.

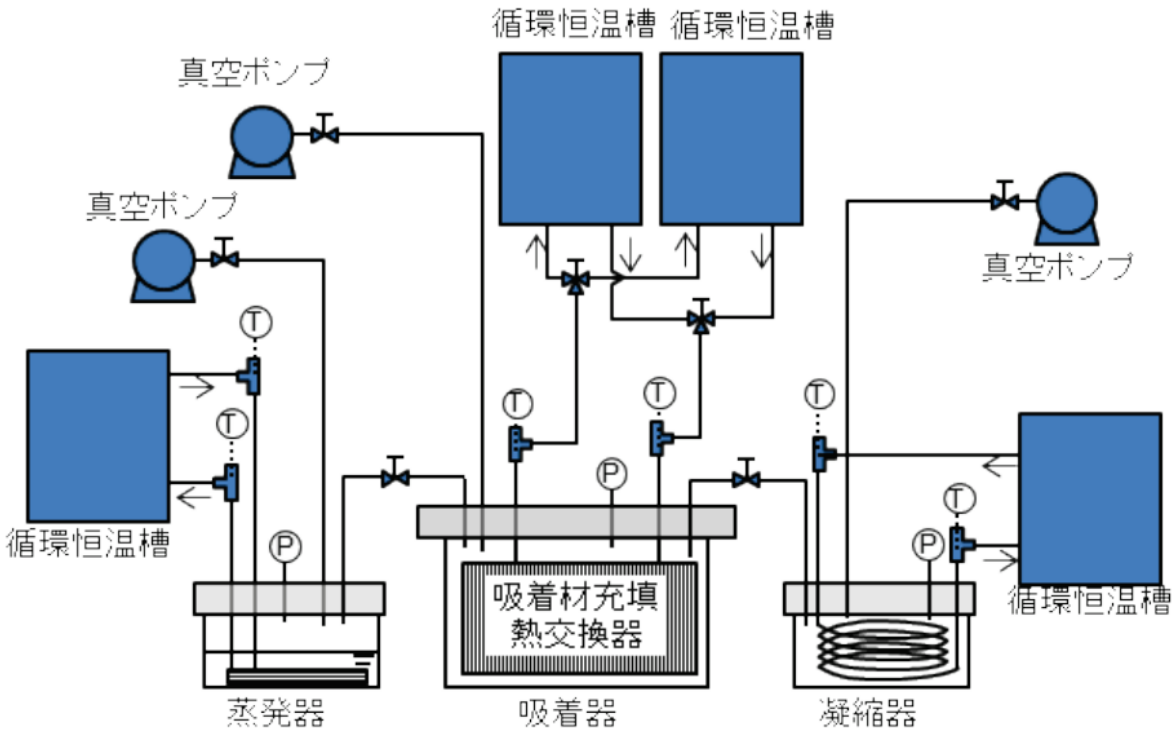

Fig. 2.10 Experiment schematic.

2.3.6. Development and Performance Evaluation of a 1 kW Lab-scale [27]

As a previous step of final objective of 20~30 kW scale AHP development, a 1 kW lab-scale AHP was developed to investigate the methods, feasibility, and cooling performance. As shown in **Fig. 2.11**, two of adsorber chambers were built to provide constant cooling ability.

Experiments were conducted at following conditions: 80 ºC-regeneration, 30 ºC-sorption, 30 ºC-condensation, 15 ºC-evaporation, 14 minutes cycle period. The result shown that COP of 0.33 and SCP of 0.15 kW/kg were achieved. However, the water accumulated in the bottom of the adsorber chambers with the cycle repeat, which led to decrease of cooling performance.

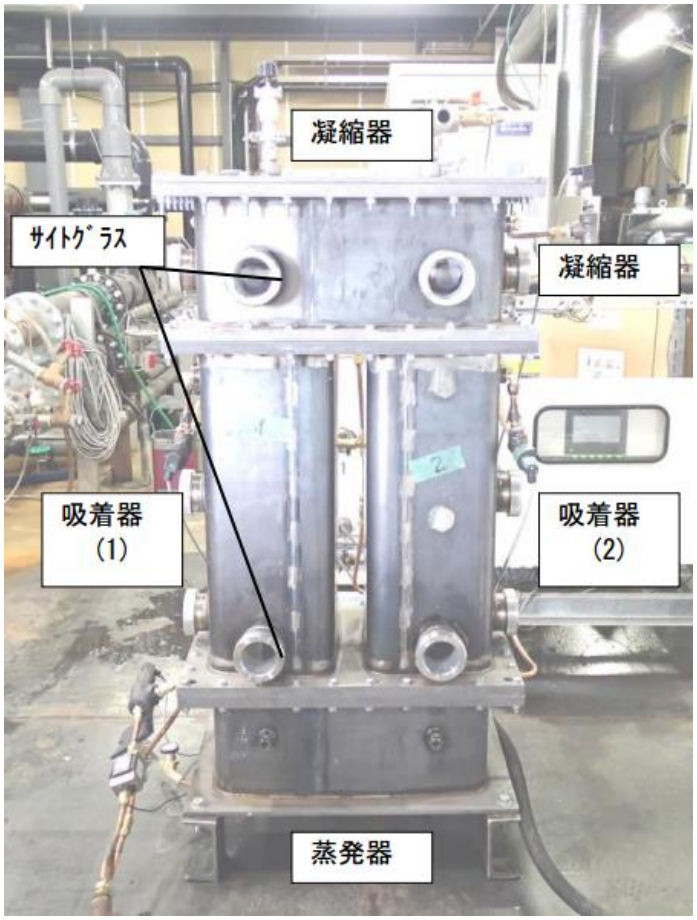

Fig. 2.11 View of 1kW-laboratory scale AHP.

2.3.7. 3D Numerical Modeling Simulation Development [28]

A 3D numerical modeling of LiCl-WSS based AHP was built to investigate the cooling HEX shape and physical properties. Moreover, COP and VCP were predicted with the simulation. Thus the HEX shape can be

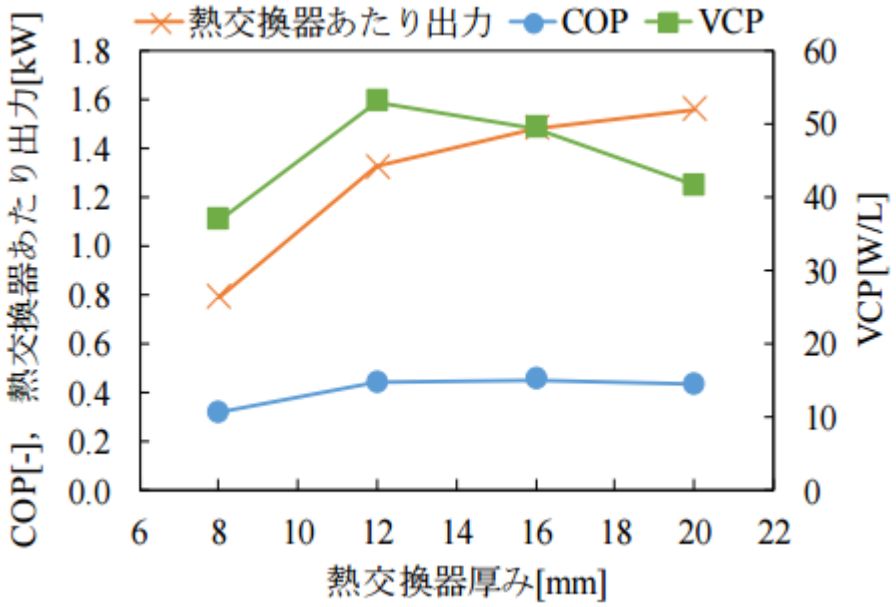

Fig. 2.12 Output over one piece of heat exchanger COP and VCP based on the thickness of heat exchanger.

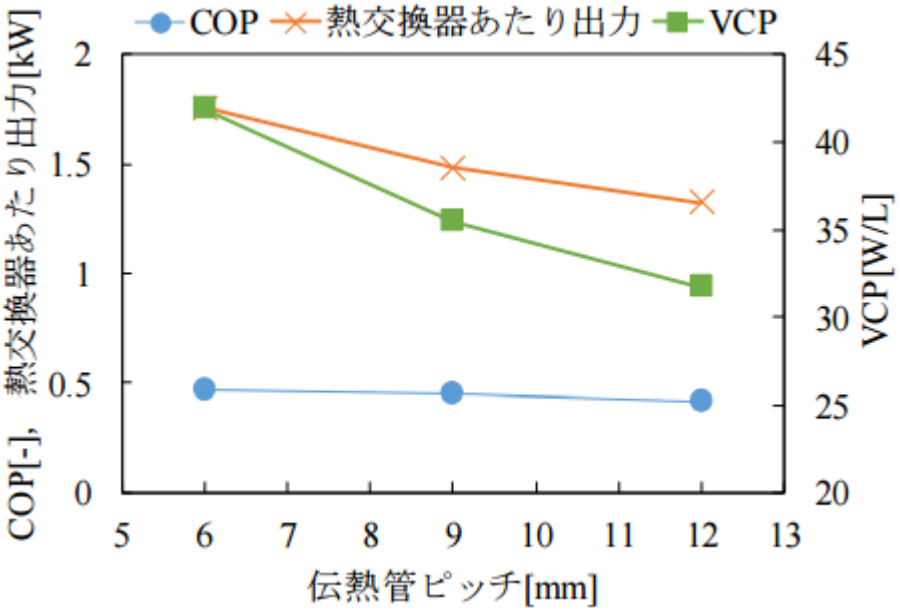

Fig. 2.13 Output over one piece of heat exchanger COP and VCP based on the pitch of heat exchanger.

optimized.

Simulation results are shown in **Fig. 2.12** and **Fig. 2.13**. Both the highest COP and SCP can be achieved at HEX thickness of 12 mm (**Fig. 2.12)**. Smaller pitch between refrigerant roads leads to less adsorbent in a HEX, however, higher COP and VCP were obtained (**Fig. 2.13)**.

2.4. Position of Current Study

AQSOA-FAM are generally used as adsorbent of commercial AHP. Moreover, MOFs has been studied a lot recent year. These adsorbents are artificially synthesized, and cooling performance can be enhanced by adjusting elements. However, the high production cost of these artificially synthesized adsorbents leads to market barrier. For example, the price of commercial 10 kW scale AHP made by Invensor Co. Ltd. is more than 26 thousand dollars and about 1/3 of it is for adsorbent. A natural mesoporous material called Wakkanai Siliceous Shale (WSS) was proposed as composite adsorbent matrix by our laboratory to reduce the cost. The price of this material crushed into powder was about 1 dollar per kilogram, which is very cheap compared with AQSOA-FAM and MOFs. AHP applied this new composite adsorbent was developed and improved to provide the competitive cooling capacity with the commercial AHP. Hence the spread of AHP can be enhanced and the dependence on the fossil fuel can be reduced.

The prior studies focused on simulation prediction, adsorbent development, small prototype building and parameter investigation. However, the small prototype is affected a lot by the heat loss, the practical development is needed. The further enhancement of the cooling performance is required to make the AHP competitive to the conventional compress type air-conditioner. In this study, a low-cost mesoporous material adsorbent based AHP is developed as the practical application of the AHP using the WSS composite. The advanced cycle of the heat recovery and the mass recovery are introduced to improve COP of the AHP. Then a new filling method called Dip-coating is adapted to improve the mass and heat transfer of the HEX filled with the adsorbents (ad-HEX). Some new ad-HEXs such as Dip-HEX, Dip-Filled-HEX are prepared to compared with the conventional Filled-HEX. Finally, a three-dimensional numerical modeling simulation is built to predict the cooling performance of AHP. The parameter studies of the AHP can be numerically studied to find the optimal conditions, thus the cooling performance of AHP can be enhanced.

Reference

[1] F. Meunier (1985) “Second law analysis of a solid adsorption heat pump operating on reversible cascade cycles_Application to the Zeolite-water pair”, *Heat Recovery System* Vol.5, No.2, pp. 133-141.

[2] Douss (1988) “Predictive Model and Experimental Results for a Two-Adsorber Solid Adsorption Heat Pump”, *Ind. Eng. Chem. Res* 27, pp. 310-316.

[3] L.W. Wang (2009) “A renewable on adsorption working pairs for refrigeration”, *Renewable and sustainable energy reviews* 13, pp. 518-534.

[4] B. Xue (2012), “Numerical simulation for steam generation process in a novel zeolite-water adsorption heat pump”, *Journal of Chemical Engineering of Japan*, 45(6), pp. 408‐416.

[5] E. Oktariani (2012), “Experimental investigation on the adsorption process for steam generation using a zeolite-water system”, *Journal of Chemical Engineering of Japan*, 45(5), pp. 355–362.

[6] A. Akahira (2004), “Mass recovery adsorption refrigeration cycle - improving cooling capacity”, International Journal of Refrigeration 27, pp.225-234.

[7] Q.W. Pan (2015), “Comparison of different kinds of heat recoveries applied in adsorption refrigeration system”, International Journal of Refrigeration 55, pp.37-48.

[8] Q.W. Pan (2016) “Design and experimental study of a silica gel-water adsorption chiller with modular adsorbers”, *Refrigeration* 67, 336-344.

[9] Q.W. Pan (2017), “Experimental study on operating features of heat and mass recovery processes in adsorption refrigeration”, Energy 135, pp.361-369.

[10] Q.W. Pan (2018), “Study on operation strategy of a silica gel-water adsorption chiller in solar cooling application”, *Solar Energy* 172, pp. 24-31.

[11] A. Akahira (2005), “Mass recovery four-bed adsorption refrigeration cycle with energy cascading”, Applied Thermal Engineering 25, pp.1764-1778.

[12] H.J. Dakkama (2017) “Integrated evaporator-condenser cascaded adsorption system for low temperature cooling using different working pairs”, *Applied Energy* 185, pp. 2117-2126

[13] Mikio Kumita (2018) “Methanol adsorption behaviors of compression-molded activated carbon fiber with PTFE”, *International Journal of Refrigeration* 94, pp. 127-135

[14] 「低温水利用 AQSOA 吸着式冷凍機」, 日本機械学会誌 (2010), Vol. 113, No.1094 Adsorption news (2011), Vol. 25, No. 4, pp. 6–11, http://www.j-ad.org/adsorption_news/25_4.pdf , (2019 年 2 月 4 日)

[15] 垣内博行 (2005)「水蒸気吸着材 FAM-Z02 の基礎特性評価および吸着ヒートポンプへの適応性検討」, 化学工学論文集 31, No.4, pp.273-277.

[16] 垣内博行 (2005)「水蒸気吸着材 FAM-Z01 の基礎特性評価および吸着ヒートポンプへの適応性検

討」，化学工学論文集 31, No.4, pp.361-364.

[17] A. Sapienza (2011) “Influence of the management strategy and operating conditions on the performance of an adsorption chiller”, *Energy* 36, pp. 5532-5538.

[18] H.Z. Liu (2015) “Experimental testing of a small sorption air cooler using composite material made from natural siliceous shale and chloride”, *Applied Thermal Engineering* 82, pp.68-81.

[19] S.K. Henninger (2017) “New materials for adsorption heat transformation and storage”, *Renewable Energy* 111, pp. 59-68.

[20] H.Z. Liu (2018) “Performance of LiCl impregnated mesoporous material coating over corrugated heat exchangers in a solid sorption chiller”, *Energies*.

[21] L.J. Ma (2016) “Performance evaluation of shaped MIL-101-ethanol working pair for adsorption refrigeration”, *Applied Thermal Engineering* 95, pp.223-228.

[22] Z.S. Lu (2013), “Performance improvement by mass-heat recovery of an innovative adsorption air-conditioner driven by 50-80ºC hot water”, Applied Thermal Engineering 55, pp.113-120.

[23] S. Nakabayashi (2011), “Improvement of water vapor adsorption ability of natural mesoporous material by impregnating with chloride salts for development of a new desiccant filter”, *Adsorption* 17, pp. 675-686.

[24] A. Morita (2015), “Study on Low-cost Adsorption Heat Pump using Natural Mesoporous Material”, *Master thesis*.

[25] M. Inoue (2016), “R and D of Low-Cost Adsorption Heat pump using Natural Mesoporous Material Part 6: Enhancement of effective thermal conductivity and measurement of overall mass transfer coefficient”, *SHASEJ Conference Hokkaido Branch*

[26] J. Togawa (2016), “R and D of Low-Cost Adsorption Heat pump using Natural Mesoporous Material Part 4: Examination of the adsorption-regeneration cycle time for the cooling power evaluation using small size testing apparatus ”, *SHASEJ Conference Hokkaido Branch*

[27] S. Oomae (2018), “Development of adsorption heat pump using natural mesoporous materials with LiCl part-2 Development and evaluation of 10kW type adsorption heat pump”, Proceeding of the 9th ACRA2018

[28] A. Komaki (2016), “R and D of Low-cost Adsorption Heat pump using Natural Mesoporous Material Part 7: Numerical Simulation Using Three-Dimensional Model and the Performance Prediction” , *SHASEJ Conference Hokkaido Branch*

Chapter 3

Development and Performance Enhancement of 1 kW Scale Adsorption Heat Pump

3.1. Experimental Apparatus and Procedure

3.1.1. Adsorbent

WSS is a natural mesoporous material composed of silicon dioxide [1]. Mined quarries offers significant advantages over adsorbents such as silica gel and synthetic zeolites [2]. LiCl is usually used as additives of WSS to improve the adsorption amount [3-7]. Though the LiCl with crystal water produces HCl when the drying temperature is beyond 98 ℃ according to Zhang’ s report [8], the WSS adsorbent can keep stable because the regeneration temperature in this study is set below 80℃. Considering the balance of sorptive ability and stability, WSS with 20 wt. % LiCl (WSS-LiCl) was adopted as the adsorbent in this study. After crushing the WSS into a powder (**Fig. 3.1 (a)**), 20 wt.% of LiCl was impregnated into it as an additive to improve its sorption amount (**Fig. 3.1 (b)**) [2,3], [5-7], [9]. The WSS composite adsorbent was dissolved in slurry (**Fig. 3.1 (c)**), and its water vapor sorption isotherms are shown as **Fig. 3.2** [7]. The physical properties of the WSS composite adsorbent are shown in **Table 3.1**, and their pore diameter distributions is shown in **Fig. 3.3** and [7], respectively. The

(a) **(b)** **(c)**

Fig. 3.1 WSS material: (a) WSS powder; (b) WSS + 20 wt.% LiCl; (c) Slurry of WSS – LiCl.

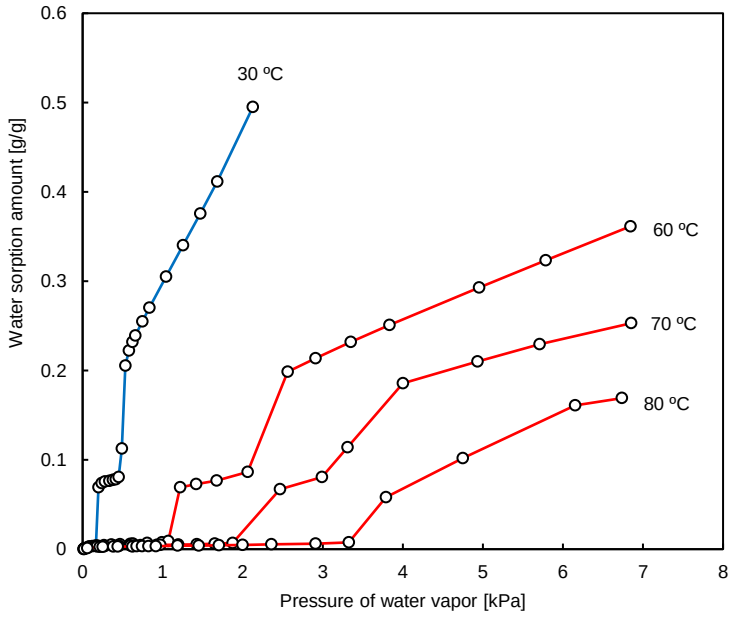

Fig. 3.2 Water vapor sorption isotherms of WSS+20 wt.% LiCl at the various temperature.

Table 3.1 Measured physical properties of WSS composite adsorbent

Density	Porosity	Specific heat	Effective thermal conductivity of dried adsorbent
2.14×10^{-3} [g/L]	0.28 [-]	1.13 [J/(g·K)]	0.18 [W/(m·K)]

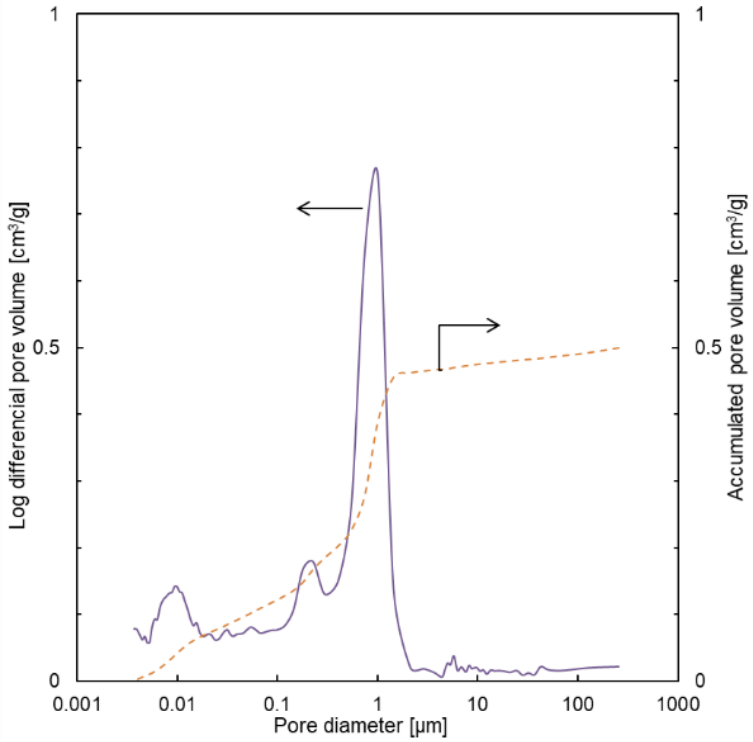

Fig. 3.3 Pore diameter distribution.

accumulated pore volume until 1 μm is about 0.5 cm^3/g, as **Fig. 3.3** shown [7]. It is obviously that the theoretical maximum vapor sorption amount at conditions of 30 °C and 1.7 kPa is limited under 0.5 g/g from **Fig. 3.2**. Hence the impregnated LiCl solution can be kept in the mesopore to avoid sorption ability decrease with the cycle repeat [7].

3.1.2. Corrugated Heat Exchanger

The aluminum corrugated microchannel heat exchanger (HEX) was employed owing to its superior performance. The HEXs used as adsorber are coated by epoxy resin, which is the cationic eletro-deposition coating, on the surfaces of micro channels, corrugated fins, pitches and header to prevent corrosion. The optimal thickness of the HEX was 12 mm, according to the results of the numerical calculations [6]. The corrosion tests were carried out. Four pieces of samples (W45 × H20 × D12), which were cut off from the HEXs, were prepared and shown in **Fig. 3.4**: No.1 and No.2 are the original HEXs without coating, No.3 and No.4 are the HEXs with epoxy resin coating. Besides, the micro channel of No.2 and No.4 are blocked with silicon. The samples were placed into the solution with LiCl wt.% 40, the mass reduction ratio over elapsed days is shown in **Fig. 3.5**. The

No.1 Original

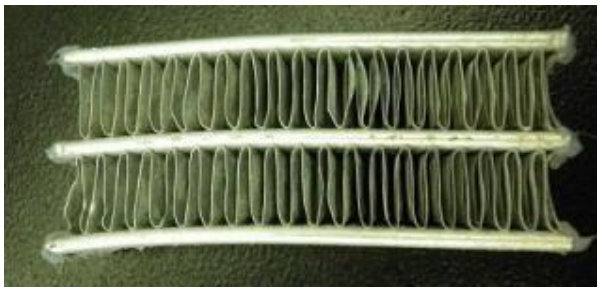

No.2 Original (Inlet / outlet blocked)

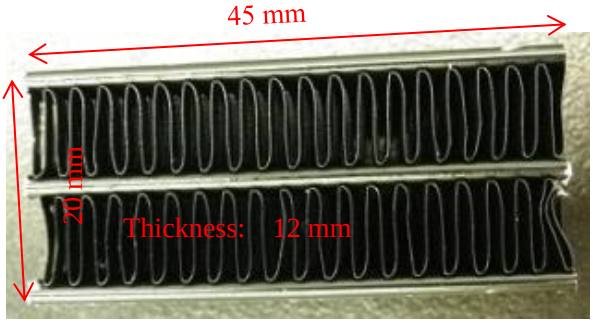

No.3 Epoxy resin coated

No.4 Epoxy resin coated (Inlet / outlet blocked)

Fig. 3.4 HEX Samples.

mass of No.1 and No.2 reduced more than 2% after 50 days, meanwhile the mass of No.3 and No.4 reduced only 0.2%. In fact, the O_2 that contribute to corrosion did not exist inside the AHP chambers, in which the HEXs are used. It is estimated that the HEX with epoxy resin coating can be stable for 10 years.

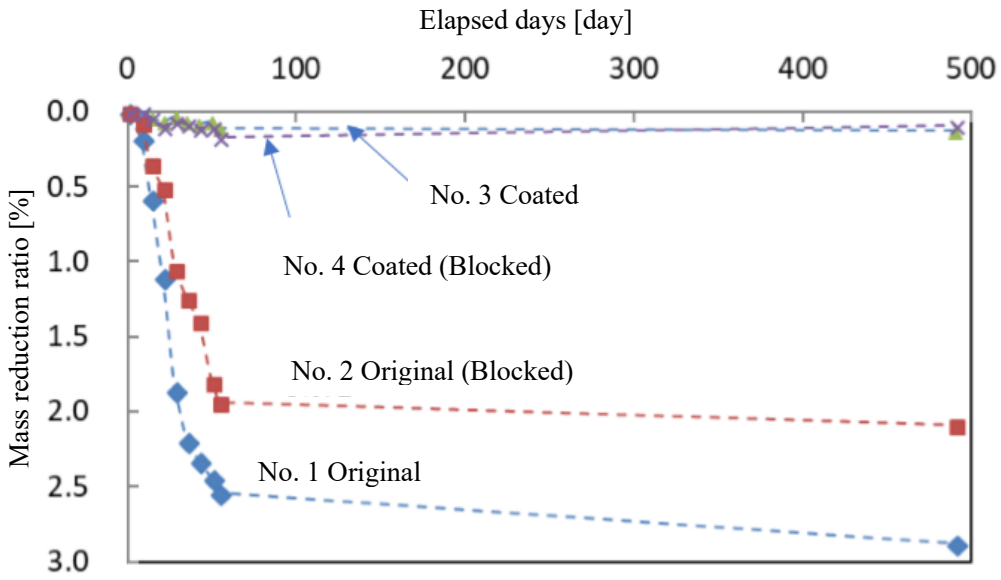

Fig. 3.5 Mass reduction ratios over elapsed days.

3.1.3. Manufacture of Adsorbent-filled HEX

A special thin blank HEX (bk-HEX) was ordered from Chinese manufactory, it was applied as the holder of adsorbent is shown in **Fig. 3.6 (a)**. The bk-HEX whose dimensions are W400 × H300 × D12 mm possessed a weight and volume of 850 ±10 g and 1.44 L, respectively. Further, the fin pitch between the microchannel was 8.1 mm, and the surface of the bk-HEX was coated using a thin epoxy resin layer to prevent corrosion, as mentioned in the previous section.

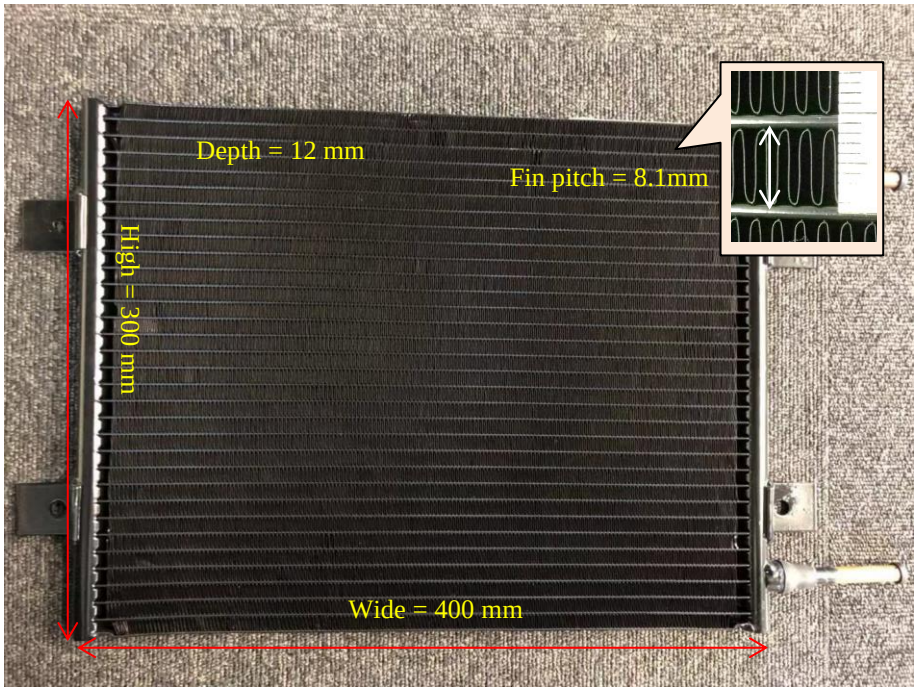

Fig. 3.6 Empty heat exchanger.

Firstly, the slurry of WSS-LiCl prepared in **Fig. 3.1 (c)** was filled into the space between the water channels of bk-HEX (**Fig. 3.7 (a)**), and the bk-HEX needs rap to reduce bubbles within the slurry. The filling of slurry was repeated until the space between the water channels of bk-HEX was fully filled with the slurry, then the bk-HEX with adsorbent slurry was put into an oven to dry at 120 °C for 24 hours (**Fig. 3.7 (b)**). Finally, the heat exchanger with the adsorbent (ad-HEX) was obtained (**Fig. 3.7 (c)**). The Features of ad-HEX are shown in **Table 3.2**. The adsorbent weight and adsorbent packing density in one piece of HEX was 500 (±15) g and 350 (±10) g / L, respectively. Eight pieces of ad-HEX were prepared, and 4065 g of adsorbent was filled.

(a) Filling of adsorbent

(b) Oven

(c) HEX with adsorbent

Fig. 3.7 Procedure of filling adsorbent.

Table 3.2 Features of ad-HEX

Number of HEX	A	B	C	D	E	F	G	H
Weight of HEX [kg]	0.845	0.835	0.855	0.835	0.835	0.850	0.845	0.850
Weight of adsorbent [kg]	0.535	0.520	0.500	0.555	0.520	0.490	0.485	0.490
Total weight of adsorbent [kg]	2.11				1.99			
Adsorbent density [kg/L]	0.37	0.36	0.35	0.39	0.36	0.34	0.34	0.34

3.1.4. AHP Apparatus

The 1 kW-AHP unit consisted of an evaporator, a condenser, and two adsorbers. An acrylic cylinder of 450 mm internal diameter and 20 mm thickness was used as the body of AHP to carry out observations inside the AHP, as shown in **Fig. 3.8**.

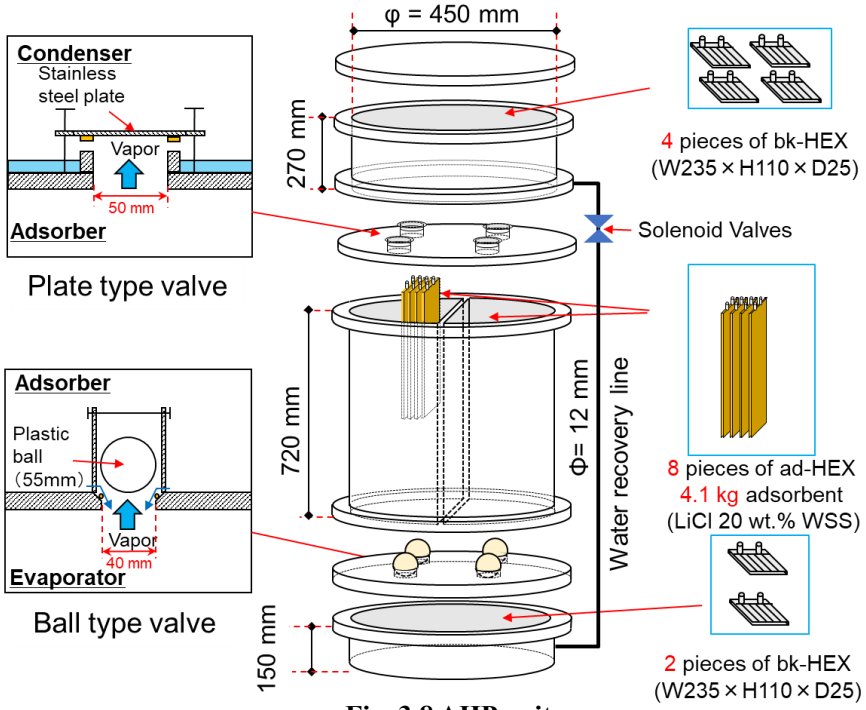

Fig. 3.8 AHP unit.

The depth of the evaporator is 150 mm. Two pieces of small corrugated fin-type bk-HEXs (W270 × H100 × D25.6), which is shown in **Fig.3.9**, were set in the chambers of the evaporator. A plastic support was set in the center of evaporator chamber to against sunken bottom due to the atmosphere pressure. In addition, several stainless-steel connecters were set in the bottom of evaporator chamber for water supply / return of bk-HEXs and pressure gauge. Four of ball type valves were set in the cover plate of evaporator chamber, which is also the bottom of adsorber chambers. The vapor can only move from the evaporator chamber to the adsorber chamber by the pressure difference, meanwhile the accumulated water in adsorber chamber bottom can return to the evaporator chamber.

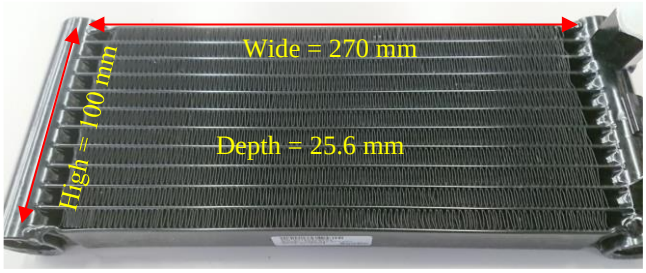

Fig. 3.9 bk-HEX for evaporator and condenser.

An acrylic cylinder with a depth of 720 mm was separated into two adsorber chambers by an acrylic plate of 20 mm thickness. Four pieces of ad-HEX prepared in section **3.1.3** were combined as the adsorber set (Ads.), it was covered by aluminum sheets of 0.3 mm thickness to reduce the heat loss from radiation (**Fig. 3.10**). Adsorber

sets were placed in each chamber, total 8 pieces of ad-HEXs were applied in this AHP. Several polyvinyl chloride frameworks were set inside to prevent atmospheric pressure. Moreover, ethylene propylene diene monomer was posted to the connection section of bottom and top covers to prevent leak.

The depth of the condenser is 270 mm. Four pieces of small corrugated fin-type bk-HEXs that same to that in evaporator were set in the chambers of the condenser. A plastic support was set in the center of condenser chamber to against sunken top cover. Four of plate type valves were set in the bottom plate of evaporator chamber, which is also the top cover of adsorber chambers. The vapor can only move to the condenser chamber by the pressure difference; however, the valve pedestal prevent the water in the condenser chamber bottom return to the adsorber chamber. In addition, the water supply / return and pressure gauge tubes for adsorber chamber passed through the condenser chamber, which is covered by the thermal insulation sheet. A bypass was set to recover the water accumulated in the condenser chamber to the evaporator chamber.

Fig. 3.11 shows the view of this AHP, inside observation is clearly obtained. However,the whole AHP was generally covered with polystyrene foam to reduce heat loss,. The inside observation can be obtained while needed.

Fig. 3.10 Adsorber set (Ads.).

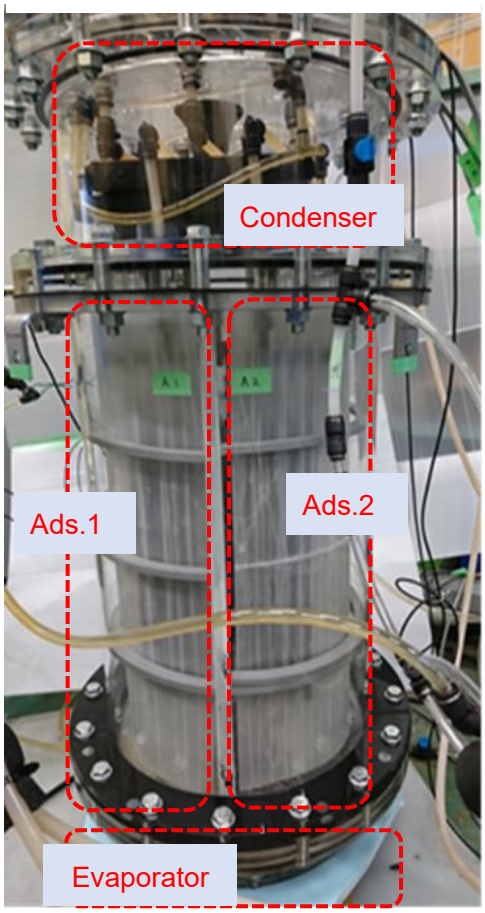

Fig. 3.11 View of AHP.

3.1.5. System Description

The experimental system schematic for this study is shown in **Fig. 3.12**. The hot water used for the regeneration process was heated using a water heater and stored in a hot water tank of capacity 300 L. A chiller of 8.7 kW supplied the cooling water for the sorption process. Two cryogenic thermostats of 1 kW supply the chilled water to the evaporator and cooling water to the condenser. The cooling and condensation capacities in this study were designed to be more than 1 kW; hence, the auxiliary heating and cooling were provided by a 1 kW tube heater and plate heat exchanger, respectively. The timing of closing and opening the valves was automatically

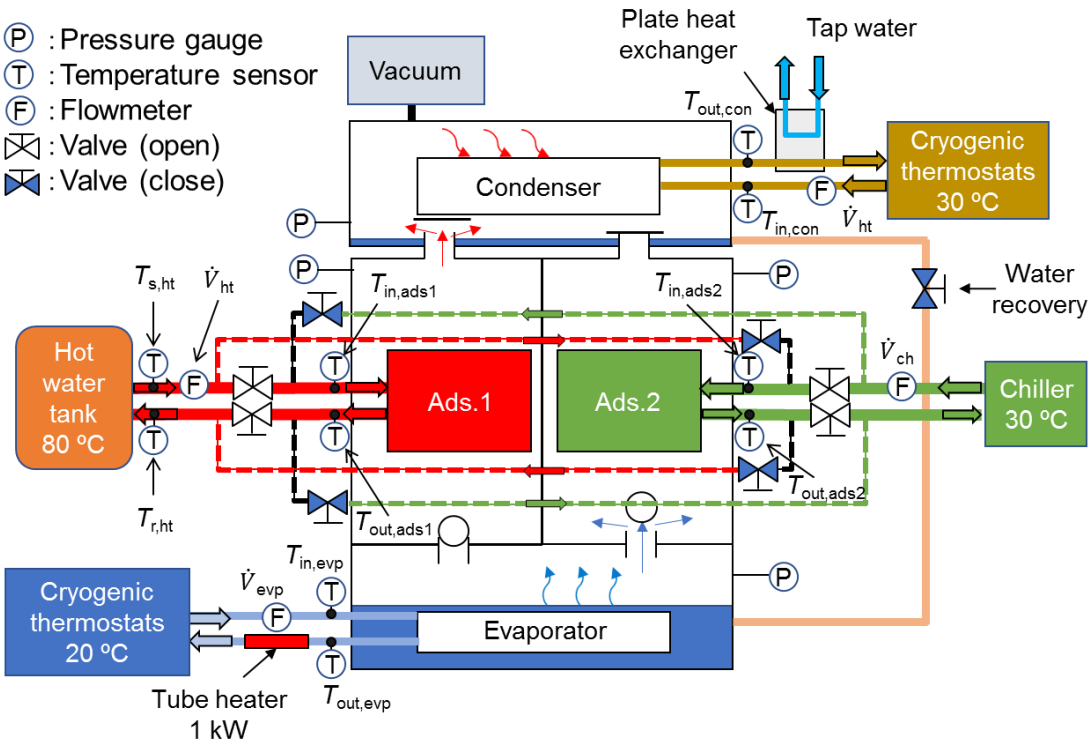

Fig. 3.12 Experiment schematic.

controlled. The inlet and outlet temperatures of the evaporator, the adsorbers, and the condenser were measured using PT100 sensors. The flow rates of the evaporator, the adsorbers, and the condenser were measured by means of flowmeters that were set at the inlet of each chamber. Solenoid valves were used to control the hot water/cooling water supply.

3.2. Operating Methodology

3.2.1. Experimental Procedure

The pressure in the evaporator chamber, the adsorber chamber, and the condenser chamber was evacuated to 2.3, 4.8, and 4.3 kPa, respectively, before the start of the experiment. Water at 20 °C and 30 °C was circulated into the evaporator and condenser, respectively. Both adsorbers were dried with hot water at 80 °C, cooling water for the sorption process was circulated into Ads.1, instead of hot water at the start of the experiment, and the cooling water/hot water supply exchange was performed every few minutes. The standard experimental conditions were 80 ℃ for regeneration, 30 ℃ for sorption, 30 ℃ for condensation, 20 ℃ for the evaporator inlet, and 7 min each for the sorption and regeneration process. Experiments on different regeneration temperatures (60–80 ℃), the evaporator inlet temperature (12–20 ℃), and the cycle period (10–18 min) were also conducted. The temperature and flow rate data were recorded by means of a logger and analyzed to evaluate the system performance.

3.2.2. Evaluation Indices

COP and SCP are used to evaluate the system's performance in this study. $Q_{\mathrm{i,c}}$ and $Q_{\mathrm{i,reg}}$ are the amount of cooling and regeneration heat for the i$^{\mathrm{th}}$ cycle. The equations for $Q_{\mathrm{i,c}}$, and $Q_{\mathrm{i,reg}}$ are shown in **Eqs. (3.1)** and **(3.2)**, respectively. In this study, COP and SCP are the average of all the cycles except for the 1$^{\mathrm{st}}$ and the 2$^{\mathrm{nd}}$ cycle, which are unstable, and defined by **Eq. (3.3)** and **Eq. (3.4)**. Besides, volumetric cooling power (VCP) is used to compare with other AHP in the **section 3.4**. The adsorber pack VCP and the entire machine VCP are defined as

$$Q_{\mathrm{i,c}} = \int_{t_{\mathrm{i,b,sor}}}^{t_{\mathrm{i,e,sor}}} \dot{V}_{\mathrm{evp}} \rho_{\mathrm{w}} C_{\mathrm{p,w}} \left(T_{\mathrm{in,evp}} - T_{\mathrm{out,evp}}\right) dt \tag{3.1}$$

$$Q_{\mathrm{i,reg}} = \int_{t_{\mathrm{i,b,reg}}}^{t_{\mathrm{i,e,reg}}} \dot{V}_{\mathrm{ht}} \rho_{\mathrm{w}} C_{\mathrm{p,w}} \left(T_{\mathrm{in,ads}} - T_{\mathrm{out,ads}}\right) dt \tag{3.2}$$

$$\mathrm{COP} = \sum_{\mathrm{i=3}}^{\mathrm{n}} Q_{\mathrm{i,c}} \Big/ \sum_{\mathrm{i=3}}^{\mathrm{n}} Q_{\mathrm{i,reg}} \tag{3.3}$$

$$\mathrm{SCP} = \sum_{\mathrm{i=3}}^{\mathrm{n}} Q_{\mathrm{i,c}} \Big/ \left(m_{\mathrm{dry}} \cdot t_{\mathrm{cyc}}(n-2)\right) \tag{3.4}$$

$$\mathrm{VCP_{ads}} = \sum_{\mathrm{i=3}}^{\mathrm{n}} Q_{\mathrm{i,c}} \Big/ \left(V_{\mathrm{ads}} \cdot t_{\mathrm{cyc}}(n-2)\right) \tag{3.5}$$

$$\mathrm{VCP_{en}} = \sum_{\mathrm{i=3}}^{\mathrm{n}} Q_{\mathrm{i,c}} \Big/ \left(V_{\mathrm{en}} \cdot t_{\mathrm{cyc}}(n-2)\right) \tag{3.6}$$

Eq. (3.5) and **Eq. (3.6)**, respectively.

3.2.3. Uncertainty analysis

The uncertainties of COP and SCP are combined uncertainties, which can be determined by the propagation of individual uncertainties. The following equation is used to calculate the uncertainties of COP and SCP. Here the R in the **Eq. (3.7)** indicates COP or SCP [10], [11]. **Table 3.3** presents the experimental measured parameters (x_i) and their uncertainties (u_{x_i}).

$$u_{\mathrm{R}} = \sqrt{\sum_{I=1}^{I=N} \left(u_{x_I} \frac{\partial R}{\partial x_I}\right)} \tag{3.7}$$

Table 3.3 Experimental uncertainties.

Parameter	$\dot{V}_{\mathrm{evp}}$ [m^3/s]	$\dot{V}_{\mathrm{ht}}$ [m^3/s]	$T_{\mathrm{in,evp}}$, $T_{\mathrm{out,evp}}$, $T_{\mathrm{in,ads}}$, $T_{\mathrm{out,ads}}$ [°C]	m_{dry} [kg]
Uncertainty	±4.9×10^{-7}	±8.33×10^{-6}	0.3 (T≤60) or 0.5%×|T| (T>60)	±0.01

3.3. Experimental Results and Discussion

3.3.1. Test Experiment

Test experiments were conducted to estimate the working condition of this 1 kW AHP. The experimental conditions are shown in **Table 3.4**. The circulation water in HEX of evaporator is chilled by the water evaporation evaporator, and the vapor moves to the Adsorber 2 to be adsorbed by the adsorbent, the sorption heat amount is taken away by the cooling water. It called sorption process. Meanwhile the adsorbed water is regenerated by the hot water in the Adsorber 1 and move to the condenser to be condensed, the condensation heat amount is taken

Table 3.4 Experimental conditions.

	Evaporator	Condenser	Adsorber (sorption)	Adsorber (regeneration)
Temperature [°C]	20	30	30	80
Flowrate [L/min]	4.38	5.22	6.20	6.36

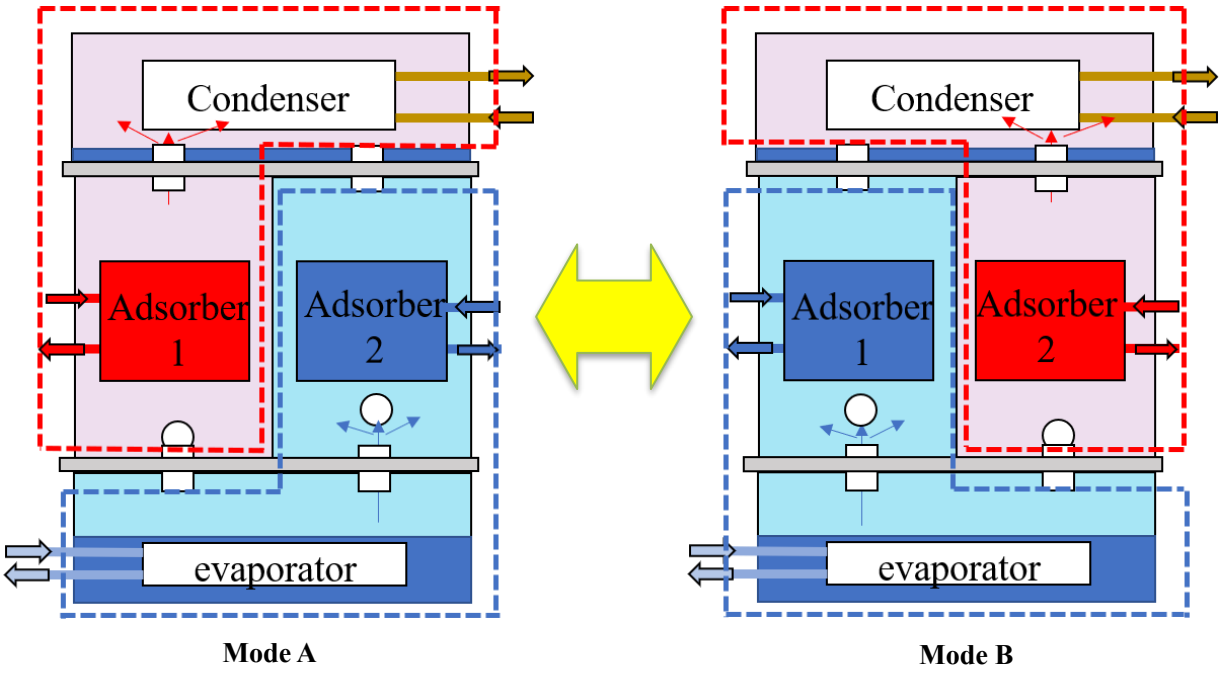

Fig. 3.13 (a) Working modes of Sorption/Desorption cycle.

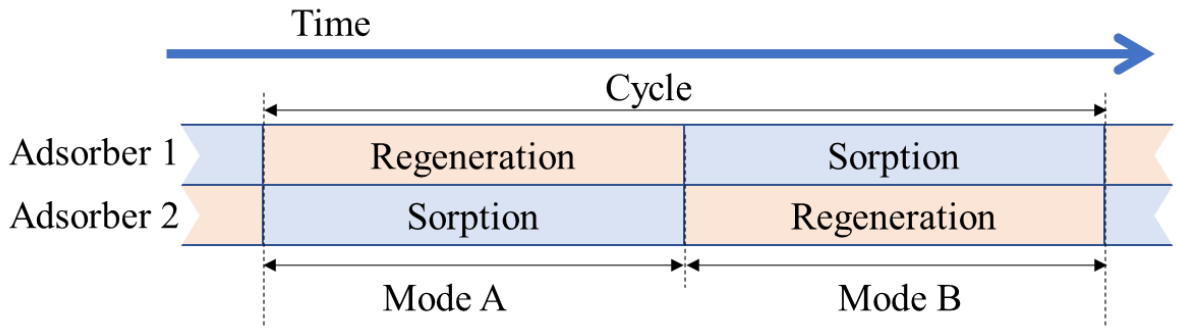

Fig. 3.13 (b) Time schedule of state change.

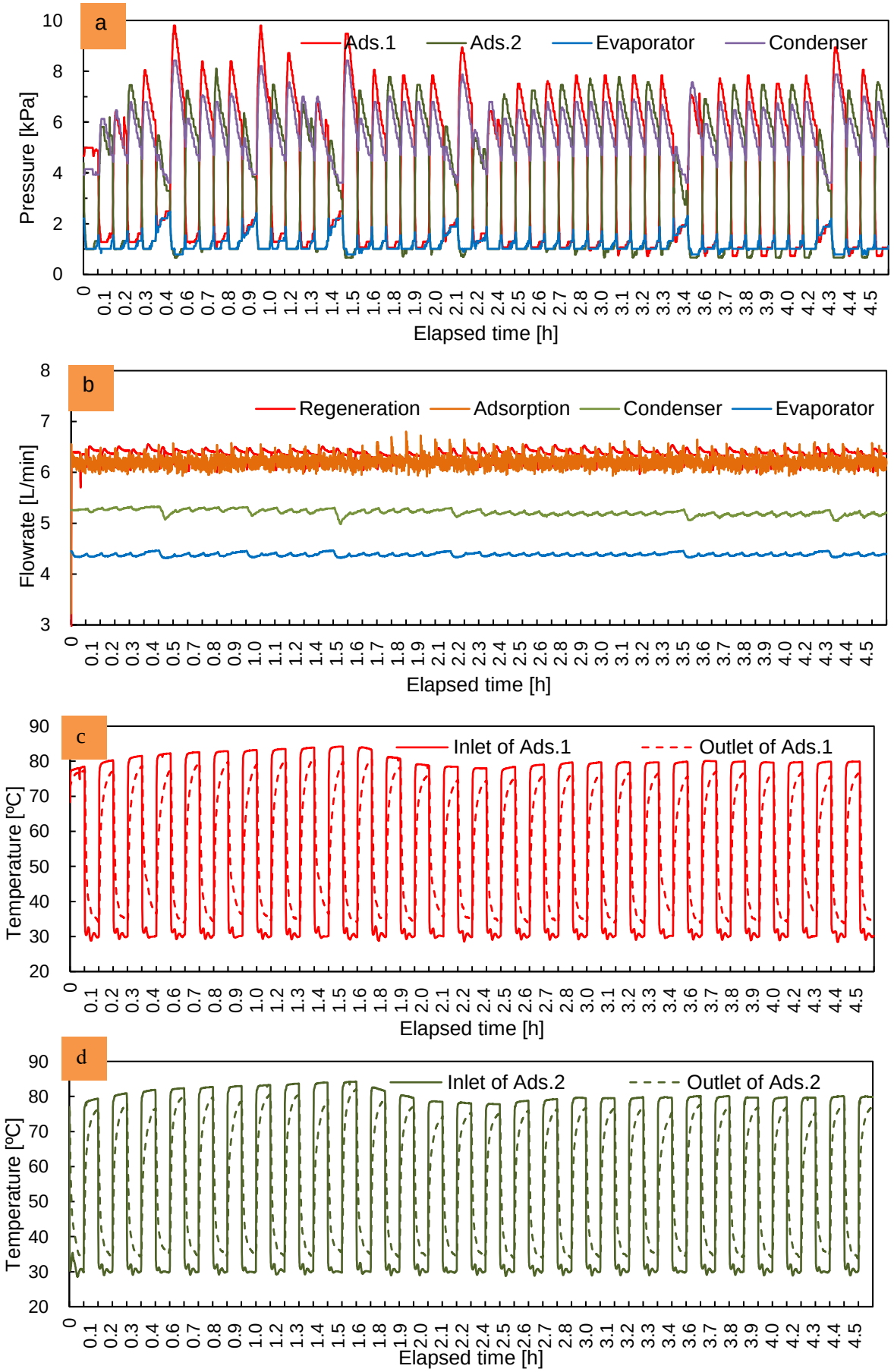

Fig. 3.14 Result of constant experiment.

away by the cooling water. It called regeneration process, as **Fig. 3.13 (a) Mode A** shown. The sorption / regeneration processes are switched every half cycle, as **Fig. 3.13 (a) Mode B** shown.

With the exchange of Mode A and Mode B, the cooling ability can be provided continuously, as **Fig. 3.13 (b)** shown. The cycle period was set at 600 s (t_{cyc} = 10 min) and the 5-hours experimental results are shown in **Fig. 3.14**. The pressure transients are shown in **Fig. 3.14 (a)**, some extreme low or high pressure in one sorption / regeneration can be observed. The not perfect valves moving can be considered to be the reason. Other parts shown a periodical stable change. All the chambers kept a very stable flowrates, as shown in **Fig. 3.14 (b)**. **Fig. 3.14 (c)** and **Fig. 3.14 (d)** show the inlet / outlet temperature change of Ads.1 and Ads.2, respectively. The inlet temperatures of regeneration process changed in the first 2 hours due to the temperature adjusting of the hot water tank, they were stable after 3 hours from the start of experiment. On the other hand, the inlet temperature fluctuation of sorption process in a narrow arrange can be observed because of the capacity limitation of the chiller. Hence this AHP system can work stably for the experiments.

The regeneration heat capacities are calculated based on the adsorber temperature differences are shown in **Fig. 3.14 (e)** and **Fig. 3.14 (f)**. These transients change similar to those of the adsorber temperature, they are stable after 3 hours from the start of experiment.

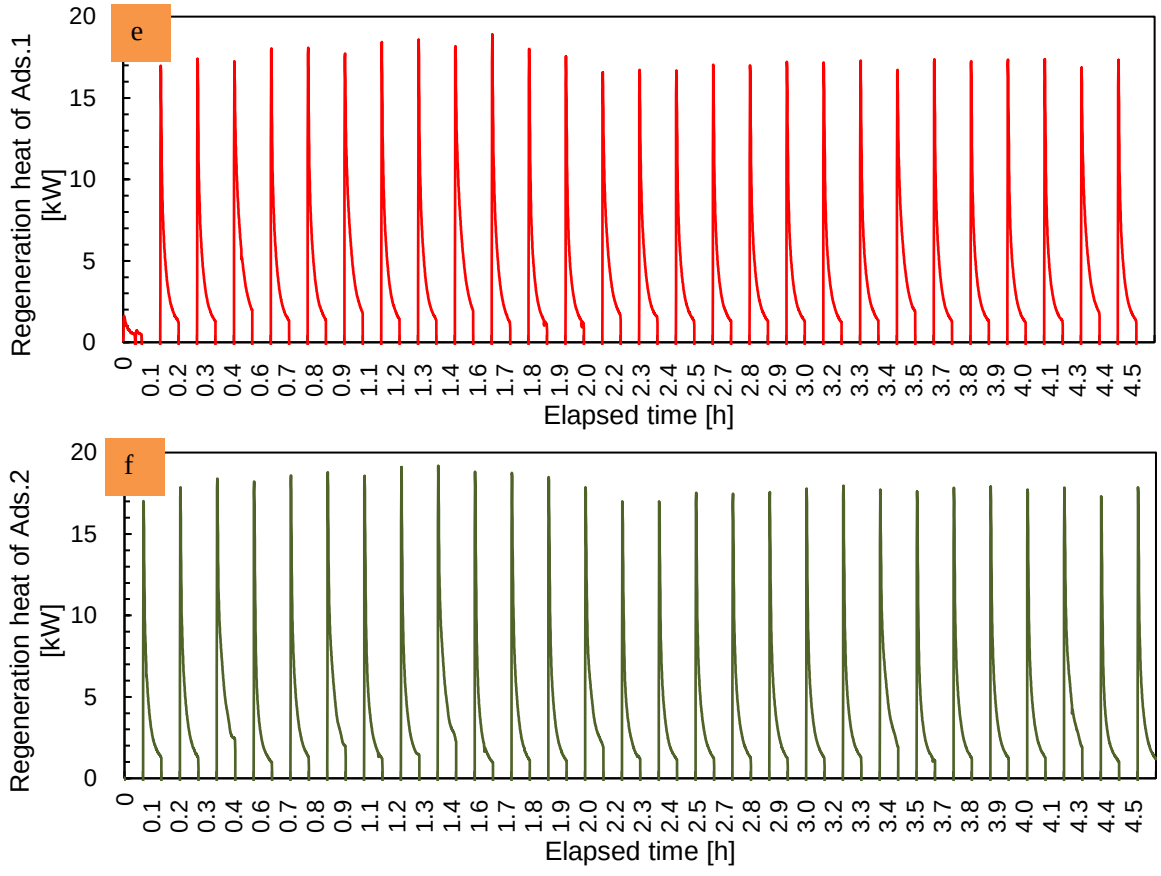

Fig. 3.14 Result of constant experiment.

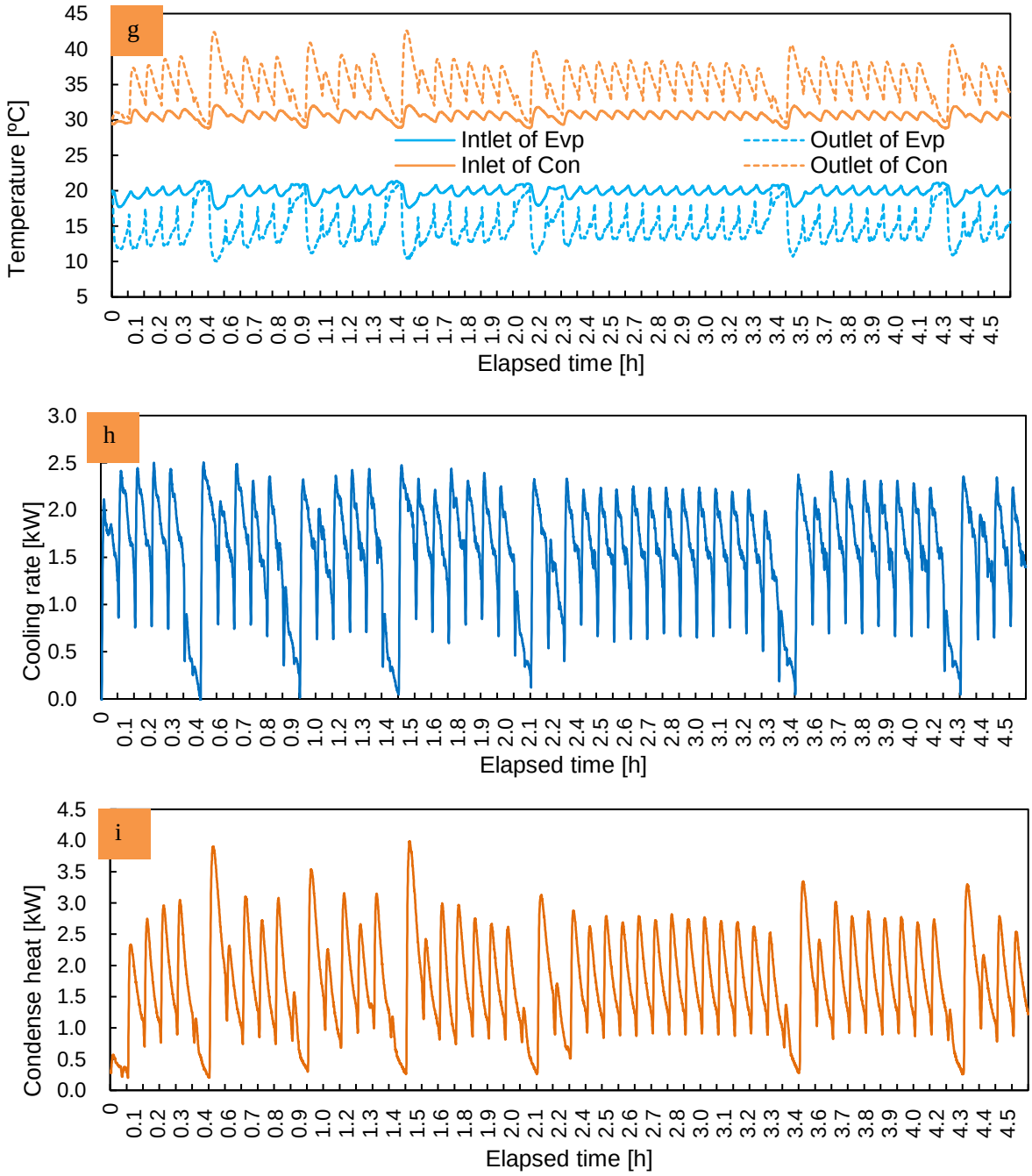

Fig. 3.14 Result of constant experiment.

Fig. 3.14 (g) shows the inlet/outlet temperature of evaporator and condenser, the cooling capacity and condensation capacity based on **Fig. 3.14 (g)** are shown in **Fig. 3.14 (h)** and **(i)**. these curves show periodical stable change except several cycle for the same reason to **Fig. 3.14 (a)**.

Fig. 3.15 shows the results of two representative cycles. The $T_{in,ads}$ for the hot water for the regeneration process is kept at 80 ± 0.5 ℃ meanwhile, the $T_{in,ads}$ for the cooling water for the sorption process is kept at 30.5 ± 1.5 ℃ as seen in **Fig. 3.15 (a)**. On the other hand, $T_{in,evp}$ and $T_{out,evp}$ are maintained at 20 ± 0.6 ℃ and 14.4 ± 1.2 ℃, respectively, and are obtained over various periods expect during the switching between the regeneration and sorption process as observed in **Fig. 3.15 (b)**. As **Fig. 3.15 (c)** shows, the evaporator pressure of 1.7 ± 0.3 kPa is

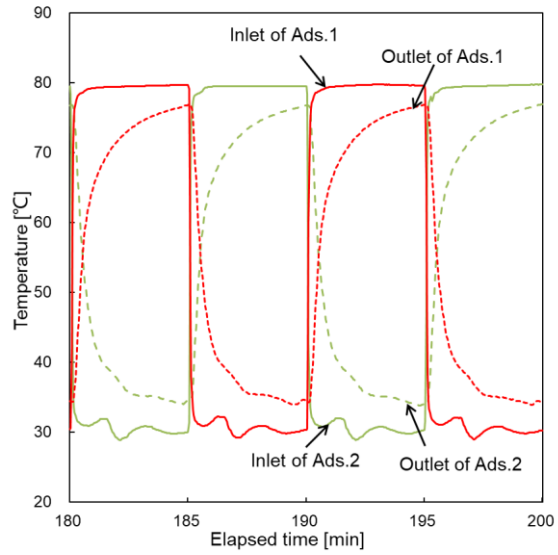

(a) Temperature change of adsorbers.

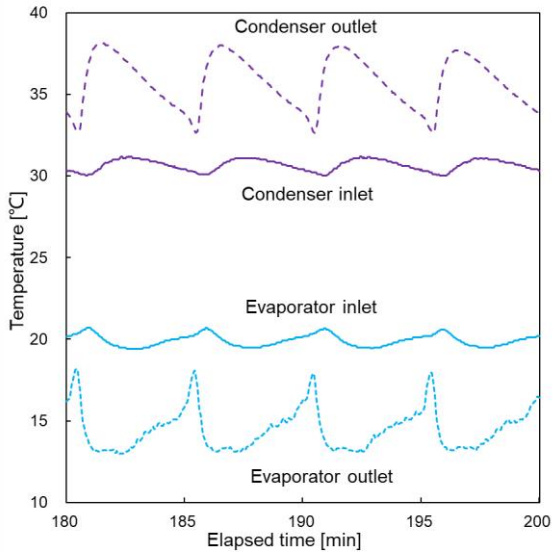

(b) Temperature change of condenser and evaporator.

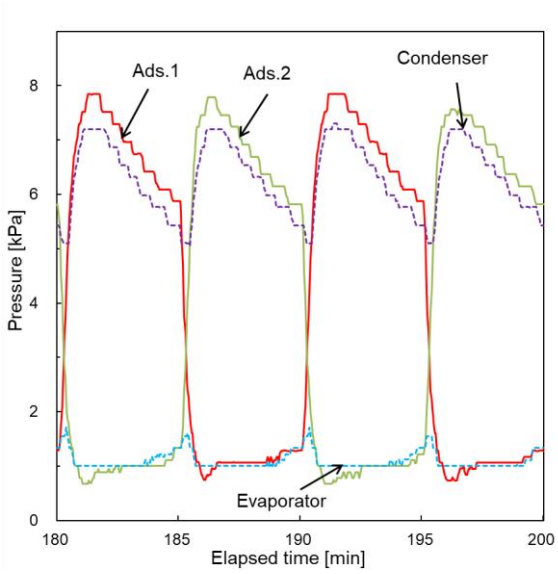

(c) Pressure changes of each chamber.

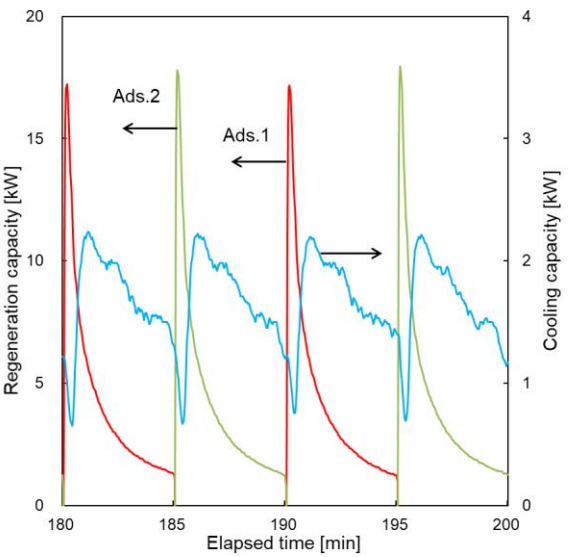

(d) Regeneration and cooling capacities.

Fig. 3.15 Results of basical performance (19th~20th cycle).

maintained, thus ensuring evaporation speed. The pressure of the condenser increases to 6.8 kPa owing to the desorption of a large amount of vapor. The pressure differences of evaporator-adsorber and adsorber-condensor are 0.1 kPa and 0.3 kPa at the end of cycle, respectively. The Myat's study showed that the similar pressure difference is required to open the valves [12]. It indicates that the ball-type valves and the plate valves can work well over those pressure difference. The peak of the cooling output is 2.3 kW and drops to 1.25 kW at the end of the sorption process based on **Fig. 3.15 (d)**, and an average cooling output of 1.67 kW is obtained in this case. The COP and SCP are 0.4 and 0.41 kW/kg, respectively.

3.3.2. Cycle Period Changed Experiment

Fig. 3.16 shows the changes in COP and SCP against the t_{cyc} from 10 to 18 min. COP is found to increase to 0.48 from 0.4 when a longer t_{cyc} is considered owing to the regeneration heat amount that is mainly used to reheat the HEX, adsorbent and water remaining in the HEX when a new cycle begins. On the other hand, the SCP decreases from 0.41 kW/kg to 0.34 kW/kg. This is due to the gradual decrease in the cooling capacity, during the regeneration process, as shown in **Fig. 3.15 (d)**. The temperature difference between the inlet and outlet of the evaporator was kept at 14.9 ± 0.5 ℃.

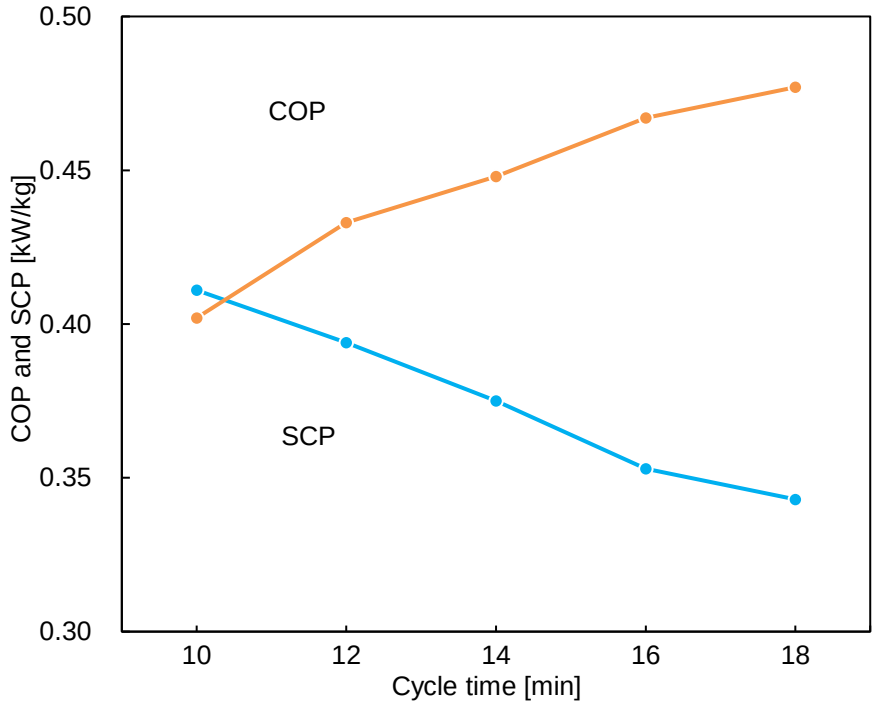

Fig. 3.16 COP and SCP against the cycle period.

The cooling amount $Q_{i,c}$ is 768 kJ when the cycle period is 18 minutes. The actual adsorbed water amounts q_{actual} of 0.16 g/g is calculated by the **Eq. (3.8)**. It is within the theoretical maximum water sorption amount q_{max} of 0.33 g/g, which can be obtained with the water vapor sorption amount isotherms in **Fig. 3.2** that reported by J.Togawa [7]. The cooling capacity of 0.8 kW can be observed at the end of cycle. It indicates that the actual adsorption equilibrium is not obtained yet. On the other hand, the cooling capacity curve is stable after long-term operation, as shown in **Fig. 3.17**. From these facts, it is confirmed that this experiment operates well when the cycle period is under 18 minutes. In this study, the cycle period t_{cyc} is set to 14 min to correspond to prior research [5]. The SCP and COP are 0.39 kW/kg and 0.43, respectively.

$$q_{\mathrm{actual}} = \frac{Q_{\mathrm{i,c}}}{m_{\mathrm{dry}} \times h_{\mathrm{w}}} \tag{3.8}$$

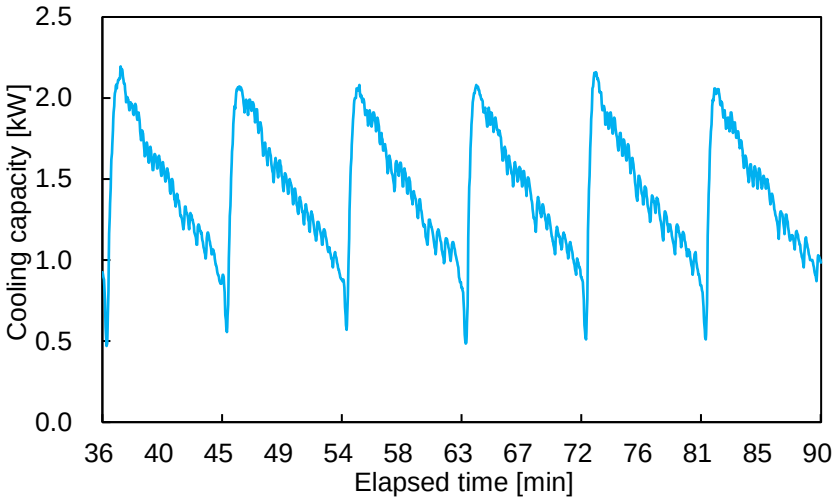

Fig. 3.17 Cooling capacity at cycle period of 18 minutes.

The COP for this AHP was not as high as the expected value of 0.5 and can be attributed to the heat loss from the heat radiation of the adsorber sets. Thermal insulation was used to reduce heat loss and increase the COP. Aluminum sheets of 0.3 mm thickness were posted on the surface of the adsorber sets, and the adsorber chambers were wrapped with a polyethylene sheet of 6 mm thickness. The experimental conditions and results are listed in **Table 3.5**. The regeneration heat amount of 40 kJ was reduced and the COP improved from 0.43 to 0.45 while using the polyethylene sheet (Cases A and C, or cases B and D). On the other hand, the regeneration heat amount increased by 70 kJ and the cooling amount increased by 35 kJ while using the aluminum sheets (Cases A and B, or cases C and D), which deviates from our expected outcome. The results show that a COP of 0.45 and SCP of 0.41 kW/kg can be obtained using thermal insulation.

To determine the reason for the unexpected results, the surface temperature changes of the adsorbent after the process change are shown in **Fig. 3.18**. The surface temperatures for cases A and C increased faster than those of cases B and D, which indicates that the aluminum sheets can reduce the heat loss from radiation, and the adsorbent can be preheated. Hence, the adsorbent can be drier, and more vapor can be adsorbed during the next sorption process, and consequently, the SCP can be improved.

Table 3.5 Result of heat insulation.

Case	Polyethylene sheet	Aluminum sheet	COP [-]	SCP [kW/kg]	Regeneration heat amount [kJ]	Cooling amount [kJ]
A	with	with	0.45	0.41	1551	698
B		without	0.45	0.39	1483	660
C	without	with	0.43	0.4	1597	689
D		without	0.43	0.39	1522	660

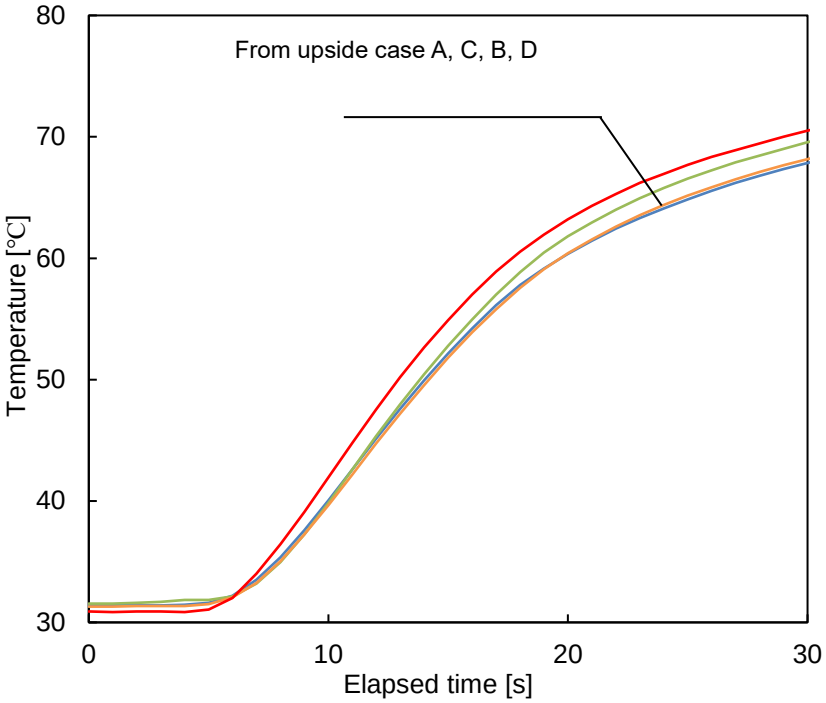

Fig. 3.18 Adsorbent surface temperature changes.

3.3.3. Evaporation & Regeneration Temperature Changed Experiment

AHP can be driven by a low-grade heat source, which is one of the most attractive advantages of AHP. In this section, regeneration temperatures in the range of 60-80 ℃ and an evaporation inlet temperature of 12-20 ℃ were used to examine the performance of the system, as **Table 3.6** shows. The flowrate of the evaporator is adjusted from 1.08 L/min to 4.39 L/min to keep the temperature difference of 5 K between the inlet and the outlet of the evaporator. The results are shown in **Fig. 3.19**. When the regeneration temperature decreased to 60 ℃ and the evaporator inlet temperature decreased to 12 ℃, a COP of 0.14 and an SCP of 0.04 kW/kg were recorded.

Table 3.6 Experiment conditions.

Case	1-1	1-2	1-3	2-1	2-2	2-3	3-1	3-2	3-3
Regeneration water inlet temperature [℃]		80			70			60	
Chilled water inlet temperature [℃]	20	15	12	20	15	12	20	15	12

The evaporator outlet temperature can decrease to 9.6 ℃, though the minimum flow rates are limited by the adjustable flow rate range of the thermostats. The cooling amount and the regeneration heat amount decrease simultaneously, with the decrease in regeneration temperature, which leads to a slight decrease in the COP

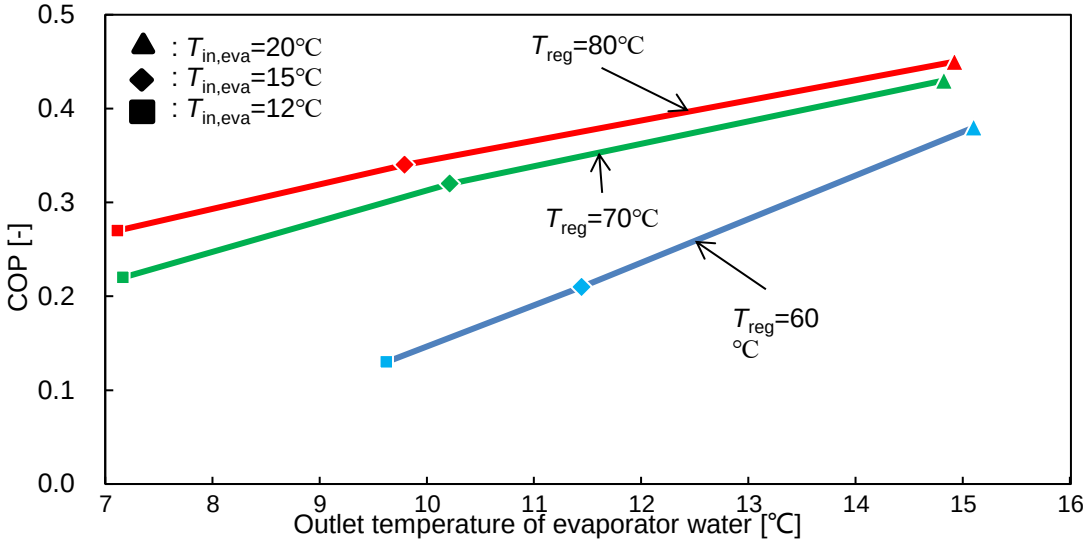

(a) COP as a function of outlet temperature in evaporator

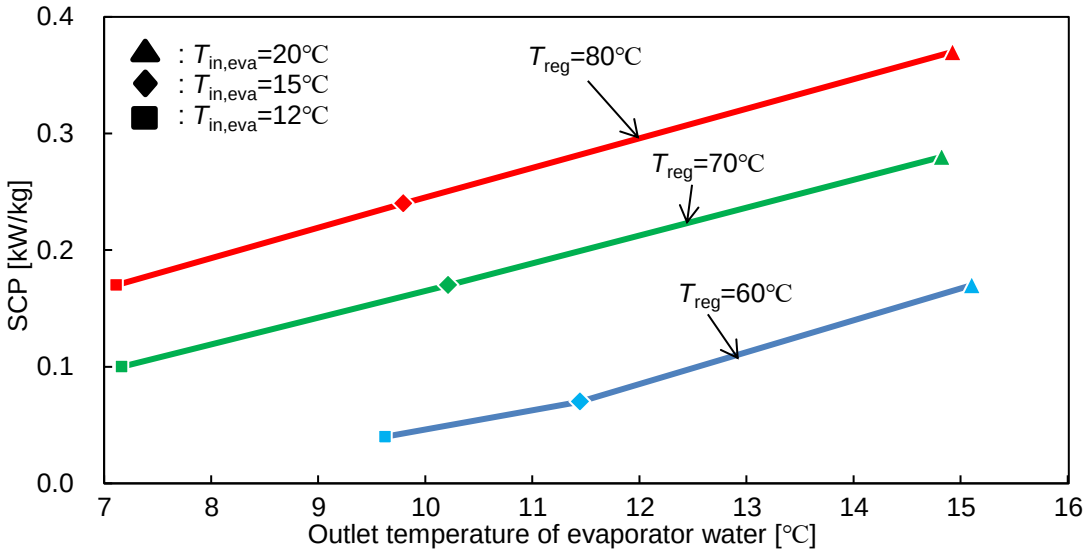

(b) SCP as a function of outlet temperature in evaporator

Fig. 3.19 SCP and COP as a function of outlet temperature in evaporator.

according to **Eq. (3.3)** and a distinct decrease in SCP according to **Eq. (3.4)**. A COP of 0.38 and SCP of 0.17 kW/kg can be obtained when the regeneration temperature decreases to 60 ℃. It was confirmed that a low-grade heat source could drive the AHP.

3.3.4. Uncertainties Evaluation

The uncertainties of COP and SCP are shown in **Table 3.7**. All of $\frac{u_{COP}}{COP}$ and $\frac{u_{SCP}}{SCP}$ are less than 2.5% (up to 2.4% of $\frac{u_{COP}}{COP}$ and up to 0.13% of $\frac{u_{SCP}}{SCP}$, case 3-3) in this experiment, thus the calculated COP and SCP are credible in this experiment.

Table 3.7 (a) Uncertainties of COP and SCP in different cycle period experiment.

t_{cyc}	10	12	14	16	18
u_{COP} [$\times 10^{-3}$]	3.315	3.384	3.393	3.398	3.339
u_{SCP} [$\times 10^{-3}$ kW/kg]	2.597	2.291	2.022	1.802	1.717

Table 3.7 (b) Uncertainties of COP and SCP in different regeneration/evaporation experiment.

Regeneration water inlet temperature [ºC]	80			70			60		
Chilled water inlet temperature [ºC]	20	15	12	20	15	12	20	15	12
u_{COP} [$\times 10^{-3}$]	3.39	3.35	3.42	3.76	3.76	3.74	4.37	3.83	3.25
u_{SCP} [$\times 10^{-4}$ kW/kg]	3.25	4.89	6.46	3.78	5.66	8.58	5.10	9.56	12.83

3.4. Heat Recovery

3.4.1. Heat Recovery Method

The COP of the current AHP is still limited to less than 0.5 and could be attributed to the low-temperature side adsorber (LTS, Ads.2) needs to be pre-heated to 80 ℃ from 30 ℃ and the high-temperature side adsorber (HTS, Ads.1) needs to be pre-cooled to 30 ℃ from 80 ℃ post the process exchange, which increases the amount of heat required (**Fig. 3.20**). The system efficiency can be improved by pre-heating the LTS with the heat capacity of the HTS or pre-cooling the HTS with the heat capacity of the LTS when the process is exchanged. Hence the regeneration amount can be reduced, and COP can be improved. This process is termed as the heat recovery process.

The heat recovery process is classified into three types: serial heat recovery (SHR), circulation heat recovery (CHR), and passive heat recovery (PHR) [13], as shown in **Fig. 3.21 (a),(b),(c)**.

SHR (**Fig. 3.21 (a)**): The LTS of Ads.2 is pre-heated by the hot water from the HTS of Ads.1. Two sets of bypasses and solenoid valves are added to connect the Ads.2 inlet and the Ads.1 outlet, or the Ads.1 inlet and the Ads.2 outlet.

CHR (**Fig. 3.21 (b)**): The LTS of Ads.2 is pre-heated by the hot water from the HTS of Ads.1, while the HTS of Ads.1 is pre-cooled using the cooling water from the LTS of Ads.2. The additional bypasses and valves are the same as those used for the SHR.

PHR (**Fig. 3.21 (c)**): The cold-water inflow into the heat source is prevented by delaying the action of the outlet solenoid valves of the adsorbers; hence, the heating amount inputted can be reduced. Additional bypasses and valves are not needed as compared to those required by the SHR and CHR.

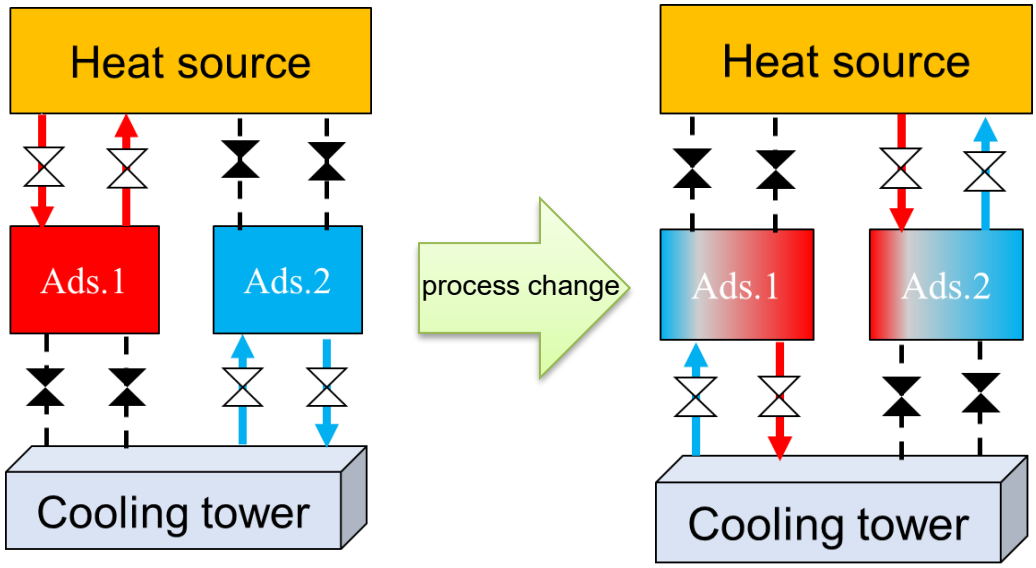

(a) Before process change **(b) Basic type**

⋈ : Opened valve ⋈ : Closed valve

Fig. 3.20 Basic type.

In this study, experiments with SHR and PHR were conducted as they are more effective in improving the COP and are better suited for heat recovery under practical applications [13]. CHR needs lots of extra apparatus and long period to fulfill, thus it was ignored in this study.

3.4.2. System Update

2 sets of bypass / solenoid valves were added to connect the outlet of Ads.1 / the inlet of Ads.2 and the outlet of Ads.2 / the inlet of Ads.1 to fulfill the SHR, as shown in **Fig. 3.21 (a)**. The PHR can be conducted by delaying the action of the outlet solenoid valves of the adsorbers, thus the extra apparatus is not necessary.

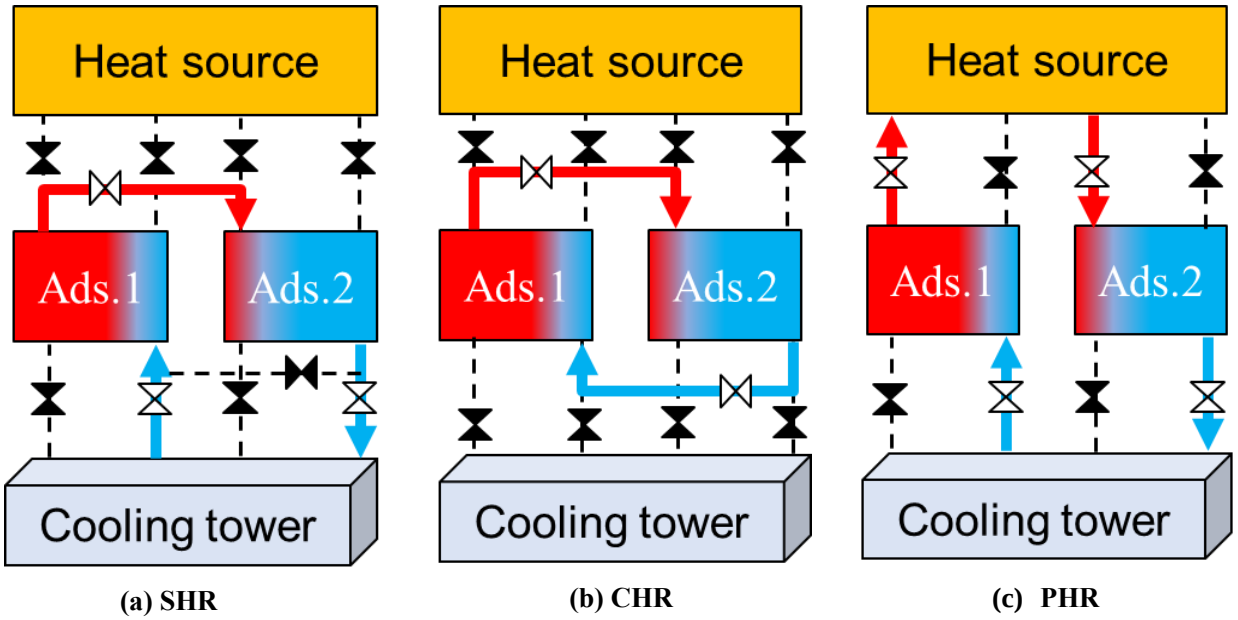

(a) SHR **(b) CHR** **(c) PHR**

⋈ : Opened valve **⋈ : Closed valve**

Fig. 3.21 Three types of heat recoveries.

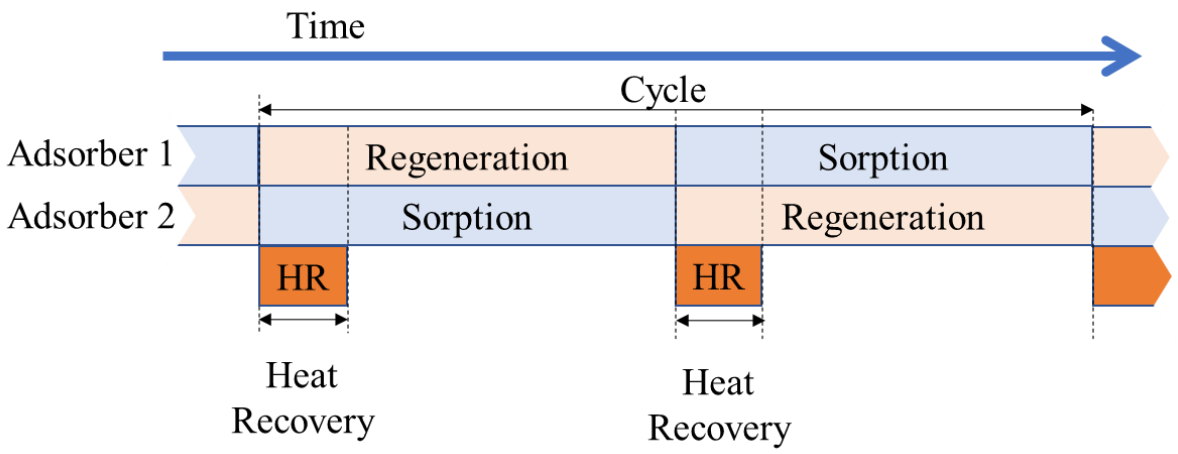

Fig. 3.22 Time schedule of heat recovery and common process.

The heat recovery processes are combined with the common regeneration/sorption processes. The heat recovery processes start when the sorption/regeneration process switch and end with the heat recovery period finish. The PHR independent of the sorption/regeneration process and the SHR only effect on the regeneration process slightly, hence the combination takes the same period to the common regeneration/sorption processes, as shown in **Fig. 3.22**.

The heat amount input of this system is considered as the regeneration amount in the case where heat recovery is introduced, and two temperature sensors are set at the supply and return sides of the hot water tank, respectively. The equation for calculating the regeneration heat amount is defined as follows:

$$Q_{\mathrm{i,reg,hr}} = \int_{t_{\mathrm{i,b,reg}}}^{t_{\mathrm{i,e,reg}}} \dot{V}_{\mathrm{ht}} \rho_{\mathrm{w}} c_{\mathrm{p,w}} \left(T_{\mathrm{s,ht}} - T_{\mathrm{r,ht}}\right) dt \tag{3.9}$$

The standard experiment conditions are shown in **Table 3.8**, the heat recovery period was changed to evaluate the cooling performance.

Table 3.8 Standard experiment condition.

Regeneration temperature [ºC]	Sorption temperature [ºC]	Condensation temperature [ºC]	Evaporation inlet temperature [ºC]	Regeneration period [s]	Sorption period [s]
80	30	30	20	420	420

3.4.3. SHR

As mentioned above, the LTS of Ads.2 is pre-heated by the hot water from the HTS of Ads.1. The inlet temperature change of the Ads.1 is the same to the sorption process, therefore the investigation fucuses on the Ads. 2, which is switched to the regeneration process. The inlet/outlet temperature changes of Ads.1 and Ads.2 during the endless SHR are shown in **Fig. 3.23**.

The SHR started from 0 s (t_0), inlet temperature of Ads.1 decrease due to switching of cooling water, and outlet temperature of Ads.1 decreases in several seconds. The hot water in Ads.1 was recovered to pre-heat Ads.2, thus the inlet temperature transient of Ads.2 follows that of Ads.1 outlet in a little hysteresis. The outlet temperature transient of Ads.2 follows that of Ads.1 inlet in about 20 s of hysteresis.

3 of representative moment were pick up:

t_1: The inlet temperature of Ads.2 increase and reach the peak.

t_2: The inlet and outlet temperature of Ads.2 are the same.

t_3: The inlet and outlet temperature of Ads.2 are the same.

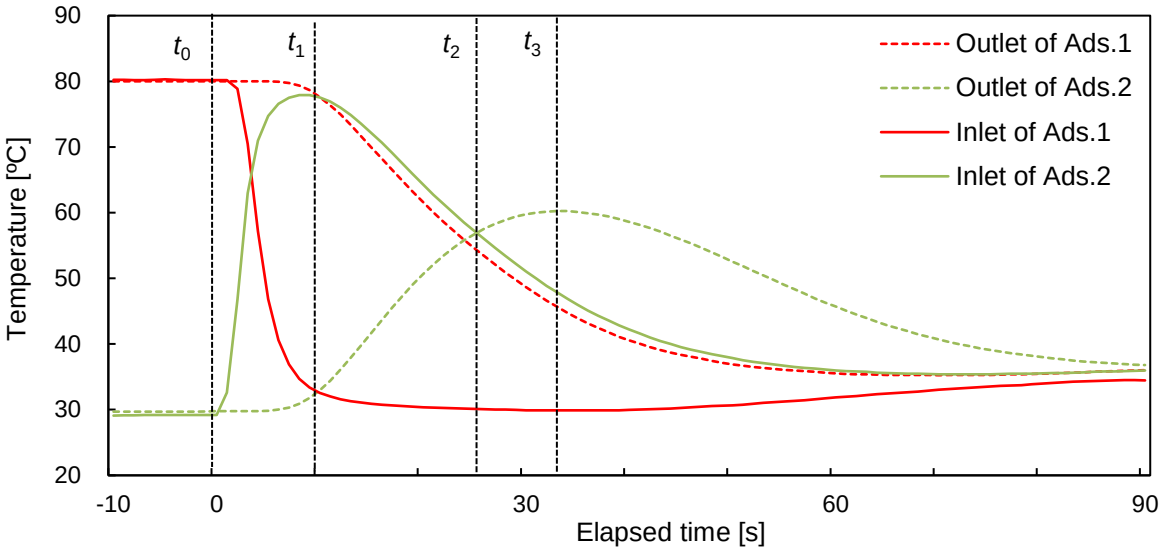

Fig. 3.23 Temperature change based on elapsed time.

The hot water from Ads.1 was flowed into Ads.2 and inlet temperature of Ads.2 kept increasing from t_0 to t_1, which indicate that the pre-heating is ongoing until t_1, and the optimal heat recovery period should be longer than t_1. On the other hand, both inlet and outlet of Ads.2 start decreasing after t_3, it obviously proved that the pre-heat of Ads.2 was finished, the optimal heat recovery period should be less than t_3. It was proved that the optimal period of SHR was within t_1(10 s) to t_3 (34 s).

The inlet/outlet temperature transients with SHR of t_2 (34 s) are shown in **Fig. 3.24**. Compared with the basic case (Ads.2-basic), inlet temperature transient of Ads.2 increase earlier due to the closer distance from Ads.1/Ads.2 than that of hot water tank/Ads.2. The inlet temperature transient of Ads.2 reach the peak and decrease until the end of SHR period follows that Ads.1 outlet, which follows the transient of Ads.1 outlet temperature change. The regeneration water from hot water tank started to be flowed into Ads.2 after 28 s, hence

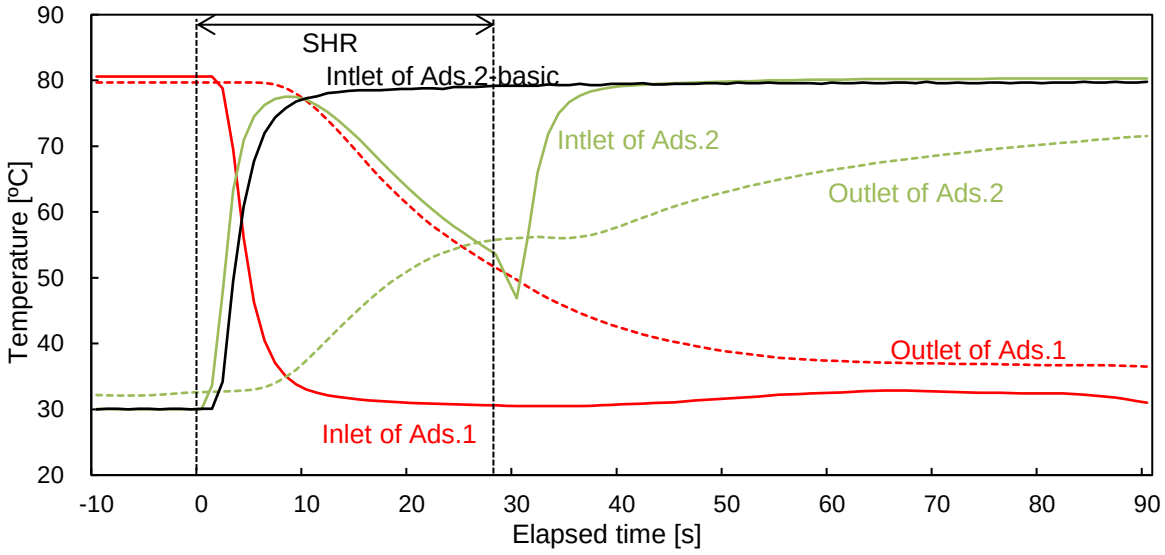

Fig. 3.24 Temperature change of SHR based on elapsed time.

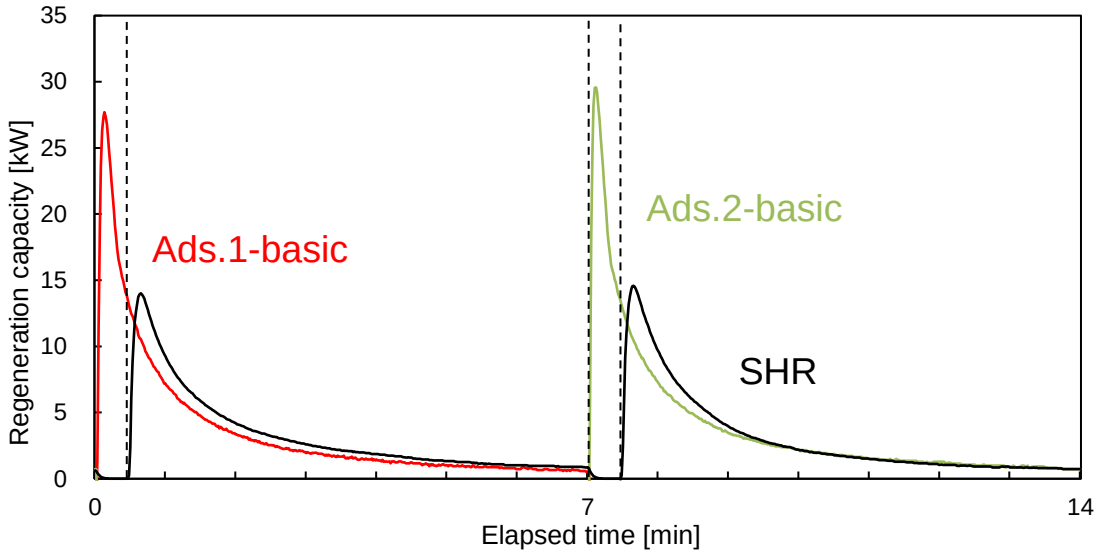

Fig. 3.25 Regeneration heat changes of SHR based on elapsed time.

the inlet temperature of Ads.2 increased again. Ads.2 was pre-heated during SHR period without hot water from hot water tank to reduce the regeneration heat, as shown in **Fig. 3.25**.

Then the experiments with SHR were performed at heat recovery period from 10 s to 34 s. The experimental results are shown in **Fig. 3.26**. COP was obviously improved with SHR, it was enhanced up to 0.54 from 0.47 at SHR period of 28 s. The enhanced COP increases with longer SHR period until 28 s, then it started decreasing. On the other hand, the inlet temperature of Ads.2 starts decreasing and is lower than that of basic case after reaching the peak, as shown in **Fig. 3.26**, which result in slower regeneration progress than the basic case. Therefore, SCP with SHR keeps slight decreasing with the SHR period increasing.

The inlet/outlet temperatures at the end of SHR period based on heat recovery period are shown in **Fig. 3.27**. At SHR period of 28 s, when the highest COP of 0.54 is obtained, the inlet/outlet temperatures of Ads.2 are

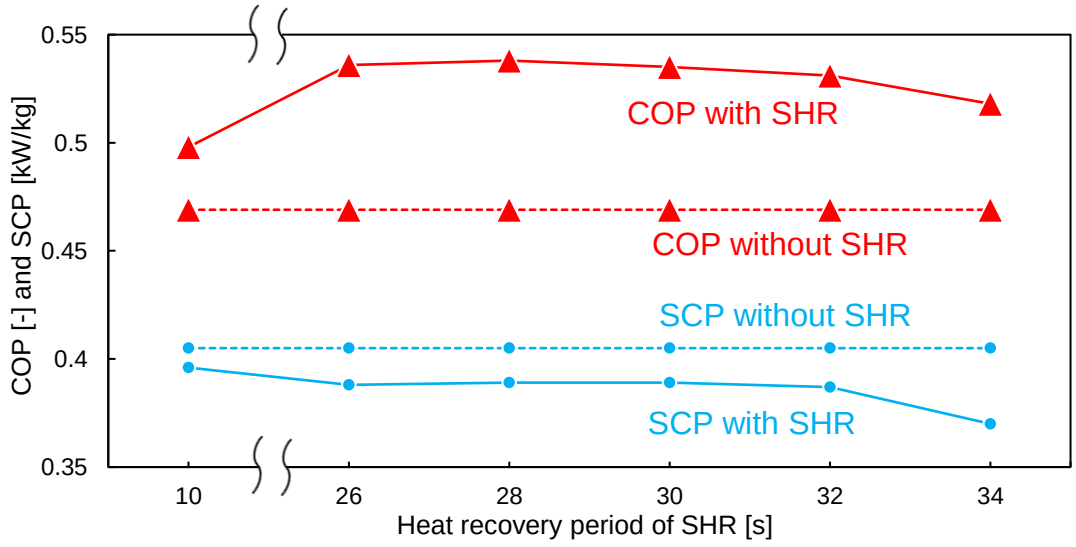

Fig. 3.26 COP and SCP based on period of SHR.

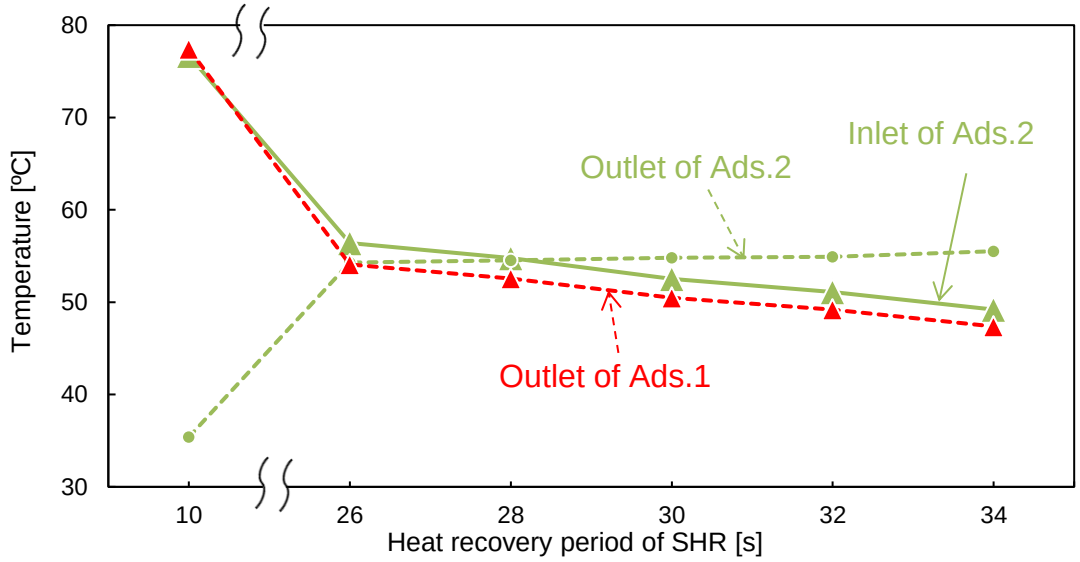

Fig. 3.27 Outlet temperatures of SHR based on heat recovery period.

54.77 ºC and 54.55 ºC, respectively. The outlet temperature of Ads.1 shows a slight lower 52.56 ºC, it is expected to be the same to the inlet temperature of Ads.2 while the water capacity and heat loss can be ignored.

3.4.4. PHR

The inlet/outlet temperature changes of Ads.1/Ads.2 and supply/return of hot water at a PHR period of 35 s are shown in **Fig. 3.28**. PHR have no effect on the generation/sorption processes, thus the generation heat without PHR can be calculated based on the inlet/outlet temperature of Ads.2. The transient of hot water return temperature follow that of Ads.1 outlet during the PHR period then follow that of Ads.2 outlet in several seconds of hysteresis. According to **Eq. (3.9)**, the regeneration capacity with PHR is calculated based on the temperature different between hot water supply and return. It is obviously smaller than the temperature difference between

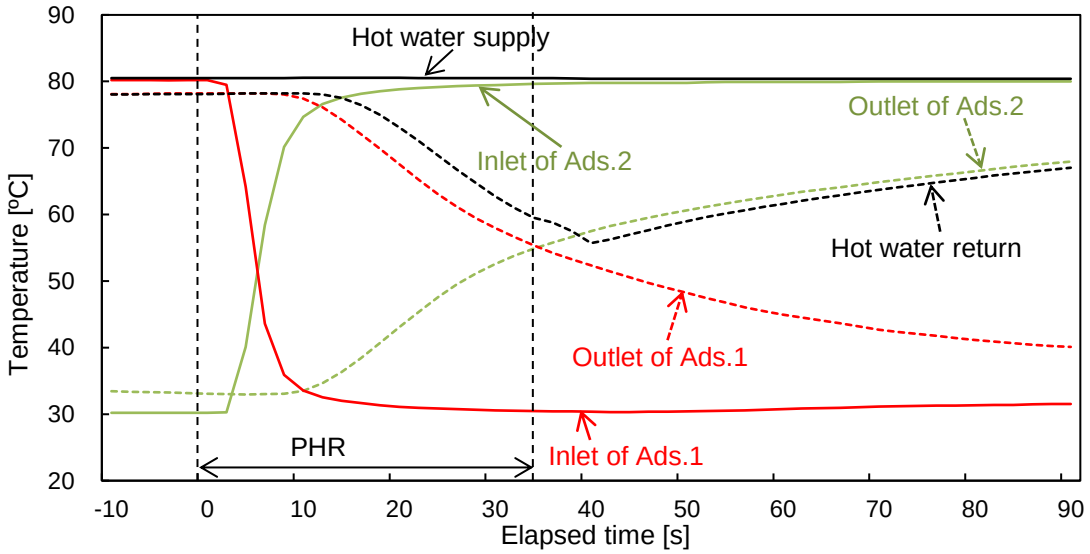

Fig. 3.28 Temperature change of PHR based on elapsed time.

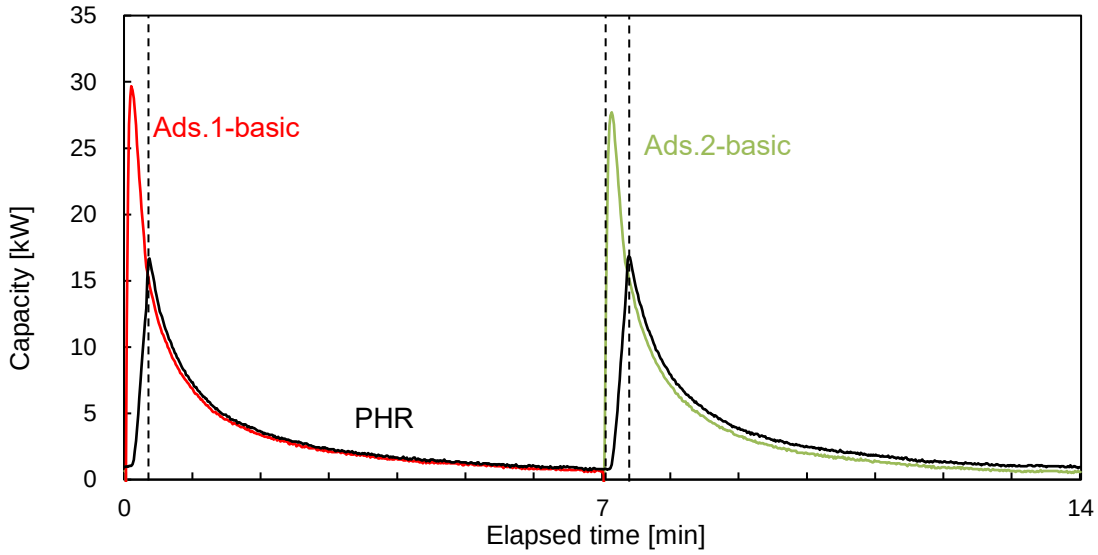

Fig. 3.29 Regeneration heat changes of PHR based on elapsed time.

the inlet and outlet of Ads.2, which is applied to calculate the regeneration capacity without PHR in **Eq. (3.2)**. The regeneration capacity of basic case and PHR are shown in **Fig. 3.29**. Hot water for the regeneration process is still provided and the regeneration capacity is partly reduced during the PHR, which is different from the SHR.

The experiments with PHR at period of 25-45 s were performed, the results are shown in **Fig. 3.30**. COP with PHR is enhanced up to 0.54, which is the same level to that of SHR. The highest COP is observed at PHR period of 35s though COP is slightly fluctuated with the PHR period increasing due to the experiment error. As mentioned above, PHR have no effect on SCP, SCP is stable while the error is ignored. The inlet/outlet temperatures at the end of SHR period based on heat recovery period are shown in **Fig. 3.31**. With the longer PHR period taken, Ads.1 outlet temperature increases while Ads.2 outlet temperature decreases. The inlet temperature of Ads.2 approaches the hot water supply temperature of 80 ºC, which is different from that in SHR.

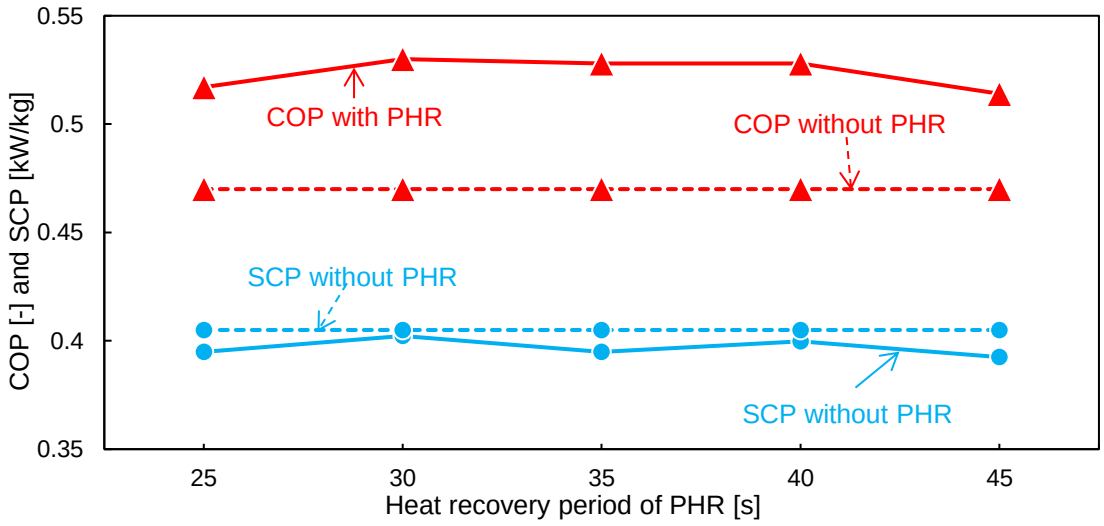

Fig. 3.30 COP and SCP based on period of PHR.

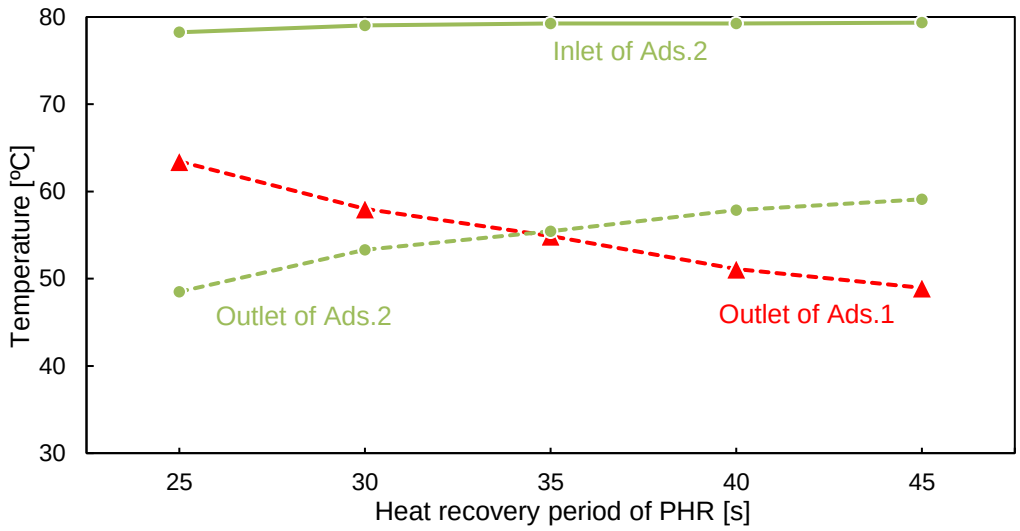

Fig. 3.31 Outlet temperatures of PHR based on heat recovery period.

The outlet temperature of Ads.1 and Ads.2 are 54.9 ºC and 55.45 ºC, respectively.

3.4.5. Discussion

As shown in **Fig. 3.26** and **Fig. 3.30**, both the SHR and PHR can improve the COP value up to 0.54 in the case where the heat recovery period of the SHR and PHR are 28 s and 35 s, respectively. The highest value of COP can be achieved in the case where the heat recovery process is completed and when the outlet temperatures of Ads.1 and Ads.2 close to 55 ºC, which is the average temperature of 80 ºC for regeneration and 30 ºC for cooling. Both SHR and PHR are applied to recover the sensible heat amount of Ads.1 (HTS) by heat transfer water, half of maximum sensible heat amount is recoverable due to the application of symmetric adsorber. Therefore the optimal outlet temperatures to end both SHR and PHR is supposed to be the average temperature of regeneration and cooling, as shown in **Fig. 3.27** and **Fig. 3.31**. The regeneration heat amount $Q_{i,reg,hr}$ is reduced by 14% compared with $Q_{i,reg}$ using heat recovery , which is very similar to the formal research calculation result of 15 % [13].

Two sets of bypasses and two additional solenoid valves are needed for SHR and CHR, meanwhile CHR requires an extra circulate pump, which leads to a higher capital cost and more complex system. Besides, the heat recovery time of CHR is very long, which also negatively influence the cooling capacity and system pesrformance [13]. In additions, SHR result in slight SCP decreas. Therefore, although the same COP of 0.54 can be obtained using both types of heat recoveries in this study, PHR is reasonable for this study because additional tubes and valves are not required.

3.5. Evaluation of Heat Balance

The heat balance of the regeneration heat input is analyzed to improve the system's thermal efficiency, and the experimental conditions provided in **Table 3.8** were applied. The heat balance equation for the regeneration process is shown in **Eq. (3.10)**, and **Eq. (3.11)** can be used to calculate the sensible heat amount

$$Q_{reg} = Q_{lt,des} + Q_{ss,HEX} + Q_{ss,adsorbent} + Q_{ss,rw} + Q_{ss,Al} + Q_{ss,connector} + Q_{loss} \quad (3.10)$$

$$Q_{ss} = m \times C_p \times \Delta T \quad (3.11)$$

A representative regeneration process is examined, and the elemental values of the heat balance equation are listed in **Table 3.9**. Q_{reg} of 1444 kJ is the regeneration heat input, and $Q_{lt,des}$ is the latent heat amount of water desorption, which is the same as the condensation heat amount of 743 kJ. $Q_{ss,HEX}$ is the sensible heat amount of the HEX and is calculated to be 146 kJ. $Q_{ss,Al}$ is the sensible heat amount of the aluminum sheets, and $Q_{ss,connector}$ is the sensible heat amount of the copper connector between the HEXs and the tubes measured as 17 and 18 kJ, respectively. A blank experiment was conducted to measure the sensible heat amount of the adsorbent ($Q_{ss,adsorbent}$) and the remaining cooling water ($Q_{ss,rw}$). The bk-HEXs are used in Ads.1 as the reference, and the adsorbate

Table 3.9 Element of heat balance equation under standard experiment condition.

	Q_{reg}	$Q_{lt,des}$	$Q_{ss,HEX}$	$Q_{ss,adsorbent}$	$Q_{ss,rw}$	$Q_{ss,Al}$	$Q_{ss,connector}$	Q_{loss}
Heat amount [kJ]	1444	743	146	236	122	17	18	162

water inside the AHP chamber was removed to avoid sorption/desorption. The results show that the regeneration heat amounts of Ads.1 and Ads.2 are 303 kJ and 539 kJ, respectively. $Q_{ss,adsorbent}$ works out to be 236 kJ from the difference in the regeneration heat amount. $Q_{ss,rw}$ of 122 kJ can be obtained from the difference between the regeneration heat amount of Ads.1 and the sum of $Q_{ss,HEX}$, $Q_{ss,Al}$, and $Q_{ss,connector}$. The unknow-heat loss, Q_{loss} of 162 kJ, represents the remainder of Q_{reg} term.

Nineteen percent of the regeneration heat can be reduced when half of the $Q_{ss,HEX}$, $Q_{ss,adsorbent}$, $Q_{ss,rw}$, $Q_{ss,Al}$, and $Q_{ss,connector}$ are recovered completely. The regeneration heat amount can be reduced to 1174.5 kJ from 1444 kJ, and the COP can be improved to 0.57. In the case of heat recovery, the regeneration heat amount $Q_{i,reg}$ (**Eq. (3.2)**) is changed to $Q_{i,reg,hr}$ (**Eq. (3.5)**), and more cooling water needs to be reheated when the regeneration and sorption processes are exchanged. The regeneration heat amounts based on the experiment are listed in **Table 3.10**. For the basic case, the difference between $Q_{reg,bs,hr}$ and $Q_{reg,bs}$ is 239 kJ, which is the sensible heat amount of the cooling water and the tubes between the hot water tank and the adsorber sets. The actual regeneration amount increases to 1294 kJ from 1174.5 kJ when half of 239 kJ is recovered and is close to that of the $Q_{reg,p,hr}$ value of

Table 3.10 Regeneration heat amount based on different side.

	Regeneration heat amount [kJ]	
Case	Heat exchanger base	Hot water tank base
Basic	$Q_{reg,b}$ = 1426	$Q_{reg,b,hr}$ = 1665
PHR	$Q_{reg,ps}$ = 1444	$Q_{reg,ps,hr}$ = 1251

1251 kJ. It was confirmed that 13.4% of the regeneration heat could be recovered using heat recovery, and COP could be improved to 0.54 from 0.46. The tubes between the hot water tank and the heat exchanger need to be reduced; thus, the COP can approach 0.57, which is the calculated value, based on the evaluation above.

3.6. Examination of Performance

The performances of the current AHP and three other AHP studies, which have similar temperature conditions, are compared in **Table 3.11**.

Table 3.11 Cooling performance comparison.

Case	Current study	Q. W. Pan [20]	A. Sapienza [4]	U. Wittstadt [38]
Adsorbent	WSS+20 wt. % LiCl	Silica-gel	AQSOA-FAM-02	SAPO-34
Cycle period t_{cyc} [s]	840	1568	420	400
Sorption/evaporation temperature [℃]	30 / 15	30 / 14.7	30 / 15	27 / 17.5
Regeneration/ condensation temperature [℃]	80 / 30	86 / 30	80 / 35	85 / 27
Heat recovery	With	With	Without	Without
Mass recovery	Without	With	Without	Without
SCP [W/kg]	380	146	235	421
COP [-]	0.54	0.65	0.44	0.35
VCP_{ads} [W/m^3]	13.4×10^4	4.5×10^4	13.3×10^4	8.2×10^4
VCP_{en} [W/m^3]	1.152×10^4	0.44×10^4	/	/

The COP of the current AHP is improved to 0.54 with the introduction of heat recovery when the cycle period is 14 min (840 s). The SCP of the current AHP demonstrates a high value of 380 W/kg. Formal research shows that a COP of 0.65 can be obtained in the AHP, which is a popular adsorbent made of silica gel [14]. The extended cycle period of 26 min (1568 s) and introduction of heat recovery causes a higher COP as compared to the current AHP. However, the SCP of the silica-gel AHP is only 146 W/kg. The COP of 0.44 and SCP of 235 W/kg was obtained in another study [15], in which a type of synthetic zeolite AQSOA-FAM-02 was used as an adsorbent. A type of control strategy enhances the SCP of this synthetic zeolite AHP. On the other hand, this synthetic zeolite AHP shows a lower COP of 0.44 as compared to those of silica-gel AHP owing to the shorter cycle period of 420 s. The AHP using another synthetic zeolite of SAPO-34 achieved high SCP of 421 W/kg with short cycle period of 400, which leads to low COP of 0.35.

The current AHP has the advantage of high SCP as compared with the AHP using silica-gel and the AHP using AQSOA. The COP of the current AHP can be enhanced by considering a long cycle period though the SCP may decrease. Some advanced cycles, such as mass recovery, can be introduced to improve the COP of the current

AHP further. The current AHP shows adsorber VCP of 13.4×10^4 W/m^3, which is almost the same to those of the AQSOA AHP (13.3×10^4 W/m^3) and higher than the silica-gel AHP (4.5×10^4 W/m3) and SAPO-34 AHP (8.2×10^4 W/m^3). The current AHP is more compact than the silica-gel AHP due to higher entire machine VCP (1.152×10^4 W/m^3) compared to those of the silica-gel AHP (0.44×10^4 W/m3).

As mentioned above, the widespread adoption of the commercial products has been disrupted owing to the high price of the synthetic zeolite. For example, the commercial production of 10kW AHP made in Germany is 28,000 US$/kg [16]. The synthetic zeolite made by Japanese is estimated to approximate 50 US$/kg [17]. A type silica gel, which is usually used as adsorbent of AHP, can be purchased in 9.3 US$/kg from Japanese market. The WSS with 20 wt. % LiCl adsorbents is available can be obtained in 1.3 US$/kg, which is obviously cheaper than A type silica gel and synthetic zeolite. In addition, WSS adsorbent in current AHP shows as competitive cooling performance as synthetic zeolite, which is higher than silica gel. As a result, the WSS is proved to be a potential alternative adsorbent.

On the other hand, it is challenging to confirm that the WSS with 20 wt.% LiCl is a comprehensive adsorbent compared with other kinds of adsorbents such as synthetic zeolite or silica gel due to different experimental conditions and heat exchangers. The influence of different types of heat exchangers will be studied in the future.

3.7. Conclusion

In this part, a 1 kW adsorption chiller prototype was developed for practical application of natural mesoporous material, WSS, and heat recovery was introduced to improve the system's performance. The conclusions are summarized as follows.

1) A 1 kW adsorption chiller prototype, in which WSS with 20 wt. % LiCl was used as an adsorbent to reduce the initial cost, was developed to evaluate the system's performance. Under standard experimental conditions of 80 °C for regeneration, 30 °C for sorption, 30 °C for condensation, 15 °C for the evaporator outlet, and proper cycle period of 14 min, the COP and SCP are calculated as 0.43 and 0.39 kW/kg, respectively. The uncertainties of COP and SCP are 2.4% and 0.13%, respectively.

2) Aluminum plates and polyethylene sheets were used to reduce heat loss. The results show that the aluminum sheets could help increase the SCP. With heat isolation, the COP and SCP could be improved to 0.45 and 0.41 kW/, respectively.

3) The COP of 0.38 and SCP of 0.17 kW/kg are shown when the regeneration temperature decreases to 60 °C. It was confirmed that a low-grade heat source could drive the AHP. The lowest evaporator outlet temperature of 9.6 °C could be obtained when the regeneration temperature decreases to 60 °C and the evaporator inlet temperature decreases to 12 °C.

4) For both SHR and PHR, the highest COP of 0.54 could be obtained when the outlet temperature of the Ads.1 and Ads.2 are the same, 55 °C, which is the average temperature of the regeneration and sorption. The PHR is reasonable in this study given that additional tubes and valves were not needed, although the same COP could be obtained.

5) The heat balance evaluation shows that the COP of the AHP can be further improved to 0.57 by means of heat recovery by reducing the tubes between the hot water tank and the heat exchangers. The current AHP has the advantage of SCP and shows a reasonable COP of 0.54. A better COP can be expected when other types of advanced cycles are introduced.

6) The WSS with 20 wt. % LiCl is proved to be a valuable adsorbent due to low-cost and high cooling performance.

NOMENCLATURE

C_p : Specific heat [J/(g·K)]

h_w : Sorption latent heat [J/g]

m : Mass [g]

m_{dry} : Mass of the dry adsorbent [g]

q : Sorption amount [g/g]

Q : Amount of heat [J]

R : Parameter [-]

T : Temperature [℃]

t : Time [s]

t_{cyc} : Cycle time [s]

u : Uncertainty [-]

x : Measured parameter [-]

V : Volume [m^3/s]

$\dot{V}$: Flowrate [m^3/s]

GREEK SYMBOLS

ρ : Density [g/m^3]

ΔT : Temperature difference [℃]

SUBSCRIPTS

actual : Actual

ads : Adsorber

adsorbent : Adsorbent

Al : Aluminum sheet

bs : Basic case

b : Begin

c : Cooling

connector : Connector

des : Desorption

e : End

en : Entire machine

evp : Evaporator

HEX : Heat exchanger

hr : Heat recovery

ht : Hot water tank

i : Number of cycles

I : Number of parameter

in : Inlet

loss : Unknown heat loss

lt : Latent heat

max : Maximum

n : Number of cycles in all

N : Number of parameters in all

out : Outlet

ps : Passive heat recovery

r : Return

rw : Remained water

reg : Regeneration process

R : Parameter

s : Supply

sor : Sorption process

ss : Sensible heat

w : Water

Reference

[1] S. Nakabayashi, K. Nagano, M. Nakamura, J. Togawa, A. Kurokawa. Improvement of water vapor adsorption ability of natural mesoporous material by impregnating with chloride salts for development of a new desiccant filter. *Adsorption* 2011;17:675-686.

[2] F. He, K. Nagano, J. Togawa; Experimental Study and Development of a Low-Cost 1 kW Adsorption Chiller using Composite Adsorbent based on Natural Mesoporous Material. *Energy* 2020;209:118365.

[3] H. Liu, K. Nagano, A. Morita, J. Togawa, M. Nakamura. Experimental testing of a small sorption air cooler using composite material made from natural siliceous shale and chloride. *Applied Thermal Engineering* 2015;82:68-81.

[4] H. Liu, K. Nagano, J. Togawa. Performance of LiCl impregnated mesoporous material coating over corrugated heat exchangers in a solid sorption chiller. *Energies* 2018;11,1565:1-15

[5] S. Oomae, J. Togawa, H. Kuroishi, K. Ochi, K. Nagano. Development of adsorption heat pump using natural mesoporous materials with LiCl – Part 2 Development and evaluation of 10 kW type adsorption heat pump. *Proceedings of the Asian Conference on Refrigeration and Air Conditioning* 2018;9.

[6] A. Komaki, M. Inoue, K. Nagano, J. Togawa. R and D of Low-cost Adsorption Heat pump using Natural Mesoporous Material-Part 7: Numerical Simulation Using Three-Dimensional Model and Performance Prediction, proceedings of the Society of Heating. *Air-Conditioning and Sanitary Engineers of Japan 2017 of hokkaido branch.*

[7] J. Togawa, A. Kurokawa, K. Nagano. Water sorption property and cooling performance using natural mesoporous siliceous shale impregnated with LiCl for adsorption heat pump. *Applied Thermal Engineering* 2020;173:115241

[8] H. Zhang, Y. Yuan, Q. Sun, X. Cao, L. Sun, Steady-state equation of water vapor sorption for CaCl2-based chemical sorbents and its application, *Si. Rep* 2016;6:34115.

[9] A.D. Grekova, L.G. Godeeva, Z. Lu, R. Wang, Y. Aristov. Composite. “LiCl/MWCNT” as advanced water sorbent for thermal energy storage: Sorption dynamics. *Solar Energy Materials and Solar Cells* 2018;176:273-279.

[10] P.C. Thimmaiah, A. Sharafian, W. Huttema. C. McCague, M. Bahrami. Effects of capillary-assisted tubes with different fin geometries on the performance of a low-operating pressure evaporator for adsorption cooling system applications. *Applied Energy* 2016;171:256-265.

[11] P.C. Thimmaiah, A. Sharafian, M. Rouhani, W. Huttema. Evaluation of low-pressure flooded evaporator performance for adsorption chillers. *Energy* 2017;122:144-158.

[12] A. Myat, N.K. Choon, K. Thu, Y.D. Kim. Experimental investigation on the optimal performance of

Zeolite-water adsorption chiller. *Applied Energy* 2013;102:582-590.

[13] Q.W. Pan, R.Z. Wang, L.W. Wang. Comparison of different kinds of heat recoveries applied in adsorption refrigeration system. *Refrigeration* 2015;55:37-48.

[14] Q.W. Pan, R.Z. Wang, L.W. Wang, D. Liu. Design and experimental study of a silica gel-water adsorption chiller with modular adsorbers. *Refrigeration* 2016;67:336-344.

[15] A. Sapienza, S. Santamaria, A. Frazzica, A. Freni. Influence of the management strategy and operating conditions on the performance of an adsorption chiller. *Energy* 2011;36:5532-5538.

[16] AAA machine, Inc. http://www.aaasaveenergy.com/jp/index.html, May 2020.

[17] Mitsubishi Chemical. https://www.mitsubishichem-hd.co.jp, May 2020.

Chapter 4

Revolution of Adsorbent-filled Heat Exchanger and Introduction of Mass Recovery

Introduction

Heat exchangers (HEXs) filled with adsorbents are generally used as adsorbers in AHPs, and the mass transfer and heat transfer of the adsorbent depend on the HEX type and filling method. The fin-tube HEX has a simple structure and is used not only as an adsorbent holder [1], [2], [3], [4], but also as an evaporator and condenser HEX [5], [6]. The plate-fin-tube HEX is similar to the in-tube HEX, and its relatively large heat transfer area renders it one of the most frequently used HEXs in AHPs [7], [8], [9], [10], [11]. The aluminum corrugated microchannel HEX, which exhibits good heat transfer performance, has been used in a few recent studies [12], [13], [14], [4], [15]. Adsorbents were added to HEXs using different methods. The adsorbent, which is granular, is typically embedded in HEXs [8], [12], [16]. Adsorbents can be densified in this manner, although the contact between the adsorbent and HEX is not favorable. Powder adsorbents are generally dissolved in a solution with a binder, and HEXs filled with this solution require drying after filling is performed [14], [4]. Consequently, the mass transfer is disrupted, and the packing density is low; however, this method enhances the contact between the adsorbent and HEX. Meanwhile, the coating method can overcome the problems of contact and mass transfer [11], [17], and an advanced method known as the dip-coating method has been proposed [15], [18]. An SCP of 0.675 W/g was achieved using a dip-coated HEX [15], thereby proving the effectiveness of the dip-coating method in improving the performance of AHPs. Furthermore, a type of adsorber fluidization method, in which the heat exchanger is removed and the adsorber bed is fluidized, has been investigated to intensify heat and mass transfer. It is typically applied in desiccants under atmospheric conditions [19]. However, researchers have recently applied fluidized beds in the adsorption chiller of vacuum systems [20].

Some advanced cycles have been investigated and then applied to AHPs to improve system performance. Heat recovery is a type of advance cycle that can reduce regeneration input [14] and has been primarily implemented in 1988 [21]. Three types of heat recovery, which were summarized and proposed by Pan et al. [2], have been primarily employed in recent years [16], [22]. Mass recovery is a type of advanced cycle that is achieved by connecting two adsorber chambers during regeneration/sorption exchange [23]. Mass recovery has been reported to be effective in enhancing the COP and SCP in several studies [7], [8], [23], [24]. In addition, Sapienza et al. proposed another advanced method that changes the relative duration of sorption/regeneration to increase the COP and SCP by up to 10% [8] by changing the relative sorption/regeneration duration. This method has been used in some studies, although it resulted in complex systems [6], [25].

In this chapter, the studies on the types of HEX, the filling methods and the mass recovery are performed.

4.1. Experimental Apparatus and Procedure

4.1.1. Apparatus for Performance Evaluation

In this chapter, some new Ad-HEXs are studied, and more than 8 pieces of bk-HEXs are needed in each case with the 1 kW AHP used in **Chapter 3**. Thus a 100 W scale prototype AHP is applied instead of the 1 kW AHP to reduce the preparation period and cost [26].

The 100 W AHP prototype used for performance evaluation in this study is shown in **Fig. 4.1**. It comprises an evaporator (Evp.), a condenser (Con.) and two adsorbers (Ads.). Stainless steel buckets were used as a container in each chamber, and their dimensions are shown in **Table 4.1**. One ad-HEX (Explained in the sections below) was set in each adsorber chamber. Meanwhile, an aluminum corrugated microchannel HEX (W90 mm × D80 mm × H16 mm) and a spiral coil HEX were set in the evaporator and condenser chambers, respectively. An acrylic plate with a thickness of 10 mm was used as the lid of each chamber. The inside and outside spaces were connected by connectors on an acrylic plate. The chambers were connected to a tube with an inner diameter of 14 mm, which was controlled by several solenoid valves. All chambers were shielded with polystyrene foam to reduce heat loss. Hot water, cooling water, and chilled water were supplied using 1 kW cryogenic thermostats. Pt100 sensors were set at the inlet and outlet of the evaporator, condenser, and adsorbers to measure their temperatures. The pressures were measured using gauges set in each chamber. The flow rates of the evaporator, condenser, and adsorbers were measured using flowmeters set at the inlet of each chamber. Eight solenoid valves were used to control the hot/cooling water supply. All the solenoid valves were controlled automatically by

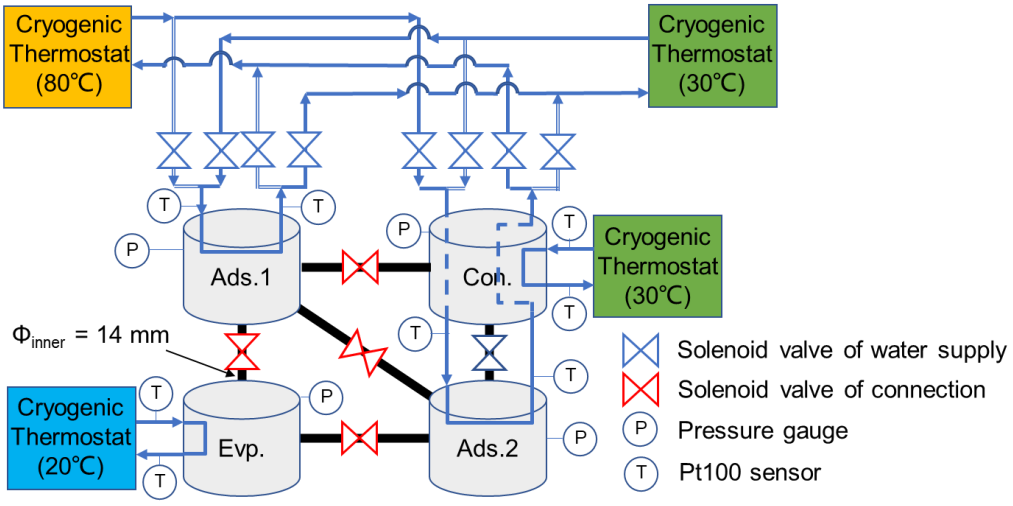

Fig. 4.1 Schematic illustration of experimental setup.

Table 4.1 Dimensions of each chamber.

	Adsorber	Evaporator	Condenser
Volume [L]	4.58	1.08	2.16
Diameter [mm]	180	140	140
Depth [mm]	180	70	140

timers.

4.1.2. Operation Method

The operation method of 100 W AHP is similar to that of 1 kW AHP. Cooling water (30 °C) and the chilled water (20 °C) were circulated into the condenser and evaporator, respectively. Meanwhile, regeneration hot water (80 °C) was flowed into the adsorbers to dry the adsorbent. Subsequently, the pressures of the evaporator, adsorber, and condenser chambers were evacuated to 2.3, 4.3, and 4.3 kPa, respectively. The cooling water used for the sorption process was circulated into the Ads. 1 instead of the generation hot water to begin the experiment. The timer was set to exchange the cooling/hot water supply every few minutes.

AHPs can operate in a wide range of temperature conditions, and they have been experimentally investigated in our prior studies [14], [4]. In this study, the comparison of Ad-HEXs with different filling methods was prioritized; in this regard, the standard conditions used are as shown in **Table 4.2**. The regeneration temperature, sorption temperature, condensation temperature, and evaporator inlet temperature were 80 °C, 30 °C, 30 °C, and 20 °C, respectively. The flow rates of the regeneration hot water, sorption cooling water, condensation cooling water, and evaporator inlet chilled water were 1.62, 1.58, 0.64, and 0.24 L/min, respectively. Hence, the temperature difference between the inlet and outlet of each chamber was 5 K. The cycle period was changed from 10 to 18 min. The temperature, flow rate, and pressure data were recorded using a logger.

Table 4.2 Experimental conditions.

	Regeneration	**Sorption**	**Condensation**	**Evaporator inlet**
Temperature [°C]	80	30	30	20
Flow rate [L/min]	1.62	1.58	0.64	0.24

4.1.3. Evaluation Indices

In this chapter, the system performance was evaluated based on the COP, SCP, and adsorber pack volumetric cooling power (VCP_{ads}) [8], [14], [27], which are the same to **Chapter 3**. In addition, η_u, as defined by **Eq. (4.1)** is used to evaluate the effective utilization rate. Here, q_{max} is the maximum sorption amount, which is shown in **Fig. 4.2** as 0.35 g/g, and ΔH_w is the latent heat of water.

$$\eta_u = \frac{\sum_{i=3}^{n} Q_{i,c}}{(n-i+1)\Delta H_w m_{dry}} \times \frac{1}{q_{max}} \tag{4.1}$$

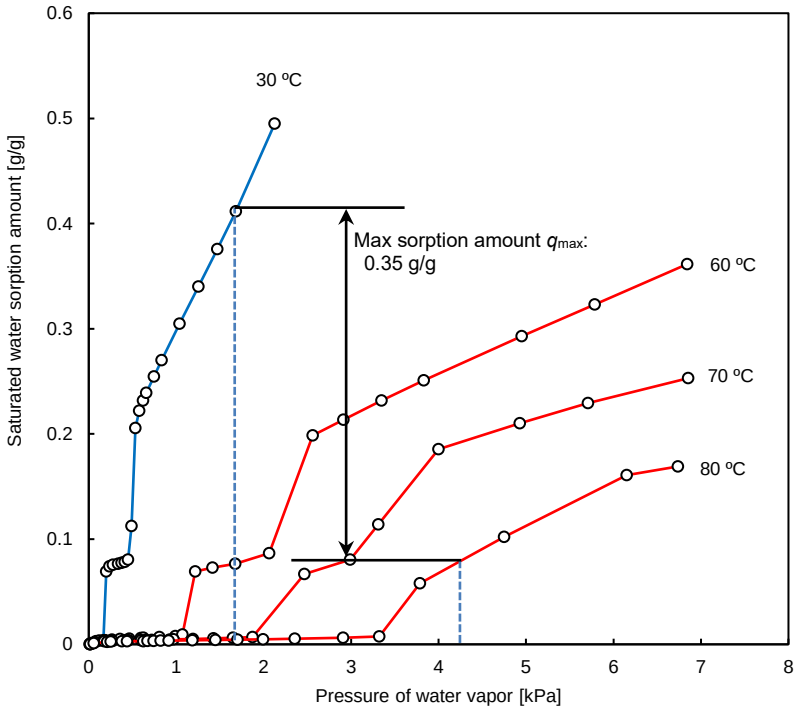

Fig. 4.2 Water vapor sorption isotherms of WSS+20 wt.% LiCl at various temperatures.

The equation expressing the accumulated regeneration amount of the regeneration process and that expressing the cooling amount of the sorption process are shown below. They are used to determine the sorption/desorption characteristics [14].

$$Q_{reg} = Q_{lt,des} + (Q_{ss,ads,adsorbent} + Q_{ss,ads,HEX} + Q_{ss,ads,rw} + Q_{ss,ads,tube} + Q_{ads,loss}) \quad (4.2)$$

$$Q_{c} = Q_{lt,evporation} - (Q_{ss,evp,w} + Q_{ss,evp,HEX} + Q_{ss,evp,rw} + Q_{ss,evp,tube} + Q_{evp,loss}) \quad (4.3)$$

The heat balance equation for the regeneration heat amount Q_{reg} in a cycle is shown in **Eq. (4.2)**, whereas the heat balance equation for the cooling amount Q_c in a cycle is shown in **Eq. (4.3)**. In the ideal state, the regeneration heat is used to desorb vapor in the adsorbent, and Q_{reg} equals the desorption heat amount $Q_{lt,des}$. The evaporation heat is used to chill the refrigerant of the evaporator, and Q_c equals $Q_{lt,evaporation}$. The vaporized water is absorbed by the adsorbent during the sorption process and then desorbed during the desorption process. The measured latent heat of sorption/desorption was similar to the evaporation latent heat amount of water (±2%) [4]; therefore, $Q_{lt,evp}$ was assumed to be equal to $Q_{lt,des}$. However, the adsorbers were always heated from 30 °C to 80 °C; hence, the sensible heat amounts of the adsorbent ($Q_{ss,ads,adsorbent}$), HEX ($Q_{ss,ads,HEX}$), remaining water in the HEX ($Q_{ss,ads,rw}$), and tube ($Q_{ss,ads,tube}$), as well as the heat loss $Q_{ads,loss}$ were unchanged, whereas the regeneration heat amount Q_{reg} increased. By contrast, the temperature of the evaporator fluctuated periodically, and the sensible heat of the adsorbate water in the evaporator ($Q_{ss,evp,w}$), HEX ($Q_{ss,evp,HEX}$), remaining water in

the HEX ($Q_{ss,evp,rw}$), and tube ($Q_{ss,evp,tube}$) was 0. Hence, the cooling amount Q_c decreased owing to the heat loss Q_{loss}.

The uncertainties of the COP, SCP, and VCP are combined uncertainties, which can be determined by the propagation of uncertainty as the same as **Eq. (3.7)** in **Section 3.2.3** shown.

4.1.4. Uncertainty Analysis

The uncertainties of the COP, SCP, and VCP are combined uncertainties, which can be determined by the propagation of uncertainty. **Eq. (4.4)** is used to calculate the uncertainties of the COP and SCP [28], [29], where R represents the COP, SCP, or VCP. **Table 4.3** presents the measured parameters (x_i) and their uncertainties (u_{x_i}).

$$u_{\mathrm{R}} = \sqrt{\sum_{\mathrm{I}=1}^{\mathrm{I}=N} \left(u_{x_{\mathrm{I}}} \frac{\partial R}{\partial x_{\mathrm{I}}}\right)^2} \tag{4.4}$$

Table 4.3 Uncertainties of measurement apparatus.

Parameter	$\dot{V}_{evp}$ [m^3/s]	$\dot{V}_{ht}$ [m^3/s]	$T_{in,evp}$, $T_{out,evp}$, $T_{in,ads}$, $T_{out,ads}$ [K]	m_{dry} [kg]
Uncertainty	± 4.17×10^{-8}	± 4.17×10^{-6}	0.1	± 1×10^{-5}

4.2. Study on Different Types of HEX

4.2.1. Bk-HEX

As mentioned in **Section 4.1**, different types of HEXes such as the fin-tube type HEX, the plate-fin-tube type HEX and the aluminum corrugated microchannel type HEX (**Fig. 4.3(c)**) are applied as holder of adsorbent. The fin-tube type HEX (**Fig. 4.3(a)**) shows a cheap price for its simple structure, however, its unregular shape results in low space utilization and small heat exchange area. The plate-fin-tube type HEX (PFT-HEX), which is shown in **Fig. 4.3(b)**, is an advanced version of the fin-tube type HEX. Its thin and folded shape of refrigerant road provide stronger support to the fin and contribute to larger heat exchange area; thus the PFT-HEX is the most common HEX in lots of AHP systems. The aluminum corrugated microchannel type HEX is shown in **Fig. 4.3(c)**. The refrigerant road is separated into several parallel micro channel, the corrugated fins are set between the micro channels. This structure provides great strength to protect the fins, hence the thickness of the fins is reduced to 0.09 mm, which leads to increasing of surface area and heat transfer performance. However, the thin

(a) Fin-tube type HEX

(b) Plate-fin-tube type HEX

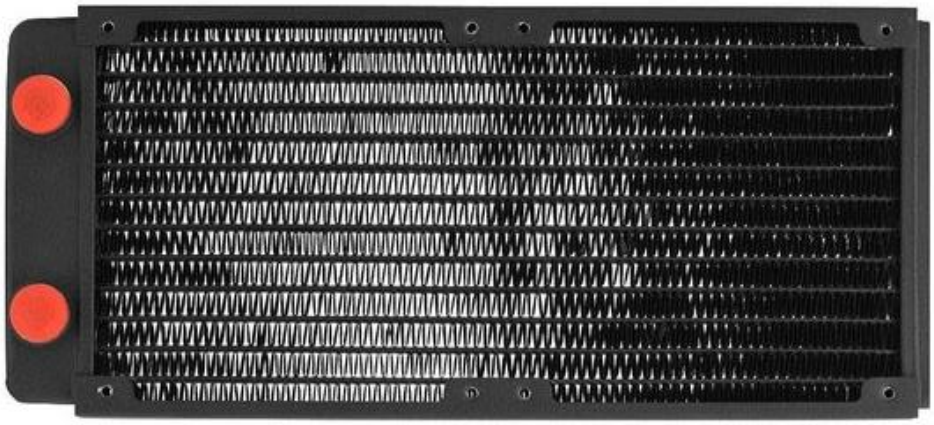

(C) Aluminum corrugated microchannel type HEX

Fig. 4.3 Different types of HEXes.

refrigerant road limits the maximum flowrate.

In this part, the PFT-HEX and the MC-HEX are studied in experiments.

4.2.2. Preparation of Ad-HEX

The commercial PFT-HEX (W235 × H110 × D25) and the MC-HEX (W125 × H120 × D25) ARE used in this studied. In order to manufacture the ad-HEX possessed the same size of the adsorbent layer, some fins of PFT-HEX and MC-HEX are removed and to adapt the dimension of both bk-HEX into the same W120 × H110 × D25, as **Fig. 4.4** shows. The same adsorbent slurry of 1 kW AHP, which is WSS impregnated with 20 wt. % of LiCl, is filled into this HEX, the information of obtained ad-HEXs is shown in **Table 4.4**. The adsorbent filled into the PFT-HEX and the MC-HEX is adapted to the same level to each other, the packing densities of the PFT-

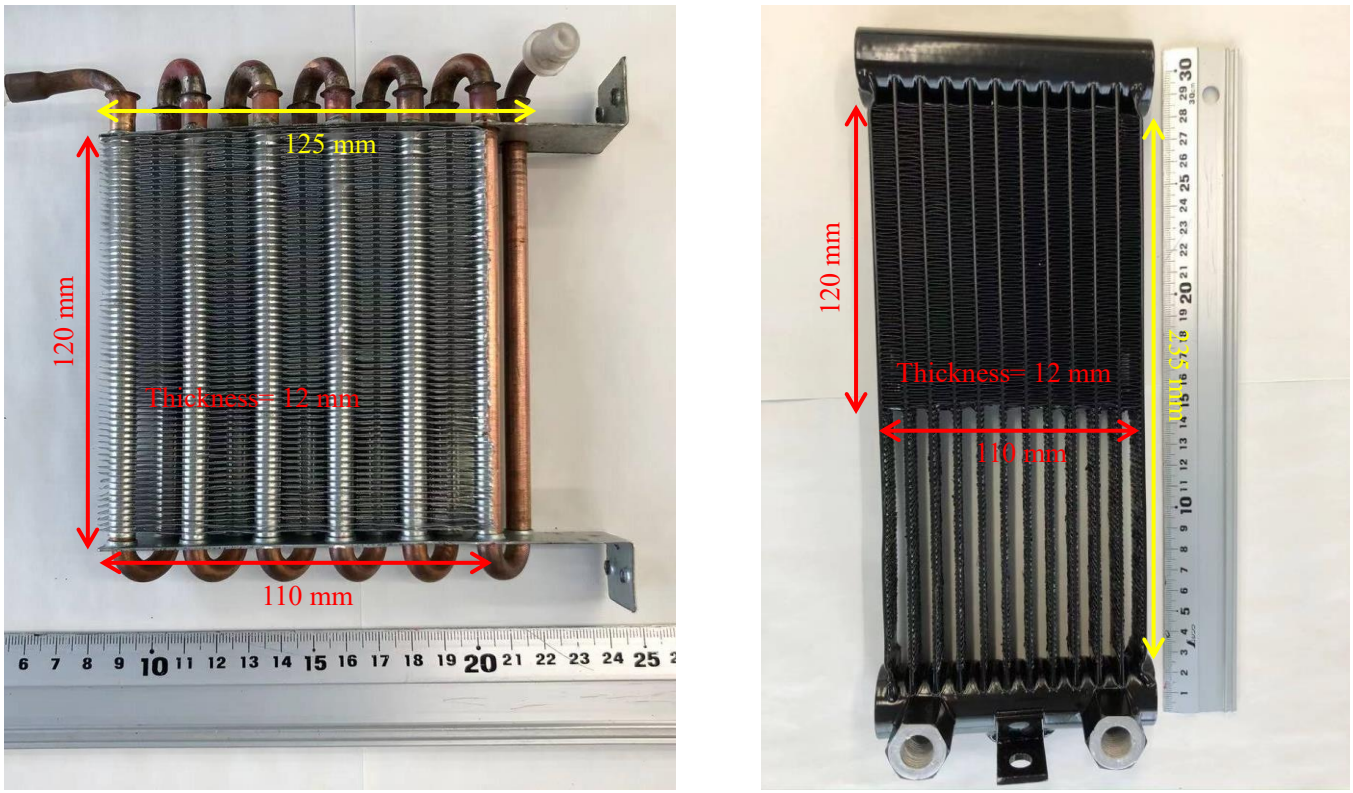

(a) PFT-HEX **(b) MC-HEX**

Fig. 4.4 Bk-HEXes applied in this study.

Table 4.4 Heat exchangers filled with adsorbent.

Type	PFT-HEX	MC-HEX	SMC-HEX
Weight of HEX [g]	238	493	190
Weight of adsorbent [g]	109.3	111.4	58.85
Packing density [g/L]	331.2	337.6	445.8
Remained water [g]	61.7	165.6	27.6

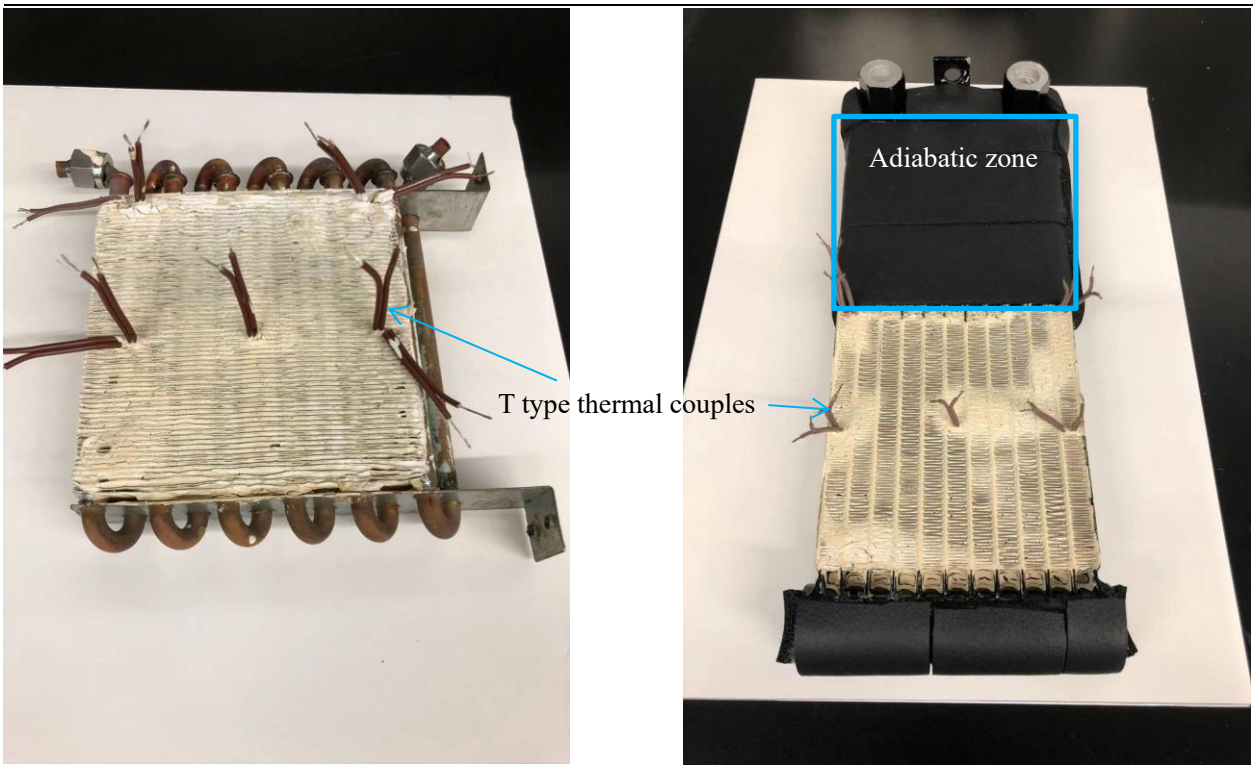

(a) Ad-HEX of PFT-HEX. **(b) Ad-HEX of MC-HEX.**

Fig. 4.5 Ad-HEXes made from different bk-HEX.

HEX and the MC-HEX are 331.2 g/L and 337.6 g/L, respectively. On the other hand, half of the fins are removed from the original MC-HEX to fit the size of PFT-HEX, the weight of HEX and the remained water of the MC-HEX are much higher than those of PFT-HEX. The part of ad-HEXs without adsorbent are thermal isolated, and several T type thermal couples are set at the surface of the adsorbent layer to measure the surface temperature transient. The obtained ad-HEX are shown in **Fig. 4.5**.

4.2.3. Performance Evaluation

The basic experiments are performed to evaluate the cooling performance of both Ad-HEX. The PFT-HEX and the MC-HEX are set in adsorber chamber, respectively. In addition, an ad-HEX made from the ordered small micro channel (SMC-HEX) is used to compare with the MC-HEX, its information is shown in **Table 4.4.** The standard experiment conditions are shown in **Table 4.5**.

Table 4.5 Standard experimental conditions.

	Regeneration	Sorption	Condensation	Evaporation (inlet)
Temperature [ºC]	80	30	30	20
Flowrate [L/min]	1.47	1.6	0.5	0.31

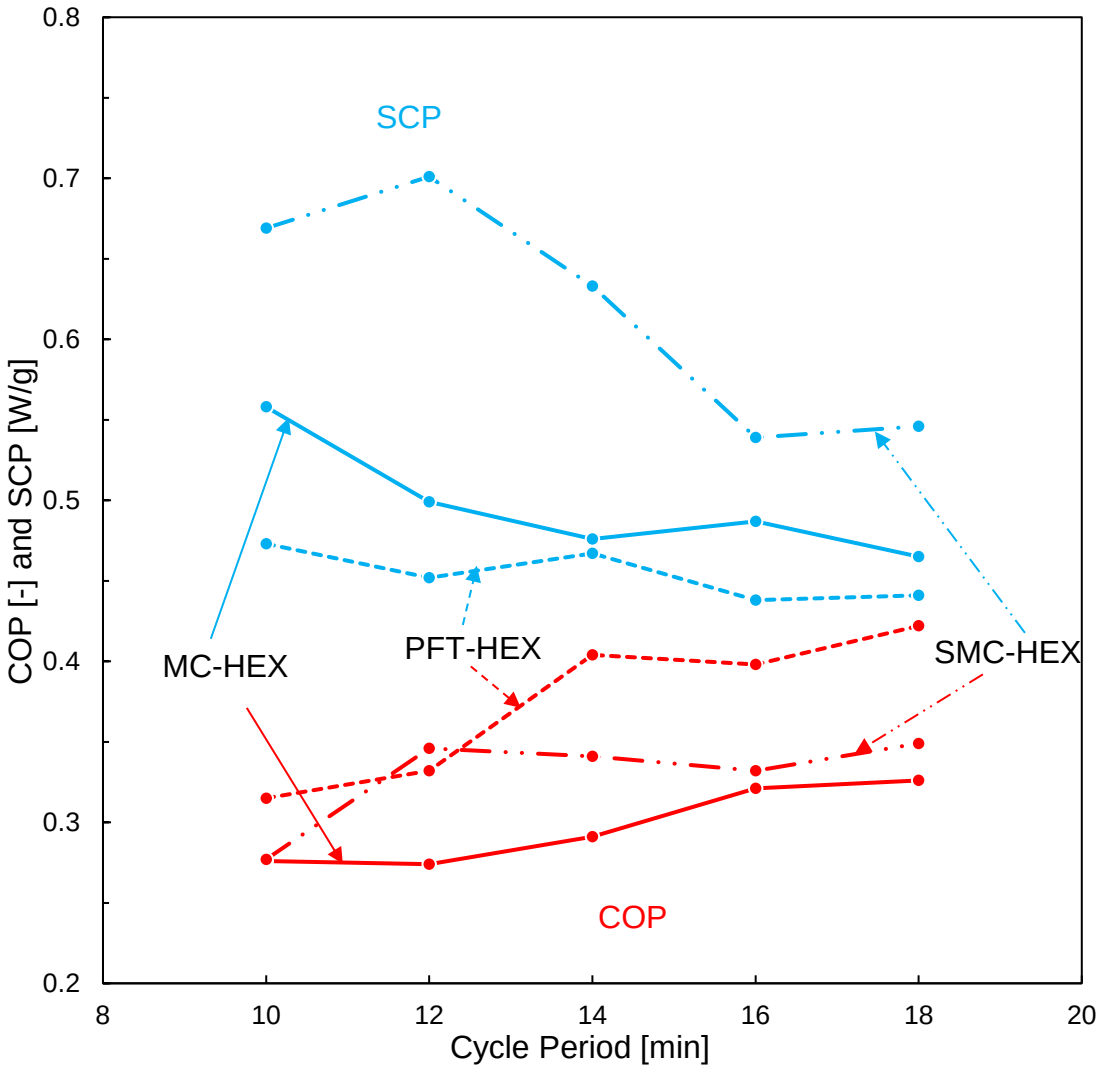

Fig. 4.6 COP and SCP based on cycle period.

The cycle period is change from 10 to 18 minutes, and the results are shown in **Fig. 4.6**. COP of three types of HEX increase with the longer cycle period is taken, meanwhile SCP decrease, which is like those of 1 kW AHP experiment in **Chapter 3**. Compared with PFT-HEX, MC-HEX shown lower COP. On the other hand, MC-HEX can provide higher SCP than PFT-HEX. The SMC-HEX, which is a special ordered corrugated micro channel HEX, possess thinner depth and larger packing density. It shows higher COP than the MC-HEX. In addition, the much higher SCP than the PFT-HEX and the MC-HEX is achieved by the SMC-HEX.

The experiment results at cycle period of 14 minutes are pick up and compared in **Table 4.6**. The cooling amount of the MC-HEX is higher than that of the PFTH-HEX, however, the regeneration amount of the MC-HEX is much more than that of the PFTH-HEX due to larger weight of HEX and remained water. The SMC-HEX is a well-designed version of the MC-HEX, the thinner depth contributes to better mass transfer of vapor, the weight of the HEX and the remained water are much reduced compare with those of the MC-HEX; meanwhile the thinner depth of HEX enhances the mass and heat transfer, which leads to higher SCP than those of the PFT-HEX and the MC-HEX.

Table 4.6 Experimental result of 14 minutes cycle.

HEX type	PFTH-HEX	CH-HEX	SMC-HEX
Cooling amount [J]	43845	45571	32034
Regeneration amount [J]	110108	157346	94681
COP [-]	0.4	0.29	0.34
SCP [W/g]	0.47	0.48	0.63

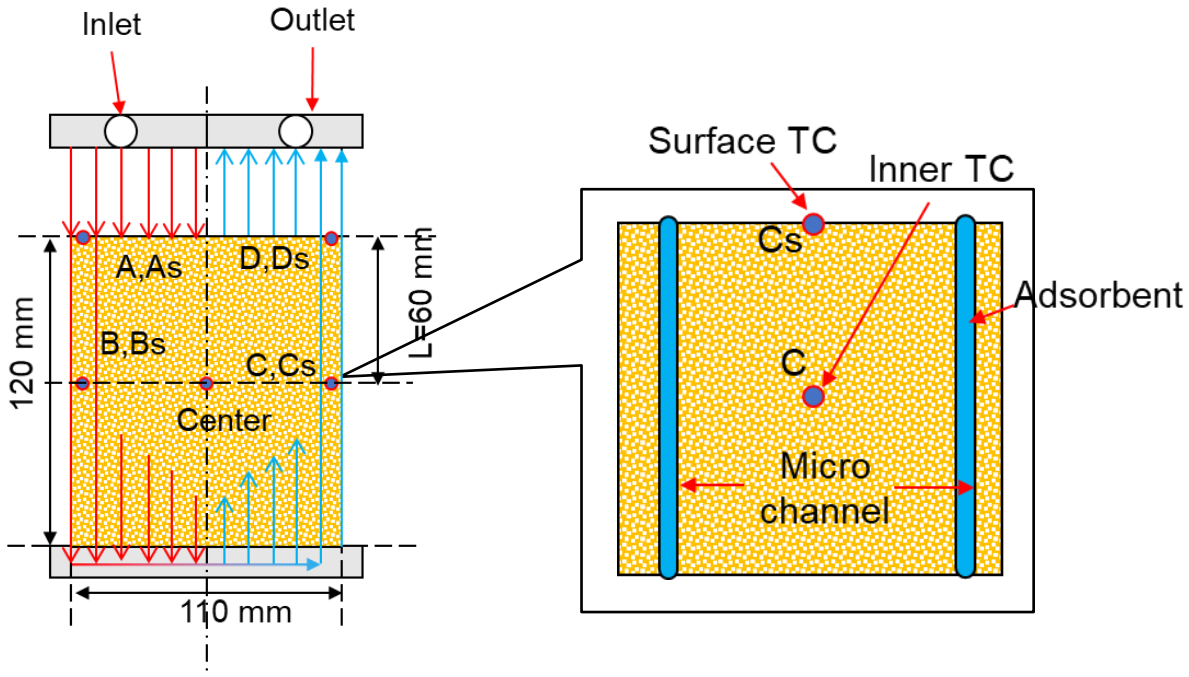

(a) PFT-HEX.

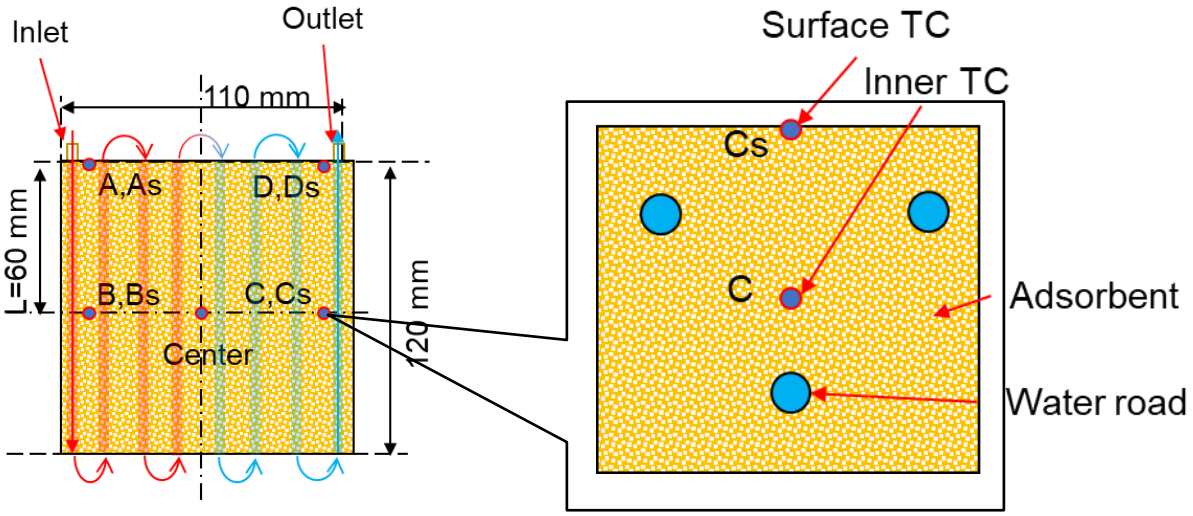

(b) PFT-HEX.

Fig. 4.7 Measure point of thermal couples.

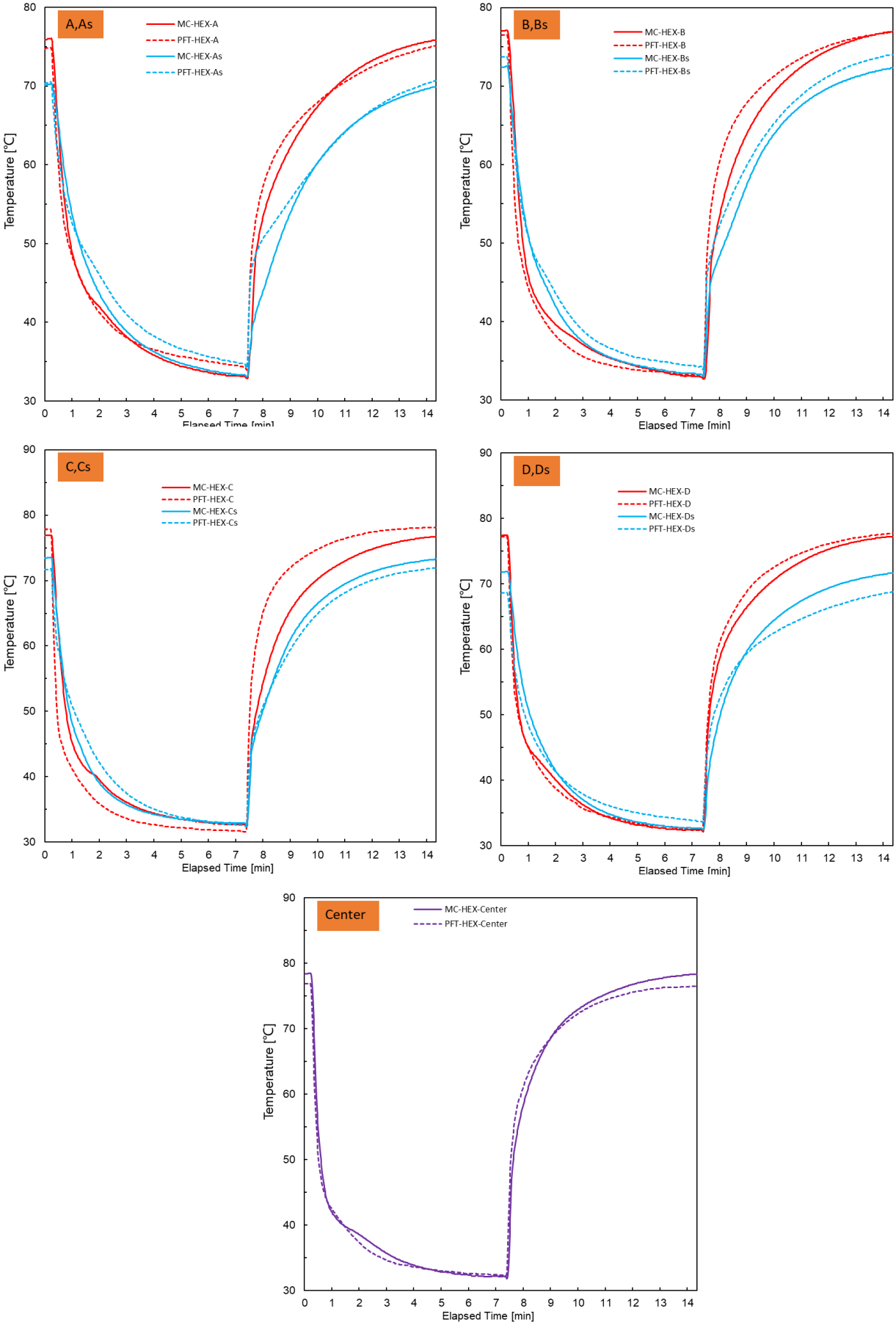

Fig. 4.8 Temperature responds.

4.2.4. Surface Temperature Responds

As mentioned above, the corrugated micro channel HEX is proposed to have advantages on mass and heat transfer, which are reflected on the surface temperature transient of the adsorbent. Therefore several thermal couple (TC) are set on the surface of adsorbent to measure the temperature transient. As shown in **Fig. 4.7**, 4 points of each ad-HEX are chosen, they are marked as A, B, C, D following the refrigerant direction. In addition, the center of the whole adsorbent layer is chosen as a reference. A and D are at the inlet and the outlet of refrigerant, respectively. B is 60 mm from A, meanwhile C is 60 mm from D. 2 of thermal couple are set at the adsorbent surface and inner middle (depth 12.5 mm) for each point.

The experiment conditions are the same to those shown in **Table 4.5**, and the temperature responds of a representative cycle at cycle period of 14 minutes are shown in **Fig. 4.8**. The inner temperature responds of the PFT-HEX are faster than those of the MC-HEX for both sorption (0-7 min) and regeneration process (7-14 min). It can be explained that the MC-HEX needs more heat and cooling amount due to larger weight of HEX and remained water, as mentioned above. The surface temperatures of the PFT-HEX change a little faster than those of the MC-HEX after regeneration/sorption process switch. However, the MC-HEX shows a higher surface temperature at the end of the regeneration process and a lower surface temperature at the end of the sorption process, which indicate that heat transfer of MC-HEX is better than that of PFT-HEX. For the same measure point, the temperature differences between the surface and the inner of the regeneration process are larger than that of the sorption process, the faster regeneration speed and the heat loss are the reasons. The center temperature transients show the same trend to the inner temperature transient of other measure point.

4.2.5. Discussion

SCP of the MC-HEX is higher than that of the PFT-HEX, it proved the larger surface area contributes better heat transfer, which is reflected to the faster temperature responds. With the usage of well-designed corrugated micro channel HEX, SCP can be further enhanced up to 0.63 kW/kg. On the other hand, the MC-HEX show a lower COP than the PFT-HEX because the larger weight of HEX and remained water need more energy to heat or cool down. In addition, the PFT-HEX possess more space between the fins. The gaps of the PFT-HEX are not full filled (**Fig. 4.9**) at the same packing density to the MC-HEX, whose gaps are full filled. For the merits of lighter HEX, less remained water and more space, COP of the PFT-HEX can be improved further with the packing density increase and longer cycle period. However, the MC-HEX shows the better heat transfer, higher SCP can be obtained. In addition, the limit thickness of the commercial PTF-HEX is 25 mm while that of the MC-HEX can be reduced to 12 mm owing to its structure, which can enhance the heat transfer further.

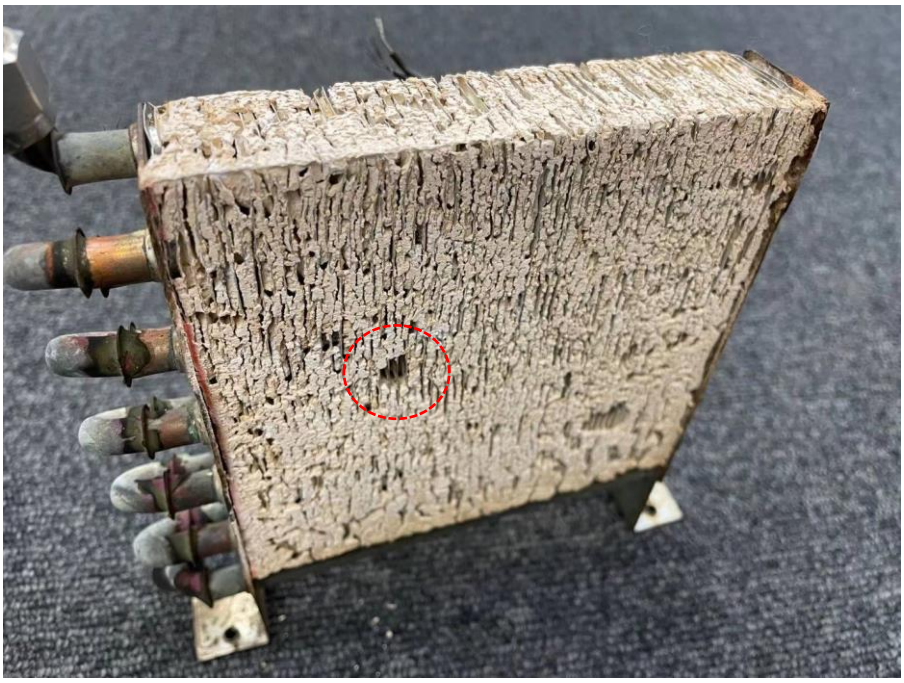

Fig. 4.9 Gaps of the PFT-HEX.

4.3. Filling Method Update

4.3.1. Dip-coating Method

The conventional filling method is shown in **Fig. 4.10 (a)**, the composite adsorbent was dissolved in slurry, filled into a corrugated HEX, and then dried at 120 °C. The improvement in its packing density was limited by the bubble space inside the adsorbent, which appeared owing to the evaporation of liquid. In addition, the mass transfer was disrupted as a mass transfer channel was not adopted.

To improve the packing density, Zhen et al. [18] proposed a filling method known as the dip-coating method.

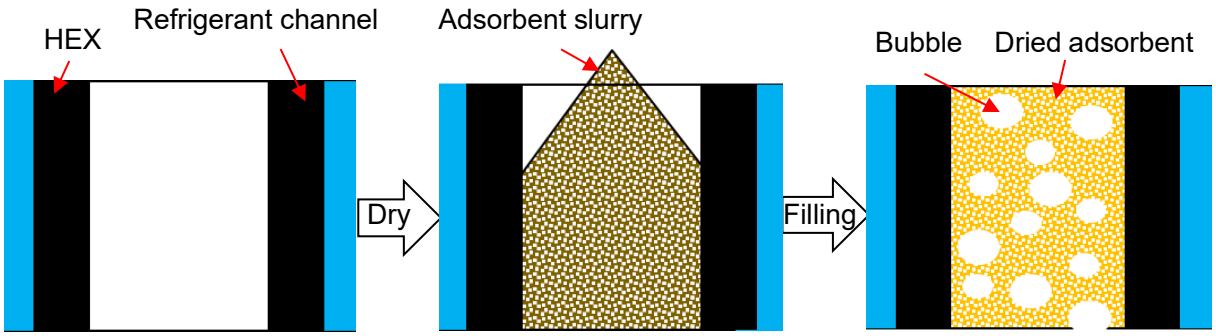

(a) Conventional filling method.

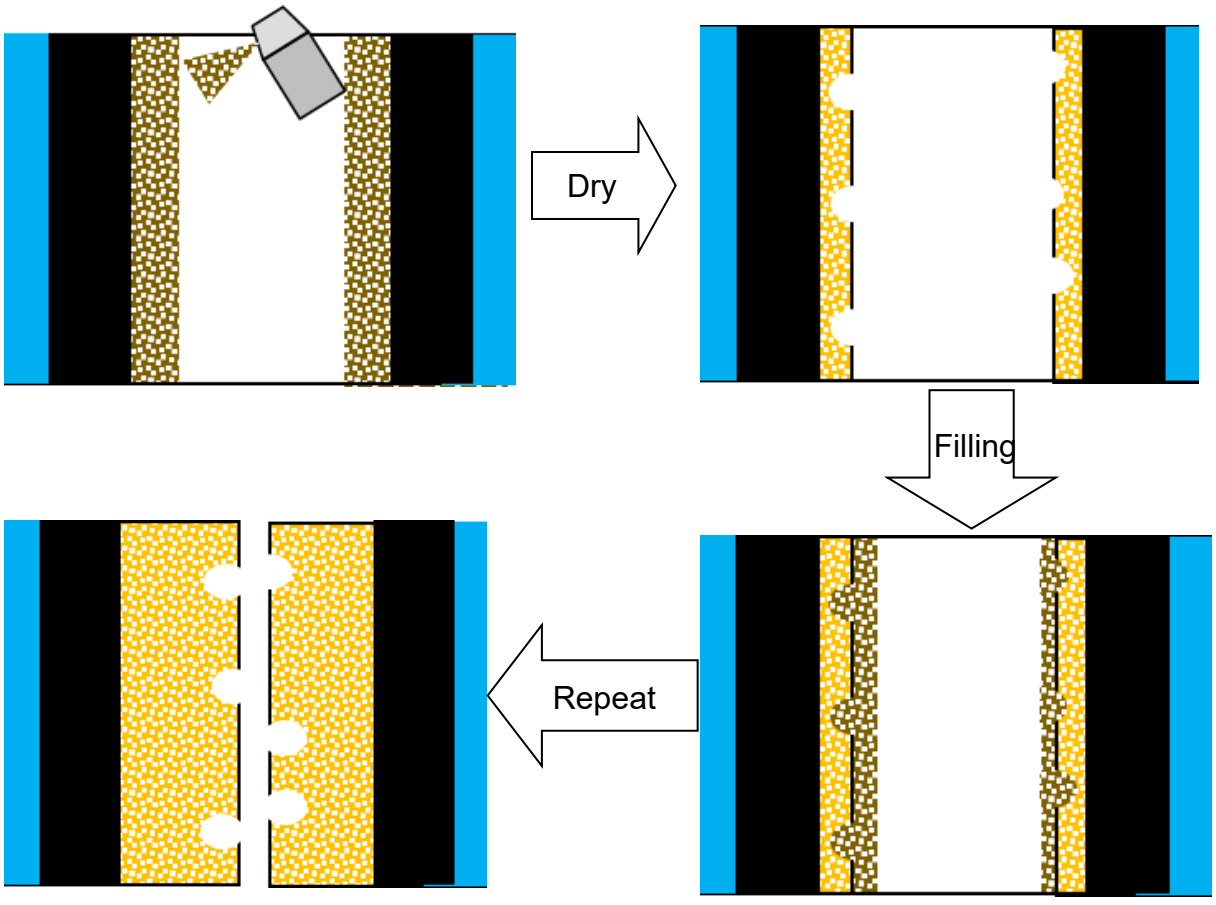

(b) Dip-coating method

Fig. 4.10 Manufacture procedure of different HEXs: (a) Filled-HEX; (b) dip-HEX.

However, the mass ratios of the WSS and additive, which are vital to WSS composite adsorbents [14], [4], are difficult to control using the dip-coating method. Hence, as shown in **Fig. 4.10 (a)**, the dip-coating method was adapted as follows to accommodate the WSS composite adsorbent.

1) The HEX was weighted without an adsorbent. Subsequently, the WSS composite adsorbent slurry was sprayed onto the surface of the corrugated HEX.

2) The corrugated HEX was dried at 120 °C to achieve a coated-HEX;

3) The WSS composite adsorbent slurry was diluted with distilled water to achieve a 1:3 ratio of WSS composite adsorbent to distilled water.

4) The dried HEX was deposited into the diluted slurry prepared in step **3)** for 10 s

5) The HEX was removed from the slurry and dried in an oven at 120 °C for 30 min. The HEX was weighed with the adsorbent to calculate the weight of the adsorbent filled into the HEX.

6) Steps **4)** and **5)** were repeated until a filled WSS composite adsorbent was obtained.

In step **1)**, the extremely thin coating layer of the WSS composite adsorbent slurry enhanced the contact between the adsorbent and HEX for forming a coated-HEX. Furthermore, this thin coating layer serve as the base of the dip-HEX. The viscosity of the WSS composite adsorbent slurry used in the filled-HEX was 25.1 mPa·s, which is much higher than that of water (1.002 mPa·s). This renders the dipping process difficult. Hence, the WSS composite adsorbent slurry was diluted (in step **3)**) to reduce the viscosity to 2.71 mPa·s. According to Togawa et al., the excessive sorption of vapor results in salt leakage and deteriorated performance [4]. Therefore, the dipping process performed in step **4)** was designed to be extremely short (10 s) as compared with the dip-coating method proposed by Zhen et al. to prevent leakage. In addition, an air spray was used to remove the adsorbent block in step **4)** when necessary.

4.3.2. Ad-HEX Preparation

In this study, several new ad-HEXs were prepared for comparison with the conventional filled-HEX. The same series of aluminum corrugated microchannel HEXs was employed in a previous study [14]. As shown in **Fig. 4.11 (a)**, the dimensions and volumes of the original HEX were 140 mm Width × 110 mm Depth × 12 mm Height and 0.1848 L, respectively. The thickness of the microchannel was 1.2 mm, and the span between the microchannels was 8.1 mm. Using the different methods mentioned above, 20 wt.% LiCl impregnated WSS was filled into this HEX to obtain the ad-HEXs. The conventional filled-HEX is shown in **Fig. 4.11 (b)**. The weight of the filled adsorbent and the packing density were 55.96 g and 303 g/L, respectively. Some cracks appeared inside the dried adsorbent owing to the evaporation of the solution during the drying process. **Fig. 4.11 (c)** shows the coated-HEX prepared in step **2)** of **Section 4.4.1**. The weight of the filled adsorbent and the packing density

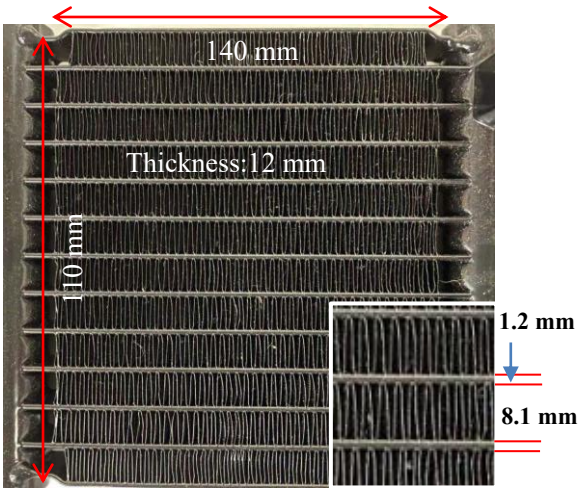

(a)

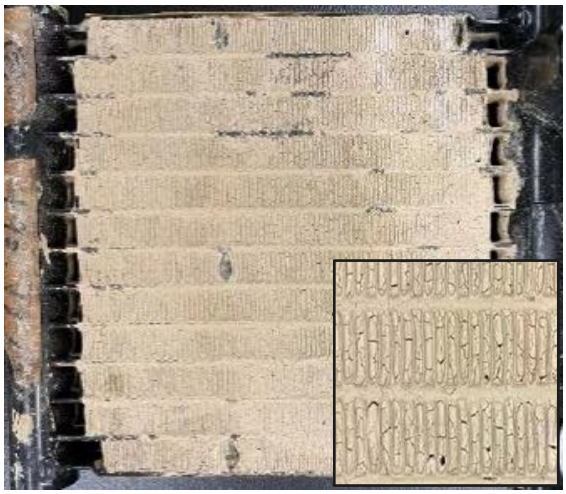

(b)

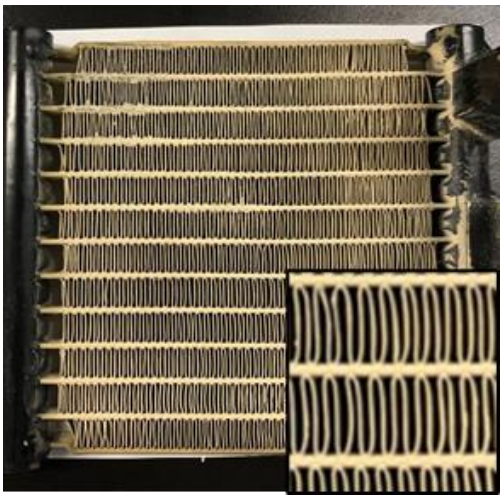

(c)

(d)

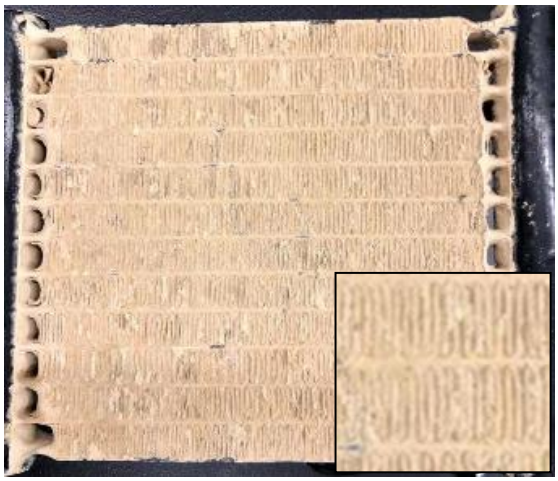

(e)

Fig. 4.11 Ad-HEXs prepared using different method: (a) Original HEX; (b) Filled-HEX; (c) Coated-HEX; (d) Dip-HEX; (e) Dip-filled-HEX.

were 11.72 g and 63 g/L, respectively. The space between the fins was large, which provided a smooth mass transfer. The packing density increased as steps **4)** and **5)** of **Section 4.4.1** were repeated to obtain a dip-HEX, as shown in **Fig. 4.11 (d)**. The weight of the filled adsorbent and packing density were 58.85 g and 318 g/L, respectively, which were similar to those of the filled-HEX. Most of the mass transfer channels remained, although the space between the fins was obstructed partially by the adsorbent. Hence, the dip-coating method was proven to be effective in densifying the adsorbent. As steps **4)** and **5)** of **Section 4.4.1** were further repeated, the dip-HEX transformed into the dip-filled-HEX, as shown in **Fig. 4.11 (e)**. The dip-filled-HEX is similar to the filled-HEX, and the space between the fins was fully filled with the adsorbent. However, almost no crack appeared inside the adsorbent of the dip-filled-HEX; the weight of the filled adsorbent and the packing density were 68.96 g and 380 g/L, respectively.

4.3.3. Performance Evaluation

The weight of the filled adsorbent increased as the dip-coating process was repeated. The system cooling performance afforded by the ad-HEX for different adsorbent weights was assessed. The cycle period was set to 620 s, which included a 300 s sorption/regeneration process and a 10 s pre-cooling/pre-heating process. Ads. 1 was used to evaluate one ad-HEX, and the experimental conditions are listed in **Table 4.7**. The variations in the COP and SCP, as well as the effective rate of utilization of η_u for different adsorbent weights are shown in **Fig.4.12**. The adsorbent weight of the ad-HEX was increased from 11.72 to 54.06 g. The adsorbent weight of the coated-HEX was the lightest at 11.72 g; therefore, it required only a low amount of heat for a full regeneration/sorption. Consequently, a maximum SCP of 0.818 W/g was obtained. However, the cooling amount was relatively low compared with the fixed regeneration amount of the HEX, as shown in **Eqs. (4.2)** and **(4.3)**. Consequently, an extremely low COP of 0.11 was obtained. When the weight of the adsorbent was increased to 54.06 g (dip-HEX), more heat was required for a full regeneration/sorption, and η_u decreased from 60% to 46%. Although the SCP of the dip-HEX decreased slightly to 0.62 W/g because of the decrease in η_u, it remained at a relatively high level compared with those of other adsorbents [30], [8]. However, an increase in the adsorbent amount increased the cooling amount, which improved the VCP from 53 to 185 W/L and significantly improved the COP to 0.28. Hence, increasing the amount of adsorbent used in a HEX can effectively improve the COP of

Table 4.7 Experimental conditions of the dip-coating method experiment.

	Regeneration	Sorption	Condensation	Evaporator inlet
Temperature [°C]	80	30	30	20
Flow rate [L/min]	1.62	1.58	0.64	0.24

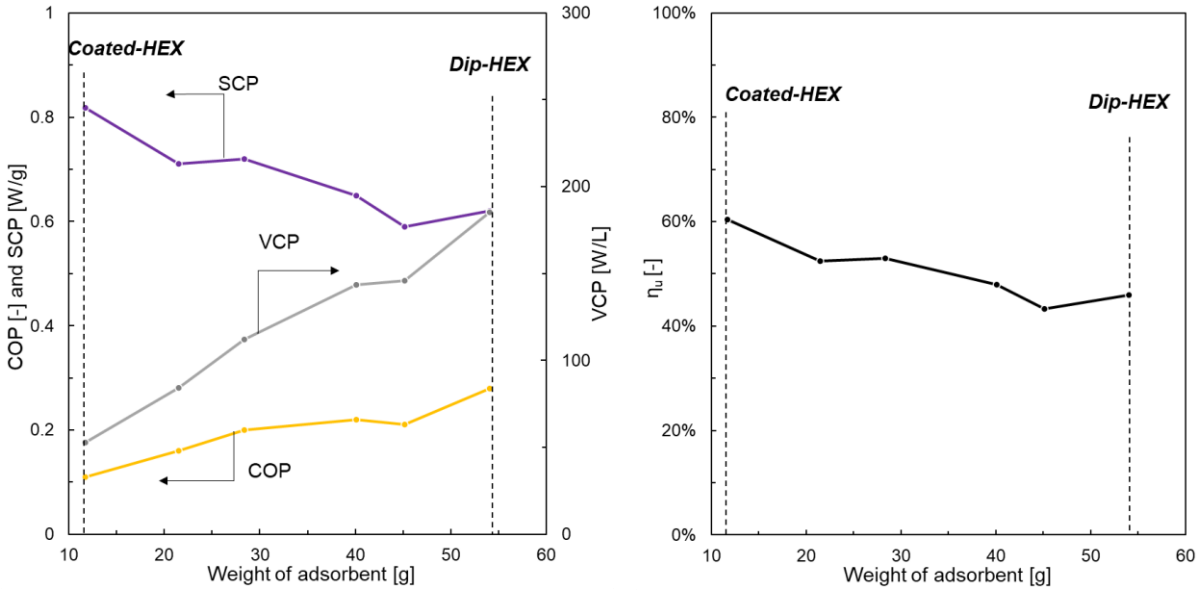

Fig. 4.12 Trends of COP, SCP, and VCP; η_u vs. adsorbent amount on HEX.

AHPs employing this type of ad-HEX, accompanied with an acceptable decrease in the SCP.

Then basic performance experiments were performed to compare the conventional filled-HEX with the dip-HEX and dip-filled-HEX, based on the steps provided in **Section 4.4.1**. Information regarding the filled-HEX, dip-HEX, and dip-filled-HEX are shown in **Table 4.8**. The average packing density of the dip-HEX was 301 g/L; it was well controlled to approximately 308 g/L, which is the average packing density of the filled-HEX. The average density of the dip-filled-HEX was 380 g/L. Thermal couples were set at the surface center of the ad-HEX to measure the temperature response. In this experiment, both sides of the adsorber functioned as intended. The cycle period was changed from 10 to 18 min, and the pre-cooling/pre-heating period was fixed at 10 s.

The results of a representative 18 min cycle are shown in **Fig. 4.13**. **Fig. 4.13 (a)** shows the center temperature responses of each ad-HEX vs. the elapsed time. Compared with the filled-HEX, the dip-HEX and dip-filled-HEX indicated faster temperature responses owing to the densified adsorbent. The temperature response of the dip-filled-HEX was slightly slower than that of the dip-HEX because of the higher amount of adsorbent of the

Table 4.8 Adsorbent used for HEX and packing density of various HEXs.

		Filled-HEX		**Dip-HEX**		**Dip-Filled-HEX**	
		Ads. 1	Ads. 2	Ads. 1	Ads. 2	Ads. 1	Ads. 2
Adsorbent of HEX [g]	individual	57.21	54.70	54.92	54.24	72.44	65.48
	average	55.96		54.58		68.96	
Packing density [g/L]	individual	315	302	303	299	400	358
	average	308		301		380	

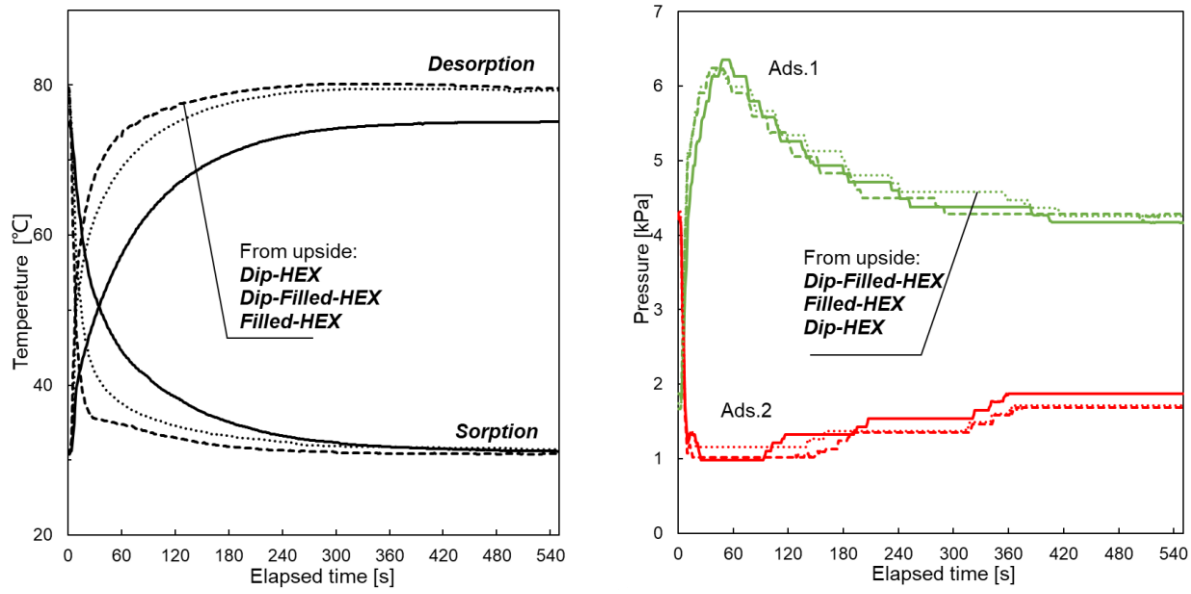

Fig. 4.13 Temperature, pressure, and cooling capacity vs. elapsed time of representative cycle in 18 min: (a) Center temperature response of each ad-HEX; (b) Adsorber pressure of each Ad-HEX; (c) Cooling capacity and integrated cooling amount of each ad-HEX.

dip-filled-HEX. The pressure changes of each ad-HEX vs. the elapsed time are shown in **Fig. 4.13 (b)**. The pressure of both the filled-HEX and dip-HEX decreased to 1 kPa in 10 s of the sorption process; however, the pressure of the filled-HEX was maintained for 90 s, whereas that of the dip-HEX was maintained until 150 s. The pressure of the dip-filled-HEX decreased to 1.2 kPa and then returned to 1.7 kPa at the end of the sorption process, which is also observed in the dip-HEX; however, the abovementioned values were lower than those of the filled-HEX. The pressure changes during the regeneration process were similar to those in the sorption process. The faster temperature response resulted in a more significant pressure change in the dip-HEX than that

in the filled-HEX. The cooling capacity and integrated cooling amount are shown in **Fig. 4.13 (c)**. The cooling capacity of the filled-HEX increased to 115 W and then decreased rapidly to 30 W. The dip-filled-HEX exhibited a mild curve of the cooling capacity, which indicated a peak at 103 W and ended at approximately 48 W. The cooling capacity curve of the dip-HEX was between those of the filled-HEX and dip-filled-HEX. The integrated cooling amount during the sorption process of the dip-HEX was 5% higher than that of the filled-HEX, although almost the same adsorbent amount was filled in the HEXs. It was discovered that the mass transfer channel enhanced mass transfer.

Fig. 4.14 shows the experimental results of a representative cycle in which the dip-HEX was applied vs. the elapsed time in cycle periods of 10, 14, and 18 min. The variations in the cooling capacity were similar to each other, as shown in **Fig. 4.14 (a)**. In all these cases, the cooling capacity increased to 100 W for approximately 60 s, and then the cooling capacity for the cases of 10, 14, and 18 min decreased slightly to 58, 40, and 34 W at the end of the sorption process, respectively. The variations in the regeneration amount almost overlapped with each other. In fact, they increased up to 3.5 kW in only 6 s and then decreased significantly (**Fig. 4.14 (b)**). Hence, the integrated values of the cooling amount increased smoothly over time, whereas the rapid increase in the integrated regeneration amounts lasted until 60 s. The COP, SCP, and η_u calculated based on the cooling and regeneration amounts vs. cycle period curves are shown in **Fig. 4.15**. The COP increased with the cycle period for all the ad-HEXs, as shown in **Fig. 4.15 (a)**. The COP of the dip-HEX was higher than that of the dip-Filled-HEX by up to 11% in a cycle period of 18 min. The dip-Filled-HEX indicated the best COP, which was higher than that of the filled-HEX up to 15% in 18 min of the cycle period. The SCP decreased as the cycle period

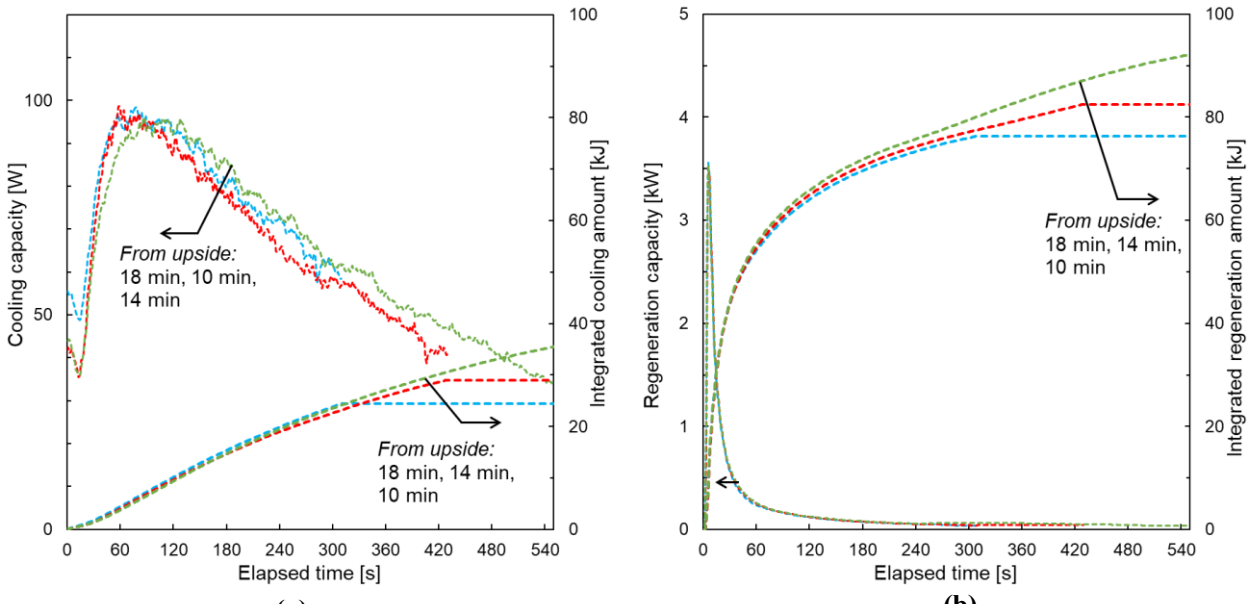

Fig. 4.14 Cooling capacity and regeneration capacity of representative cycle applying dip-HEX vs. elapsed time in cycle periods of 10, 14, and 18 min: (a) Cooling capacity and integrated cooling amount; (b) Regeneration capacity and integrated regeneration amount.

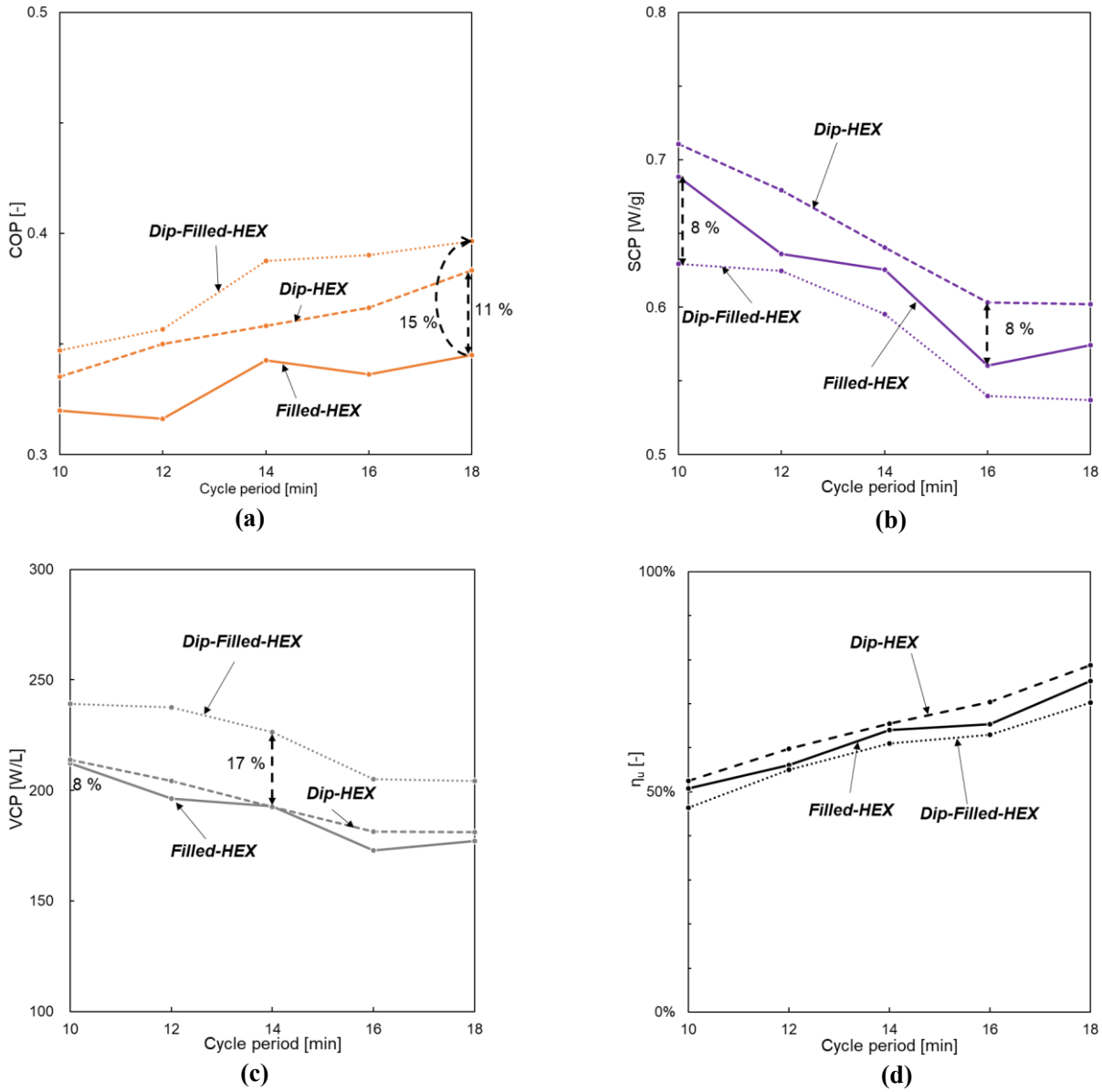

Fig. 4.15 COP, SCP, VCP and η_u vs. cycle period: (a) COP of each ad-HEX; (b) SCP of each ad-HEX; (c) VCP of each ad-HEX; (d) η_u of each ad-HEX.

increased, as shown in **Fig. 4.15 (b)**. The SCP of the dip-HEX was higher than that of the filled-HEX by up to 8%, which is consistent with the result of the integrated cooling amount shown in **Fig. 4.13 (c)**. By contrast, the SCP of the dip-filled-HEX was lower than that of the filled-HEX by 8%. The densified adsorbent without a mass transfer channel resulted in a slower mass transfer. The filled-HEX and the dip-HEX indicated similar VCP values, whereas the VCP of the dip-filled-HEX improved by 17% in a cycle period of 14 min (**Fig. 4.15 (c)**). **Fig. 4.15 (d)** shows the η_u of each ad-HEX vs. the cycle period. The η_u of the filled-HEX was lower than that of the dip-HEX and higher than that of the dip-Filled-HEX; this trend was similarly observed for the SCP. Meanwhile, as the cycle period was changed from 10 to 18 min, the η_u of the filled-HEX, dip-HEX, and dip-Filled-HEX improved from 51%, 52%, and 49% to 75%, 79%, and 71%, respectively. Hence, it was confirmed that the higher cooling performance of the dip-HEX was better than that of the filled-HEX. In this study, the

packing density of the dip-filled-HEX used in Ads. 1 increased to 400 g/L, which was 30% higher than that of the filled-HEX. Hence, the dip-filled-HEX demonstrated a relatively lower SCP; however, its best COP of 0.4 can be attributed to its higher packing density. The COP of the dip-filled-HEX is expected to increase further as the cycle period increases.

4.3.4. Uncertainty

The results of the uncertainties are listed in **Table 4.9**. Because of the small scale of the AHP, the results were affected significantly by the measure error effect. The uncertainties of the COP were primarily 3.1%–4.5%, and only one case indicated a COP of 5%. Meanwhile, the uncertainties of the SCP were 2.5%–3.5%, whereas the uncertainties of the VCP were 2.5%– 4.1%. All these uncertainties were less than 5%; hence, the results of this study were confirmed to be credible.

Table 4.9 Uncertainties of COP, SCP, and VCP.

(a) Experiment based on filling weight.

m_{dry} [g]	11.7	21.5	28.37	40.1	45.14	54.06
COP × 10^{-3} [-]	5.49	7.16	7.85	8.58	8.14	9.20
SCP ×10^{-2} [W/g]	3.86	2.66	2.52	2.11	2.03	1.71
VCP ×10 [W/L]	2.45	3.09	3.87	4.58	4.97	5.01

(b) Basic performance experiment

Cycle period [min]		10	12	14	16	18
COP ×10^{-2} [-]	Filled-HEX	1.03	0.97	1.08	1.14	1.42
	Dip-HEX	1.06	1.20	1.28	1.34	1.62
	Dip-filled-HEX	1.20	1.32	1.42	1.49	1.53
SCP ×10^{-2} [W/g]	Filled-HEX	1.98	1.79	1.67	1.77	2.41
	Dip-HEX	1.78	1.82	1.81	1.78	2.08
	Dip-filled-HEX	1.85	1.88	1.87	1.83	1.82
VCP [W/L]	Filled-HEX	6.30	5.69	5.32	5.63	7.66
	Dip-HEX	5.94	6.08	6.01	5.93	6.94
	Dip-filled-HEX	6.91	7.01	7.00	6.81	6.81

4.3.5. Discussion

The dip-coating method was adapted to accommodate the WSS composite adsorbent. The dip-HEX and dip-filled-HEX were fabricated using this adopted dip-coating method. As shown in **Fig. 4.11 (b)**, the mass transfer of the dip-HEX was smoother as compared with that of the others because of the mass transfer channel, although its packing density was the same as that of the filled-HEX. In addition, a thinner adsorbent layer results in faster mass transfer [31]. Therefore, the COP and SCP of the dip-HEX were higher than those of the filled-HEX, as shown in **Fig. 4.16 (a)** and **(b)**. The packing density can be improved by approximately 30% up to 400 g/L to achieve the dip-Filled-HEX via the dip-coating method. The high packing density of the dip-filled HEX significantly increased the COP; however, this resulted in a slight decrease in the SCP.

The adapted dip-coating method resulted in the effective filling of the ad-HEXs. The mass transfer pass of the ad-HEX was maintained, and the surface area increased, which enhanced sorption/desorption. Meanwhile, the adsorbent packing density can be increased to improve the COP. However, an excessive amount of adsorbent (dip-filled-HEX) resulted in a block of mass transfer pass, as shown in **Fig. 4.12 (e)**, which indicates that the SCP and VCP decreased as the COP increased. In this study, the ad-HEX with an adsorbent weight of 54.6 g (dip-HEX) is optimal.

4.4. Mass Recovery

4.4.1. Mass Recovery Method

The isotherms of WSS impregnated with 20 wt. % of LiCl are shown in **Fig. 4.16**. At the standard experiment conditions shown in **Table 4.2**, the maximum sorption amount depends on the vapor pressure of 1.8 kPa from the evaporation and the sorption temperature of 30 °C, meanwhile the minimum sorption amount depends on the condensation vapor pressure of 4.2 kPa and the regeneration temperature of 80 °C. The theoretical maximum sorption amount q_{max} is the difference between the maximum sorption amount and the minimum sorption amount, it is 0.35 g/g.

A mass recovery method is proposed to change the pressure condition to improve the cooling performance. Two adsorber chamber is connected at the end of the sorption/regeneration processes, the pressure of chamber in regeneration process decreases and the minimum sorption amount decrease, meanwhile the pressure of chamber in sorption process increases and the maximum sorption amount increase, as shown in **Fig. 4.16**. Hence, the theoretical maximum sorption amount is improved from q_{max} to q'_{max} and the sorption/regeneration process can be enhanced to improve SCP/COP.

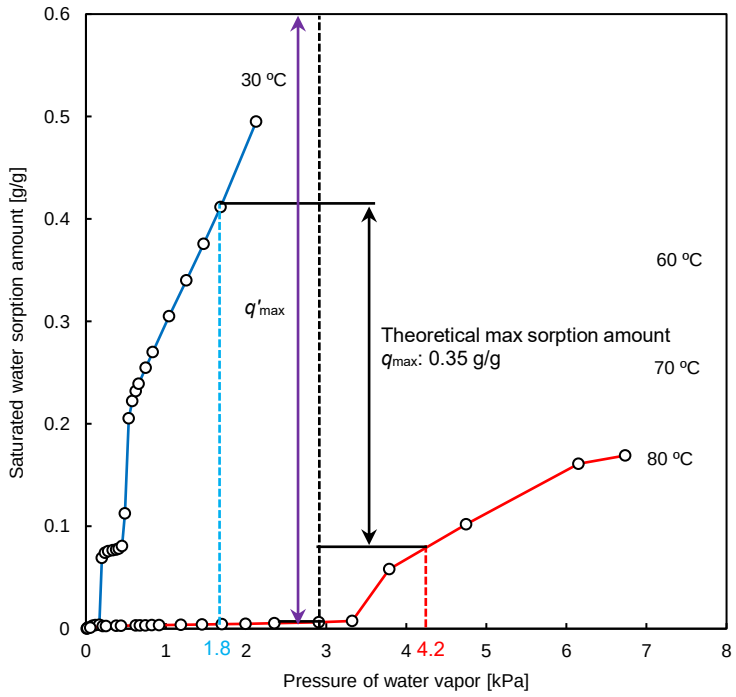

Fig. 4.16 Water vapor sorption isotherms of WSS+20 wt.% LiCl at various temperatures.

4.4.2. Schematic of the Mass Recovery

The schematic illustration of the mass recovery process is shown in **Fig. 4.17**. **Fig. 4.17 (a)** shows the adsorber chambers at the end of the regeneration and sorption processes. The pressures at the high-temperature (HTS)

side absorber (Ads. 1) and low-temperature side (HTS) adsorber (Ads. 2) are 4.2 and 1.8 kPa, respectively. Based on the isotherms shown in **Fig. 4.16**, the adsorbent water sorption amounts approached the saturated water sorption amount, and the regeneration/sorption is almost completed. Subsequently, the hot/cooling water supply is terminated, and two adsorber chambers are connect to each other to begin the mass recovery process, which called A type mass recovery and is shown in **Fig. 4.17 (b)**. The pressure on both sides is 3 kPa because of the connection between the adsorber chambers. The saturated water sorption amount at the HTS decreases and the desorption enhances, whereas the saturated water sorption amount at the LTS increases and the sorption enhances. The LTS can be preheated by the sorption heat without additional heating/cooling to reduce the sensible heat, and the COP can be improved based on **Eq. (4.2)**. Moreover, the sorption amount at the HTS in the next sorption process can be enhanced owing to the desorption at the HTS during the mass recovery process, which results in an increase in Q_c. Hence, the SCP and VCP can be enhanced using **Eq. (4.3)**. Moreover, another type of mass recovery (B type Mass Recovery) is shown in **Fig. 4.17 (c)**. The hot/cooling water during the mass recovery is still provided, the desorption of the HTS and the sorption of the LTS are obviously enhanced. This type of mass recovery focuses on the cooling capacity improvement though COP decreases [23]. In this section, the A type Mass Recovery is introduced because it can improve both COP and SCP. The Filled-HEX, the Dip-HEX and the Dip-Filled-HEX are compared in the cases that the Mass Recovery is introduced. The cycle period and pre-cooling/preheating duration were fixed at 14 min and 10 s, respectively. The mass recovery period is varied from 0 to 60 s.

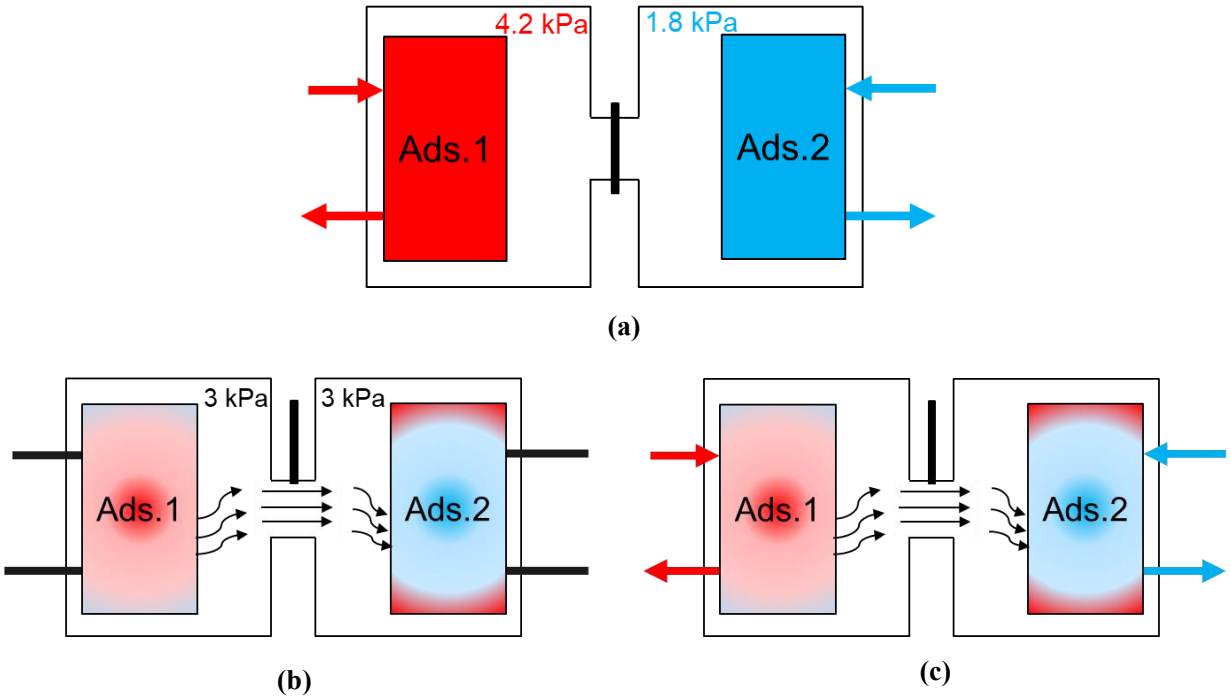

Fig. 4.17 Schematic illustration of mass recovery: (a) End of sorption/regeneration process; (b) A type mass recovery process. (c) B type mass recovery process.

4.4.3. Experiment Results

The experimental results for a mass recovery period of 60 s are shown in **Fig. 4.18**. **Fig. 4.18 (a)** shows the center temperature responses of each ad-HEX vs. the elapsed time during the mass recovery process. For the first 20 s of the mass recovery process, vapor is absorbed rapidly, and the temperatures of the three types of ad-HEXs increase rapidly. As the water sorption progressing, the water sorption amount of the adsorbent approached the saturated water sorption amount, and the temperature increase becomes less significant. The temperature response of the dip-HEX is the fastest and increases up to 41.9 °C, which is 1.4 °C higher than that of the filled-HEX. The larger surface area of the dip-HEX contributes to more sorption and a faster temperature change compared with the filled-HEX. Meanwhile, the dip-filled-HEX demonstrates the slowest temperature response, although its surface area is similar to that of the filled-HEX; this is because its higher amount of adsorbent required a higher amount of heat for heating. Its temperature response is the slowest until 35 s; however, it increases to 41.6 °C at the end of the mass recovery process. The regeneration capacities with and without mass recovery are shown in **Fig. 4.18 (b)**. For the first 15 s of the regeneration process, the regeneration capacities reduced wing to mass recovery, and the preheating effect was confirmed.

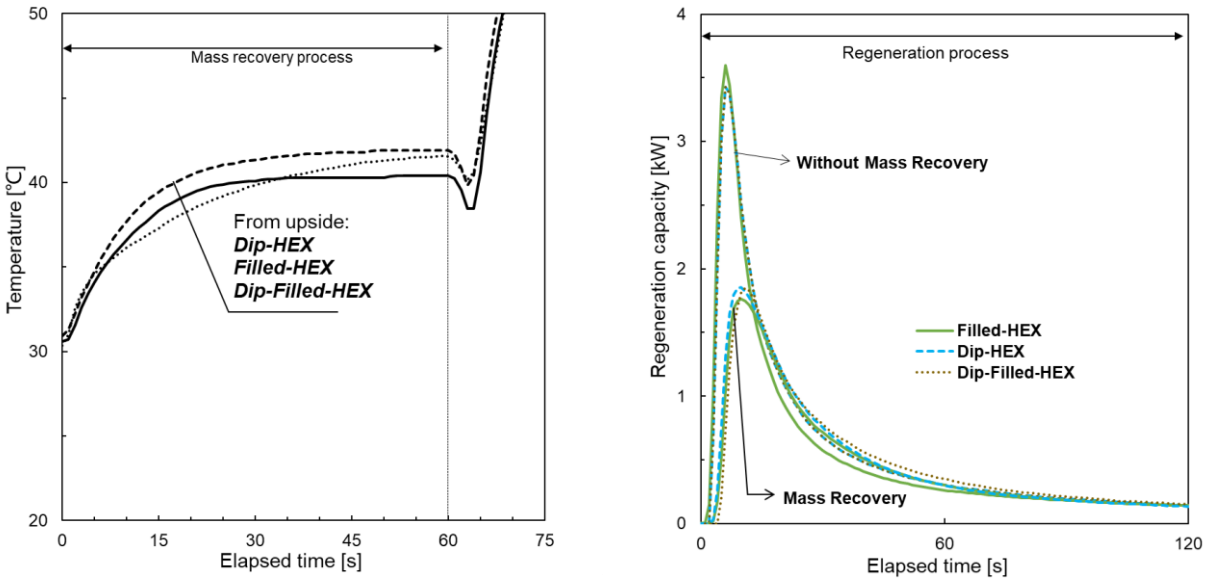

(a) (b)

Fig. 4.18 Temperature and regeneration capacity vs. elapsed time for mass recovery period of 60 s: (a) Temperature responses of each ad-HEX; (b) Regeneration capacity of each ad-HEX.

Fig. 4.19 shows the experimental results of a representative cycle applying dip-HEX vs. the elapsed time for different mass recovery periods. The temperature responses are shown in **Fig. 4.18 (a)**. As shown, that at the HTS decreased to 74 °C in a short mass recovery period of 10 s compared with the HTS of 72.8 °C in the mass recovery period of 60 s. This indicates that 10 s was sufficient for the mass recovery process of desorption/pre-cooling. By contrast, the temperature at the LTS increased to 36.6 °C, 40.6 °C, and 41.6 °C in mass recovery

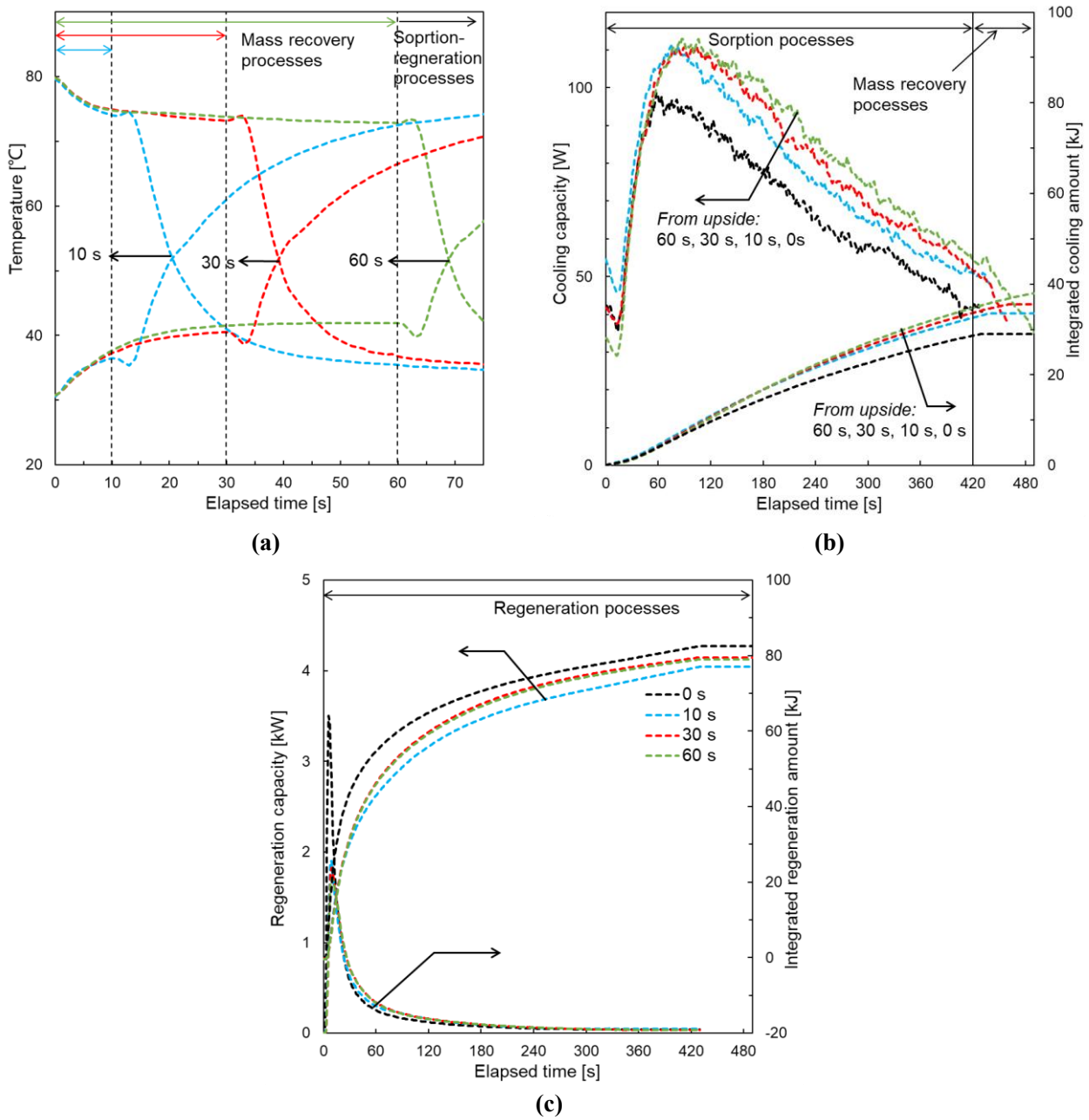

Fig. 4.19 Temperature, cooling capacity, and regeneration capacity of dip-HEX vs. elapsed time for different mass recovery periods: (a) Temperature responses; (b) Cooling capacity; (c) Regeneration capacity.

periods of 10, 30, and 60 s, respectively. Higher temperatures benefit the speed of sorption/desorption [12]; therefore, the LTS required more time to fulfill sorption/pre-heating as compared with the HTS to fulfill desorption/pre-cooling. The variations in the cooling capacity are shown in **Fig. 4.19 (b)**; it was clear that they improved even after 10 s of mass recovery. A longer period of mass recovery can improve the cooling capacity slightly because the HTS desorption is fulfilled. Meanwhile, the cooling capacity decreased rapidly during the mass recovery process because of the absence of evaporation; this indicates that an excessively long mass recovery period results in a decrease in the average cooling capacity, as supported by **Eqs. (3.1)** and **(3.4)**. In addition, the regeneration amount reduced significantly after 10 s of mass recovery, as shown in **Fig. 4.19 (c)**.

Based on these experimental results, a mass recovery period of 10 s was confirmed to be appropriate for the dip-HEX of the current AHP.

The regeneration amount reduction and the cooling amount improvement versus the mass recovery period is shown in **Fig. 4.20.** The regeneration amount reduction of the Dip-HEX can up to 12.5 % in extreme short 5 s, meanwhile the Filled-HEX needs about 30 seconds to achieve the same reduction, which indicate that the enough mass recovery period has been taken. The regeneration amount of the Dip-Filled-HEX can be reduced 15.4 % in 10 seconds. The cooling amount improvement curve of the Filled-HEX and the Dip-Filled-HEX almost overlap with each other. They rise rapidly within 10 seconds, then increase slightly due to the little cooling capacity during the mass recovery process. The Dip-HEX shows a rapid cooling amount improvement within 5 seconds while at least 10 seconds are needed for the Filled-HEX and the Dip-Filled-HEX.

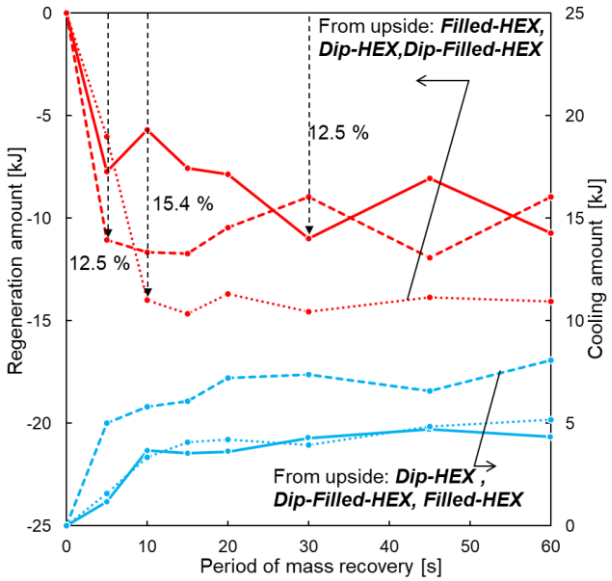

Fig. 4.20 Regeneration amount and cooling amount of different ad-HEXs vs. period of mass recovery.

COP of these Ad-HEX are shown in **Fig. 4.21 (a)**. To obtain the relatively high COP, the Dip-HEX needs only 5 seconds of the mass recovery to raise COP from 0.34 to 0.45, meanwhile the Dip-Filled-HEX needs 10 seconds to raise COP from 0.39 to 0.5. COP of the Filled-HEX can be increased from 0.34 to 0.45 in 30 seconds of the mass recovery period. With the mass recovery period increasing, mass recovery is progressed and SCP of these three kinds of Ad-HEX rise to the peak around 10-20 seconds, as **Fig. 4.21 (b)** shows. SCP of the Filled-HEX, the Dip-HEX and the Dip-Filled-HEX can be enhanced from 0.63 W/g, 0.63 W/g, 0.6 W/g up to 0.69 W/g, 0.75 W/g and 0.64 W/g, respectively. However, the longer period of mass recovery with little increase of cooling amount leads to decrease of SCP. VCP improvement of the Dip-HEX is more than that of the Filled-HEX, as **Fig. 4.21 (c)** shown. VCP of the Filled-HEX, the Dip-HEX and the Dip-Filled-HEX are enhanced up to 212 W/L,225 W/L and 244 W/L, respectively. η_u of each Ad-HEX versus the period of the mass recovery are shown in **Fig. 4.21 (d)**. It was reported that too much sorption of vapor result in leakage of salt and performance

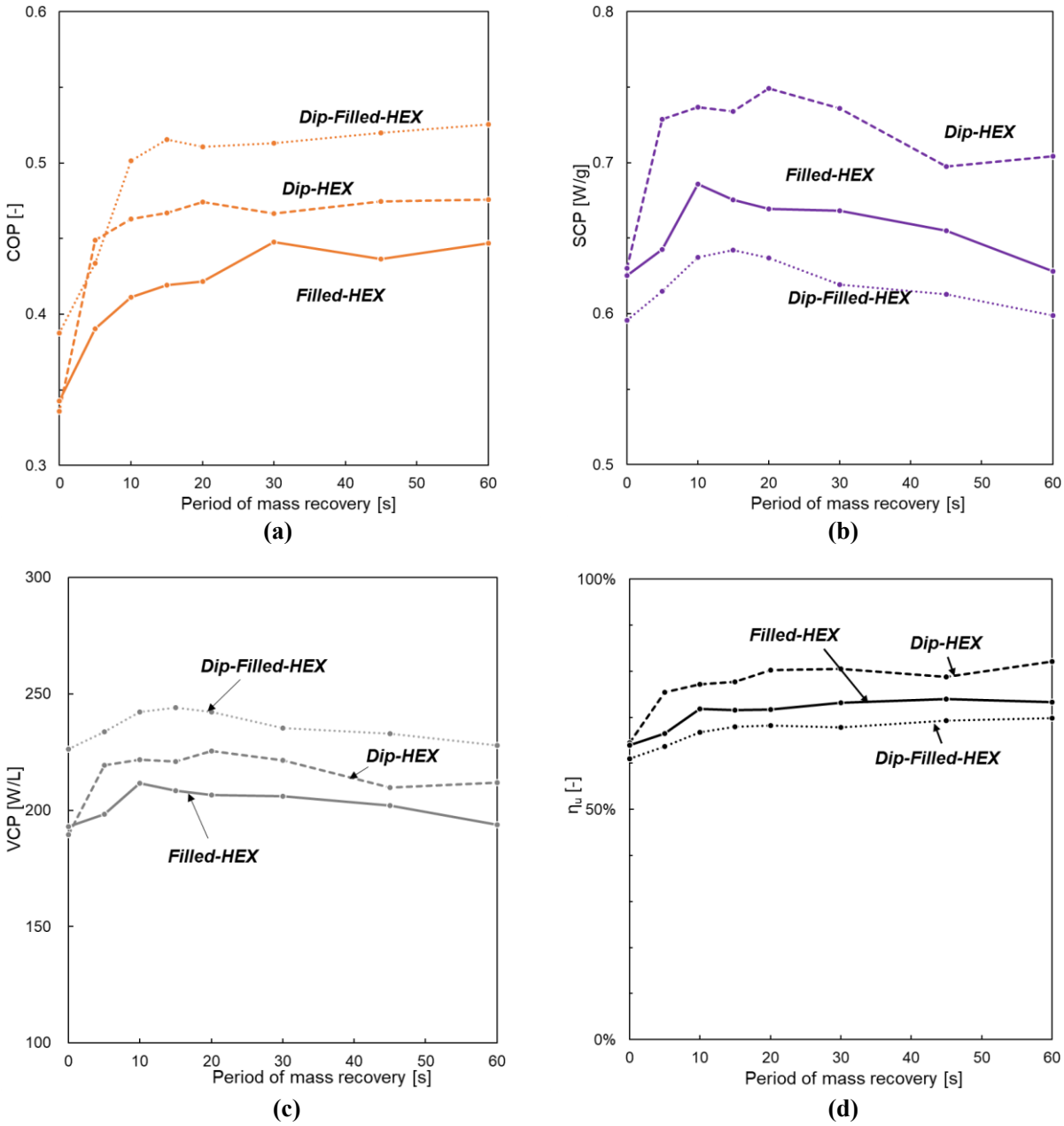

Fig. 4.21 Experimental result of different ad-HEXs vs. period of mass recovery: (a) COP of each ad-HEX; (b) SCP of each ad-HEX; (c) VCP of each ad-HEX; (d) η_u of each ad-HEX.

reduction by Togawa et al. [4]. In this study, all the adsorbed water is still maintained in the mesoporous pores though η_u of the Dip-HEX is enhanced from 64 % up to 82 %. Besides, η_u of the Filled-HEX and the Dip-Filled-HEX are improved from 64 %, 61 % to 73 %, 70 % with the mass recovery of 60 seconds, respectively.

4.4.4. Discussion

An advanced cycle called the Mass Recovery is introduce and experimentally studied. All these Ad-HEX shows obvious improvement of COP and SCP with the mass recovery (**Fig. 4.21 (a)** and **(b)**). According to the method of Seol et al., the interfacial mass transfer of the adsorbent is stable and much larger than the internal mass transfers. For a short period of sorption/desorption, the sorption/desorption amount mainly depend on the

surface area. As **Fig. 4.20** shown, the cooling amount increasing of the Dip-Filled-HEX almost overlap that of the Filled-HEX due to the same surface area, and 10 seconds of mass recovery is needed to enhance the cooling amount to a relative high level. Meanwhile, the cooling amount increasing of the Dip-HEX is more than others and only 5 seconds is enough to fulfill. On the other hand, high temperature of the adsorbent contributes much faster desorption. The Dip-HEX need only 5 seconds of mass recovery to reduce the regeneration amount fully, however, its reduction amount is the same level to those of the Filled-HEX over 30 seconds of mass recovery. The Dip-Filled-HEX shown more regeneration amount reduction than the Filled-HEX and the Dip-HEX while the mass recovery period of 10 seconds is taken. The internal mass transfers is enhanced due to the high temperature and the larger packing density benefit the regeneration amount reduction. As the result, the mass recovery is proved to be a very effective advanced cycle to enhance COP and SCP. The Dip-HEX is a better Ad-HEX compared with others, because its large surface area contributes to void longer mass recovery period that may cause SCP and VCP decrease.

The cooling performance of the current AHP is tried to compare with some prior researches. Current AHP shows VCP of 244 W/L, which is a great advantage over the silica gel AHP [7], the synthetic zeolites AHP [8], [15], [17], [25] and the composite AHP [27]. Meanwhile the highest SCP of 0.74 W/g can be obtained by current AHP. It is higher than other AHP [1], [24], [16], [27]. COP achieved by current AHP is 0.46, which is not high compared with that of silica gel AHP [1], [16]. COP improvement is limited by the small scale of current AHP. It could be enhanced with the scale up of AHP in the future. On the other hand, the WSS composite adsorbent used in current AHP is obviously cheaper than the synthetic zeolites and the silica gel [14]. Thus, the combine of the Dip-HEX and the mass recovery are proved to be competitive way to improve the cooling performance of AHP.

4.4.5. Uncertainty

The results of the uncertainties are listed in **Table 4.10**. All these uncertainties were less than 5%; hence, the results of this study were confirmed to be credible.

Table 4.10 Uncertainties of COP, SCP and VCP in the Mass Recovery Experiment.

Period of mass recovery [s]		5	10	15	20	30	45	60
COP $\times 10^{-2}$ [-]	Filled-HEX	1.48	1.30	1.74	1.93	1.90	1.41	2.08
	Dip-HEX	1.67	1.69	1.76	1.71	1.67	1.85	1.74
	Dip-Filled-HEX	1.46	1.67	1.82	1.80	1.75	1.78	1.84
SCP $\times 10^{-2}$ [W/g]	Filled-HEX	2.14	2.13	2.72	2.76	2.79	2.00	2.79
	Dip-HEX	2.26	2.32	2.28	2.25	2.20	2.25	2.16
	Dip-Filled-HEX	1.88	1.89	1.89	1.87	1.86	1.88	1.86
VCP [W/L]	Filled-HEX	6.51	6.45	8.24	8.36	8.45	6.05	8.44
	Dip-HEX	6.86	7.05	6.93	6.84	6.67	6.81	6.56
	Dip-Filled-HEX	7.02	7.06	7.04	6.99	6.93	7.01	6.94

4.5. Conclusion

In this chapter, the ad-HEX and an advanced cycle of the Mass Recovery are studied in a 100 W AHP.

Two types of the HEX, which are the PFT-HEX and the MC-HEX, are applied as the holder of the adsorbent to manufacture the ad-HEX. For the merits of lighter HEX, less remained water and more space, COP of the PFT-HEX can be improved further with the packing density increase and longer cycle period. However, the MC-HEX shows the better heat transfer, higher SCP can be obtained. In addition, the limit thickness of the commercial PTF-HEX is 25 mm while that of the MC-HEX can be reduced to 12 mm owing to its structure, which leads to compact of the ad-HEX. Thus the MC-HEX is proved to be better than the PFT-HEX.

Subsequently, a Dip-coating method is introduced and adjusted to accommodate the WSS composite adsorbent. Three kinds of Ad-HEX (Filled-HEX, Dip-HEX, Dip-Filled-HEX) are fabricated using this adopted Dip-coating. Compared with the conventional Filled-HEX, the Dip-HEX possesses the mass transfer channels inner the adsorbent layer, which contribute to better mass transfer [31]. Therefore, COP and SCP of the Dip-HEX were higher than those of the filled-HEX. The packing density can be improved by approximately 30% up to 400 g/L to achieve the Dip-Filled-HEX via the adopted Dip-coating method. The high packing density of the dip-filled HEX significantly increased the COP; however, this resulted in a slight decrease in the SCP.

Then an advanced cycle called the Mass Recovery is introduce and experimentally studied. With the proper mass recovery period of 10 seconds, COP of the current AHP applied the Filled-HEX, the Dip-HEX and the Dip-Filled-HEX are improved up to 0.41, 0.46 and 0.5, respectively. SCP of the current AHP applied the Filled-HEX, the Dip-HEX and the Dip-Filled-HEX increases up to 0.69 W/g, 0.74 W/g and 0.64 W/g, respectively, meanwhile VCP are increased to 211 W/L, 222 W/L and 242 W/L. Sorption/desorption of adsorbent during the mass recovery process depend on the filling type of the Ad-HEX, larger surface area obviously increase the sorption/desorption speed and enhances then mass recovery.

It is found that the Dip-HEX is a completely advanced Ad-HEX than the conventional Filled-HEX at both COP and SCP. Larger surface of the Dip-HEX contributes to faster regeneration/sorption at a short period, such as 10 seconds of the mass recovery.

NOMENCLATURE

C_p : Specific heat [J/(g·K)]

m : Mass [g]

m_{dry} : Mass of the dry adsorbent [g]

q : Sorption amount [g/g]

q_{max} : Theoretical maximum sorption amount [g/g]

Q : Amount of heat [J]

R : Parameter [-]

T : Temperature [℃]

t : Time [s]

t_{cyc} : Cycle time [s]

u : Uncertainty [-]

x : Measured parameter [-]

V : Volume [m^3/s]

$\dot{V}$: Flowrate [m^3/s]

GREEK SYMBOLS

η : Coefficient of efficiency [-]

ρ : Density [g/m^3]

$\triangle T$: Temperature difference [℃]

$\triangle H_w$: Vaporization latent heat of the water [J/g]

SUBSCRIPTS

ads : Adsorber

adsorbent : Adsorbent

Al : Aluminum sheet

bs : Basic case

b : Begin

c : Cooling

con : Condenser

connector : Connector

des : Desorption

e	: End
en	: Entire machine
evp	: Evaporator
evporation	: Evaporation
HEX	: Heat exchanger
hr	: Heat recovery
ht	: Hot water tank
i	: Number of cycles
I	: Number of parameter
in	: Inlet
loss	: Unknown heat loss
lt	: Latent heat
max	: Maximum
n	: Number of cycles in all
N	: Number of parameters in all
out	: Outlet
ps	: Passive heat recovery
r	: Return
rw	: Remained water
reg	: Regeneration process
R	: Parameter
s	: Supply
sor	: Sorption process
ss	: Sensible heat
tube	: Tube
u	: Effective utilization rate of the adsorbent
w	: Water

Reference

[1] Jung-Yang San, Fu-Kang Tsai. Testing of a lab-scale four-bed adsorption heat pump. *Applied Thermal Engineering* 2014;70:274-281.

[2] Q. W. Pan, R. Z. Wang, L. W. Wang. Comparison of different kinds of heat recoveries applied in adsorption refrigeration system. *Refrigeration* 2015;55:37-48.

[3] M. M. Saleh, A. D. Raya, M. Saad, E. Eman, E. S. Osama. Wire fin heat exchanger using aluminium fumarate for adsorption heat pumps. *Applied Thermal Engineering* 2020;164:114426.

[4] J. Togawa, A. Kurokawa, K. Nagano. Water sorption property and cooling performance using natural mesoporous siliceous shale impregnated with LiCl for adsorption heat pump. *Applied Thermal Engineering* 2020;173:115241.

[5] H. Liu, K. Nagano, A. Morita, J. Togawa, M. Nakamura. Experimental testing of a small sorption air cooler using composite material made from natural siliceous shale and chloride. *Applied Thermal Engineering* 2015;82:68-81.

[6] V. Palomba, B. Dawoud, A. Sapienza, S. Vasta. On the impact of different management strategies on the performance of a two-bed activated carbon/ethanol refrigerator: An experimental study, *Energy Conversion and Management* 2017;142:322-333.

[7] Z.S. Lu, R.Z. Wang. Performance improvement by mass-heat recovery of an innovative adsorption air-conditioner driven by 50-80 ºC hot water. *Applied Thermal Engineering* 2013; 55:113-120.

[8] A. Sapienza, S. Santamaria, A. Frazzica, A. Freni. Influence of the management strategy and operating conditions on the performance of an adsorption chiller. *Energy* 2011; 36:5532-5538.

[9] Q.W. Pan, R.Z. Wang. Experimental study on operating features of heat and mass recovery processes in adsorption refrigeration. *Energy* 2017;135:361-369.

[10] M. M. Tokarev, L. G. Gordeeva, A. I. Shkatulov, Y. I. Aristov. Testing the lab-scale “Heat from Cold” prototype with the “LiCl/silica – methanol” working pair. *Energy Conversion and Management* 2018;159:213-220.

[11] A. Myat, N.K. Choon, K. Thu, Y.D. Kim. Experimental investigation on the optimal performance of Zeolite-water adsorption chiller. *Applied Energy* 2013;102:582-590.

[12] M. Verde, L. Cortes, J.M. Corberan, A. Sapienza, S. Vasta, G. Restuccia. Modelling of an adsorption system driven by engine waste heat for truck cabin A/C. performance estimation for a standard driving cycle. *Applied Thermal Engineering* 2010;30:1511-1522.

[13] H. Liu, K. Nagano, J. Togawa. Performance of LiCl impregnated mesoporous material coating over corrugated heat exchangers in a solid sorption chiller. *Energies* 2018;11(6):1565:1-15.

[14] F. He, K. Nagano, J. Togawa; Experimental Study and Development of a Low-Cost 1 kW Adsorption Chiller using Composite Adsorbent based on Natural Mesoporous Material. *Energy* 2020;209:118365.

[15] A. Freni, L. Bonaccorsi, L. Calabrese, A. Caprì, A. Frazzica, A. Sapienza. SAPO-34 coated adsorbent heat exchanger for adsorption chillers. *Applied Thermal Engineering* 2015;82:1-7

[16] Q.W. Pan, R.Z. Wang, L.W. Wang, D. Liu. Design and experimental study of a silica gel-water adsorption chiller with modular adsorbers. *Refrigeration* 2016;67:336-344.

[17] A. Sapienza, G. Gullì, L. Calabrese, V. Palomba, A. Frazzica, V. Brancato, D. La Rosa, S. Vasta, A. Freni, L. Bonaccorsi, G. Cacciola. An innovative adsorptive chiller prototype based on 3 hybrid coated/granular adsorbers. *Applied Energy* 2016;179:929-938.

[18] X. Zheng; T. S. Ge; Y. Jiang, R. Z. Wang. Experimental study on silica gel-LiCl composite desiccants for desiccant coated heat exchanger. *International Journal of Refrigeration* 2015, 51, 24-32.

[19] Chiang, Y. C., Chen, C. H., Chiang, Y. C., & Chen, S. L., Circulating inclined fluidized beds with application for desiccant dehumidification systems. *Applied Energy* 2016, 175, 199–211.

[20] Grabowska, K., Zylka, A., Kulakowska, A., Skrobek, D., Krzywanski, J., Sosnowski, M., Ciesielska, K., & Nowak, W., Experimental Investigation of an Intensified Heat Transfer Adsorption Bed (IHTAB) Reactor Prototype, *Materials* 2021.

[21] N. Douss, F. N. Meunier, Lian-Ming Sun. Predictive model and experimental results for a two-adsorber solid adsorption heat pump. *Ind. Eng. Chem. Res* 1988;27:310-316.

[22] Z.S. Lu, R.Z. Wang, T.X. Li, L.W. Wang, C.J. Chen. Experimental investigation of a novel multifuncion heat pipe solid soption icemaker for fishing boats using CaCl2 - activated carbon compound – ammonia. *Refrigeration* 2007;30:76-85.

[23] A. Akahira, K.C.A. Alam, Y. Hamamoto, A. Akisawa, T. Kashiwagi. Mass recovery adsorption refrigeration cycle - improving cooling capacity. *Refrigeration* 2004;27: 225-234.

[24] A. Akahira, K.C. A. Alam, Y. Hamamoto, A. Akisawa, T. Kashiwagi. Mass recovery four-bed adsorption refrigeration cycle with energy cascading. *Applied Thermal Engineering* 2005;25:1764-1778.

[25] A. Sapienza, V. Palomba, G. Gulli, A. Frazzica, S. Vasta. A new management strategy based on the reallocation of ads-/desorption times: Experimental operation of a full-scale 3 beds adsorption chiller, *Applied Energy* 2017;205:1081-1090.

[26] F. He, K. Nagano, S. H. Seol, J. Togawa. Thermal performance improvement of AHP using corrugated heat exchanger by dip-coating method with mass recovery. *Energy* 2022;239:122418.

[27] L. Jiang, R. Z. Wang, L. W. Wang, J. Y. Liu, P. Gao, F. Q. Zhu, A. P. Roskilly. Performance analysis on a novel compact two-stage sorption refrigerator driven by low temperature heat source. *Energy* 2017;135:476-485.

[28] P.C.Thimmaiah, A.Sharafian, W.Huttema. C.McCague, M.Bahrami. Effects of capillary-assisted tubes with different fin geometries on the performance of a low-operating pressure evaporator for adsorption cooling system applications. *Applied Energy* 2016;171:256-265.

[29] P.C.Thimmaiah, A.Sharafian, M.Rouhani, W.Huttema. Evaluation of low-pressure flooded evaporator performance for adsorption chillers. *Energy* 2017;122:144-158.

[30] A. Akahira, K. C. A. Alam, Y. Hamamoto, A. Akisawa, T. Kashiwagi. Experimental investigation of mass recovery adsorption refrigeration cycle. *Refrigeration* 2005;28:565-572

[31] S. H. Seol, K. Nagano, J. Togawa. A new experimental method to separate interfacial and internal mass transfer on coated adsorbent. *Applied Thermal Engineering* 2019;159:113869.

Chapter 5

Parameter Studies with a Three-Dimensional Model

Introduction

Numerical simulation is an economic and effective way to analyze and evaluate the AHP. The new method and design can be employed easily with the simulation [1], [2], [3], and the long-term performance prediction in different conditions is available [4], [5], [6]. The zero-dimensional model is generally applied for the AHP system performance prediction in lots of researches [1], [4], [6], meanwhile the three-dimensional model is used for analysis of the HEX [2], [3] or adsorbent layer [5]. A zero-dimensional model has been built in our prior study for the performance prediction [7]. However, the distributions of the temperature and sorption speed in different adsorbent layers are unavailable in this zero-dimensional model, which is very important for the mass recovery process.

The objective of this chapter is to predict and analyze the cooling performance of the AHP. A three-dimensional model of the adsorber filled with the adsorbent was built. At the standard conditions of 80℃-regeneration, 30℃-sorption, 30℃-condensation, 20℃-evaporator inlet and cycle period of 14 minutes, an acceptable error of COP and SCP were confirmed for this model. This model is available for the prediction and parameter study. Then the HR [2], [8] was performed and a new induce of Value Factor (VF) was proposed to determine the optimal system parameters. Subsequently, the MR [1] was introduced and combined with the HR to enhance the cooling performance. It was found that the recoverable sensible heat amount in a representative cycle is limited and shared by the MR and the HR. The HR shows higher heat amount reduction rate, meanwhile the MR not only enhance the sorption process but also reduce the regeneration heat.

5.1. Description of System

The target AHP unit, which has been described in **Chapter 3** [8], is shown in **Fig. 5.1 (a)**. This AHP unit consisted of an evaporator, a condenser and two adsorbers, their dimensions are shown in **Fig. 5.1 (b)**. Two and four pieces of small corrugated fin-type blank HEXs (bk-HEXs, W270 × D100 × H25.6) were set in the chambers of the evaporator and condenser, respectively. The evaporator chamber and the adsorber chambers were connected by four of ball type valves, meanwhile the adsorber chambers and the condenser chamber were connected by four of plate type valves.

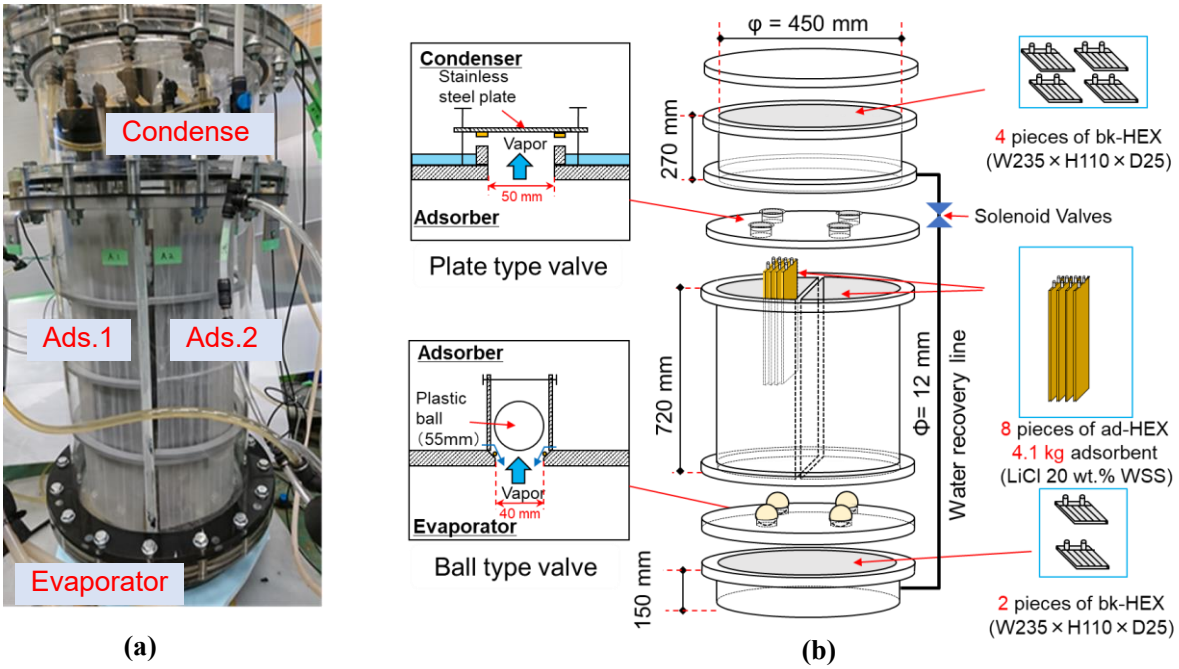

Fig. 5.1 Experiment devices: (a) View of AHP; (b) AHP unit.

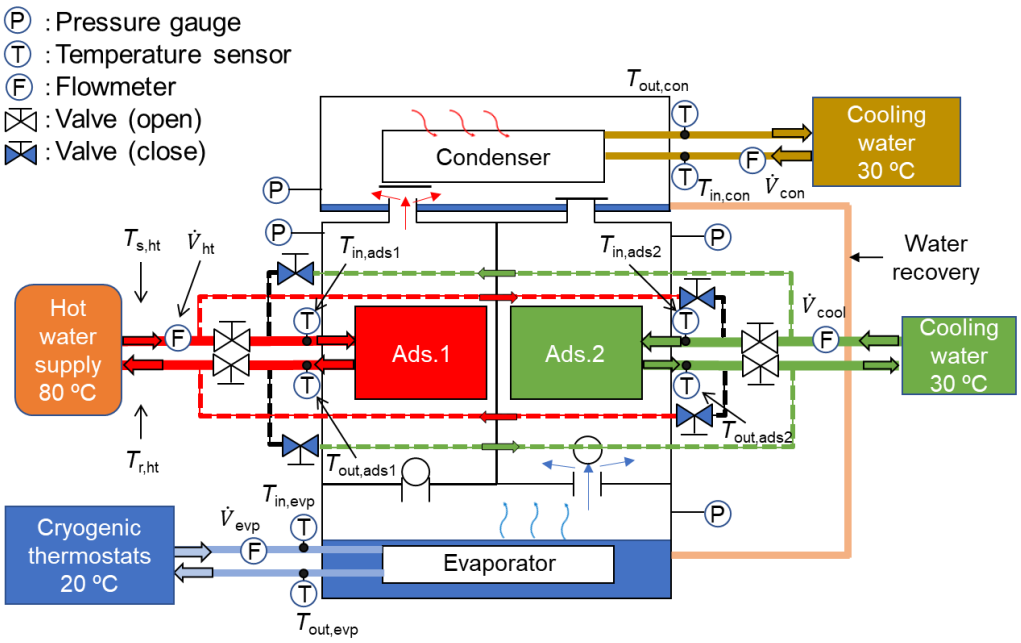

Fig. 5.2 Experiment schematic.

Fig. 5.2 shows the schematic of the AHP system. The hot/cooling water are circulated into different adsorbers with the time pass to switch this AHP between **Mode A** and **Mode B**, which are described as following:

Mode A: The evaporator chamber is connected to the Ads.2 chamber and they are in sorption process. The cooling ability is provided by the vaporization of the water in the evaporator chamber. The vapor from the evaporator chamber move to Ads.2 to be adsorbed, the released sorption heat is taken off by the cooling water. Meanwhile the Ads.1 chamber is connected to the condenser chamber, and they are in regeneration process. The hot water is flowed into Ads.1, in which the vapor is desorbed then move to the condenser to be condensed. The released condensation heat is taken off by the cooling water.

Mode B: The evaporator chamber is connected to the Ads.1, they are in sorption processes. Meanwhile the Ads.2 chamber is connected to the condenser chamber, they are in regeneration processes. The mass transfer and the heat transfer are switched with the mode switching.

5.2. Numerical Modeling of AHP

An overall model is developed to simulate the working of the AHP and evaluate its performance. This AHP is separated to several parts and described by some functions based on the heat and mass transfer to simplify this system. Some advanced cycles are studied in this paper, they depend on the properties of the adsorbers. Furthermore, some phenomenon such as transients of temperature and sorption amount are reflected to the adsorber. Therefore a three-dimensional model is built to describe the adsorbers in detail. The zero-dimensional models are applied for the evaporator and the condenser. For this overall model, the assumptions have been considered as following:

1) The temperature of the whole evaporator chamber, including the HEX, tubes and the container, is uniform. The same condition is fitted to the temperature of the condenser.
2) There is no leakage for the whole AHP system. The inner space of the AHP is always full of vapor.
3) The vaporized water amount equals the vapor amount adsorbed by the adsorbent, meanwhile the condensed water amount equals the vapor amount desorbed from the adsorbent.
4) The vapor mass transfer between the evaporator-adsorber/adsorber-condenser only depends on the sorption/regeneration speed, the speed of evaporation/condensation is not considered.
5) The water amount in evaporator/condenser is constant. The vaporized water amount is replenished by the recovered water from the condenser immediately, meanwhile the water amount returned back to the evaporator is replenished by the vapor condensation from the adsorber immediately.
6) The specific heat of the adsorbent, the HEX and the water are independent of their temperature, their values are taken account as the constant.

All the basic governing equations applied for this AHP in the following depend on these assumptions above. The overall model has been developed with MATLAB. This overall model includes models of evaporator, condenser and 2 adsorber chambers, they are described in the next sections.

5.2.1. Reactor Model

5.2.1.1 Modeling of the Adsorber

The composite adsorbent of Wakkanai Siliceous Shale (WSS) impregnated with 20 wt.% of LiCl, which is a kind of salt inside porous matrix and has been studied by our team in the prior studies [7-14], was employed as

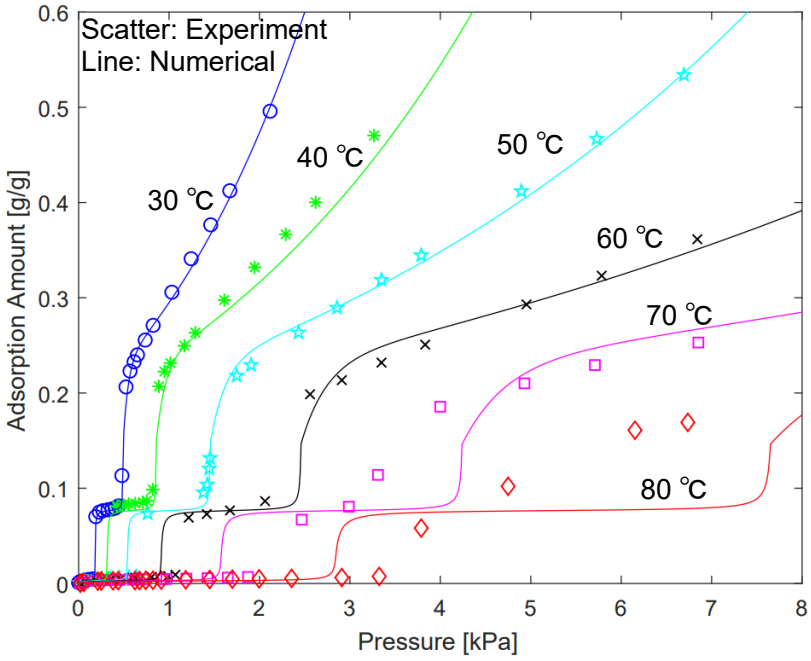

Fig. 5.3 Isotherms of WSS composite adsorbent.

$$q^* = 6.257 \times 10^{-4} \times \tan\left(77 \times (50 \times Pr \times Np\ -\ 1)\right) + 2.736 \times 10^{-3} \quad (P_r < 0.0431/Np)$$

$$q^* = 1.453 \times 10^{-3} \times \tan\left(24.36 \times (100 \times Pr \times Np\ -\ 7.925)\right) + 7.65 \times 10^{-2} \quad (0.0431/Np \le P_r \le 0.1157/Np) \tag{5.1}$$

$$q^* = 0.1837 \times \exp(2.01 \times Pr \times Np)\ - 560.1 \times \exp(-75.93 \times Pr \times Np) \quad (0.1157/Np < P_r)$$

$$Np = 0.999999 \times (T_a - 30)^{3.25} \tag{5.2}$$

the adsorbent. The isotherms of this adsorbent were measured by Togawa et al [15], then Seol et al built a zero-dimensional model for performance prediction [7], in which the isotherms of the WSS composite were presented with a special function [16]. In this study, a simplified function of the **Eqs. (5.1)** and **(5.2)** is applied, the measured equilibrium adsorption isotherm and the numerically fitted adsorption isotherm are shown in **Fig. 5.3**. The numerical isotherm curves fit the experiment results well in low pressure range (1-2 kPa) at 30 ℃, which is the common sorption process condition. This WSS composite was filled in the bk-HEX (W400 × D300 × H12) to obtain the adsorbent filled HEX (ad-HEX), as shown in **Fig. 5.4**. The specification of the ad-HEX is shown in **Table. 5.1**. Each bk-HEX possesses 33 of micro channels, the adsorbent is filled into the gap of the micro channels and dried, as shown in **Fig. 5.5 (a)**. The adsorbent layer between the micro channels is separated into 4 of symmetric small area, the mass transfer only occurs from 2 directions, which are the surface of the adsorbent. The adsorbent layer is separated into 4 of representative symmetric small area, as shown in **Fig. 5.5 (c)**. Hence

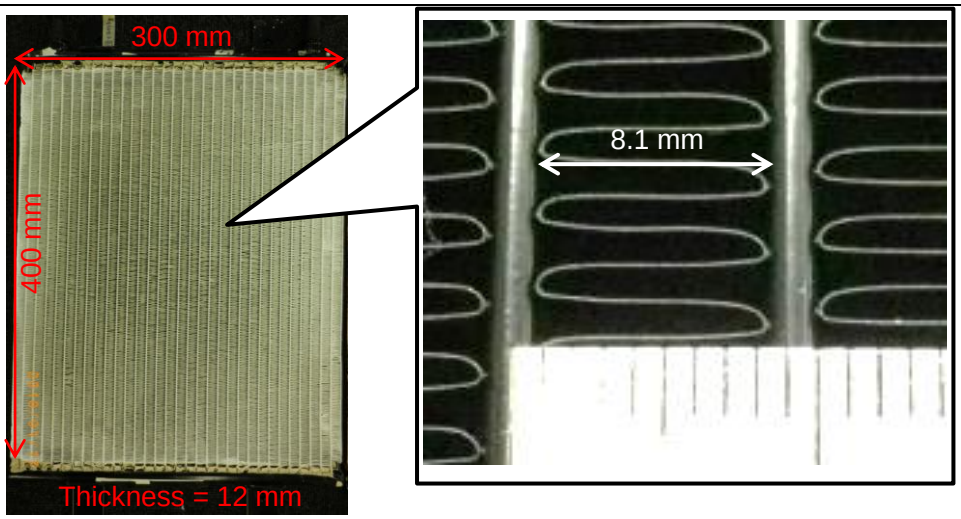

Fig. 5.4 Adsorbent filled HEX (ad-HEX).

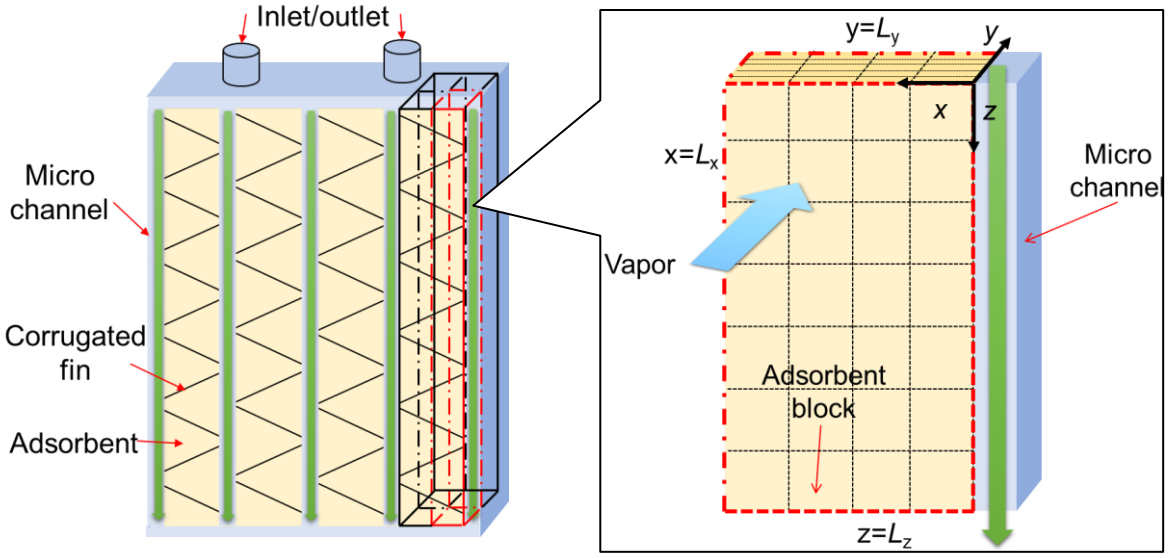

(a) **(b)**

Fig. 5.5 Modeling of the ad-HEX: (a) Schematic of the ad-HEX; (b) Schematic of a representative absorbent small area.

Table 5.1 Specification of the ad-HEX.

Dimension of HEX	Material of HEX	Weight of HEX	Numbers of HEX in each reactor chamber
400 mm × 300 mm × 12 mm	Aluminum	850 g	4
Adsorbent	Weight	Packing density	Total weight in each reactor chamber
WSS + 20 wt.% LiCl	512.5	356 g/L	2.05

the sorption/desorption of the entire adsorber can be calculated by the numerical analysis of this representative small area. The representative small area is further separated into blocks, in which the heat and mass transfer are numerically calculated in the direction of *x*, *y* and *z*. In this model, *x* is the direction of the depth, *y* is the direction of the high, *z* is the direction of the wide. The representative small area is separated into 4, 5 and 7 parts in the directions of *x*, *y* and *z*, respectively. The micro channel is next to the adsorbent blocks, as shown in **Fig. 5.5 (c)**. Following assumptions are applied to simplify the model:

1) The adsorbent block includes the liquid phase and the gas phase.
2) The heat transfer occurred only between the adjacent liquid phases, in which the mass transfer is ignored.
3) The mass transfer occurred only between the adjacent gas phases due to vapor diffusion, in which the heat transfer is ignored.
4) The pressure of the gas phase is determined by the ideal gas law, in which the liquid phase temperature is applied as the gas temperature.
5) The temperature of the micro channel and the cooling/regeneration water are determined with a one-dimensional model in the direction of *z*. Their temperatures are uniform with the same *z*. Moreover,

The temperature of the cooling/regeneration water and the micro channel in a block is the same. The cooling/regeneration water direction and their flowrates are the same.

5.2.1.2. Heat Transfer Equation

The heat transfer equation of the adsorbent blocks is shown in **Eq. (5.3)**:

$$C_{\mathrm{p,a}}\rho_{\mathrm{a}}\frac{\partial T_{\mathrm{a}}}{\partial t}=\frac{\partial}{\partial x}\left(\lambda_{\mathrm{a}}\frac{\partial T_{\mathrm{a}}}{\partial x}\right)+\frac{\partial}{\partial y}\left(\lambda_{\mathrm{a}}\frac{\partial T_{\mathrm{a}}}{\partial y}\right)+\frac{\partial}{\partial z}\left(\lambda_{\mathrm{a}}\frac{\partial T_{\mathrm{a}}}{\partial z}\right)+\Delta H\rho_{\mathrm{a}}\frac{\partial q}{\partial t} \tag{5.3}$$

The left side of the equation presents the liquid phase temperature change on the elapsed time. The first, second and third parts of right side are the thermal conduction on the *x, y* and *z* directions. The fourth part is the sorption/regeneration heat capacity. $\frac{\partial q}{\partial t}$ is the sorption/desorption speed, which is presented by a Line Driving Force (LDF) model that shown in **Eq. (5.4)** [17], [18]. ΔH is the water sorption/desorption latent heat. q^* is the equilibrium water vapor sorption amount, which is described above and can be calculated by **Eqs. (5.1)** and **(5.2)**. q is the instantaneous water vapor sorption amount of the adsorbent.

$$\frac{dq}{dt}=k_{\mathrm{m}}\left(q^*-q\right) \tag{5.4}$$

The overall mass transfer coefficient of k_{m} is expressed by **Eq. (5.5)** [17].

$$k_m=\frac{15}{{r_{\mathrm{s}}}^2}D_{\mathrm{s0}}exp\left(-\frac{E_{\mathrm{a}}}{RT}\right) \tag{5.5}$$

In addition, λ_a is the effective thermal conductivity of adsorbent, which depends on the instantaneous vapor sorption amount q. It is reported by Freni's team [5] and presented as **Eq. (5.6)**.

$$\lambda_{\mathrm{a}}=\lambda_{\mathrm{a,dry}}+q\lambda_{\mathrm{w}} \tag{5.6}$$

5.2.1.3. Mass Transfer Equation

The mass transfer equation of the ad-HEX is shown in **Eq. (5.7)**:

$$\frac{\partial C_{\mathrm{v}}}{\partial t} = D\left(\frac{\partial^2 C_{\mathrm{v}}}{\partial x^2} + \frac{\partial^2 C_{\mathrm{v}}}{\partial y^2} + \frac{\partial^2 C_{\mathrm{v}}}{\partial z^2}\right) - \frac{\rho_{\mathrm{a}}}{\varepsilon}\frac{1}{M_{\mathrm{r}}}\frac{\partial q}{\partial t} \tag{5.7}$$

The left side of the equation presents the gas phase vapor concentration change on the elapsed time. The first part of right side is the vapor diffusion in the *x*, *y* and *z* directions. The second part is the vapor concentration change due to the sorption and regeneration. ρ_{a}, ε and M_{r} are the density of the adsorbent layer, the porosity of the adsorbent layer and the relative molecular mass of the water, respectively. *D* is the vapor diffusion coefficient, which is calculated by **Eq. (5.8)**. T_{v} is the temperature of the vapor, meanwhile $P_{\mathrm{atmosphere}}$ and P_{v} are the atmosphere pressure and the pressure of vapor, respectively.

$$D = 0.241 \times \left(\frac{273.15 + T_{\mathrm{v}}}{288}\right)^{1.75} \times \frac{P_{\mathrm{atmosphere}}}{P_{\mathrm{v}}} \tag{5.8}$$

5.2.1.3. Boundary Conditions

In this section, the boundary conditions are described. As mentioned in **Section 3.1.1**, the representative adsorbent small area is one of four symmetric adsorbent small area, the adiabatic boundaries are expressed by **Eq. (5.9)**.

$$\begin{aligned} x = L_x: &\quad \frac{\partial T_{\mathrm{a}}}{\partial x} = 0 \\ y = 0, L_y: &\quad \frac{\partial T_{\mathrm{a}}}{\partial y} = 0 \\ z = 0, L_z: &\quad \frac{\partial T_{\mathrm{a}}}{\partial z} = 0 \end{aligned} \tag{5.9}$$

At the boundary of $x = 0$, the cooling/regeneration water is flowed in the direction of *z* to cool or heat the entire ad-HEX. The heat transfer equation in the micro channel is expressed by **Eq. (5.10)**. The left side of the equation is the micro channel and its inside water temperature change depends on the elapsed time. The first part of the right side is the heat input due to the cooling/regeneration water inflow, and the second part is the thermal conduction in the *x* direction.

$$\left(C_{\mathrm{p,w}} m_{\mathrm{w,block}} + C_{\mathrm{p,HEX}} m_{\mathrm{HEX,block}}\right)\frac{\partial T_{\mathrm{w}}}{\partial t} = \dot{m}_{\mathrm{w,block}} C_{\mathrm{p,w}}\frac{\partial T_{\mathrm{w}}}{\partial z} + \frac{\partial}{\partial x}\left(\lambda_{\mathrm{a-HEX}}\frac{\partial T_{\mathrm{HEX}}}{\partial x}\right) \tag{5.10}$$

Meanwhile, the vapor diffusion occurs only on the blocks that y equal 0, other boundaries are humidity insulated. The boundary condition of mass transfer is shown in in **Eq. (5.11)**. The concentration of the vapor at

$$
\begin{aligned}
x = L_x, 0: \quad & \frac{\partial C_\mathrm{v}}{\partial x} = 0 \\
y = L_y: \quad & \frac{\partial C_\mathrm{v}}{\partial y} = 0 \\
z = L_z, 0: \quad & \frac{\partial C_\mathrm{v}}{\partial z} = 0 \\
y = 0: \quad & C_v = \frac{P_\mathrm{ev}}{RT_\mathrm{ev}} \quad \text{(Sorption process)} \\
& C_v = \frac{P_\mathrm{co}}{RT_\mathrm{co}} \quad \text{(Regeneration process)}
\end{aligned}
\tag{5.11}
$$

y equal 0 depends on the adsorber pressure, which is governed by the evaporator or condenser pressure in the sorption or the regeneration process, respectively.

5.2.2. Evaporator Model

A zero-dimensional model is applied for the evaporator. The heat transfer is calculated by **Eq. (5.12)**, as shown in following:

$$
\begin{aligned}
&\left(m_\mathrm{w,ev}C_\mathrm{p,w} + m_\mathrm{HEX,ev}C_\mathrm{p,HEX} + m_\mathrm{v,ev}C_\mathrm{p,v}\right)\frac{dT_\mathrm{ev}}{dt} \\
&\quad = \dot{m}_\mathrm{ev}C_\mathrm{p,w}E_\mathrm{ev}\left(T_\mathrm{ev,in} - T_\mathrm{ev,HEX}\right) - L_\mathrm{w}m_\mathrm{a}\frac{dq_\mathrm{sor}}{dt} + C_\mathrm{p,w}\left(T_\mathrm{co,HEX} - T_\mathrm{ev,HEX}\right)\frac{dm_\mathrm{w,co\to ev}}{dt}
\end{aligned}
\tag{5.12}
$$

The left side of **Eq. (5.12)** is the entire temperature change of the evaporator, which includes the adsorbate water, the HEX and the vapor in the evaporator chamber. The first part of right side is the heat input of the circulation water inflow. the second part is the vaporization heat, which depends on the adsorption amount of the vapor in the adsorber. The third part is the sensible heat of the recovered water from the condenser chamber. E_ev is the heat exchange coefficient that defined by **Eq. (5.13)**.

$$
E_\mathrm{ev} = \frac{T_\mathrm{ev,in} - T_\mathrm{ev,out}}{T_\mathrm{ev,in} - T_\mathrm{ev,HEX}} \tag{5.13}
$$

On the other hand, the mass transfer is expressed by **Eq. (5.14)**. As the assumption in **Section 5.2.1.1**, the water amount in evaporator and condenser chamber is constant, **Eq. (5.14)** can be transformed to **Eq. (5.15)**.

$$
\frac{dm_\mathrm{w,ev}}{dt} = \frac{dm_\mathrm{w,co\to ev}}{dt} - m_\mathrm{a}\frac{dq_\mathrm{sor}}{dt} \tag{5.14}
$$

$$
\frac{dm_\mathrm{co\to ev}}{dt} = m_\mathrm{a}\frac{dq_\mathrm{sor}}{dt} \tag{5.15}
$$

The vapor in evaporator chamber is always saturated, it can be calculated by the Wexler-hyland equation shown in **Eq. (5.16)** [19]. The weight of vapor is calculated by the Ideal Gas Law.

$$lnP_{\mathrm{sat}} = -\frac{5.675}{T_{\mathrm{v}}} \times 10^{3} + 6.393 - 9.678 \times 10^{-3} \times T_{\mathrm{v}} + 6.222 \times 10^{-7} \times {T_{\mathrm{v}}}^{2} + 2.075 \times 10^{-9} \times {T_{\mathrm{v}}}^{3} - 9.484 \times 10^{-13} \times {T_{\mathrm{v}}}^{4} + 4.164 \times 10^{-7} \times lnT_{\mathrm{v}} \tag{5.16}$$

5.2.3. Condenser Model

The condenser is described with a zero-dimensional model, which is similar to that of the evaporator. The heat transfer is calculated by **Eq. (5.17)**, as shown in following:

$$\left(m_{\mathrm{w,co}}C_{\mathrm{p,w}} + m_{\mathrm{HEX,co}}C_{\mathrm{p,HEX}} + m_{\mathrm{v,co}}C_{\mathrm{p,v}}\right)\frac{dT_{\mathrm{co}}}{dt} = \dot{m}_{\mathrm{co}}C_{\mathrm{p,w}}E_{\mathrm{co}}\left(T_{\mathrm{co,in}} - T_{\mathrm{co,HEX}}\right) - L_{\mathrm{w}}m_{\mathrm{a}}\frac{dq_{\mathrm{des}}}{dt} - C_{\mathrm{p,w}}\left(T_{\mathrm{co,HEX}} - T_{\mathrm{ev,HEX}}\right)\frac{dm_{\mathrm{w,co\rightarrow ev}}}{dt} \tag{5.17}$$

All the parts are similar to those in the evaporator model. E_{co} is the heat exchange coefficient that defined by **Eq. (5.18)**.

$$E_{\mathrm{co}} = \frac{T_{\mathrm{co,in}} - T_{\mathrm{co,out}}}{T_{\mathrm{co,in}} - T_{\mathrm{co,HEX}}} \tag{5.18}$$

As the same assumption in **Section 5.2.1.1**, the mass transfer in condenser is governed according to **Eq. (5.15)**. In addition, the pressure of the condenser chamber is defined by **Eq. (5.16)**.

5.2.4. Advanced Cycle

In this study, the advanced cycles of the Heat Recovery and the Mass Recovery are introduced. Their principles are described in the next sections. With the introduction of the advanced cycles, the cycle period of the AHP system is changed as following:

1) For the basic cycle without the advanced cycles. The AHP system is switched between **Mode A** and **Mode B**, which are mentioned in the **Section 5.1**. The cycle is shown as the **Basic** in **Fig. 5.6**.
2) The regeneration heat can be partly recovered by the introduction of the HR, which focuses on the control strategies of the adsorber outlet. The period of the HR is included in the period of **Mode A** and **Mode B**, which are the same to those in the basic cycle, as shown in **Fig. 5.6 HR**.
3) The regeneration and the sorption of adsorbers during the MR process are different from those in **Mode A**

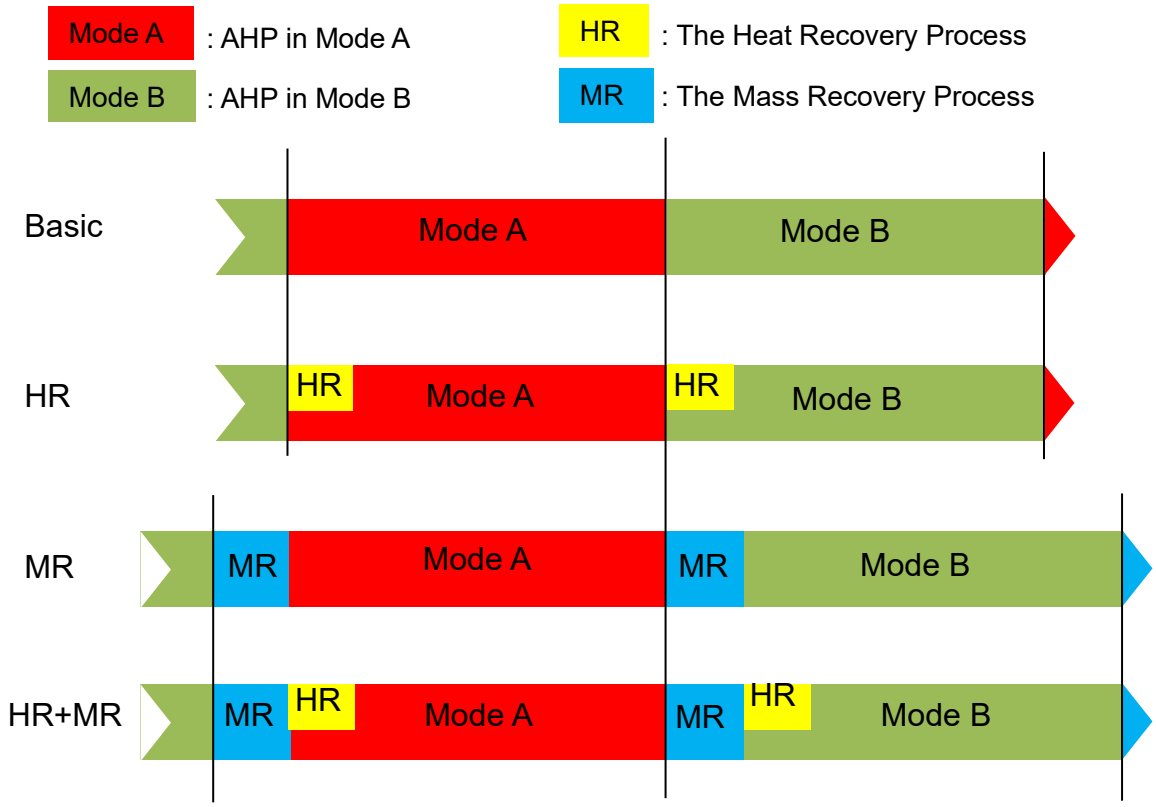

Fig. 5.6 Entire cycle period change of different cases.

and **Mode B**, thus the MR need extra time to fulfill. The longer entire cycle period is taken with the MR, as the **MR** shown in **Fig. 5.6**.

4) **HR+MR** presents the case that the HR and the MR are combined to enhance the system performance. Our prior experiment result indicates that the pressure conditions of the adsorber became unavailable for the MR before the completion of the HR. Therefore the MR is performed before the HR.

5.2.4.1 Heat Recovery

The heat recovery is a kind of advanced cycle that can improve the system efficiency by recovering the heat capacity of the High Temperature Side (HTS, Ads.1) adsorber. The heat recovery has been studied by lots of research [20], [21], [2], [8], [22]. The principle of the HR is shown in **Fig. 5.7** [2], our prior study also explained the HR in detail [8]. This study focuses on the Serial Heat Recovery (SHR) and the Passive Heat Recovery (PHR) because of their simple structure compared with the Circulated Heat Recovery (CHR).

The following assumptions are applied to the HR process model:

1) The all the heat loss is ignored.
2) The flowrate of the adsorber during the SHR process is same to that during **Mode A** or **Mode B**.

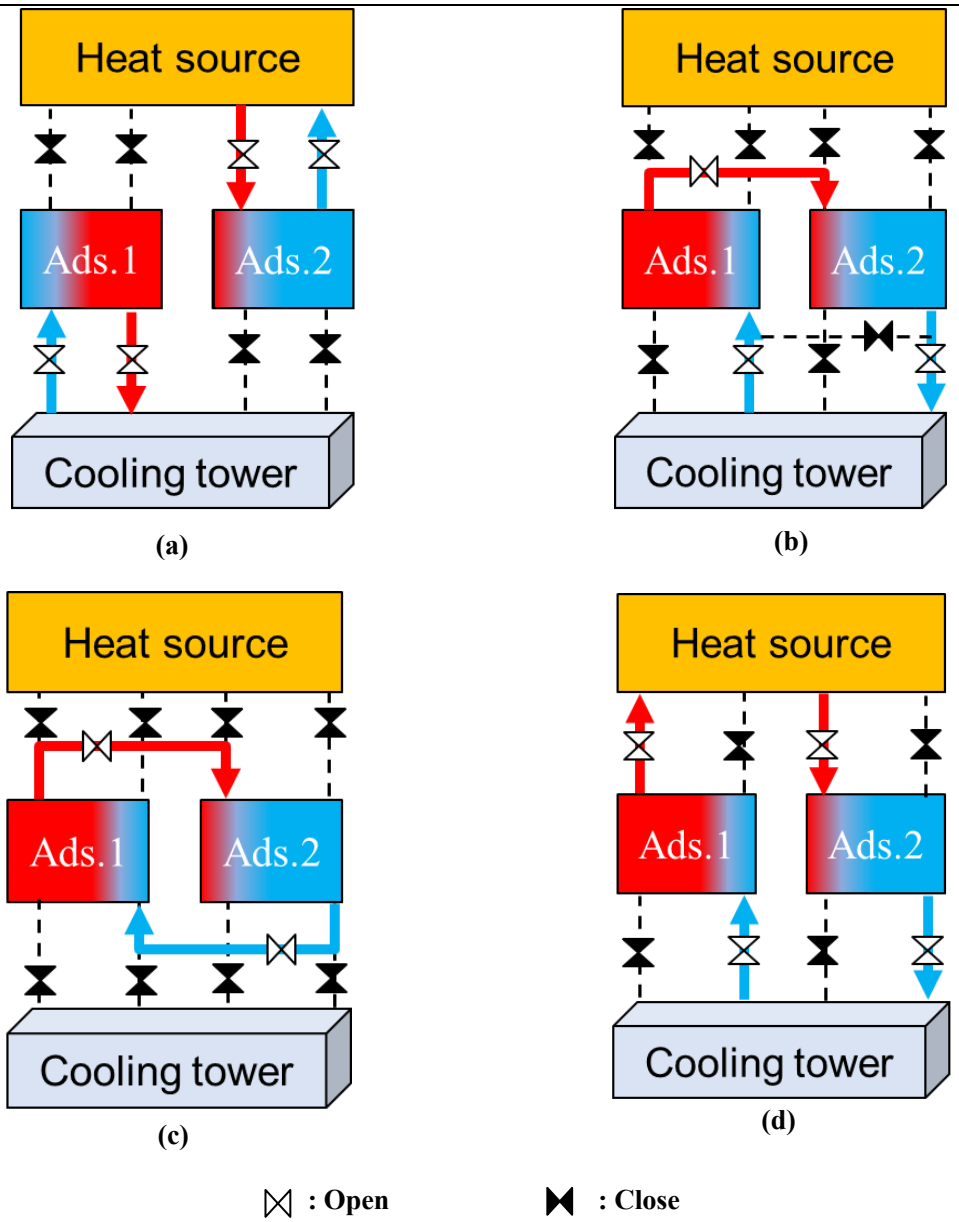

Fig. 5.7 Basic type and three types of heat recoveries: (a) Basic type; (b) Serial heat recovery (SHR); (c) Circulated heat recovery (CHR); (d) Passive heat recovery (PHR).[28]

5.2.4.2 Mass Recovery

The mass recovery has been proposed in recently years [1], [23], lots of researches have been performed [1], [23], [24]. **Fig. 5.8** presents the schematic of the MR. The HTS and the LTS are connected with each other to start the MR process, the vapor in HTS and LTS are mixed, as shown in **Fig. 5.8 (b)**. Their pressures converge with the middle value, which enhance the desorption process of the HTS and the sorption process of the LTS.

The model of the MR is built based on the following assumptions:

1) The adsorber chambers are separated with the evaporator and the condenser chamber during the MR process.

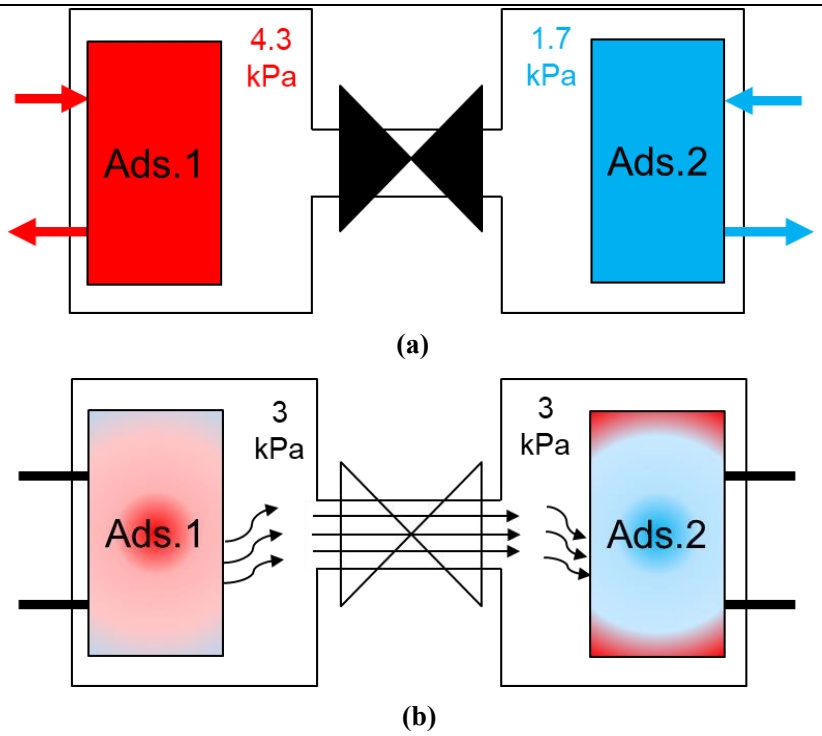

Fig. 5.8 Schematic illustration of mass recovery (based on the standard experiment conditions): (a) End of sorption/regeneration process; (b) mass recovery process.

2) The vapor in the adsorber chambers is the ideal gas, thus the pressure and the temperature of the mixture gas can be calculated by Avogadro's Hypothesis.

3) There is no heat transfer of the vapor due to the mixture during the mass recovery process.

The conditions of the vapor in the AHP can be expressed by the ideal gas law that shown in **Eq. (5.19)**. The assumption **3)** results in **Eq. (5.20)**, the temperature of the mixed vapor can be achieved by **Eq. (5.21)**.

$$PV = nTR \tag{5.19}$$

$$\int P_{\text{ads.1}} dV_{\text{ads.1}} = -\int P_{\text{ads.2}} dV_{\text{ads.2}} \tag{5.20}$$

$$T_{\text{mix}} = \frac{n_{\text{ads.1}} T_{\text{ads.1}} + n_{\text{ads.2}} T_{\text{ads.2}}}{n_{\text{ads.1}} + n_{\text{ads.2}}} \tag{5.21}$$

5.2.5. Evaluation Indices

COP, SCP are employed to evaluate the performance of the AHP system [25], [8], [26]. $Q_{\text{i,c}}$ is the cooling amount in the i$^{\text{th}}$ cycle and it is defined with **Eq. (5.22)**, meanwhile $Q_{\text{i,reg}}$ is the regeneration heat amount in the i$^{\text{th}}$ cycle and **Eq. (5.23)** is used to define it. In addition, $Q_{\text{i,reg,hr}}$ in **Eq. (5.24)** is the amount of regeneration heat in the i$^{\text{th}}$ cycle for cases that the HR is introduced. For each sorption/regeneration process, the accumulated amount of the cooling and the regeneration are defined by **Eq. (5.25)** and **(5.26)**, respectively. They are used to

analyze the sorption/desorption characteristics [8], [24]. Based on the amount of the cooling and the regeneration, COP is defined with **Eq. (5.27)**. As defined by **Eq. (5.28)**, SCP is the cooling capacity per unit weight of the adsorbent, the higher SCP indicates the lower cost of AHP. Owing to the instability of the system, the unavailable data of the first and second cycles are generally ignored.

$$Q_{\mathrm{i,c}} = \int_{t_{\mathrm{i,b,sor}}}^{t_{\mathrm{i,e,sor}}} \dot{V}_{\mathrm{ev}} \rho_{\mathrm{w}} C_{\mathrm{p,w}} \left(T_{\mathrm{ev,in}} - T_{\mathrm{ev,out}}\right) dt \tag{5.22}$$

$$Q_{\mathrm{i,reg}} = \int_{t_{\mathrm{i,b,reg}}}^{t_{\mathrm{i,e,reg}}} \dot{V}_{\mathrm{hw}} \rho_{\mathrm{w}} C_{\mathrm{p,w}} \left(T_{\mathrm{ads,in}} - T_{\mathrm{ads,out}}\right) dt \tag{5.23}$$

$$Q_{\mathrm{i,reg,hr}} = \int_{t_{\mathrm{i,b,reg}}}^{t_{\mathrm{i,e,reg}}} \dot{V}_{\mathrm{ht}} \rho_{\mathrm{w}} c_{\mathrm{p,w}} \left(T_{\mathrm{ht,s}} - T_{\mathrm{ht,r}}\right) dt \tag{5.24}$$

$$Q_{\mathrm{c}} = Q_{\mathrm{lt,evporation}} - (Q_{\mathrm{ss,ev,w}} + Q_{\mathrm{ss,ev,HEX}} + Q_{\mathrm{ss,ev,rw}} + Q_{\mathrm{ev,loss}}) \tag{5.25}$$

$$Q_{\mathrm{reg}} = Q_{\mathrm{lt,des}} + (Q_{\mathrm{ss,ads,a}} + Q_{\mathrm{ss,ads,HEX}} + Q_{\mathrm{ss,ads,rw}} + Q_{\mathrm{ads,loss}}) \tag{5.26}$$

$$\mathrm{COP} = \sum_{\mathrm{i=3}}^{N} Q_{\mathrm{i,c}} \Big/ \sum_{\mathrm{i=3}}^{N} Q_{\mathrm{i,reg}} \tag{5.27}$$

$$\mathrm{SCP} = \sum_{\mathrm{i=3}}^{N} Q_{\mathrm{i,c}} \Big/ (m_{\mathrm{a,dry}} \cdot t_{\mathrm{cyc}}(N-2)) \tag{5.28}$$

Moreover, COP and SCP are independent of each other, they show the converse change in many cases. The optimal COP and SCP for the best system performance need to determine. Therefore a new index called Value Factor (VF) is proposed, as shown in **Eqs. (5.29), (5.30)** and **(5.31)**.

$$\mathrm{VF} = \mathrm{SCP} \times \mathrm{VC_{SCP}} - \frac{\mathrm{SCP}}{\mathrm{COP}} \times \mathrm{VC_{COP}} \tag{5.29}$$

$$\mathrm{VC_{SCP}} = \frac{1}{\eta_{\mathrm{chiller}} \times \eta_{\mathrm{gen,pv}}} \tag{5.30}$$

$$\mathrm{VC_{COP}} = \frac{1}{\eta_{\mathrm{heater,solar}}} \tag{5.31}$$

One of another air-conditioner is generally chosen as the reference, and η_{chiller} is its efficiency coefficient. $\eta_{\mathrm{gen,pv}}$ is the efficiency coefficient of the photovoltaic generation system. $\eta_{\mathrm{heater,solar}}$ is efficiency coefficient of the solar collector. According to the efficiency coefficient of the air-conditioner chosen as the reference, the relative value achievement of the current AHP is expressed by the first part on the right side of the **Eq. (5.29)**, which depends on SCP of the current AHP. Meanwhile, the relative value consumption, which depends on SCP

and COP of the current AHP, is expressed by the second part on the right side of the **Eq. (5.29)**. Hence both SCP and COP are connected with the same source of the solar power to determine the optimal COP and SCP for the system. As the reference, VF of the conventional compress type air-conditioner is 0 owing to the equal relative value achievement and the relative value consumption. The VF higher than 0 indicates better performance of AHP than the reference air-conditioner, otherwise the reference air-conditioner is better than the AHP. Moreover, different AHP system can be compared with each other definitely. In this study, the value of the η_{chiller}, $\eta_{\mathrm{gen,pv}}$ and $\eta_{\mathrm{heater,solar}}$ are 3, 0.12 and 0.65, respectively.

5.3. Simulation Results and Discussion

5.3.1. Validation of the Numerical Model

The numerical model is validated by comparing the calculation results with the experiment results, whose standard experiment conditions are shown in **Table. 5.2**. The adsorber inlet/outlet temperature transients of the calculation results are shown in **Fig. 5.9 (a)**, they are very similar to those of the experiment results. The average adsorber inlet temperature for the sorption and the regeneration processes of the calculation results are very close to the standard experiment conditions (± 0.2 K). However, the average adsorber inlet temperature for the sorption process of the experiment results is 31.19 ℃ owing to the limitation of the chiller capacity. For the same reason, the evaporator and the condenser inlet/outlet temperature transients of the experiment results fluctuate at 20 ℃ ± 0.5 K, as shown in **Fig. 5.9 (b)**. On the other hand, the experiment results show the notably higher peaks of the condenser outlet temperature and the adsorber pressure than those of the simulation result, it indicates the experiment case have faster heat transfer speed. In this simulation, the corrugated fins are ignored to simplify the adsorber model, which decreases the heat transfer speed of the simulation. It is also reflected to the hot water supply/return temperatures change of the case that the passive heat recovery is introduced, which is expressed in **Fig. 5.9 (c)**. The cooling and the regeneration capacities that shown in **Fig. 5.9 (d)** are calculated based on the temperature differences. The average cooling capacity of the experiment result and the calculation result are 1.54 kW and 1.48 kW, respectively. Meanwhile, the average regeneration capacity of the experiment result and the calculation result are 2.93 kW and 3.38 kW, respectively. The error of the cooling capacity is 4.22 %, however, that of the regeneration capacity is 13.69 % because of the ignoring of the heat loss. The cooling/regeneration amount of a representative cycle, COP of the basic case (COP-basic), COP of the heat recovery case (COP-HR)

Table 5.2 Standard experiment conditions.

	Regeneration	Sorption	Condensation	Evaporator
Inlet temperature [℃]	80	30	30	20
Flowrate [L/min]	6.3	6.3	5.5	4.39

Table 5.3 Calculation error.

	COP-basic [-]	COP-HR [-]	SCP [kW/kg]
Experiment	0.449	0.513	0.381
Calculation	0.498	0.604	0.361
Error	10.97%	17.69 %	4.22 %

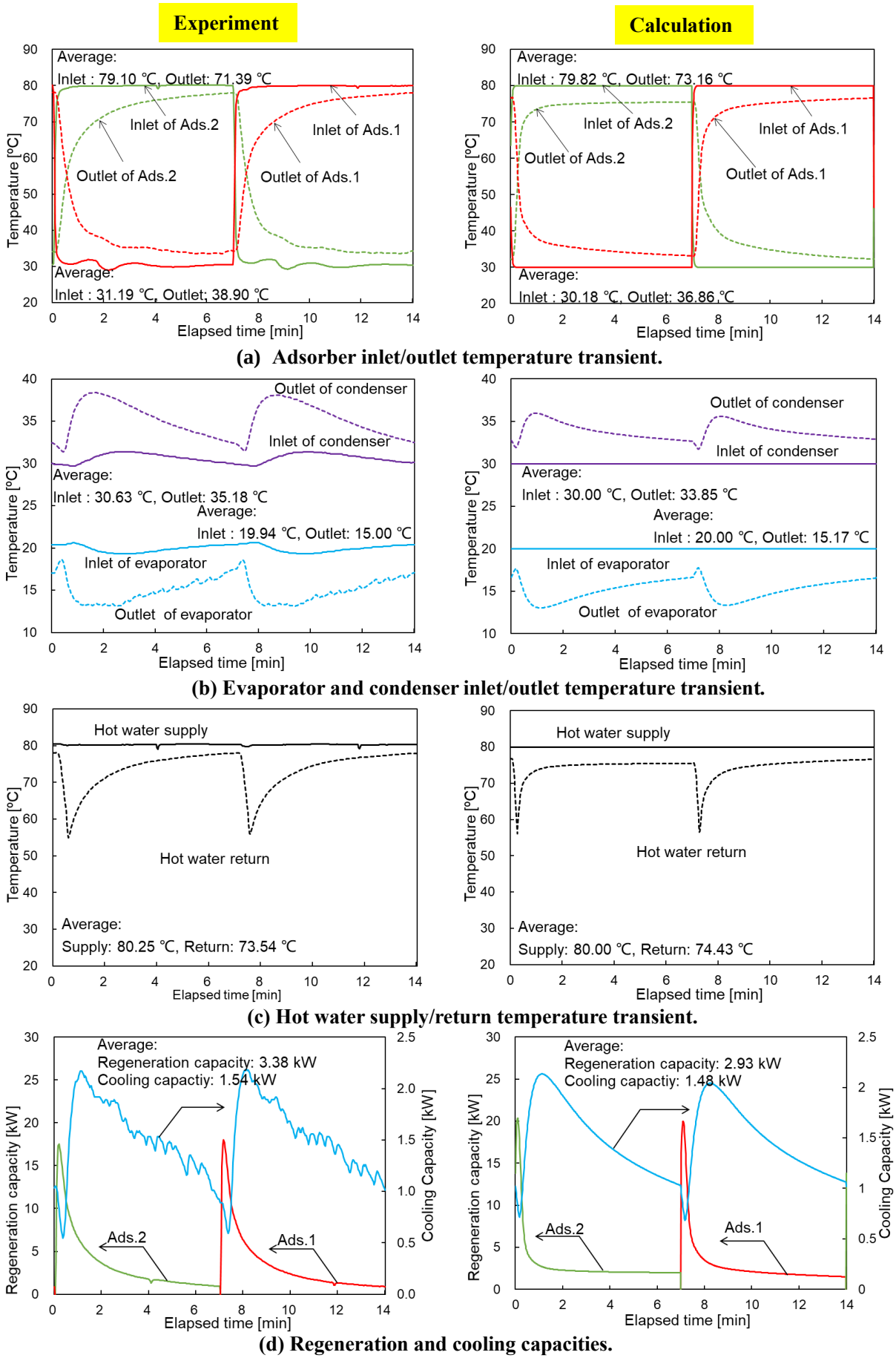

Fig. 5.9 Results of the calculation and experiment.

and SCP are shown in **Table 5.3** to compare. SCP of the calculation result is 0.361 kW/kg, its error is a reliable 4.22 %. On the other hand, the ignoring of the heat loss in this simulation leads to higher COP of the calculation result than that of the experiment result. COP-basic is 0.498 and COP-HR is 0.604, their errors are 10.97 % and 17.69 %, respectively. Therefore, COPs of the calculation results, which are the ideal value, are available for the performance evaluation.

5.3.2. Parameter Analysis of the Basic Cycle

The cycle period was changed from 2-60 minutes, COP and SCP versus the cycle period are shown in **Fig.5.10** to compare with the experiment results, which has been studied in our prior research [8]. SCP of the calculation result increases and reaches the peak of 0.367 kW/kg at cycle period of 12 minutes, then it decreases with the longer cycle period is taken. Meanwhile, COP of the calculation result increases up to 0.581 at cycle period of 60 minutes. The experiments are performed in cycle periods from 10 to 18 minutes, SCP decreases from 0.422 kW/kg at cycle period of 10 minutes to 0.351 kW/kg at cycle period of 18 minutes. As mentioned in **Section 5.3.1**, fins of the ad-HEX are ignored in this model, which results in the slower desorption/sorption than those in the experiment, experiment SCPs decrease notably with the increasing of the cycle period. experiment COPs are lower than those of the calculation results owing to the heat loss. The calculation results show COP of 0.498 and SCP of 0.365 kW/kg at cycle period of 14 minutes, which refers the prior study [8].

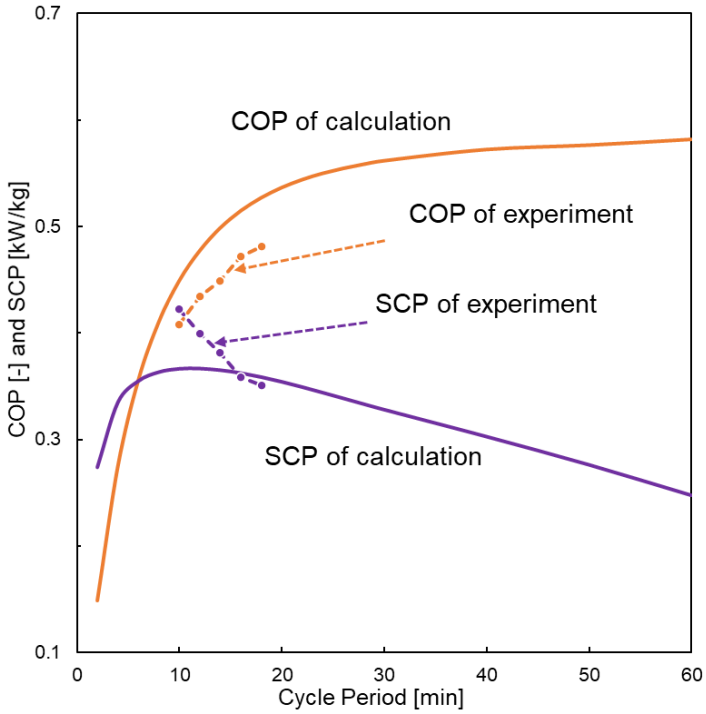

Fig. 5.10 COP and SCP versus the cycle period.

Then the cycle period is fixed at 14 minutes, the regeneration temperature is changed from 60-80 ℃ and the evaporator inlet temperature is changed from 12-20 ℃. The flowrate of the evaporator is adapted to keep the temperature difference between the inlet/outlet of the evaporator is 5 K. The results of the calculation and the experiment [8] are shown in **Fig. 5.11**. The evaporator outlet temperatures of the simulation are adapted to the target with error ± 0.05 K; on the other hand, that of the experiment is failed to be adapted in the cases of low evaporation/regeneration temperature due to the limitation of the devices. All COPs of the calculation results are higher than those of the experiment results. The heat loss leads to reduction of COP, especially for the cases of low evaporation/regeneration temperature, as shown in **Fig. 5.11 (a)**. **Fig. 5.11 (b)** shows SCP based on the evaporation/regeneration temperature. SCP of the calculation results at evaporator outlet temperature of 15 ℃ are lightly lower than those of the experiment. However, the heat loss in the evaporator increases with the evaporator outlet temperature decrease, it results in lower SCP of the experiment than those of the calculation results. In this model, COP decreases from 0.498 to 0.110 and SCP decreases from 0.365 kW/kg to 0.043 kW/kg while the regeneration temperature decreases from 80 ℃ to 60 ℃ and the evaporator outlet temperature decreases from 15 ℃ to 7 ℃.

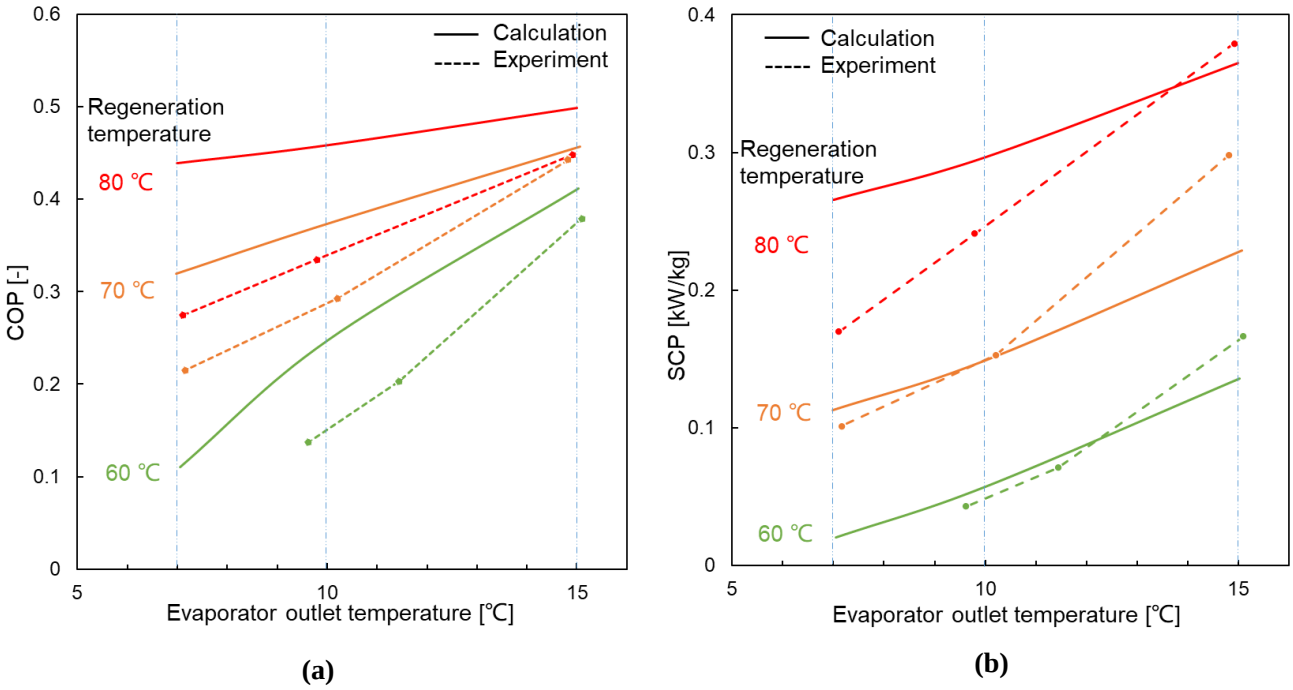

Fig. 5.11 COP and SCP versus the evaporator outlet temperature: (a) COP; (b) SCP.

5.3.3. Advanced Cycle

5.3.3.1. Heat Recovery

The SHR and the PHR that introduced in **Section 5.2.4.1** are programmed into the simulation code, the calculation results are shown in **Fig. 5.12**. The cycle period is fixed at 14 minutes referring the previous study [8], the experiment conditions in **Table 5.4** are applied and the heat recovery period is changed from 0 to 20

Table 5.4 Experiment conditions for heat recovery.

	Regeneration	Sorption	Condensation	Evaporator
Inlet temperature [℃]	80	30	30	20
Flowrate [L/min]	9.5	9.5	5.5	4.39

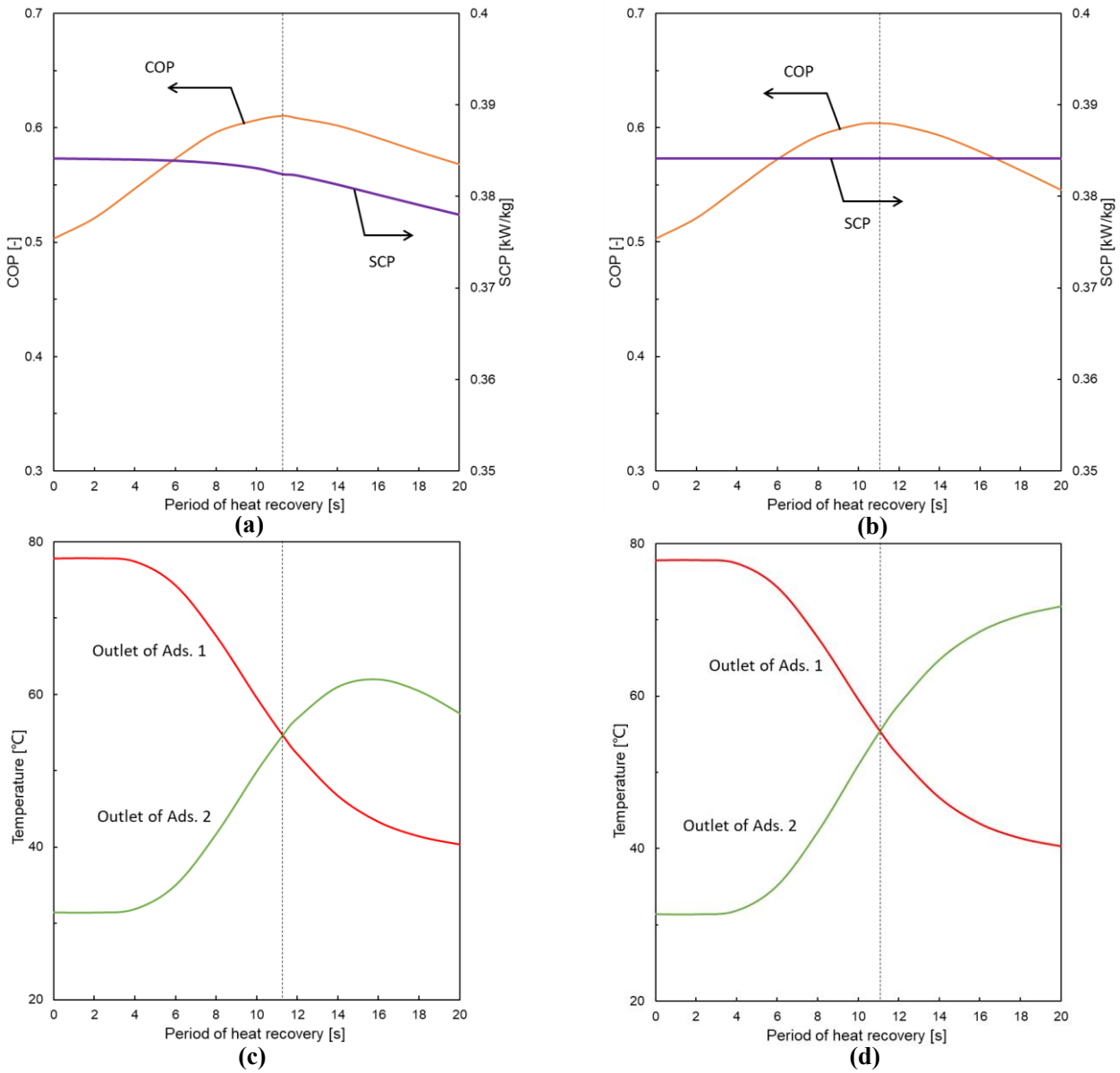

Fig. 5.12 Results versus the period of heat recovery: (a) COP and SCP of SHR; (b) COP and SCP of PHR; (c) Adsorber outlet temperature of SHR; (d) Adsorber outlet temperature of PHR.

seconds.

COP with both SHR and PHR increase to peak then decrease mildly with the longer period of the heat recovery are taken, as shown in **Fig. 5.12 (a)** and **(b)**. Compared with the basic case, COP is increased from 0.503 up to 0.610 and 0.604 with the SHR and the PHR, respectively. **Fig. 5.12 (c)** and **(d)** present the adsorber outlet temperature at the end of the SHR and the PHR, respectively. In the case of the SHR, the outlet temperature of the Ads.1 and the Ads.2 close and cross to each other while the heat recovery period increases to 11.29 seconds, in which the highest COP can be obtained. Meanwhile the case of PHR needs 11.08 seconds to cross the adsorber outlet temperatures. As described in **Section 5.2.4.1**, the hot water of the Ads.1 outlet is flowed into the Ads.2 inlet instead of the hot water from the heat source, which leads to the lower Ads.2 inlet temperature compared with that in basic case and PHR. The lower inlet temperature also disturbs the regeneration of adsorbent, hence SCP of SHR slightly decreases with the heat recovery period increasing, as shown in **Fig. 5.12 (a)**. It is also confirmed in our former study [8]. Moreover, it was found that half of the sensible heat amount, which is shown in the bracket of **Eq. (5.26)**, can be recovered by the heat recovery reasonably. In this study, the regeneration heat amount of 218.91 kJ is reduced, which is 51.24 % of the sensible heat amount. The temperature of the adsorbent in the HTS (Ads.1) decreases with the progressing of the heat recovery, which results in the sorption of vapor and the increasing of the adsorbent temperature. Thus the recovered heat amount is higher than that of the ideal value. The PHR is a better heat recovery method owing to simple structure, no extra valves and no

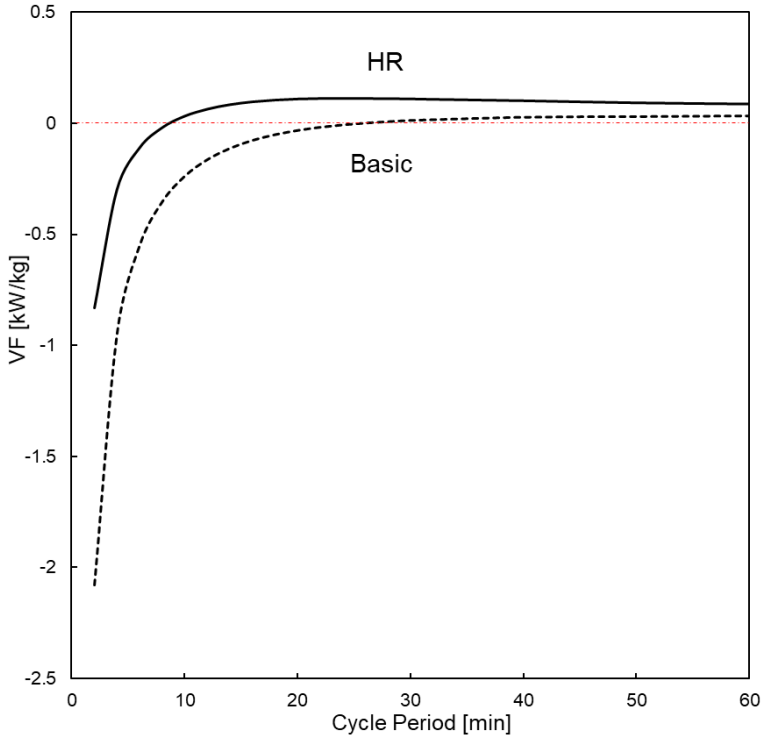

Fig. 5.13 VF versus the cycle period.

decreasing of SCP compared with the SHR. The PHR is combined with the MR in the next section.

Then VF versus the cycle period, which is defined in **Eq. (5.29)**, is presented in **Fig. 5.13**. VF of the basic cases (basic) increase and over 0 while the cycle period is longer than 24 minutes, which indicate the AHP is more efficient and valuable to utilize the solar power than the compress type air conditioner. VF are notably enhanced with the PHR (HR), the minimum of the cycle period that provide positive VF is shortened to 10 minutes. The cycle period is still set at 14 minutes refer the previous study though The highest VF of 0.113 kW/kg appears at the cycle period of 24 minutes.

5.3.3.2. Mass Recovery

The mass recovery is performed with the conditions in **Table 5.4**, the cycle period is fixed at 14 minutes and the mass recovery period is changed from 0 to 90 seconds. In additions, the flowrates for the regeneration and the sorption are set at 0 during the mass recovery period. **Fig. 5.14 (a)** shows the adsorbent surface temperature transient versus the elapsed time duringthe mass recovery process. The mixture of the vapor contributes to the pre-cooing/preheating of the adsorbers, the surface temperature of the HTS (Ads.1) and the LTS (Ads.2) decreases and increases, respectively. With the longer mass recovery period is taken, the surface temperatures of the LTS reach the peaks within 10 seconds, which indicates that the vapor sorption speed on the surface dropped and the heat amount of the adsorbent transfer to the deeper layer. A temperature bounce at the end of

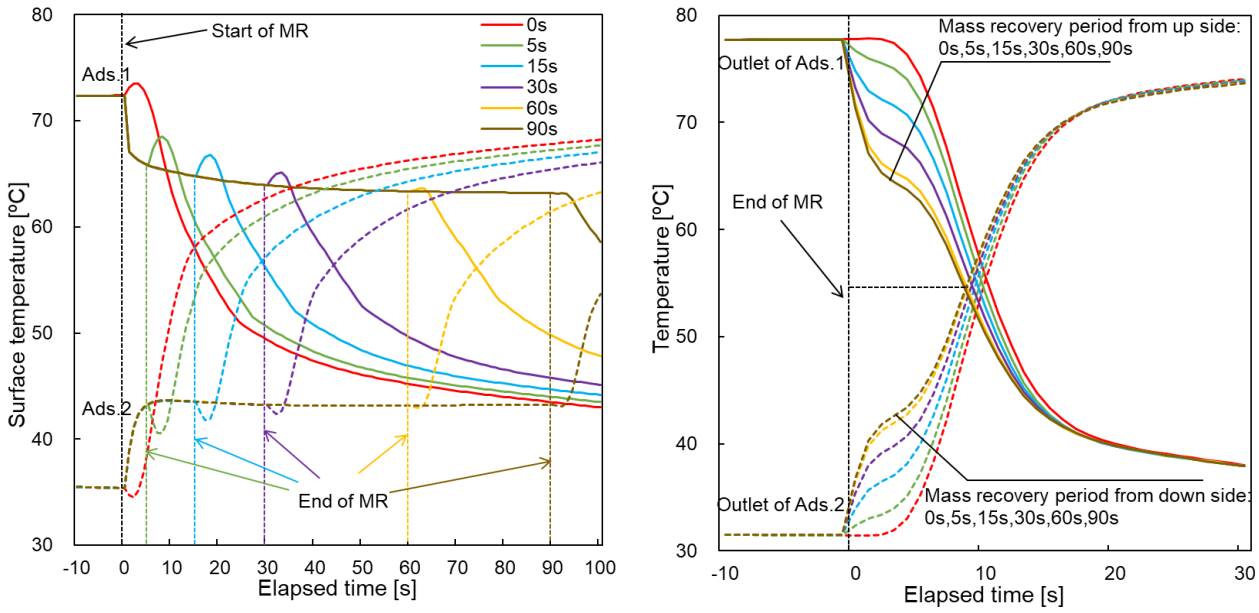

Fig. 5.14 Temperature transient versus the elapsed time: (a) Adsorbent surface temperature transient during the mass recovery process; (b) Outlet temperatures transient of adsorbers after the mass recovery process.

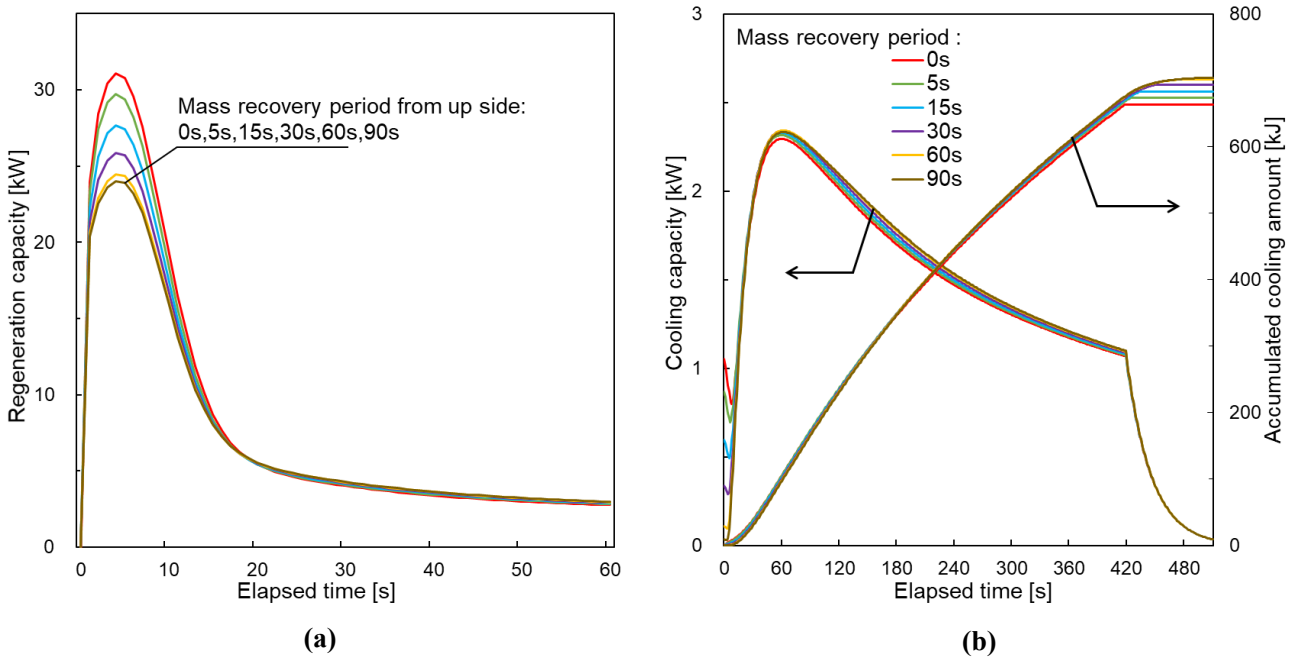

Fig. 5.15 Regeneration capacity and cooling capacity versus the elapsed time: (a) Regeneration capacity versus the elapsed time; (b) Cooling capacity and accumulated cooling amount versus the elapsed time.

the mass recovery process can be observed, it proves the uncomplete heat transfer between the adsorbent and the water remained in the HEX. The adsorber outlet temperature changes after the mass recovery process are shown in **Fig. 5.14 (b)**. The outlet temperatures of the HTS decrease meanwhile the outlet temperatures of the LTS increase obviously owing to the pre-cooling and pre-heating. It can be predicted that both side of the adsorber outlet temperature close to the black dash line in **Fig. 5.14 (b)** with a very long period of the mass recovery. The regeneration and the cooling capacities are calculated based on the temperatures shown in **Fig.5.14 (b)**, the results of a representative cycle in different mass recovery period are picked up and shown in **Fig. 5.15**. **Fig. 5.15 (a)** presents the regeneration capacity changes with the elapsed time, the regeneration capacity is reduced by the mass recovery. The cooling capacities and the accumulated cooling amounts versus the elapsed time are shown in **Fig. 5.15 (b)**. The cooling capacity is improved by the mass recovery due to the enhancement of the desorption during the mass recovery process, it is reflected to the accumulated cooling amounts.

The cooling amount and the regeneration amount versus the mass recovery period are shown in **Fig. 5.16 (a)**. The cooling amount is improved meanwhile the regeneration amount (MR) is reduced with the mass recovery period increasing. Based on the cooling/regeneration amount, COP and SCP are calculated and shown in **Fig.5.16 (b)**. SCP is enhanced up to 0.393 kW/kg from 0.389 kW/kg in mass recovery period of 1 second, then SCP decreases with the longer mass recovery period. Because of the increasing of the cooling amount and the reduction of the regeneration amount, higher COP is obtained with the longer mass recovery period. COP is improved from 0.503 up to 0.546 in mass recovery period of 90 seconds.

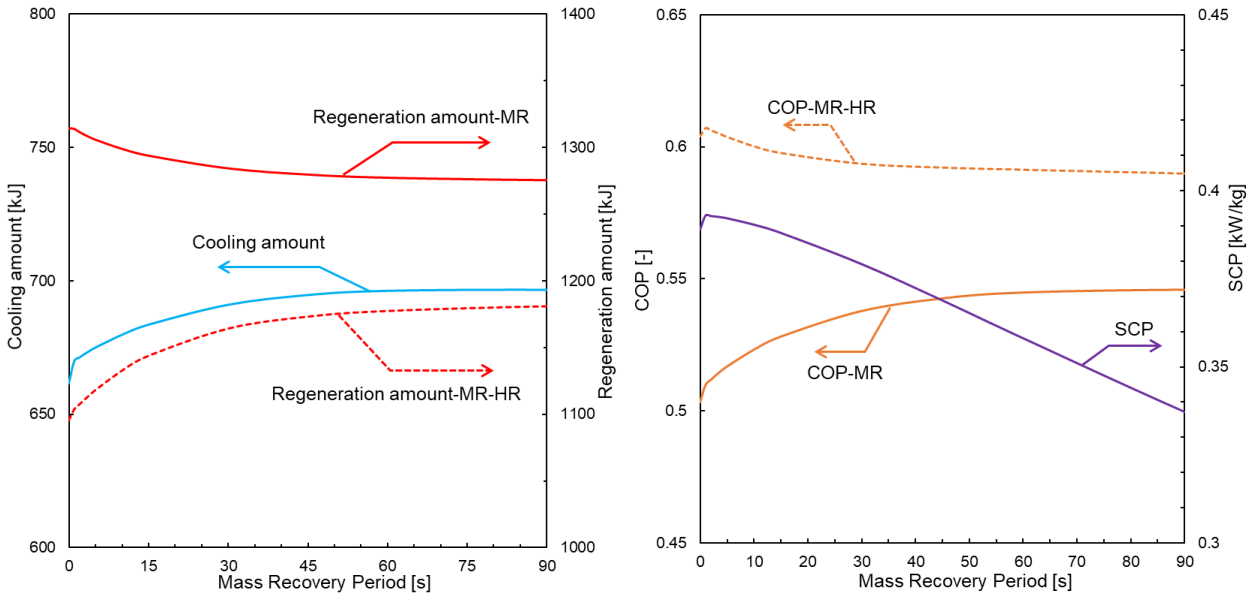

(a) (b)

Fig. 5.16 Calculation results versus the mass recovery period: (a) Cooling and regeneration amount versus the mass recovery period; (b) COP and SCP versus the mass recovery period.

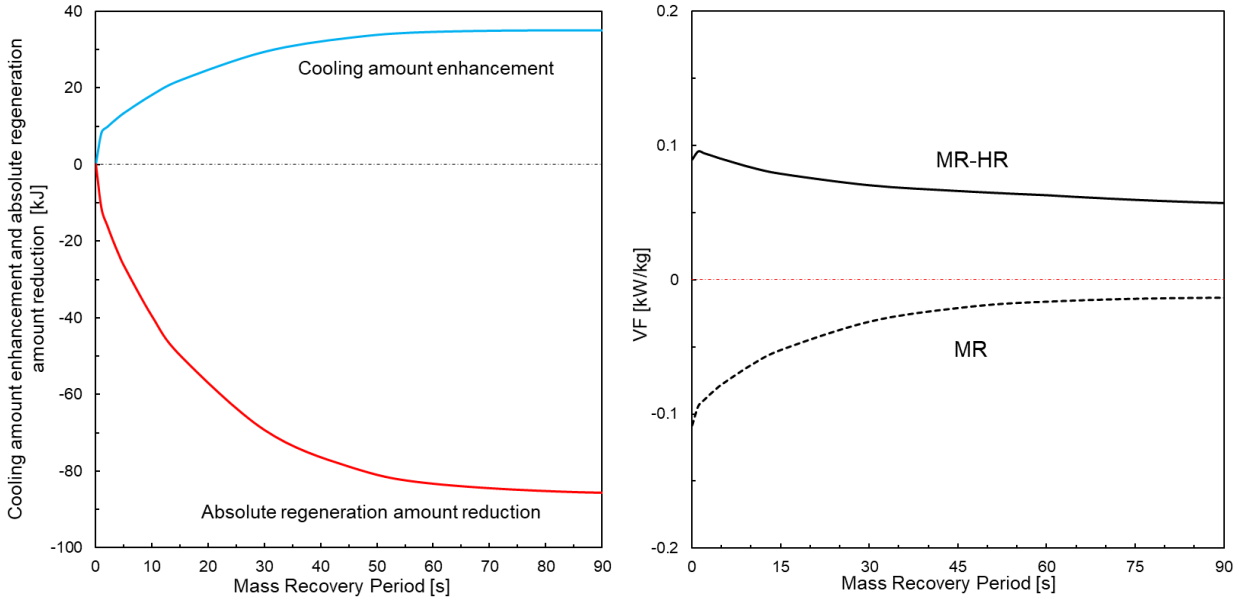

(a) (b)

Fig. 5.17 Calculation results versus the mass recovery period: (a) Cooling amount enhancement and absolute regeneration amount reduction; (b) VF versus the mass recovery period.

As mentioned in **Section 5.2.4.2**, the pre-heating of the adsorbent by the mass recovery contribute to the regeneration amount reduction (all the elements in the bracket of **Eq. (5.26)**), meanwhile the enhanced sorption process needs more regeneration amount ($Q_{lt,des}$ of **Eq. (5.26)**). The cooling amount enhancement and the absolute regeneration amount reduction are calculated and shown in **Fig. 5.17 (a)**. They increase/decrease with the mass recovery period increasing and trend to stable in the mass recovery period of 90 seconds, in which the temperature bounce also disappeared based on **Fig. 5.14 (a)**. The mass recovery process is proved to finish in

the mass recovery period of 90 seconds. The cooling amount enhancement of 35.02 kJ and the absolute regeneration amount reduction of 85.71 kJ are obtained. VF versus the mass recovery period (MR) is presented in **Fig. 5.17 (b)**. Obviously, VF is improved with the longer mass recovery period, though it is below 0.

5.3.3.3. Combination of Mass Recovery and Heat Recovery

The PHR is combined after the mass recovery. As shown in **Fig. 5.16 (a)**, the regeneration amount with the PHR (MR-HR) is notably reduced. However, it increases with the longer mass recovery period. COP with PHR versus the mass recovery period calculated based on **Fig. 5.16 (a)** is shown in **Fig. 5.16 (b)**. The highest COP of 0.607 is obtained at a very short mass recovery period of 1 second, then COP decreases gradually to 0.590 at mass recovery period of 90 seconds. According to our former study, half of the sensible heat amount in **Eq.(5.26)** can be recovered by the PHR to reduce the regeneration heat amount [8], which can be expressed by the area between the real line and the dash line in **Fig. 5.14 (b)**. The temperature transient of hot water supply/returns that picked up from **Fig. 5.14 (b)** are shown in **Fig. 5.18**. It is confirmed that the longer heat recovery period results in the regeneration amount increasing. As described in the **Section 5.3.3.2**, the temperature of the hot water returns close to the black dash line in a very long period of mass recovery. The regeneration heat amount with PHR is predicted to increase and equal the regeneration amount without PHR, absolutely, which indicates that the limitation of the regeneration heat amount reduction by the mass recovery is a half of that by the PHR (25 % of the sensible heat amount). In this study, the absolute heat amount reduction by the mass recovery is up to 85.71 kJ, which is 20.06 % of the sensible heat amount. The relative low sorption/desorption speed and the bad vapor diffusion during the mass recovery process are considered to be the reasons. It is found that the recoverable sensible heat amount is shared by the mass recovery process and the heat recovery process, and the recovery rate of the heat recovery process is higher than that of the mass recovery process. Otherwise, the mass recovery process not only reduce the heat amount of the regeneration process, but also enhance the cooling amount of the sorption process.

Fig. 5.17 (b) express the VF (MR-HR) of the case that the MR and the PHR are combined. For the same mass recovery period, VF is improved with the PHR, which is similar to the cases that only PHR is introduced. Even though VF of the basic case (MR, mass recovery period = 0 second) is -0.113 kW/kg at a short cycle period of 14 minutes, the combination of the MR (1 second) and the PHR enhanced VF up to 0.095 kW/kg, which proved that the AHP is competitive to the conventional compress type air-conditioner. The peak appears at mass

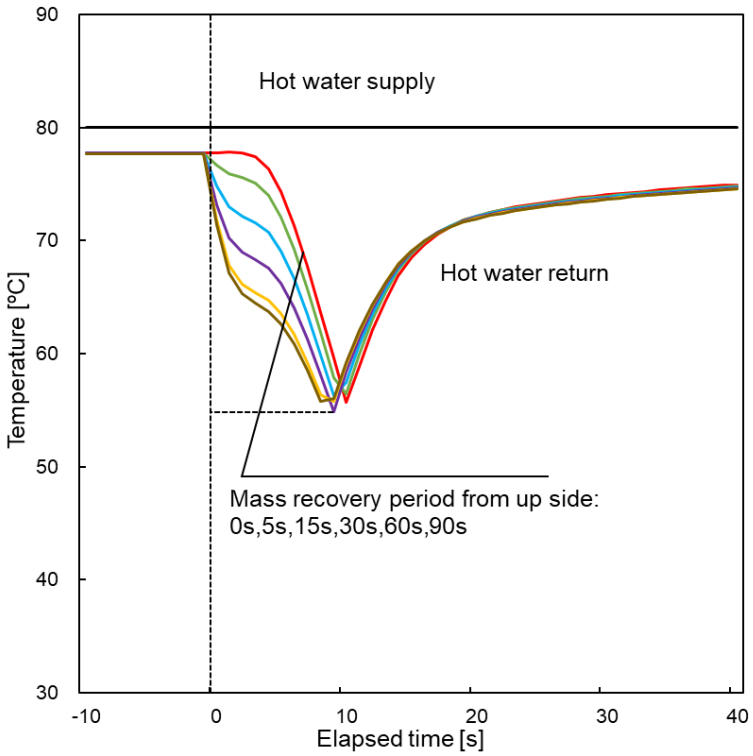

Fig. 5.18 Temperature of the hot water supply and returns versus the elapsed time.

recovery period of 1 second, which is confirmed to be optimal in this study. However, the peak is not so obvious and the period of 1 second is too short for the realistic control.

5.4. Conclusion

In this chapter, a three-dimensional model is built to predict and evaluate the performance of the AHP. The advanced cycles of the heat recovery, the mass recovery and their combination are numerically analyzed.

The 1 kW laboratory-scale AHP that experimentally studied in **Chapter 3** is applied as the target AHP. The adsorbent layers are expressed by a three-dimensional model to describe their mass and heat transfer, meanwhile a zero-dimensional model is applied in the evaporator and the condenser. In conditions of 80 ℃ & 6.3 L/min - regeneration, 30 ℃ & 6.3 L/min - sorption, 30 ℃ & 5.5 L/min - condensation, 20 ℃ & 4.39 L/min - evaporator inlet, 14 minutes cycle period, a representative cycle results of the experiment and the calculation are picked up to compared. The error of SCP is the credible 4.22 %. Though the error of COP is 10.97 % for the basic case and increased to 17.69 % owing to the ignoring of the heat loss, this model is available for the performance prediction. In the next parameter studies, COP is improved up to 0.581 meanwhile SCP decreases to 0.248 kW/kg in cycle period of 60 minutes. COP decreases to 0.110 while the temperature of the regeneration and the evaporator inlet decrease to 60 ℃ and 12 ℃, respectively. Moreover, SCP decreases to 0.020 kW/kg.

The Heat Recovery, which is one of the advanced cycles, is introduced and numerically studied. The cycle period is fixed at 14 minutes referring the experimental results in **Chapter 3**, the Serial Heat Recovery (SHR) and the Passive Heat Recovery (PHR) are applied. The optimal condition is to end the heat recovery while the outlet temperatures of adsorbers are the same, which agrees with the experiment result. Both the SHR and the PHR can improve COP up to 0.604 from 0.503. Moreover, SCP gradually decreases with the longer heat recovery period of the SHR. PHR is confirmed to be the better type of heat recovery owing to its simple structure and no extra valves.

Then the Mass Recovery is performed. COP improves up to 0.546 in mass recovery period of 90 second. SCP is enhanced up to 0.393 kW/kg from 0.389 kW/kg in mass recovery period of the extreme short 1 second, which is too short for the realistic control. The pre-heating/pre-cooling of the mass recovery contribute to the regeneration amount reduction, meanwhile the enhanced cooling amount results in the regeneration amount increasing. Thus the absolute regeneration amount reduction is calculated, and it is 20.06 % of the sensible heat amount. Subsequently, the Mass Recovery and the PHR are combined. In the cases that the mass recovery period of 1 second is taken, COP and SCP can be enhanced up to 0.607 and 0.393 kW/kg from 0.503 and 0.389 kW/kg, respectively. The longer mass recovery period leads to COP decreasing, which indicates that the recoverable sensible heat is shared by the mass recovery process and the heat recovery process. The heat recovery process

possesses better recovery rate, meanwhile the mass recovery process not only reduces the heat amount, but also improves the cooling amount.

In addition, a new evaluation index of the Value Factor (VF) is proposed to determine the optimal conditions of the AHP. A compress type air-conditioner is chosen as the reference, its efficiency coefficient is applied to connect both SCP and COP to the same source of the solar power. The VF higher than 0 indicates better performance of AHP than the reference air-conditioner. In this study, VF is obviously improved up to 0.095 kW/kg from -0.113 kW/kg with the combination of the MR and the PHR. It is confirmed that the AHP is competitive to the conventional compress type air-conditioner in this study.

CONSTANTS

$c_{p,a}$: 1.13 [kJ/(kg·K)]

$C_{p,HEX}$: 0.88 [kJ/(kg·K)]

$C_{p,w}$: 4.187 [kJ/(kg·K)]

$C_{p,v}$: 1.914 [kJ/(kg·K)]

D_{s0} : 0.63 [m^2/s]

E_a : 8.46×10^4 [J/mol]

E_{co} : 0.95 [-]

E_{ev} : 0.95 [-]

L_w : 2.472×10^3 [kJ/kg]

m_a : 4.1 [kg]

$m_{a,dry}$: 4.1 [kg]

$m_{HEX,block}$: 4.293×10^{-4} [kg]

$m_{HEX,co}$: 3.307 [kg]

$m_{HEX,ev}$: 1.102 [kg]

$m_{w,ev}$: 1.6 [kg]

$m_{w,co}$: 1.6 [kg]

$m_{w,block}$: 8.898×10^{-5} [kg]

M_r : 0.018 [kg/mol]

$P_{atmosphere}$: 1.013×10^2 [kPa]

r_s : 2.5×10^{-6} [m]

R : 8.314×10^{-3} [kJ/(mol·K)]

ΔH : 3.220×10^3 [kJ/kg]

ε : 0.56 [-]

$\eta_{chiller}$: 3 [-]

$\eta_{gen,pv}$: 0.12 [-]

$\eta_{heater,solar}$: 0.65 [-]

$\lambda_{a,dry}$: 1.8×10^{-4} [kW/(m·K)]

ρ_a : 0.412×10^{-3} [kg/m^3]

NOMENCLATURE

C_p : specific heat [J/(g·K)]

C_v : concentration of the water vapor [mol/m^3]

D : diffusion coefficient of the water vapor [m^2/s]

D_{s0} : pre-exponent constant [m^2/s]

E : heat exchange coefficient [-]

E_a : activation energy of surface diffusion [J/mol]

k_m : overall mass transfer coefficient [1/s]

L_w : latent heat of the water vaporization [J/g]

m : mass [g]

$\dot{m}$: mass flowrate [g/s]

$m_{w,co\rightarrow ev}$: mass of the water recovered from the condenser to the evaporator [g]

M_r : relative molecular mass of the water [g/mol]

n : mole [mol]

N : number of cycles in all [-]

Np : parameter [-]

P : pressure [Pa]

$P_{atmosphere}$: pressure of the atmosphere [Pa]

Pr : relative vapor pressure [-]

q : instantaneous water vapor sorption amount [g/g]

q^* : equilibrium water vapor sorption amount [g/g]

Q : heat amount [J]

r_s : average radius of the adsorbent particle [m]

R : gas constant [J/(mol·K)]

t : time [s]

T : temperature [°C]

V : volume [m^3]

$\dot{V}$: flowrate [L/s]

VC : value coefficient [-]

x, y, z	: direction [-]
ΔH	: water sorption/desorption latent heat [J/g]

GREEK SYMBOLS

ε	: porosity of the adsorbent layer [-]
η	: efficiency coefficient [-]
λ	: heat conductivity [W/(m·K)]
ρ	: density [g/L]

SUBSCRIPTS

a	: adsorbent
ads	: adsorber
a,dry	: dried adsorbent
a-HEX	: the mixture of the adsorbent and the HEX
b	: begin
block	: the block for calculation
c	: chilling
chiller	: the chiller chosen as the reference
co	: condenser
cyc	: cycle
des	: desorption process
e	: end
ev	: evaporator
evaporation	: water evaporation
gen,pv	: power generation efficiency of the PV panel chosen as the reference
heater,solar	: heating efficiency of the solar heater chosen as the reference

hr	: heat recovery
hw	: hot water
HEX	: heat exchanger
i	: number of cycles
in/out	: inlet/outlet
loss	: heat loss
lt	: latent heat
mix	: mixture of the water vapor
r	: return
reg	: regeneration process
rw	: remained water
s	: supply
sat	: saturated water vapor
sor	: sorption process
ss	: sensible heat
v	: water vapor
w	: water

Reference

[1] A. Akahira, K.C.A. Alam, Y. Hamamoto, A. Akisawa, T. Kashiwagi. Mass recovery adsorption refrigeration cycle - improving cooling capacity. *Refrigeration* 2004;27: 225-234.

[2] Q. W. Pan, R. Z. Wang, L. W. Wang. Comparison of different kinds of heat recoveries applied in adsorption refrigeration system. *Refrigeration* 2015;55:37-48.

[3] M. M. Saleh, A. D. Raya, M. Saad, E. Eman, E. S. Osama. Wire fin heat exchanger using aluminium fumarate for adsorption heat pumps. *Applied Thermal Engineering* 2020;164:114426.

[4] M. Verde, L. Cortes, J.M. Corberan, A. Sapienza, S. Vasta, G. Restuccia. Modelling of an adsorption system driven by engine waste heat for truck cabin A/C. performance estimation for a standard driving cycle. *Applied Thermal Engineering* 2010;30:1511-1522.

[5] A. Freni, G. Maggio, F. Cipitì, Y. I. Aristov. Simulation of water sorption dynamics in adsorption chillers: One, two and four layers of loose silica grains. *Applied Thermal Engineering* 2012, 44, 69–77.

[6] Q.W. Pan, R.Z. Wang. Study on operation strategy of a silica gel-water adsorption chiller in solar cooling application. *Solar Energy* 2018;172:24-31.

[7] S. H. Seol, K. Nagano, J. Togawa. Modeling of adsorption heat pump system based on experimental estimation of heat and mass transfer coefficients. *Applied Thermal Engineering* 2020;171:115089.

[8] F. He, K. Nagano, J. Togawa; Experimental Study and Development of a Low-Cost 1 kW Adsorption Chiller using Composite Adsorbent based on Natural Mesoporous Material. *Energy* 2020;209:118365.

[9] H. Liu, K. Nagano, A. Morita, J. Togawa, M. Nakamura. Experimental testing of a small sorption air cooler using composite material made from natural siliceous shale and chloride. *Applied Thermal Engineering* 2015;82:68-81.

[10] S. Nakabayashi, K. Nagano, M. Nakamura, J. Togawa, A. Kurokawa. Improvement of water vapor adsorption ability of natural mesoporous material by impregnating with chloride salts for development of a new desiccant filter. *Adsorption* 2011;17:675-686.

[11] H. Liu, K. Nagano, J. Togawa. Performance of LiCl impregnated mesoporous material coating over corrugated heat exchangers in a solid sorption chiller. *Energies* 2018;11(6):1565:1-15.

[12] S. H. Seol, K. Nagano, J. Togawa. A new experimental method to separate interfacial and internal mass transfer on coated adsorbent. *Applied Thermal Engineering* 2019;159:113869.

[13] A. Freni, L. Bonaccorsi, L. Calabrese, A. Caprì, A. Frazzica, A. Sapienza. SAPO-34 coated adsorbent

heat exchanger for adsorption chillers. *Applied Thermal Engineering* 2015;82:1-7

[14] S. Oomae, J. Togawa, H. Kuroishi, K. Ochi, K. Nagano. Development of adsorption heat pump using natural mesoporous materials with LiCl – Part 2 Development and evaluation of 10 kW type adsorption heat pump. *Proceedings of the Asian Conference on Refrigeration and Air Conditioning* 2018, 9.

[15] J. Togawa, A. Kurokawa, K. Nagano. Water sorption property and cooling performance using natural mesoporous siliceous shale impregnated with LiCl for adsorption heat pump. *Applied Thermal Engineering* 2020;173:115241.

[16] M. Ben Yahia, Y. Ben Torkia, S. Knani, M. A. Hachicha, M. Khalfaoui, A. Ben Lamine. Models for type VI adsorption isotherms from a statistical mechanical formulation. *Adsorption Science and Technology* 2013, 31(4), 341–357.

[17] A. Sakoda, M. Suzuki, Fundamental study on solar powered adsorption cooling system, *J. Chem. Eng. Japan*. 17 (1984) 52–57.

[18] A. Freni, M. M. Tokarev, G. Restuccia, A. G. Okunev, Y. I. Aristov. Thermal conductivity of selective water sorbents under the working conditions of a sorption chiller. *Applied Thermal Engineering* 2002, 22(14), 1631–1642.

[19] R. W. Hyland, A. Wexler, Formulations for the Thermodynamic Properties of the saturated Phases of H_2O from 173.15K to 473.15K, *ASHRAE Trans* 1983, 89(2A), 500-519.

[20] N. Douss, F. N. Meunier, Lian-Ming Sun. Predictive model and experimental results for a two-adsorber solid adsorption heat pump. *Ind. Eng. Chem. Res* 1988;27:310-316.

[21] Q.W. Pan, R.Z. Wang, L.W. Wang, D. Liu. Design and experimental study of a silica gel-water adsorption chiller with modular adsorbers. *Refrigeration* 2016;67:336-344.

[22] Z.S. Lu, R.Z. Wang, T.X. Li, L.W. Wang, C.J. Chen. Experimental investigation of a novel multifuncion heat pipe solid soption icemaker for fishing boats using $CaCl_2$ - activated carbon compound – ammonia. *Refrigeration* 2007;30:76-85.

[23] A. Akahira, K.C. A. Alam, Y. Hamamoto, A. Akisawa, T. Kashiwagi. Mass recovery four-bed adsorption refrigeration cycle with energy cascading. *Applied Thermal Engineering* 2005;25:1764-1778.

[24] F. He, K. Nagano, S. H. Seol, J. Togawa. Thermal performance improvement of AHP using corrugated heat exchanger by dip-coating method with mass recovery. *Energy* 2022;239:122418.

[25] A. Sapienza, S. Santamaria, A. Frazzica, A. Freni. Influence of the management strategy and operating conditions on the performance of an adsorption chiller. *Energy* 2011; 36:5532-5538.

[26] L. Jiang, R. Z. Wang, L. W. Wang, J. Y. Liu, P. Gao, F. Q. Zhu, A. P. Roskilly. Performance analysis on a novel compact two-stage sorption refrigerator driven by low temperature heat source. *Energy* 2017;135:476-485.

Chapter 6

Parameter Analysis

Introduction

According to the experiment results in the previous champers, it was confirmed that the performance of AHP is significantly influenced by the temperature conditions, which depend on the climate of the target area. **Fig. 6.1** shows some major cities, they are in different area that possess various climates. Obviously, the commercial AHP needs adaptation thus its cooling ability can fit the cooling load of the target area.

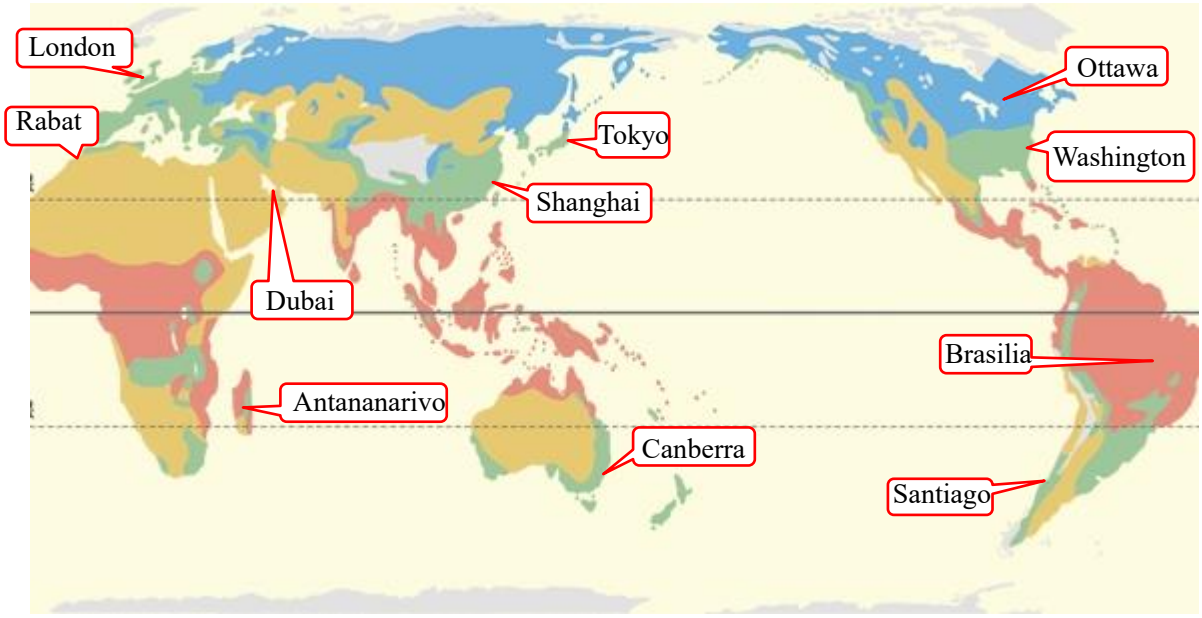

Fig. 6.1 Climate type and some major city in different area.

In this chapter, the three-dimensional model that developed in **Chapter 5** is applied for the case study. A prediction model for optimal design is proposed by the author to adapt the AHP to fit the cooling load of the target area. The temperature of regeneration, sorption, condensation and evaporation are changed to cover most temperature of the major cities. The cooling performance versus the cycle period are calculated and numerically analyzed.

6.1. Flowchart

The flowchart of performance prediction for the optimal design is shown in **Fig. 6.2**.

The cooling performance versus the cycle period, regeneration temperature and sorption/condensation temperature are calculated with the three-dimensional model that developed in **Chapter 5**. However, the prediction results are discontinuous. A function based on the prediction results is needed to fit the real continuous temperature change.

Then a target area is selected. Its climate data is applied to determine the annual transients of the cooling water temperature and the hot water temperature. Meanwhile, a representative building is selected, its annual cooling load data is applied in the optimal model. The optimal model conditions are described as following:

1) The cooling capacity can cover the cooling load.
2) The higher COP can be obtained.
3) The necessary adsorbent is least.

Based on the annual transients of the temperature and cooling load, the optimal capacity (mass of adsorbent) of the AHP can be obtained.

Subsequently, the optimized model is applied for the annual performance prediction. The annual energy consumption of the AHP is calculated to compare with that of the conventional compression type air-conditioner. The energy consumption reduction can be numerically analyzed.

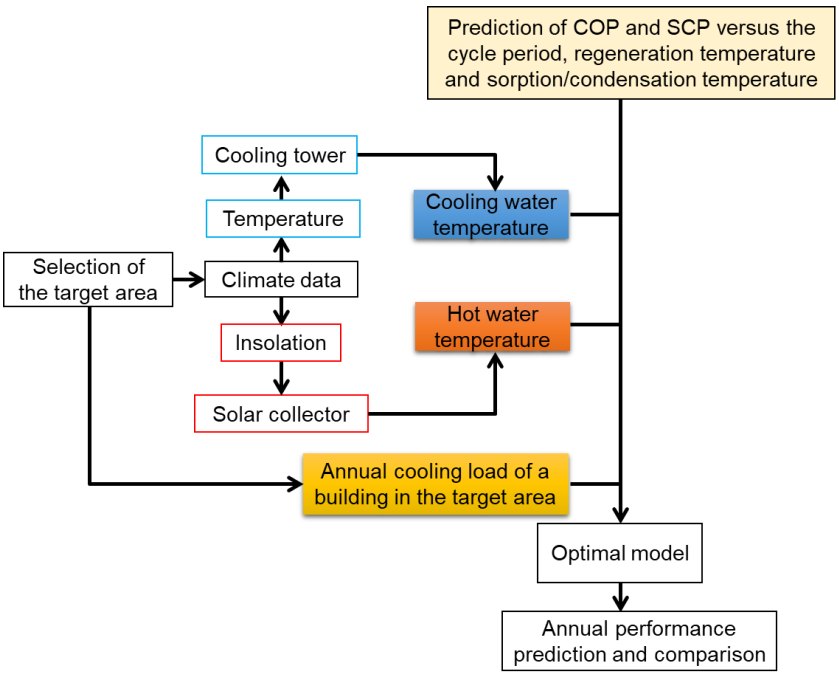

Fig. 6.2 Flowchart of performance prediction for the optimal design.

6.2. Performance Prediction versus Temperature & Cycle Period

6.2.1. Calculation Conditions

As the first step, the performance versus temperature and cycle period is predicted with the three-dimensional model developed in **Chapter 5**. The AHP described in **Chapter 3** and **5** is selected as the reference, its capacity can be adjusted by scaling up. The calculation conditions are shown in **Table 6.1**. AHP is generally applied regeneration temperature of 60-80 ℃ [1-4], meanwhile synthetic zeolites used as adsorbents in AHPs and desiccants can be regenerated at relatively low temperatures down to 50 ℃ [5-10]. For the practical application, the solar collector is used to provide the regeneration hot water because it is a well-established technology and almost no area limitation. The temperature from the solar collector based on the insolation and environment temperature, which depend on the climates of the target area and the time in one day. Pan's study also shows the temperature transient of a solar collector, which is changed between 60-80 ℃ versus the time [11]. Thus the regeneration temperature in this study is changed between 55-80 ℃. The cooling water for both sorption and condensation can be provided by the cooling tower. For the conventional compression type air-conditioner, the cooling water temperature is generally 32-37 ℃. The outlet temperature of the cooling tower is influenced by the environment temperature, it may increase above 40 ℃ in some extreme tropical area such as desert. On the other hand, some cool or coastal area can provide cooling water below 30 ℃, which will absolutely enhance the performance of the AHP. Moreover, the AHP in this study is considered as the alternative of the conventional compression type air-conditioner. It is applied for space cooling to provide comfortable indoor environment against the hot weather. In the area where can provide cooling water below 25 ℃, the space cooling is generally not necessary or can be directly provided by the natural water (River, lake, or ocean). Hence the cooling temperature for both sorption and condensation are the same and set between 25-40 ℃. The evaporation temperature of the AHP in this study is set at 15 ℃. The cycle period is changed from 2-30 minutes.

Table 6.1 Calculation conditions

	Regeneration	Sorption	Condensation	Evaporation
Temperature [℃]	55-80	25-40	25-40	15
Flowrate [L/min]	9.5	9.5	5.5	4.39

6.2.2. Calculation Results

Accumulated cooling and regeneration amount versus the cycle period are shown in **Fig. 6.3**. For the cases whose regeneration/sorption/condensation are constant, the accumulated cooling and regeneration amount

Accumulated cooling amount **Accumulated regeneration amount**

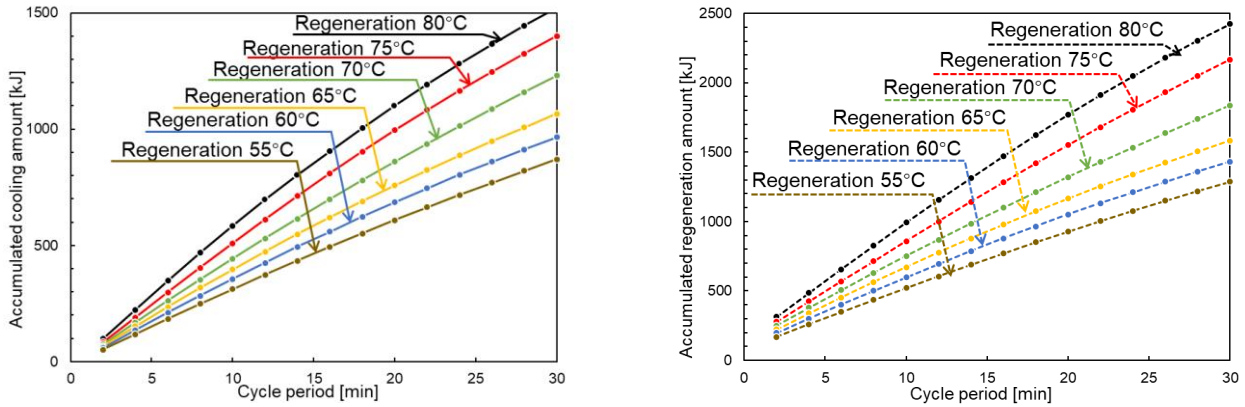

(a) Sorption/condensation temperature at 25 ℃.

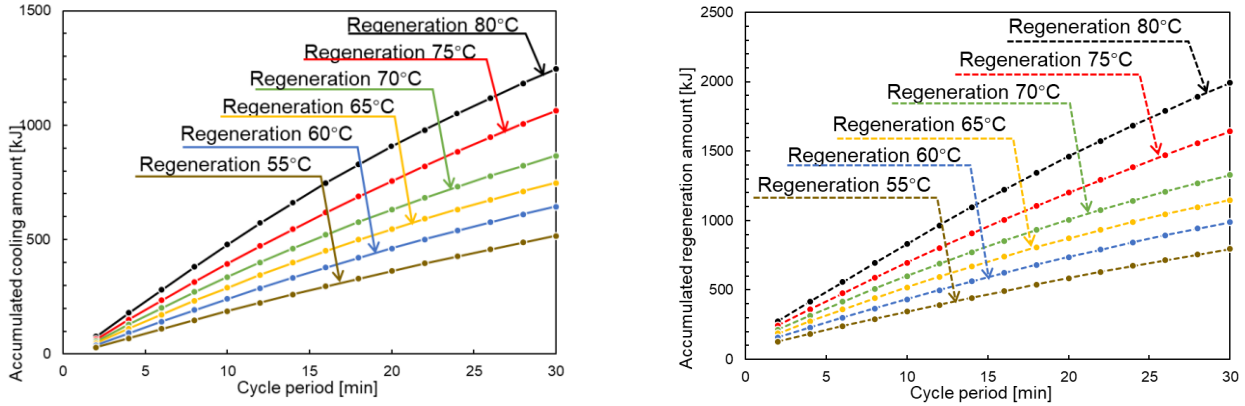

(b) Sorption/condensation temperature at 30 ℃.

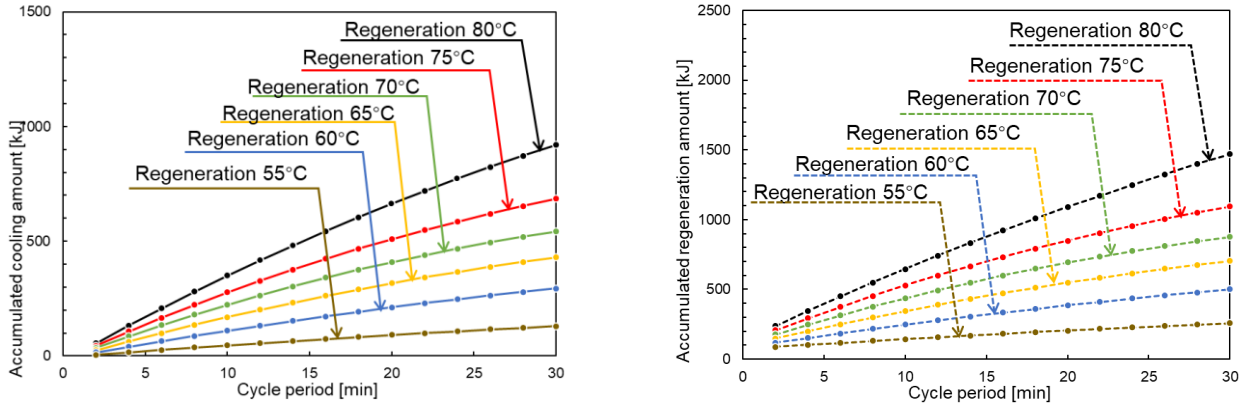

(c) Sorption/condensation temperature at 35 ℃.

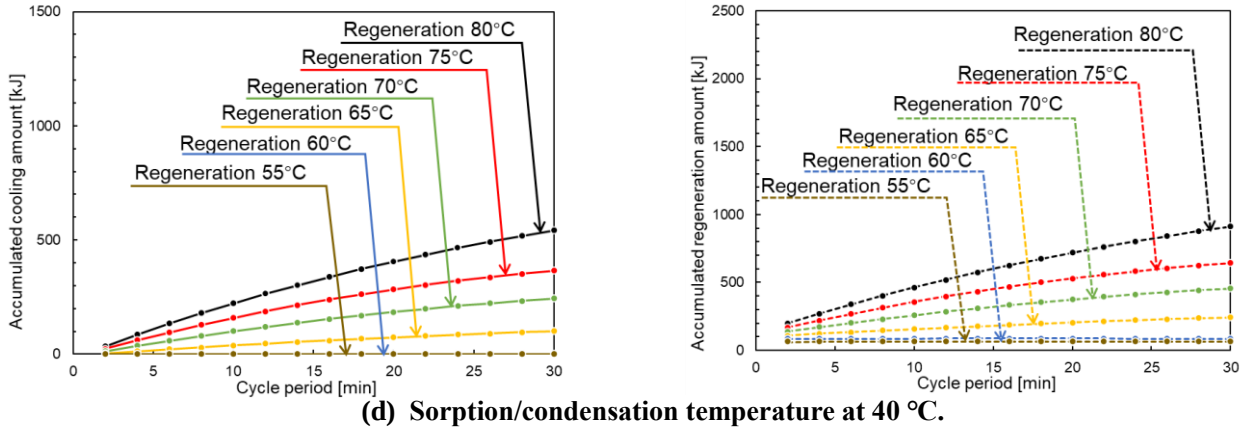

(d) Sorption/condensation temperature at 40 ℃.

Fig. 6.3 Accumulated cooling amount and accumulated regeneration amount versus the cycle period.

gradually increase with the longer cycle period is taken. It indicates that the sorption/regeneration processes have not finished completely. For the same sorption/desorption temperature, the decrease of the regeneration temperature leads to reduction of the accumulated cooling and regeneration amount. As shown in **Fig. 5.3**, the lower regeneration temperature cause decreasing of the effective sorption amount, meanwhile, the desorption speed is reduced (**Eq. 5.4**). It is considered to be the reason that the accumulated cooling and regeneration amount decrease. The increase of condensation temperature also results in effective sorption amount decreasing. In addition, the accumulated cooling amount decrease to 0 in cases that the sorption/condensation temperature increased to 40 ℃ and the regeneration temperature decrease down to 60 ℃. Based on the isotherms shown in **Fig. 5.3**, the water sorption amount in the sorption process is lower than that in the regeneration process, which indicates that the AHP is unavailable at this condition. On the other hand, the sensible heat of the HEX, adsorbent and remained water need energy to heat. Thus the accumulated regeneration amount is higher than 0 though the effective water sorption amount is minus.

Based on the results shown in **Fig. 6.3**, COP and SCP are calculated and shown in **Fig. 6.4**. SCP shows the identical trend to the accumulated cooling amount in **Fig. 6.3**, which can be explained with the definition equation of **Eq. (5.22)** and **(5.27)**. On the other hand, COP increase with the longer cycle period is taken at constant regeneration/sorption/condensation temperatures. With the increase of sorption/condensation temperatures or decrease of regeneration temperatures, the effective water sorption amount is reduced, which leads to decrease of COP. Because of the accumulated cooling amount in cases mentioned above decrease to 0, COP of those cases also down to 0. However, COP decreasing with the regeneration temperature increasing can be observed in some cases. In cases sorption/condensation temperature at 25 ℃, COP at regeneration temperatures of 75 ℃ and 80 ℃ shows obvious reduction than that at regeneration temperature of 70 ℃. In cases sorption/condensation temperature at 30 ℃, COP at regeneration temperatures of 80 ℃ is higher than others till cycle period is increased up to 14 minutes, then is lower than others.

In order to explain the COP change trend mentioned above, the calculation equation of COP based on the accumulated cooling and regeneration amount of a representative cycle is shown in **Eq. (6.1)**. Q_c is the accumulated cooling output amount of a representative sorption process, it is expressed by the difference of the vaporization latent heat $Q_{lt,evaporation}$ and the sensible heat of water recovered from the condenser $Q_{ss,recovered,w}$. On the other hand, Q_{reg} is the accumulated regeneration amount of a representative regeneration process. It consists of the sorption heat amount $Q_{lt,des}$ and the sensible heats, which are the adsorbent ($Q_{ss,ads,adsorbent}$), the sensible heats of the HEX ($Q_{ss,ads,HEX}$) and the sensible heats of the remained water ($Q_{ss,ads,rw}$). When the cycle period is long enough, the sorption and regeneration processes are absolutely finished, COP is expressed as **Eq. (6.2)**. $Q_{lt,evaporation}$ and $Q_{lt,des}$ are proportional to the theoretical maximum of

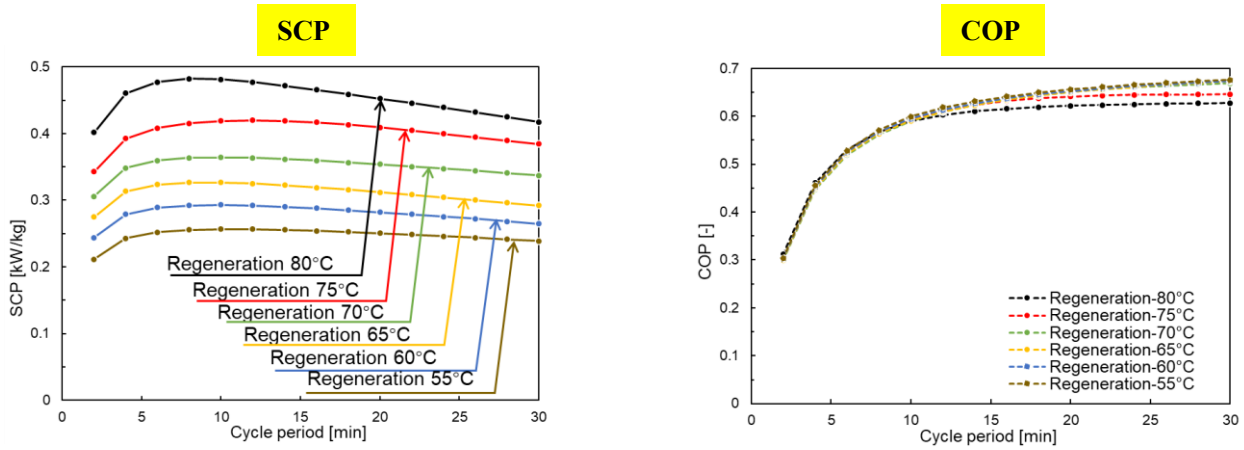

(a) Sorption/condensation temperature at 25 ℃.

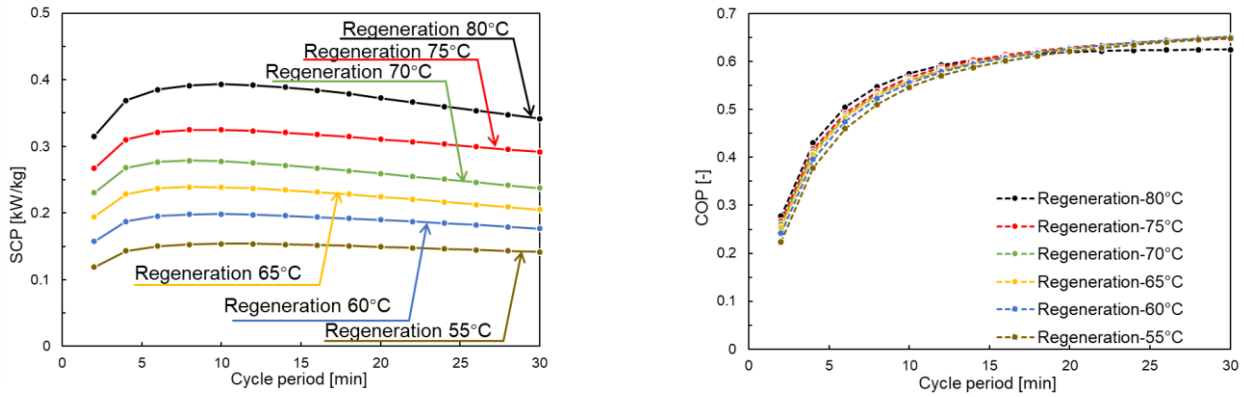

(a) Sorption/condensation temperature at 30 ℃.

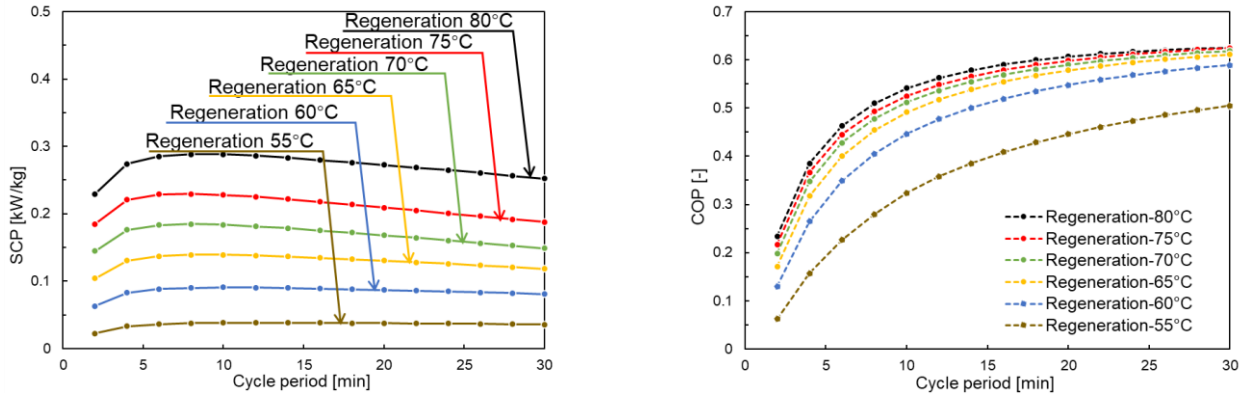

(a) Sorption/condensation temperature at

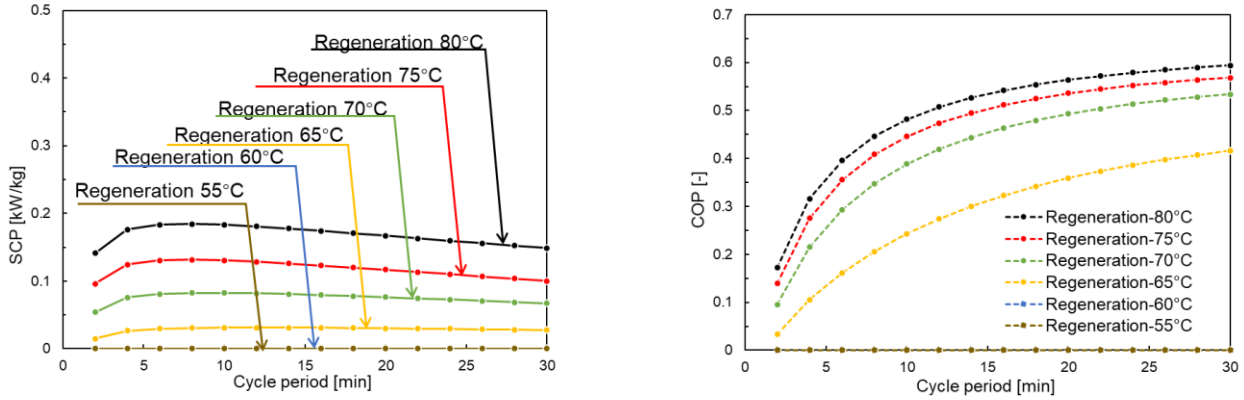

(a) Sorption/condensation temperature at

Fig. 6.4 SCP and COP versus the cycle period.

$$\mathrm{COP} = \frac{Q_c}{Q_{reg}} = \frac{Q_{lt,evporation} - (Q_{ss,recovered,w})}{Q_{lt,des} + (Q_{ss,ads,adsorbnet} + Q_{ss,ads,HEX} + Q_{ss,ads,rw})} \quad (6.1)$$

$$\mathrm{COP} = \frac{aq_{max} - cq_{max}}{bq_{max} + Q_{ss}} \quad (6.2)$$

the sorption amount q_{max} (**Fig. 6.5**), they are expressed as a*q_{max} and b*q_{max}, respectively. Meanwhile, $Q_{ss,recovered,w}$ depends on the sorption amount, it is expressed as c*q_{max}. All the sensible heat amount include $Q_{ss,ads,adsorbent}$, $Q_{ss,ads,HEX}$ and $Q_{ss,ads,rw}$, depends on the temperatures of the regeneration/ sorption and are expressed as Q_{ss}. As shown in **Fig. 6.5**, for the cases that sorption/condensation temperature are 25 ℃ (3.4 kPa) and 30 ℃ (4.25kPa), the q_{max} almost constant. However, the sensible heat Q_{ss} increase with the regeneration temperature increase, which results in the COP decrease.

This model is confirmed to be credible. Obviously, COP and SCP of AHP change a lot with the regeneration/sorption/condensation temperature changing. However, the hot/cooling water supplies are consistent in the practical application, therefore functions are needed to express COP and SCP versus the temperature of regeneration/sorption/condensation consistent. These functions will be built in the future, and the case studies will be conducted.

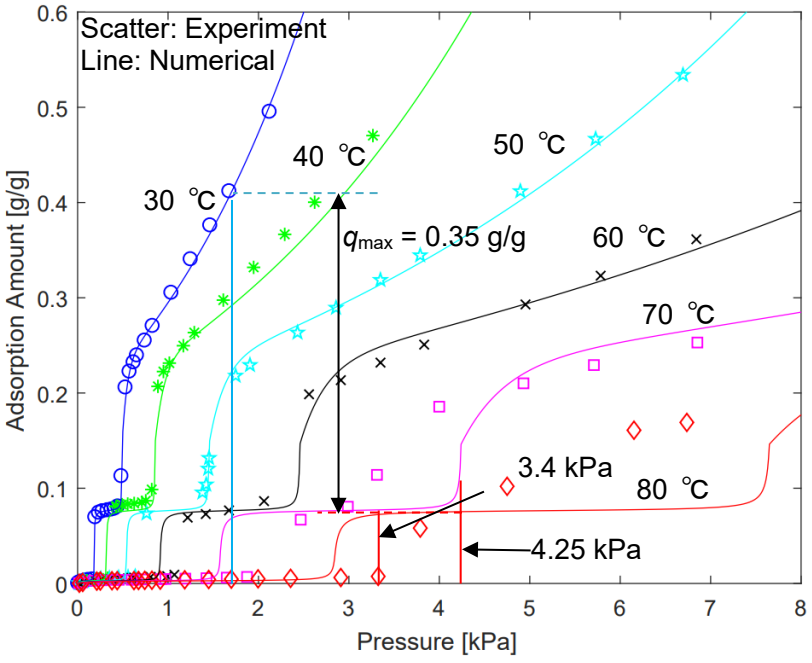

Fig. 6.5 Isotherms of WSS composite adsorbent.

NOMENCLATURE

a,b : coefficient [-]

Q : heat amount [J]

q : instantaneous water vapor sorption amount [g/g]

SUBSCRIPTS

ads : adsorber

adsorbent : adsorbent

c : chilling

des : desorption process

evaporation : water evaporation

HEX : heat exchanger

lt : latent heat

max : maximum

recovered,w : recovered water

reg : regeneration process

rw : remained water

ss : sensible heat

Reference

[1] He F, Nagano K, Togawa J. Experimental study and development of a low-cost 1 kW adsorption chiller using composite adsorbent based on natural meso- porous Material. *Energy* 2020;209:118365.

[2] Lu ZS, Wang RZ. Performance improvement by mass-heat recovery of an innovative adsorption air-conditioner driven by 50-80 ?C hot water. *Appl Therm Eng* 2013;55:113-20.

[3] Pan QW, Wang RZ. Experimental study on operating features of heat and mass recovery processes in adsorption refrigeration. *Energy* 2017;135:361-9.

[4] Akahira A, Alam KCA, Hamamoto Y, Akisawa A, Kashiwagi T. Mass recovery adsorption refrigeration cycle - improving cooling capacity. Refrigeration 2004;27:225-34.

[5] Teo HWB, Chakraborty A, Fan W. Improved adsorption characteristics data for AQSOA types zeolites and water system under and dynamic condition. *Microporous Mesoporous Mater* 2017;242:109e17.

[6] Kakiuchi H, Shimooka S, Iwade M, Oshima K, Yamazaki M, Terada S, Watanabe H, Takewaki T. Novel water vapor adsorbent FAMeZ01 and its applicability to an adsorption heat pump. *Kagaku Kogaku Ronbunshu* 2005;31:361e4.

[7] Kakiuchi H, Shimooka S, Iwade M, Oshima K, Yamazaki M, Terada S, Watanabe H, Takewaki T. Water vapor adsorbent FAM-Z02 and its applica- bility to adsorption heat pump. *Kagaku Kogaku Ronbunshu* 2005;31:273e7.

[8] Kayal S, Baichuan S, Saha BB. Adsorption characteristics ofAQSOA zeolites and water for adsorption chiller. *Int J Heat Mass Tran* 2016;92:1120e7.

[9] Chakraborty A, Leong KC, Thu K, Saha BB, Ng KC. Theoretical insight of adsorption cooling. *Appl Phys Lett* 2011;98:221910.

[10] Verde M, Cortes L, Corberan JM, Sapienza A, Vasta S, Restuccia G. Modelling of an adsorption system driven by engine waste heat for truck cabin A/C. per- formance estimation for a standard driving cycle. *Appl Therm Eng* 2010;30: 1511e22.

[11] Q.W. Pan, R.Z. Wang. Study on operation strategy of a silica gel-water adsorption chiller in solar cooling application. *Solar Energy* 2018;172:24-31.

Chapter 7

Conclusion and Prospective

Conclusion

As a competitive new adsorbent, the WSS composite had been studied in the prior research by our team members. The WSS composite had been proved to be a potential adsorbent, which possesses the similar water sorption amount but much cheaper compared with the AQSOA-FAM. This research aims at the practical application of the WSS composite as the adsorbent and the performance enhancement of the AHP. The main achievement of each chapter is summarized as following:

Chapter 1 is the general introduction. The energy structure and consumption in the world and the Japan are investigated. The space cooling requirement in the developing countries increase with the economic development, which results in fossil fuel consumption increasing. Meanwhile, the market of the air-conditioner is predicted to grow. As one of the thermal driven heat pumps, the Adsorption Heat Pump (AHP) is considered to be one of the solutions.

Chapter 2 is the reviews on the AHP. The working pairs of the AHP and their properties are investigated. Then some advanced cycles that can enhance the cooling performance of the AHP are summarized. Subsequently, our prior researches are introduced and the objective of current study is proposed.

Chapter 3 focuses on the practical application of the WSS composite. A 1 kW laboratory-scale AHP using the WSS composite as the adsorbent is developed to evaluate the cooling performance. Then the Heat Recovery (HR) is introduced and performed to reduce the regeneration heat amount. According to the results of the parameter studies, the following conclusions are obtained:

1) Under standard experimental conditions of 80 ℃ for regeneration, 30 ℃ for sorption, 30 ℃ for condensation, 15 ℃ for the evaporator outlet, and proper cycle period of 14 min, the COP and SCP are calculated as 0.45 and 0.41 kW/kg, respectively. The COP of 0.38 and SCP of 0.17 kW/kg are shown when the regeneration temperature decreases to 60 ℃. It is confirmed that a low-grade heat source could drive the AHP.

2) Two types of the HR, which are the Serial Heat Recovery (SHR) and the Passive Heat Recovery (PHR), are introduced. For both SHR and PHR, the highest COP of 0.54 could be obtained when the outlet temperature of the Ads.1 and Ads.2 are the same, 55 ℃, which is the average temperature of the regeneration and sorption. The heat balance evaluation shows that the COP of the AHP can be further improved to 0.57 by means of heat recovery by reducing the tubes between the hot water tank and the heat exchangers.

3) The WSS with 20 wt. % LiCl is proved to be a valuable adsorbent due to low-cost and high cooling performance.

Chapter 4 compares the Plate Fin-Tube type HEX (PFT-HEX) and the Micro Channel type HEX (MC-HEX). For the merits of lighter HEX, less remained water and more space, COP of the PFT-HEX can be improved further with the packing density increase and longer cycle period. However, the MC-HEX shows the better heat transfer, higher SCP can be obtained. In addition, the limit thickness of the commercial PTF-HEX is 25 mm while that of the MC-HEX can be reduced to 12 mm owing to its structure, which contributes to compact of the ad-HEX. Thus the MC-HEX is proved to be better than the PFT-HEX.

Then a new filling method called Dip-coating is introduced and adapted to accommodate the WSS composite adsorbent. Three kinds of Ad-HEX (Filled-HEX, Dip-HEX, Dip-Filled-HEX) are fabricated using this adopted Dip-coating. Compared with the conventional Filled-HEX, the Dip-HEX possesses the mass transfer channels inner the adsorbent layer, which contributes to better mass transfer. Therefore, COP and SCP of the Dip-HEX are higher than those of the filled-HEX. The packing density can be improved by approximately 30% up to 400 g/L to achieve the Dip-Filled-HEX via the adopted Dip-coating method. The high packing density of the dip-filled HEX significantly increased the COP; however, this resulted in a slight decrease in the SCP.

Then an advanced cycle called the Mass Recovery (MR) is introduce and experimentally studied. With the proper mass recovery period of 10 seconds, COP of the current AHP applied the Filled-HEX, the Dip-HEX and the Dip-Filled-HEX are improved up to 0.41, 0.46 and 0.5, respectively. SCP of the current AHP applied the Filled-HEX, the Dip-HEX and the Dip-Filled-HEX increases up to 0.69 W/g, 0.74 W/g and 0.64 W/g, respectively. Sorption/desorption of adsorbent during the mass recovery process depend on the filling type of the Ad-HEX, larger surface area obviously increases the sorption/desorption speed and enhances then mass recovery. It is found that the Dip-HEX is a completely advanced Ad-HEX.

Chapter 5 develops a three-dimensional model for the cooling performance prediction and parameter studies of the AHP. Then the advanced cycles of the HR and the MR are numerically analyzed. The achievements are shown as following:

1) In conditions of 80 ℃ & 6.3 L/min - regeneration, 30 ℃ & 6.3 L/min - sorption, 30 ℃ & 5.5 L/min - condensation, 20 ℃ & 4.39 L/min - evaporator inlet, 14 minutes cycle period, the error of SCP is the credible 4.22 %. Though the error of COP is 10.97 % for the basic case and increased to 17.69 % owing to the ignoring of the heat loss, this model is available for the performance prediction.

2) COP is improved up to 0.581 meanwhile SCP decreases to 0.248 kW/kg in cycle period of 60 minutes. COP decreases to 0.110 while the temperature of the regeneration and the evaporator inlet decrease to 60 ℃

and 12 ℃, respectively. Moreover, SCP decreases to 0.020 kW/kg.

3) The cycle period is fixed at 14 minutes referring the experimental results in **Chapter 3**, the Serial Heat Recovery (SHR) and the Passive Heat Recovery (PHR) are applied in this AHP model. The optimal condition is to end the heat recovery while the outlet temperatures of adsorbers are the same, which agrees with the experiment result. Both the SHR and the PHR can improve COP up to 0.604 from 0.503. Moreover, SCP gradually decreases with the longer heat recovery period of the SHR. PHR is confirmed to be the better type of heat recovery owing to its simple structure and no extra valves.

4) Then the Mass Recovery is performed, SCP is enhanced up to 0.393 kW/kg from 0.389 kW/kg in mass recovery period of the extreme short 1 second, which is too short for the realistic control. The absolute regeneration amount reduction is calculated, and it is 20.06 % of the sensible heat amount. In the cases the Mass Recovery and the PHR are combined, COP and SCP can be enhanced up to 0.607 and 0.393 kW/kg from 0.503 and 0.389 kW/kg, respectively. The longer mass recovery period leads to COP decreasing, which indicates that the recoverable sensible heat is shared by the mass recovery process and the heat recovery process. The heat recovery process possesses better recovery rate, meanwhile the mass recovery process not only reduces the heat amount, but also improves the cooling amount.

5) A new evaluation index of the Value Factor (VF) is proposed to determine the optimal conditions of the AHP. A compress type air-conditioner is chosen as the reference, its efficiency coefficient is applied to connect both SCP and COP to the same source of the solar power. The VF higher than 0 indicates better performance of AHP than the reference air-conditioner. In this study, VF is obviously improved up to 0.095 kW/kg from -0.113 kW/kg with the combination of the MR and the PHR. It is confirmed that the AHP is competitive to the conventional compress type air-conditioner in this study.

The three-dimensional model built in **Chapter 5** is applied for parameter analysis in **Chapter 6**. The procedure for the case study is determined, and the parameter analysis based on the temperature of the regeneration/sorption/condensation are conducted.

7.1. Prospective Study

7.1.1. Case Study

As mentioned in **chapter 6**, performance of AHP is significantly influenced by the temperature conditions, which depend on the climate of the target area. The case study is necessary for the design of commercial AHP. The procedure for the case study is determined and the parameter analysis is conducted. However, the hot/cooling water supplies are consistent in the practical application, therefore functions are needed to express COP and SCP versus the temperature of regeneration/sorption/condensation consistent in the future. Moreover, the cooling load data of some representative building in target area is applied to determine the optimal control strategy. With the optimized model, the annual performance prediction and comparison are available.

7.1.2. Adsorption Chiller

The water is generally applied as the adsorbate of AHP, which leads the AHP to an environmental friendly heat pump. However, the utilization of water also limits the lowest chilled water temperature to 0 °C. In order to achieve cooling ability under 0 °C, some adsorbates with melting point under 0 °C are proposed and studied. Methanol is an adsorbate whose melting point is -97.8 °C. It is available to provide the cooling ability under 0 °C using the methanol as the adsorbate of AHP. On the other hand, the AHP using the methanol needs rigorous check and design due to its toxicity and flammability.

7.1.3. Water Harvesting

Not only the cooling ability, the AHP or adsorption-based system also available to achieve the pure water. As mentioned in the previous chapters, the adsorbate water is vaporized in the evaporator, then move to the adsorber and finally condensed to water in the condenser. The producing of pure water, which called Water Harvesting (WH), is easily to fulfill with the AHP system. The seawater or dirty water is added into the evaporator and the pure water can be obtained in the condenser. This WH system can provide the cooling ability and pure water simultaneously, which leads the WH system is very fit the lack of drinking water and hot area. Moreover, the WH system can be adapted to improve the water output by sacrificing its cooling ability, it changes the WH system to a high drinking water producing coefficient machine.